



CIVIL ENGINEERING STUDIES
Illinois Center for Transportation Series No. 12-021
UIIU-ENG-2012-2024
ISSN: 0197-9191

FIELD PERFORMANCE EVALUATIONS OF ILLINOIS AGGREGATES FOR SUBGRADE REPLACEMENT AND SUBBASE—PHASE II

Prepared By
Debakanta Mishra
Erol Tutumluer
University of Illinois at Urbana-Champaign

Research Report FHWA-ICT-12-021

Illinois Center for Transportation
Project R27-81
Field Performance Evaluations of Illinois Aggregates for
Subgrade Replacement and Subbase-Phase II

April 2013

Technical Report Documentation Page

1. Report No. FHWA-ICT-12-021		2. Government Accession No.		3. Recipient's Catalog No.	
4. Title and Subtitle Field Performance Evaluations of Illinois Aggregates for Subgrade Replacement and Subbase—Phase II				5. Report Date April 2013	
				6. Performing Organization Code ICT-12-021 UILU-ENG-2012-2024	
7. Author(s) Debakanta Mishra and Erol Tutumluer				8. Performing Organization Report No.	
9. Performing Organization Name and Address Illinois Center for Transportation Department of Civil & Environmental Engineering University of Illinois at Urbana-Champaign 205 N. Mathews Ave., MC-250 Urbana, IL 61801				10. Work Unit No. (TRAIS)	
				11. Contract or Grant No. R27-81	
12. Sponsoring Agency Name and Address Illinois Department of Transportation Bureau of Materials & Physical Research 126 E. Ash St. Springfield, IL 62704				13. Type of Report and Period Covered	
				14. Sponsoring Agency Code	
15. Supplementary Notes					
16. Abstract: The project objective was to validate the results from ICT Project R27-1, which characterized in the laboratory the strength, stiffness, and deformation behaviors of three different aggregate types commonly used in Illinois for subgrade replacement and subbase applications, through accelerated loading of full-scale pavement working platform test sections. Six different test “cells” were constructed at different combinations of aggregate material quality and subgrade strength, and were tested to failure using the University of Illinois Accelerated Transportation Loading Assembly (ATLAS). Each cell was tested along two different wheel paths representing two different aggregate layer moisture contents (Cells 1-5), or geotextile reinforcement conditions (Cell 6). Performances under loading were monitored through surface profile measurements as well as transverse scanning with ground-penetrating radar (GPR). Field and laboratory test results highlighted the importance of considering aggregate quality in the thickness design of aggregate layers for construction platforms. Thick layers of uncrushed gravel placed over a weak subgrade mainly underwent internal shear failure due to excessive movement of the aggregate particles. Crushed aggregate layers constructed with high relative compaction, on the other hand, showed significantly higher resistance to internal shear deformation and permanent deformation accumulations. Prolonged exposure to moisture and freeze-thaw effects was found to be beneficial for a crushed dolomite material with high amounts of nonplastic fines probably due to carbonate cementation within the fine fraction. Failure of test sections under flooded conditions was primarily caused by excessive deformation in the subgrade layer. Recommendations were made based on the study findings for improved material selection and thickness designs of aggregate working platforms.					
17. Key Words Unbound Aggregates, Subgrade Stability, Permanent Deformation, Accelerated Pavement Testing, Unsurfaced Pavements, Working Platforms			18. Distribution Statement No restrictions. This document is available to the public through the National Technical Information Service, Springfield, VA 22161		
19. Security Classif. (of this report) Unclassified		20. Security Classif. (of this page) Unclassified		21. No. of Pages 65 + appendices	22. Price

ACKNOWLEDGMENT, DISCLAIMER, MANUFACTURERS' NAMES

This publication is based on the results of R27-81, Field Performance Evaluations of Illinois Aggregates for Subgrade Replacement and Subbase, Phase II. R27-81 was conducted in cooperation with the Illinois Center for Transportation; the Illinois Department of Transportation; and the U.S. Department of Transportation, Federal Highway Administration.

Members of the Technical Review Panel are the following:

Gregory B. Heckel, Chair
Riyad M. Wahab
Edward M. Frank
Thomas A. Ripka
Heather Z. Shoup
Juan Pava
Joseph Vespa
William M. Kramer
Wayne Phillips
Tom Bukowski
Brian Pfeifer
Patty Broers
Sheila A. Beshears

The authors would also like to extend their acknowledgements to ICT Director Professor Imad Al-Qadi, ICT research engineer James Meister, and graduate students Hasan Kazmee, Huseyin Boler, Marcus Dersch, Anthony Mareno, and Yu Qian for their help during the construction, testing, and performance monitoring of the full-scale pavement sections. Special thanks go to Maziar Moaveni and Yuanjie Xiao for their help with the in-situ stiffness measurement during construction as well as the accelerated pavement testing.

The contents of this report reflect the view of the authors, who are responsible for the facts and the accuracy of the data presented herein. The contents do not necessarily reflect the official views or policies of the Illinois Center for Transportation, the Illinois Department of Transportation, or the Federal Highway Administration. This report does not constitute a standard, specification, or regulation.

Trademark or manufacturers' names appear in this report only because they are considered essential to the object of this document and do not constitute an endorsement of product by the Federal Highway Administration, the Illinois Department of Transportation, or the Illinois Center for Transportation.

EXECUTIVE SUMMARY

This report presents findings from Illinois Center for Transportation (ICT) Project R27-81, “Field Performance Evaluations of Illinois Aggregates for Subgrade Replacement & Subbase—Phase II.” This project was carried out as the second phase of ICT research Project R27-1 (“Characterization of Illinois Aggregates for Subgrade Replacement and Subbase”), which characterized in the laboratory the strength, stiffness, and deformation behaviors of three different aggregate types commonly used in Illinois for subgrade replacement and subbase applications. An experimental test matrix was developed to engineer gradations and study the individual effects of major aggregate properties such as particle shape, texture and angularity, fines content, and plasticity index (PI) or plasticity of fines, as well as compaction (moisture density) conditions on aggregate behavior. The overall objective was to incorporate material quality aspects into the thickness designs of aggregate layers for pavement construction platform applications through modification of the design curve presented in Figure A-2 of the Illinois Department of Transportation (IDOT) Subgrade Stability Manual (SSM). Phase II of the research study documented in this report had an overall objective of validating the laboratory test results reported in the Phase I project report through accelerated loading of full-scale pavement working platform test sections.

Six different full-scale pavement working platform test “cells” were constructed representing different combinations of aggregate material quality and subgrade strength and were tested to failure using the University of Illinois Accelerated Transportation Loading Assembly (ATLAS). Selection of aggregate materials for construction of the test sections was based on Phase I research findings. Each of Cells 1 through 5 comprised three “sections” representing three different aggregate layer thicknesses constructed over a subgrade layer of controlled strength. Cell 6 comprised three sections of equal thicknesses but was constructed using different types of large-size aggregate materials over a subgrade of immediate bearing value (IBV) = 1%. Each test cell was tested along two different wheel paths. For Cells 1 through 5, the two wheel paths represented different aggregate layer moisture conditions, whereas for Cell 6, the two wheel paths were used to evaluate the effects of geotextile reinforcement on pavement working platform performance. Test section performances under loading were monitored through surface profile measurements as well as transverse scanning with ground-penetrating radar (GPR). Transverse trenches were excavated after failure of the test sections to distinguish between rut accumulations in the aggregate and subgrade layers. Different aggregate types used for constructing the test sections were also tested in the laboratory for strength, modulus, and permanent deformation characterization.

Accelerated testing of full-scale sections, as well as laboratory characterization of aggregates, highlighted the importance of considering aggregate quality in the thickness design of aggregate layers for construction platform applications. Particle shape, linked to crushed or uncrushed aggregate type, was found to be the most important physical property affecting aggregate layer behavior. Thick layers of uncrushed gravel placed over a weak subgrade were observed to undergo internal shear failure resulting from a high amount of fines and excessive movement of the aggregate particles. Crushed aggregate layers, on the other hand, showed significantly higher resistance to internal shear deformation, while test sections constructed using crushed aggregates failed primarily as a result of subgrade deformation. The influence of compactive effort on aggregate layer performance was clearly apparent: higher relative compaction exhibited better resistance to permanent deformation accumulation. Prolonged exposure to moisture and freeze-thaw effects was found to have a beneficial effect on the crushed dolomite that contained high amounts of nonplastic fines.

Carbonate cementation within the fine fraction was identified as the most probable mechanism contributing to stiffening of the aggregate sections, which resulted in the aggregate layer sustaining a significantly higher number of load applications without undergoing shear failure. Finally, the failure of test sections under flooded conditions was caused primarily by excessive deformation in the subgrade layer. Water intrusion into the subgrade under flooded conditions significantly reduced the subgrade strength, ultimately leading to subgrade shear failure.

On the basis of combined analyses of laboratory and full-scale testing results, this report makes important recommendations for thickness designs of aggregate working platforms through inclusion of improved material selection. This report also relates aggregate quality and material properties to layer performance and based on the study findings presented in detail recommends incorporation of new construction procedure specifications into the IDOT SSM.

CONTENTS

CHAPTER 1 INTRODUCTION	1
1.1 Introduction and Background	1
1.2 Research Objectives	2
1.3 Research Methodology	2
1.3.1 Mechanistic Evaluation of Pavement Layer Response During Construction	3
1.3.2 Construction of Test Sections for Field Validation	3
1.3.3 Accelerated Testing and Performance Monitoring	4
1.3.4 Analysis of Field Section Performance, and Recommendations for Implementation of Research Findings	4
1.4 Report Organization	4
CHAPTER 2 SUMMARY OF PAST RESEARCH	6
2.1 Introduction	6
2.2 Previous Research on IDOT Subgrade Improvement Curve	6
2.2.1. Original Research by Thompson et al.....	6
2.2.2. Verification Research by Thompson and Tutumluer in 2005	6
2.2.3. Test Loop and Field Verification Studies by Heckel.....	6
2.3 ICT Project R-27-1	7
CHAPTER 3 CONSTRUCTION OF FULL-SCALE TEST SECTIONS.....	9
3.1 Introduction	9
3.2 Mechanistic Evaluation of Pavement Layer Response During Construction	9
3.3 Experimental Design Through Material Selection	10
3.4 Laboratory Characterization of Aggregates	11
3.4.1 Particle Size Distribution and Atterberg Limits	11
3.4.2 Compaction Characteristics and IBV	12
3.4.3 Resilient Modulus and Permanent Deformation Characteristics.....	13
3.4.4 Summary of Findings from Laboratory Characterization of Aggregates	16
3.5 Layout and Cross-Sectional Profile of Full-Scale Test Sections	17
3.6 Subgrade Characterization	19
3.7 Engineering Subgrade Strength through Moisture Adjustment.....	21
3.8 Aggregate Placement and Compaction	21
3.9 Summary.....	24
CHAPTER 4 ACCELERATED TESTING AND PERFORMANCE MONITORING.....	25
4.1 Introduction	25
4.2 Test Section Loading and Performance Monitoring	25
4.3 Effect of Moisture Conditions on Test Section Performance.....	26
4.4 Cell 1: Uncrushed Gravel with High Amounts of Nonplastic Fines	27
4.4.1 Performance Under Near-Optimum Conditions	27
4.4.2 Performance Under Flooded Conditions.....	33
4.5 Cell 2: Crushed Limestone with Low Amounts of Plastic Fines	34
4.5.1 Performance at Near-Optimum Moisture Conditions	34
4.5.2 Performance Under Flooded Conditions.....	38

4.6 Cell 3: Crushed Dolomite with High Amounts of Nonplastic Fines.....	40
4.6.1 Performance Under Near-Optimum Aggregate Moisture Conditions.....	41
4.6.2 Performance Under Flooded Conditions.....	44
4.7 Cell 4: Crushed Limestone with High Amounts of nonplastic Fines.....	45
4.7.1 Performance at Near-Optimum Moisture Conditions	45
4.7.2 Performance Under Flooded Conditions.....	47
4.8 Cell 5: Crushed Limestone with Low Amounts of Plastic Fines	48
4.8.1 Performance at Near-Optimum Moisture Conditions	48
4.8.2 Performance Under Flooded Conditions.....	50
4.9 CELL 6: Large-Size Aggregate Applications for Construction Platforms.....	51
4.9.1 North Wheel Path: Unreinforced	52
4.9.2 South Wheel Path: Geotextile Reinforced	53
4.10 Summary of Test Section Performance	53
CHAPTER 5 DISCUSSION AND RECOMMENDATIONS	55
5.1 Summary of Research Scope	55
5.2 Modification of Design Curve for Aggregate Cover Layer Thickness.....	55
5.3 Recommendations for Modification of IDOT SSM	59
5.3.1 Aggregate Type	59
5.3.2 Compactive Effort	60
5.3.3 Construction Lift Thickness.....	60
5.3.4. Curing Time for Aggregate Layers.....	61
5.3.5 Effects of Moisture Conditions	61
5.3.6 Realistic Construction Traffic Coverage and/or Allowable Rut Depth for Aggregate Construction Platforms.....	61
REFERENCES.....	63
APPENDIX A MECHANISTIC EVALUATION OF PAVEMENT LAYER RESPONSE DURING CONSTRUCTION	A-1
APPENDIX B PROPERTIES OF AGGREGATE MATERIALS USED IN CONSTRUCTION OF FULL-SCALE TEST SECTIONS	B -1
APPENDIX C ACCELERATED PAVEMENT TESTING AND PERFORMANCE MONITORING.....	C-1
APPENDIX D INVESTIGATION OF FREEZE-THAW EFFECTS ON CELL 3.....	D-1
APPENDIX E SURFACE PROFILE MEASUREMENTS DATA.....	E-1

CHAPTER 1 INTRODUCTION

1.1 INTRODUCTION AND BACKGROUND

The current Illinois Department of Transportation (IDOT) Subgrade Stability Manual (SSM) recommends the remedial aggregate thickness above subgrade based on the immediate bearing value (IBV) as a performance index of the subgrade soil (IDOT SSM 2005). The required cover thickness is determined from the subgrade IBV using Figure A-2 in the IDOT SSM (Figure 1.1). However, it is important to note that Figure A-2 of the IDOT SSM does not distinguish between among aggregate types when specifying the required subgrade cover thickness.

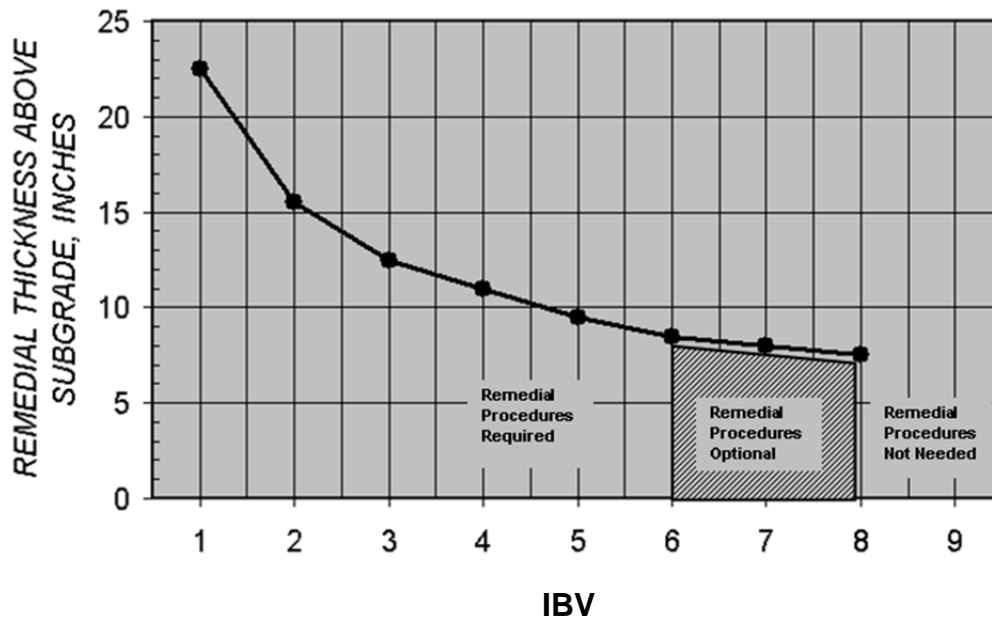


Figure 1.1. IBV-based remedial action (IDOT SSM 2005).

Several researchers have established that unbound aggregate layers perform differently based on the type and quality of aggregate material used (Gray 1962; Barksdale 1972; Allen 1973; Rowshanzamir 1995; Lekarp et al. 2000; van Niekerk 2002). Moreover, Heckel (2009) observed that an 8-in.-thick layer of crushed aggregates performed as well as a 12-in.-thick layer of uncrushed gravel because of better particle interlock and the resulting increase in shear strength in a crushed aggregate layer. Therefore, designing construction platforms without giving adequate consideration to aggregate material type and quality may lead to uneconomical overdesigns or premature failures of pavement working platforms. Heckel (2009) argued that an adjustment in aggregate thickness based on aggregate properties had the potential to save IDOT approximately \$9 million annually.

Accordingly, a recent study titled “Characterization of Illinois Aggregates for Subgrade Replacement and Subbase” was undertaken at the Illinois Center for Transportation (ICT) with an overall objective to develop aggregate thickness correlations with aggregate properties to modify and improve the thickness requirement curve in the IDOT SSM (see Figure 1.1). The scope of the research project comprised laboratory testing of three different aggregate types commonly used in Illinois for construction platform

applications. A factorial laboratory test matrix was developed for both plastic and nonplastic fines (passing through No. 200 sieve, or 0.075 mm) blended in engineered gradations of crushed limestone, crushed dolomite, and uncrushed gravel at 4%, 8%, 12%, and 16% target fines contents. The laboratory tests consisted of standard Proctor moisture density, IBV, imaging-based aggregate shape characterization, rapid shear strength, directional resilient modulus, and permanent deformation tests conducted at different combinations of the aggregate physical properties studied.

On the basis of extensive laboratory testing of the three different aggregate types at different combinations of the physical properties under investigation, the researchers recommended developing a flowchart-based approach for aggregate material selection for construction platform applications. Moreover, based on the laboratory test results, the researchers recommended preliminary correction factors to take into account changes in aggregate material quality (i.e., properties), and accordingly, modify the aggregate cover design thicknesses recommended by the IDOT SSM.

$$H_{\text{corrected}} = H_{\text{SSM}} * C_{\text{fines}} * C_{\text{PI}} * C_{\text{angularity}} * C_{\text{moisture}} * C_{\text{traffic}} \quad (1)$$

where H_{SSM} is the design thickness recommended by Figure A-2 of the IDOT SSM, and C_{fines} , C_{PI} , $C_{\text{angularity}}$, C_{moisture} , and C_{traffic} are correction factors accounting for fines content, plasticity of fines, particle angularity, moisture content, and traffic applications, respectively.

Before implementing any such correction factors into the IDOT SSM, it was important to validate the laboratory test results through accelerated testing of full-scale construction platform test sections. Therefore, with this objective, the second phase of the research study, titled “Field Performance Evaluations of Illinois Aggregates for Subgrade Replacement and Subbase—Phase II” was initiated in January 2010.

1.2 RESEARCH OBJECTIVES

The overall objective of the ICT R27-81 research project was to validate the findings of Phase I of the research study (ICT Project R27-1), “Characterization of Illinois Aggregates for Subgrade Replacement and Subbase.” Apart from the primary objective stated above, several secondary objectives of this research study involved the following:

1. Identify effects of aggregate type and quality on construction platform performance and mechanisms contributing to failure;
2. Develop guidelines for material selection for construction platform applications; and
3. Compare the effectiveness of large-size aggregate materials in construction platform applications over very weak subgrades.

1.3 RESEARCH METHODOLOGY

To achieve the above listed research objectives, full-scale pavement working platform test sections were constructed using different aggregate materials at the University of Illinois Advanced Transportation Research and Engineering Laboratory (ATREL) facility. The test sections were designed for loading to failure using the Accelerated Transportation Loading Assembly (ATLAS). Individual research objectives for the study were accomplished through completion of the following tasks.

1.3.1 Mechanistic Evaluation of Pavement Layer Response During Construction

To adequately design and construct the field sections for accelerated testing, it was important to properly assess the relative performances of different aggregate property combinations from a mechanistic-empirical pavement design perspective. To some degree, this could be accomplished by conducting mechanistic evaluation of the layer response parameters—stresses and strains experienced by the subgrade and the aggregate cover layer, due to the loads imposed by construction equipment. The research work conducted under this task therefore involved conducting mechanistic analyses of typical construction platform sections using the finite element-based pavement analysis program GT-PAVE developed by Tutumluer (1995).

The GT-PAVE axisymmetric finite element (FE) program uses isoparametric 8-node quadrilateral elements to analyze flexible pavement structures consisting of linear or nonlinear elastic layers. Details on the nonlinear solution technique used in GT-PAVE are described elsewhere (Tutumluer 1995; Tutumluer and Barksdale 1995). Unbound aggregate material characterization models developed from the laboratory tests in Phase I of this research study (ICT Project R27-1) were used in the nonlinear FE program GT-PAVE to predict effects of the varying aggregate physical properties on mechanistic response of typical construction platform section. Construction platform sections constructed using different aggregate types on top of weak subgrade layers were analyzed using GT-PAVE to determine critical pavement responses. Subgrade shear strength was characterized by the IBV, which in turn was related to the modulus values by commonly used empirical correlations in Illinois found in IDOT's Bureau of Local Roads & Streets Flexible Pavement Design Guide and given by Garcia and Thompson (2003).

The primary response parameter evaluated from the GT-PAVE analyses was the subgrade deviator stress (σ_{DEV}) used to compute subgrade stress ratio (SSR = subgrade deviator stress σ_{DEV} / unconfined compressive strength Q_u). Similar to the procedure adopted to develop the original IDOT cover thickness determination chart, the maximum SSR values allowed were fixed to 0.75, indicating allowable subgrade shear stress as high as 75% of its shear strength (Thompson et al. 1977). The cover layer thickness for different aggregate types was adjusted to analyze the effects of different aggregate physical properties on subgrade stress levels for typical pavement working platform test sections. Comparison of critical pavement responses for aggregate layers constructed using different quality materials also helped in evaluating the effects of different aggregate physical properties on construction platform performance. For the sake of brevity, detailed findings from this task are presented in Appendix A as a stand-alone technical research publication.

1.3.2 Construction of Test Sections for Field Validation

The second task under the scope of this research study involved construction of full-scale pavement working platform sections for accelerated pavement testing. Six different test "cells" were constructed at the University of Illinois ATREL facility in Rantoul, Illinois. A major advantage of the ATREL location was that it provided a controlled environment to build similar test sections using consistent construction techniques and procedures. The consistency in the constructed test section strength, stiffness, and overall quality was achieved with nuclear gauge moisture-density and dynamic cone penetrometer (DCP) test measurements during and after the construction. DCP tests were used for measuring IBV, and light weight deflectometer (LWD) and soil stiffness gauge (GeoGauge™) tests were used for quantifying achieved modulus properties of the constructed aggregate layers. Such field testing to enforce quality control helped adequately to identify anomalies in construction conditions. Finally, aggregate materials used for constructing the field sections were tested

in the laboratory to characterize their mechanical behavior and evaluate them for strength, modulus, and deformation characteristics.

1.3.3 Accelerated Testing and Performance Monitoring

The main thrust of the field testing effort was to study effects of aggregate angularity, type and amount of fines, and moisture content on pavement working platform performance. The test cells were loaded to failure under unidirectional loading using the University of Illinois ATLAS. A maximum of 1,000 load repetitions of a standard 10-kip wheel loading was sufficient for evaluating the performances of pavement working platform test sections. Each test cell was tested under two different aggregate moisture conditions along two wheel paths separated by a distance of 8 ft. Performances of the test sections under loading were monitored through surface profile measurements as well as transverse scanning using ground-penetrating radar (GPR). Transverse trench sections were excavated after failure of the test sections to distinguish rut accumulations in the aggregate and subgrade layers.

1.3.4 Analysis of Field Section Performance, and Recommendations for Implementation of Research Findings

The final task under the scope of this research study comprised analyses of full-scale test section performances under loading and evaluation of aggregate types, physical properties, and hence, quality on pavement working platform performance. Different mechanisms contributing to failure of the test sections were identified, and the role of aggregate physical properties in governing the failure mechanisms emphasized. The ultimate objective was to check the validity of the preliminary correction factors recommended in Phase I of the project for modifying the design curves for aggregate cover layer thickness in the IDOT SSM. On the basis of combined analyses of laboratory and field test results, several recommendations are made for revision and modification of the IDOT SSM.

1.4 REPORT ORGANIZATION

Chapter 2 of this report presents a summary of different research tasks dedicated to the development and modification of the aggregate cover thickness design curve in the IDOT SSM. Primary findings from Phase I of the research study are presented followed by a summary of the preliminary thickness correction factors recommended based on Phase I laboratory test results.

Chapter 3 includes detailed information on the construction of full-scale pavement working platform sections for accelerated pavement testing. The scientific approach adopted for aggregate material selection used in the construction of the test sections is presented, followed by results from laboratory characterization of the materials. Details on subgrade characterization and moisture-control methods adopted for preparing subgrade layers with controlled strengths are also presented together with detailed information on aggregate placement and compaction.

Observed performance trends of full-scale test sections under loading are presented in Chapter 4. Different mechanisms contributing to the accumulation of rutting are analyzed using surface profile measurements and GPR scans, as well as visual inspection of pavement layer boundaries obtained from excavation of transverse trenches across the wheel paths. Effects of individual aggregate physical properties on rut mechanisms leading to failure of the test sections are also discussed.

Chapter 5 summarizes the main findings of this field study and presents a discussion of performance trends the observed test section, including comparisons of measured rut

depths with the IDOT-specified field rutting threshold value. Applicability and potential problems with the correction-factors approach for modifying the thickness design of construction platforms are discussed, and recommendations are made regarding aggregate material selection, construction practice, and realistic rut depth considerations for inclusion in the IDOT SSM.

CHAPTER 2 SUMMARY OF PAST RESEARCH

2.1 INTRODUCTION

This chapter presents a summary of past research studies on developing and modifying the aggregate cover thickness design curve used by the IDOT SSM.

2.2 PREVIOUS RESEARCH ON IDOT SUBGRADE IMPROVEMENT CURVE

2.2.1. Original Research by Thompson et al.

The IDOT SSM design chart for aggregate cover thickness was originally an outcome of a multi-year study of subgrade stability conducted at the University of Illinois (Thompson et al. 1977). During that study, the researchers conducted stress-dependent finite element analyses of several pavement sections using AREA No. 4 ballast-type granular material over very soft, soft, medium, and stiff subgrades. Up to 5,000 coverages of a 32-kip tandem axle were considered. They recommended a minimum subgrade IBV requirement of 6 to 8 to limit rutting to 0.5 in. or less through the use of tire sinkage criteria and for adequate support for compaction of the overlying layers. The findings from the study were adopted by IDOT and were included in the 1982 IDOT Subgrade Stability Manual (SSM).

2.2.2. Verification Research by Thompson and Tutumluer in 2005

The thicknesses for a selected range of subgrade IBV values were recently validated (Tutumluer et al. 2005) with the ILLI-PAVE finite element analysis computer program (Raad and Figueroa 1980; Thompson and Elliott 1985) used in the development of IDOT's flexible pavement design procedure. For ILLI-PAVE analysis purposes, Tutumluer et al. (2005) represented a 20-kip (88.9-kN) single axle by a 10-kip (44.5-kN) single wheel load at 115-psi (794-kPa) tire pressure. From the analyses, they found that the computed surface deflections indicated good uniformity, and the subgrade deviator stresses predicted were typically less than 75% of the subgrade's unconfined compressive strength for the entire range of evaluated subgrade strengths and unbound aggregate thicknesses. High subgrade deviator stresses (σ_{DEV}) and subgrade stress ratios ($SSR = \sigma_{DEV}/Q_u$ where Q_u is the unconfined compressive strength) indicate high subgrade rutting potentials, and large surface deflections often lead to difficulty in compaction and can even cause tension cracking/tearing on the surface of asphalt concrete layers. From the ILLI-PAVE analyses, the researchers concluded that the current IDOT thickness requirements were reasonable for 10-kip (44.5-kN) wheel loading conditions. However, the analysis results did not distinguish between the types of aggregates used for subgrade replacement and subbase cover purposes.

2.2.3. Test Loop and Field Verification Studies by Heckel

Heckel (2009) evaluated the performance of pavement working platform sections comprising three dense-graded aggregates with varying physical properties compacted to different thicknesses using different methods. Through controlled loading in a test loop, he identified the following three factors as primarily affecting working platform performance: (1) aggregate angularity, fines content, and fines plasticity; (2) aggregate layer compaction; and (3) loading.

From the test loop results, Heckel identified a crushed limestone (CLS) having low-plasticity fines, compacted to at least 95% of the maximum laboratory density as the best

practice, and suggested that this material can be constructed to layer thicknesses lower than those recommended by the SSM. He also observed that for subgrades with IBV of 3 or greater, loading caused little or no permanent deformation in the subgrade, therefore indicating aggregate properties as the primary factors affecting performance. Moreover, Heckel reported significantly poor performance of uncrushed gravel materials when used in construction platform applications and recommended limiting the use of such materials to capping layers over large-size aggregates only.

2.3 ICT PROJECT R-27-1

On the basis of on Heckel's findings (2009) regarding the scope for possible reduction in the aggregate cover layer thickness values currently used by IDOT, a research study titled "Characterization of Illinois Aggregates for Subgrade Replacement and Subbase" was undertaken at the Illinois Center for Transportation (ICT) with an overall objective to develop aggregate thickness correlations with aggregate properties to modify and improve the thickness requirement curve in the IDOT SSM. The scope of the research project comprised laboratory testing of three different aggregate types commonly used in Illinois for construction platform applications. A factorial laboratory test matrix was developed for both plastic and nonplastic fines (passing No. 200 sieve or 0.075 mm) blended in engineered gradations of crushed limestone, crushed dolomite and uncrushed gravel at 4%, 8%, 12%, and 16% target fines contents (Tutumluer et al. 2009). Specimens were prepared in the laboratory at engineered gradations, and tested to evaluate the effects of individual aggregate properties on shear strength, resilient modulus, and permanent deformation behavior.

From the laboratory test results, it was observed that particle shape and angularity played the most important role in governing aggregate behavior irrespective of other physical properties. Crushed aggregates showed consistently higher shear strength, modulus, and lower susceptibility to permanent deformations when compared with the uncrushed gravel. An aggregate matrix comprising crushed particles exhibited higher tolerance to the amount of fines and showed lower moisture sensitivity even at high fines contents. For nonplastic fines, the variation in shear strength (IBV used as shear strength index) with moisture content was erratic and did not indicate any significant trends at low fines contents. However, at higher fines contents, the effect of moisture was significant and caused a rapid reduction in shear strength values. High moisture contents combined with high amounts of plastic fines presented the worst combination and rapidly deteriorated aggregate matrix conditions. The effect of fines type (nonplastic or plastic) was not significant for aggregate matrices comprising low amount of fines. However, as the amount of fines in a matrix was increased, specimens with plastic fines clearly showed poor performance compared with those having nonplastic fines.

Individual effects of the physical properties (test factors) were found to be significantly dependent on other test factor levels. For example, the effect of moisture on aggregate behavior changed significantly depending on the amount of fines in the aggregate matrix. Similarly, the type of fines (plastic or nonplastic) affected aggregate behavior significantly only for materials comprising high amounts of fines.

Permanent deformation test results clearly identified the importance of fines in an aggregate matrix. Crushed aggregate specimens with low fines contents (around 4%) showed unstable behavior compared with the ones having a moderate amount (around 8%) of fines. This behavior was attributed to the higher amount of voids in the aggregate matrix comprising crushed particles. At low fines contents, the aggregate particles moved and reoriented with respect to each other, thus resulting in higher permanent deformations and lower resilient modulus values. As the fines content increased to around 8%, a larger proportion of voids in the aggregate matrix were filled by the fines and a stable matrix

behavior was observed. The uncrushed gravel matrix did not show any such stabilizing behavior because of the low amount of voids in an aggregate matrix comprising uncrushed particles. On the basis of these findings, different threshold values for the allowable fines content in an aggregate material were proposed for crushed and uncrushed aggregates. Moreover, crushed aggregate matrices showed higher tolerance to variations in fines content compared with uncrushed ones.

Slight variations in test factor values did not reflect clearly on the resilient modulus behavior of aggregates. For example, increasing the amount of fines by 4% did not result in significant changes in aggregate modulus values. However, large variations induced in the fines content (increase from 4% to 16%) was often reflected as a significant reduction in resilient modulus values. Crushed aggregates showed consistently higher modulus values compared with uncrushed ones because of better particle-to-particle interlock.

On the basis of the laboratory test results, the researchers recommended developing a flowchart-based approach for aggregate material selection for construction platform applications. Several tentative correction factors (see Table 2.1) were recommended for use alongside the aggregate cover thickness design curve in the IDOT SSM. These tentative correction factors were developed by assuming that Figure A-2 of the IDOT SSM was developed for a crushed aggregate with high amounts of plastic fines at optimum (standard compactive effort) aggregate moisture conditions. Therefore, as shown in Table 2.1 the fourth aggregate type has unity (1.0) values assigned to the correction factors for type and amount of fines, as well as aggregate angularity.

The primary objective of the research study documented in the current report was to validate the laboratory test results from the Phase I study through accelerated loading of full-scale pavement working platform test sections. Through careful comparison of laboratory and field-observed performance trends for aggregates with different physical properties, the current study evaluated the feasibility of using correction factors to modify the aggregate cover thickness design curve in the IDOT SSM.

Table 2.1 Correction Factors Recommended for Use Based on Laboratory Findings

Aggregate Type*	Correction Factors				
	C _{FINES}	C _{PI}	C _{ANG}	C _{MOISTURE**}	C _{TRAFFIC}
Crushed Aggregates with Low Amount of Nonplastic Fines	0.8	0.8	1.0	1.0 (D/O) 1.2 (W)	Will be developed from Field Testing
Crushed Aggregates with Low Amount of Plastic Fines	0.8	0.8	1.0	1.0 (D/O) 1.25 (W)	
Crushed Aggregates with High Amount of Nonplastic Fines	1.0	0.8	1.0	1.0 (D/O) 1.4 (W)	
Crushed Aggregates with High Amount of Plastic Fines	1.0	1.0	1.0	1.0 (D) 1.0 (O) 1.5 (W)	
Uncrushed Aggregates with Low Amount of Nonplastic Fines	0.8	0.8	1.4	1.0 (D/O) 1.2 (W)	
Uncrushed Aggregates with Low Amount of Plastic Fines	0.8	0.8	1.4	1.0 (D/O) 1.2 (W)	
Uncrushed Aggregates with High Amount of Nonplastic Fines	1.0	0.8	1.4	1.0 (D/O) 1.4 (W)	
Uncrushed Aggregates with High Amount of Plastic Fines	1.0	1.0	1.4	1.0 (D) 1.2 (O) 1.5 (W)	

*For crushed aggregates, the amount of fines is defined as low $\leq 8\%$ and high $> 8\%$. For uncrushed aggregates, amount of fines is defined as low $\leq 6\%$ and high $> 6\%$.

** D: Dry of optimum; O: Optimum; W: Wet of optimum.

CHAPTER 3 CONSTRUCTION OF FULL-SCALE TEST SECTIONS

3.1 INTRODUCTION

This chapter describes the material selection and construction of full-scale construction platform sections for accelerated pavement testing. Six different full-scale unsurfaced pavement test cells were constructed over weak subgrades of controlled strength through field IBV checks to evaluate the effects of different aggregate physical properties on performance. Selection of aggregate types representing different combinations of the test factors under investigation is discussed followed by laboratory characterization of individual aggregate materials used for constructing the test sections. Typical characterization and engineering behavior trends observed in the aggregate materials during laboratory experimentation are used later in Chapter 4 to describe the test section performances under loading. Details of the test section layout and construction procedure are presented along with procedures for subgrade soil characterization and test section subgrade preparations for intended IBV levels through moisture addition.

3.2 MECHANISTIC EVALUATION OF PAVEMENT LAYER RESPONSE DURING CONSTRUCTION

To adequately design and construct the field sections for accelerated testing, it was important to first properly assess the relative performances of different aggregate property combinations from a mechanistic-empirical pavement design perspective. Accordingly, mechanistic evaluation of typical pavement working platform sections under loads imposed by construction equipment was conducted using the finite element-based pavement analysis program GT-PAVE developed by Tutumluer (1995).

Unbound aggregate material characterization models developed from the laboratory tests in Phase I of the study were used in GT-PAVE to predict effects of the varying aggregate physical properties on mechanistic response of typical construction platform sections. The primary response parameter analyzed from the GT-PAVE analyses was the subgrade deviator stress (σ_{DEV}) used to compute subgrade stress ratio ($SSR = \text{subgrade deviator stress } \sigma_{DEV} / \text{unconfined compressive strength } Q_u$). For sake brevity, detailed findings from this task are presented in Appendix A of this report in the form of a stand-alone technical research publication; a summary of important findings is presented below.

From analyses of more than 200 sections comprising aggregate layers at different combinations of the test factors, it was concluded that the effect of aggregate type and quality on SSR values for a given aggregate layer thickness was not significant. However, as observed from the laboratory tests in Phase I of the research study, aggregate permanent deformation trends were significantly different at different test factor combinations. Analyses of pavement working platform sections consisting of 14-in, 12-in, and 8-in.-thick aggregate layers constructed over a subgrade of $IBV = 3\%$ showed that the SSR values corresponding to 14-in.- and 12-in.-thick aggregate layers ranged between 0.5-0.7. Therefore, with subgrade vertical stress (σ_{DEV}) levels ranging from 50-70% of the subgrade, the unconfined compressive strength these sections should resist excessive rutting from subgrade shear irrespective of the type and quality of aggregate used. The SSR values corresponding to 8-in.-thick aggregate layers were consistently greater than 1 ($\sigma_{DEV} > Q_u$) indicating subgrade shear failure.

Mechanistic analyses of typical construction platform section showed that the effect of aggregate type and quality on subgrade rutting potential was not significant. However, laboratory test results in Phase I of the research study showed a significant effect of aggregate physical properties on permanent deformation behavior. Therefore, combined inspection of these results indicated the existence of two different mechanisms, namely, subgrade deformation and aggregate shear failure contributing to the accumulation of rutting in pavement working platforms. These hypotheses were subsequently verified through careful design, construction and accelerated testing of full-scale pavement working platform test sections. Detailed results from mechanistic analyses are presented in Appendix A.

3.3 EXPERIMENTAL DESIGN THROUGH MATERIAL SELECTION

To validate the laboratory test results reported in Phase I of the research study, full-scale pavement working platform test sections were constructed with various aggregate types representing different combinations of aggregate physical properties over weak subgrades of controlled strength. As already mentioned in Chapter 1, the different aggregate physical properties (test factors) selected for investigation in this research project were (1) particle shape, texture, and angularity; (2) fines content (defined as percent by weight material passing No. 200 sieve or finer than 0.075 mm); (3) plasticity of fines (measured on material finer than 0.425 mm); and (4) compaction (moisture-density) conditions.

The number of full-scale pavement test sections needed for a complete factorial evaluation of the aggregate properties of interest was not feasible as far as space requirements and construction costs were concerned. It was therefore decided to construct a limited number of full-scale test sections using aggregate materials representing extreme boundaries of the test factors. For example, as observed from Phase I research findings (Tutumluer et al. 2009), the effect of fines content on aggregate behavior was significant only when two aggregate types representing the lowest and highest practical levels of the fines contents found in quarry sources were compared. Likewise, the observed behavior trends of crushed limestone and dolomite were similar and showed a significant difference only when compared with uncrushed gravel. Therefore, small differences in aggregate shape, texture and angularity characteristics, for example, limestone showed only slightly higher angularity and surface texture properties, were not clearly reflected from the strength, permanent deformation, and resilient modulus test results. Moreover, the effect of moisture on aggregate behavior was apparent only when moisture contents of the samples increased significantly toward the wet side of optimum. On the basis of the above observations, the following material types were selected for constructing the full-scale test sections.

- Material No. 1: Uncrushed gravel with high amounts of nonplastic fines
- Material No. 2: Crushed limestone with high amounts of plastic fines
- Material No. 3: Crushed dolomite with high amounts of nonplastic fines
- Material No. 4: Crushed limestone with low amounts of nonplastic fines

The above four material types were selected to ensure comparison of the following material pairs to evaluate the effects of individual test factors on performance. The effect of aggregate angularity could be studied through a comparison of materials 1 with 2 and/or 3. The effect of fines content could be studied by comparing materials 3 and 4 (note that the Phase I research found similar behavior for crushed limestone and dolomite). The effect of plasticity of fines could be studied by comparing materials 2 and 3. Finally, the effect of moisture on aggregate behavior could be evaluated by testing each of the four materials under two different aggregate moisture conditions, i.e., optimum or near-optimum and wet upon flooding the test section.

3.4 LABORATORY CHARACTERIZATION OF AGGREGATES

On the basis of a preliminary survey of potential aggregate sources around the state of Illinois, the four material types listed above were identified, and obtained for laboratory characterization and field construction. Upon receiving the materials from the respective sources, the first task involved in-depth laboratory characterization of each aggregate type for physical and mechanical characterization. Preliminary tests were conducted on each material type to determine its particle size distribution (AASHTO T 11), Atterberg limits (ASTM D 4318), compaction characteristics (ASTM D 698, ASTM D 1557), and unsoaked CBR (ASTM D 1883). Repeated load triaxial (RLT) tests were conducted following the AASHTO T 307 test protocol to characterize the permanent deformation and resilient modulus behavior. Findings from laboratory testing of the four aggregate materials are reported in the following sections along with figures highlighting important trends.

3.4.1 Particle Size Distribution and Atterberg Limits

Washed sieve analysis (AASHTO T 11) and Atterberg limit (ASTM D4318) tests were first conducted on the four aggregate materials and a summary of the results is provided in Table 3.1.

Table 3.1. Summary of Aggregate Properties

Material Number	Material Description	Fines Content (%) (samples 1 & 2)	Plasticity Index (%)
1	Uncrushed Gravel	11.7 & 12.0	0.0
2	Crushed Limestone	5.0 & 5.3	5.7
3	Crushed Dolomite	11.5 & 14.0	0.0
4	Crushed Limestone	9.0 & 10.9	0.2

The most significant difference between quarry-reported and actual fines contents was observed for material 2, which had significantly lower fines (5.2%) compared with the initially reported value (~12%). Moreover, material 4 had approximately 10% fines, which was higher than the threshold value of 8% recommended from Phase I of the research study (Tutumluer et al. 2009), as well as other researchers (Gray 1962; Seyhan and Tutumluer 2002) as the boundary to separate high fines from low fines for crushed aggregates. It was therefore decided to categorize materials 2 and 4 as low fines and high fines, respectively. Table 3.2 lists the final designations of the materials used in construction of the test sections. Note that the as-constructed designations for materials 2 and 4 listed in Table 3.2 are different from those originally identified in Section 3.2.

Because of the difference in material classification of the actual aggregates used in construction from those listed in Section 3.2, the effect of aggregate angularity was now evaluated through comparison of materials 1 and 3. Materials 3 and 4 were both classified as high fines; therefore, any difference in aggregate behavior would be attributed to the slight difference (~2%) in fines contents. Material 2 (crushed limestone with ~5% fines) was the only aggregate material received with plastic fines (PI = 5.7). However, as observed from laboratory testing of aggregates during Phase I of the research project, the effect of plasticity of fines on crushed aggregate behavior was significant only at high fines contents; crushed aggregate specimens with nonplastic and plastic fines showed similar behavior at fines contents below 8%. Therefore, it would appear that the low amount of plastic fines would not have a significant effect on the performance of material 2, crushed limestone). Therefore, no two material types used for constructing the full-scale test sections could be compared to assess the effect of plasticity of fines on pavement performance.

Table 3.2. Aggregate Designations Identified in the Field Study Test Matrix

Material Number	Aggregate Designation
1	Uncrushed Gravel with High Amounts of Nonplastic Fines
2	Crushed Limestone with Low Amounts of Plastic Fines
3	Crushed Dolomite with High Amounts of Nonplastic Fines
4	Crushed Limestone with High Amounts of Nonplastic Fines

3.4.2 Compaction Characteristics and IBV

The four aggregate types were tested in the laboratory for compaction characteristics using both standard (ASTM D 698) and modified (ASTM D 1557) compactive efforts. A summary of the laboratory-determined optimum moisture content (OMC) and maximum dry density (MDD) values using the two compactive efforts is provided in Table 3.3. After compaction, each specimen was penetrated by a circular plunger of 3 in² area at a rate of 0.05 in./min to determine the IBV values. Individual curves showing the variation of dry density and IBV with moisture content are presented in Appendix B.

Table 3.3. Compaction Characteristics of Aggregates Used for Constructing Full-Scale Test Sections

Material Number	Standard Compaction		Modified Compaction	
	OMC (%)	MDD (pcf)	OMC (%)	MDD (pcf)
1	8.6	136.4	8.2	140.3
2	6.5	115.4	7.3	136.8
3	7.7	141.5	5.5	142.9
4	8.1	140.9	5.7	143.6

From Table 3.3, the OMC from modified compaction for material 2 (crushed limestone with low fines) was higher than that from the standard compaction (7.3% compared with 6.5%). This contradicted commonly observed trends for compaction curves that show a decrease in OMC with increased compactive effort. This discrepancy was primarily attributed to the low fines content (~5%) in the material, which resulted in a free-draining aggregate matrix not capable of retaining moisture. Therefore, obtaining consistent compaction curves for this material was not possible, and the OMC and MDD values were determined from the best possible smooth curve joining individual data points. At this time, it is important to emphasize the inadequacy of the commonly used drop-hammer methods for establishing the compaction characteristics of open-graded and uniformly graded materials.

Two important observations can be made from Figure 3.1, which shows the change in IBV values of the four aggregate materials with moisture content under standard compaction conditions. Firstly, the IBV for the uncrushed gravel with 12% fines (material 1) decreased rapidly with an increase in moisture content even on the dry side of OMC. This reinforced findings from the laboratory tests reported in Phase I regarding the high moisture sensitivities of uncrushed aggregates with high fines. Secondly, material 2 (crushed limestone with 5% fines) did not show any significant change in IBV with increasing moisture content. This was attributed to the free-draining nature of the material, and will be referred to later in Chapter 4 when analyzing the effect of flooding on the performance trends of full-scale test sections constructed using this material. Moreover, the lack of fines in material 2 resulted in an unstable aggregate matrix under standard compaction conditions. This was clearly apparent from the low IBV (14-19%) as shown in Figure 3.1.

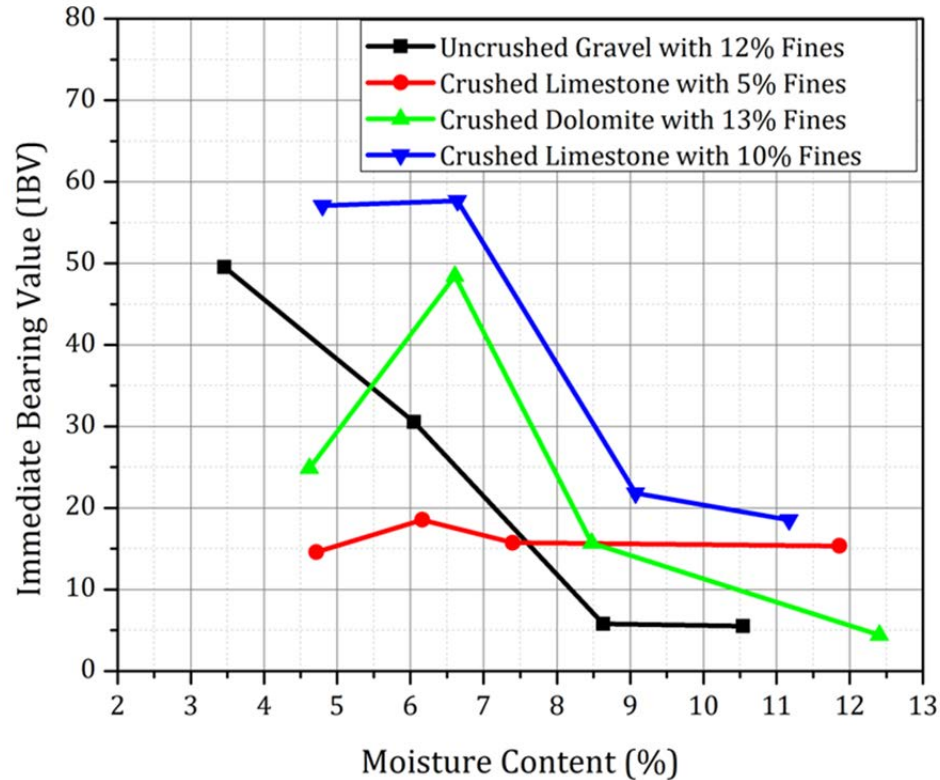


Figure 3.1. Variations in immediate bearing values (IBV) for the four aggregate materials under standard compaction conditions.

3.4.3 Resilient Modulus and Permanent Deformation Characteristics

The effect of aggregate material quality on resilient modulus and permanent deformation behavior was studied by conducting repeated load triaxial tests on each of the four aggregate materials under both standard and modified compaction conditions. Cylindrical triaxial specimens (6 in. diameter, 6 in. height) were prepared at the OMC and MDD values listed in Table 3.3, and were tested using the University of Illinois FastCell for permanent deformation and resilient modulus characteristics. The first 1,000 cycles (conditioning phase) of the resilient modulus test (AASHTO T 307) were used as an indicator of the permanent deformation susceptibility of the material. Resilient modulus tests were subsequently conducted on the specimens through pulsed load application at 15 different stress states specified in the AASHTO T 307 protocol.

Materials 1 and 2 (uncrushed gravel with high fines, and crushed limestone with low fines) both exhibited unstable matrix behavior under standard compaction conditions, and they sustained excessive deformations under a seating stress of 0.3 psi (2.1 kPa). Therefore, the permanent deformation and resilient modulus behavior of these two materials could not be characterized under standard compaction OMC and MDD conditions. However, specimens prepared with materials 3 and 4 showed stable behaviors even under standard compaction OMC and MDD conditions and were tested for permanent deformation and resilient modulus characteristics. The permanent deformation and resilient modulus trends for materials 3 and 4 are compared in Figures 3.2 and 3.3, respectively. As shown in Figure 3.2, material 3 showed higher accumulation of permanent deformation under standard compaction conditions compared with material 4. This was attributed to the higher fines content in the material 3 (13%) compared with material 4 (10%). Similarly, material 4

showed higher modulus values compared with material 3, as a result of a lower amount of fines in the matrix (see Figure 3.3).

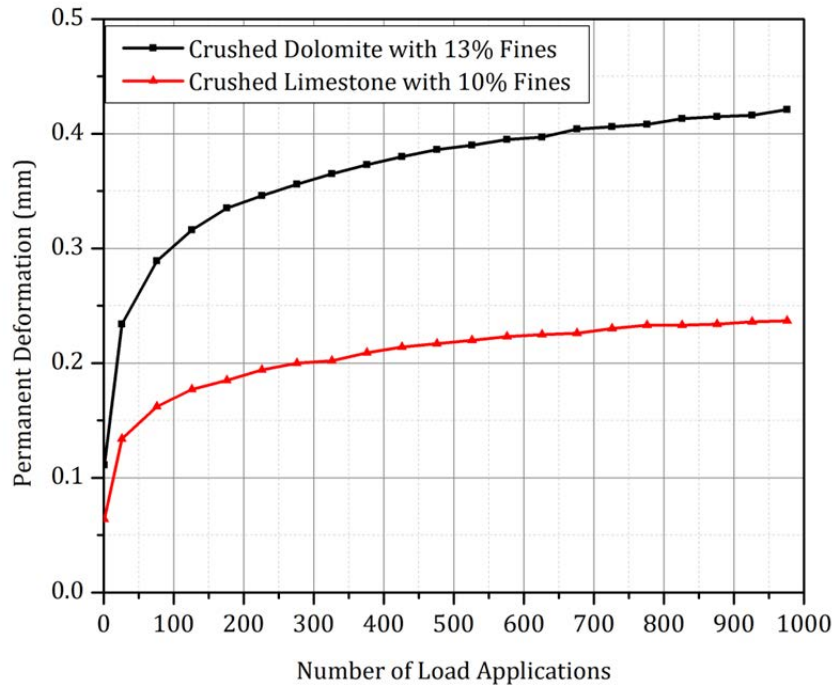


Figure 3.2. Effect of material quality on permanent deformation behavior under standard compactive effort OMC and MDD conditions.

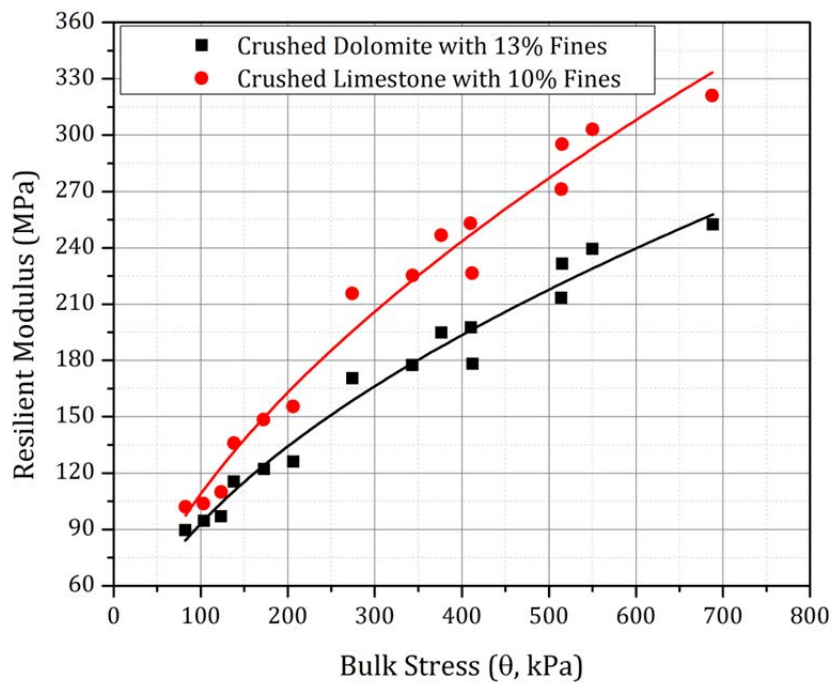


Figure 3.3. Effect of material quality on resilient modulus behavior at standard compactive effort OMC and MDD.

The effect of aggregate quality on modulus and deformation characteristics was further investigated by testing specimens compacted to modified compactive effort OMC and MDD values. Figure 3.4a shows the permanent deformation trends in the four aggregate types as determined from the conditioning phase of AASHTO T 307 resilient modulus test protocol. From the figure, it is clearly apparent that the uncrushed gravel with 12% fines (material 1) showed significantly higher permanent deformation accumulation compared with the crushed aggregates (materials 2, 3 and 4). This was consistent with the findings from Phase I research study. Figure 3.4b shows the non-stabilizing behavior (non-decreasing permanent strain rates) of the uncrushed gravel material even after the accumulation of high permanent strain values.

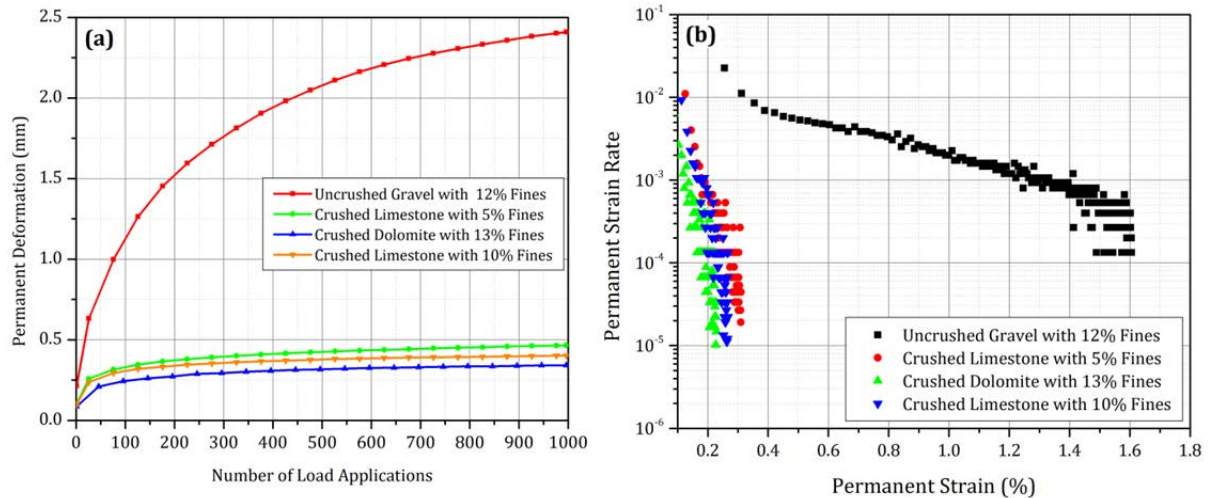


Figure 3.4. Permanent deformation trends for different aggregate types under modified compactive effort OMC and MDD.

It is important to note from Figure 3.4 that material 2 showed similar permanent deformation values as the other two crushed aggregate types (materials 3 and 4). Although material 2 included moderately plastic fines ($PI = 5.7$), the effect of plasticity of fines on aggregate behavior was not significant at such low (5.2%) fines contents. However, owing to the lack of fines, material 2 showed unstable matrix behavior under standard compaction conditions. This observation will be used later in Chapter 4 to explain the recorded performances of test sections constructed using this material.

Although materials 3 and 4 both possessed high amount of fines (13% and 10%, respectively), neither one showed progressive collapse during the permanent deformation testing as a result of low OMC values corresponding to the modified compactive effort. As observed from the laboratory test results in Phase I of the research study, at high fines contents, amount of moisture plays a critical role in governing aggregate behavior. In wet of optimum conditions, the fines and moisture combined to form a slurry that reduced the particle interlock significantly leading to rapid accumulation of permanent deformation.

Figure 3.5 compares the resilient modulus properties of the four aggregate materials for different applied bulk stresses ($\theta = \sigma_1 + \sigma_2 + \sigma_3$) determined under OMC and MDD conditions corresponding to the modified compactive efforts. The consistently higher moduli values for crushed aggregates (materials 2, 3 and 4) compared with the uncrushed gravel (material 1) are clearly apparent from Figure 3.5 (Note that similar trends were reported in the literature by Hicks and Monismith, 1971). Moduli values for materials 1 and 3 can be directly compared to assess aggregate angularity effects on stiffness characteristics of

unbound granular layers. Similarly, the effect of fines content on resilient modulus can be studied by close inspection of materials 2, 3 and 4. A direct comparison of materials 3 and 4 highlights the detrimental effect of excessive fines on resilient modulus behavior (reflected by lower moduli for material 3). The excess fines in material 3 resulted in the lower resilient modulus values when compared with those of materials 2 and 4. This is in agreement with findings by Jorenby and Hicks (1986), who observed that well-graded aggregates exhibited high resilient modulus values up to the point where the fines content of the mixture displaced the coarse particles and the properties of the fines dominated. Although material 2 showed unstable matrix behavior under standard compaction conditions, its performance at modified compaction was significantly better (higher modulus values than material 3) as a result of increased particle interlock. Material 4 contained 10% fines and showed slightly higher moduli values than material 2. However, the changes in modulus values were insignificant as the fines content increased from ~5% (material 2) to 10% (material 4).

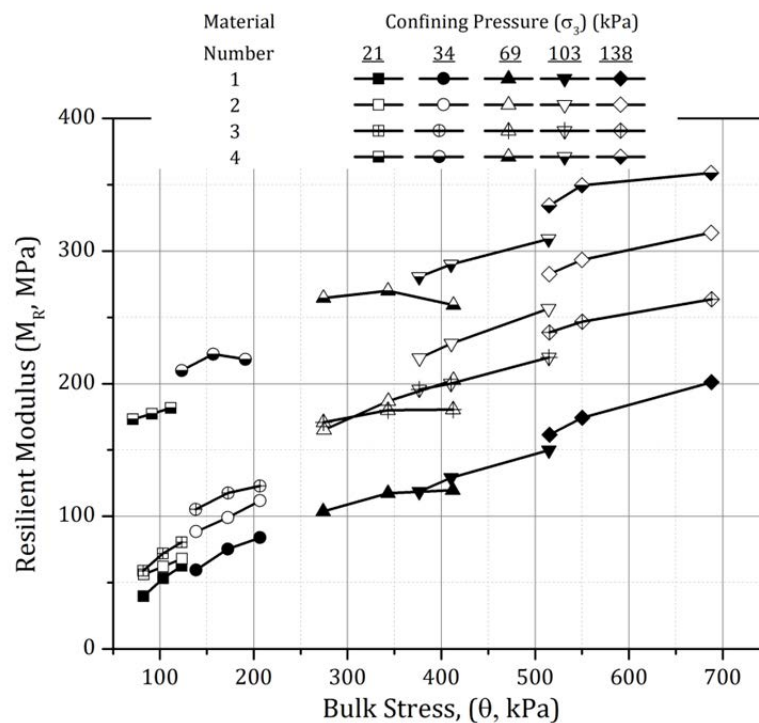


Figure 3.5. Resilient modulus trends for different aggregate types under modified compactive effort OMC and MDD conditions.

3.4.4 Summary of Findings from Laboratory Characterization of Aggregates

The four aggregate types received for use in construction of the full-scale test sections were characterized in the laboratory for strength, permanent deformation, and resilient modulus behavior. The uncrushed gravel with high fines (material 1) showed very high moisture sensitivity, whereas the crushed limestone with low fines (material 2) did not show any moisture sensitivity because it was a free-draining, open-graded matrix. Under standard compaction conditions, both materials showed unstable matrix behavior and therefore could not be tested for permanent deformation and resilient modulus characteristics. Modified compactive effort was therefore used to compare the mechanical behavior of the four aggregate types and establish links with material quality aspects.

The uncrushed gravel material showed significantly higher permanent deformation and lower resilient modulus values, compared with the three crushed aggregates. Although the crushed limestone with low fines (material 2) showed unstable behavior under standard compaction conditions, it showed significantly better performance under modified compactive effort. The crushed dolomite with 13% nonplastic fines (material 3) showed the lowest resilient modulus among the crushed aggregates. This was attributed to the stress-softening nature of the high amount of fines in the aggregate matrix. The high amount of fines in material 3, combined with high moisture contents resulted in higher permanent deformation and lower resilient modulus values compared with material 4 under standard compaction conditions. These laboratory test results will be used in Chapter 4 to explain performance trends observed under loading for the full-scale construction platform test sections.

3.5 LAYOUT AND CROSS-SECTIONAL PROFILE OF FULL-SCALE TEST SECTIONS

Six test cells (numbered 1 through 6) were constructed along three longitudinal test strips using the four aggregate types listed in Table 3.2 to evaluate the effect of aggregate type and quality on construction platform performance. Cells 1 through 4 were constructed with the four selected aggregate materials (material numbers 1 through 4, respectively, as listed in Table 3.2) over a weak subgrade of IBV = 3%. Identical subgrade conditions and aggregate layer thicknesses ensured differences in pavement performance to be directly linked to differences in aggregate quality. Cell 5 was constructed using material 2 (same as Cell 2) over a stronger subgrade of IBV = 6%. The main purpose was to evaluate the effect of subgrade strength on working platform performance and mechanisms contributing to rut accumulation. Cell 6 was constructed over a subgrade of IBV = 1% by first placing a 12-in.-thick layer of large-size aggregates, which was subsequently capped by a 6-in.-thick layer of IDOT CA-6 dense-graded aggregate (material 2 used for capping).

Figure 3.6 shows the layout of the test cells along the three longitudinal strips 237.5 ft (72.4 m) long and 18 ft (5.5-m) wide, separated by 12-ft (3.7-m) wide access roads for construction equipment operation. Longitudinal edge drains were constructed along the north side of each cell and were connected to transverse drains near the west end of the cell. The edge drains sloped from east to west, and the discharge was carried by the long transverse drain along the west boundary to a sump pit. Water was continually pumped out from the sump pit to prevent accumulation of water in the drain pipes.

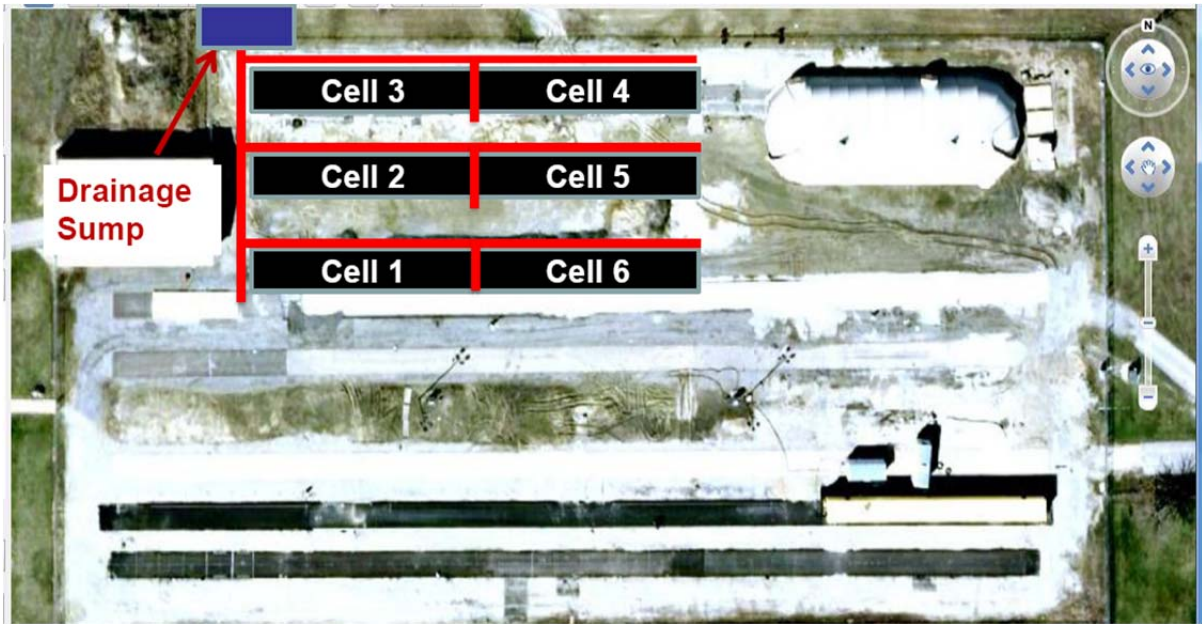


Figure 3.6. Aerial view of test section layout.

Figure 3.7 presents the plan view (on top) and cross-sectional details of a representative test cell constructed over a subgrade of $IBV = 3\%$ (same configuration for Cells 1 through 4). Each test cell constructed was 130-ft (39.6-m) long and comprised three test sections with aggregate layers of thicknesses 14 in. (356 mm), 12 in. (305 mm), and 8 in. (203 mm), respectively. Each cell was separated from the adjacent cell (longitudinally) by a 22.5-ft (6.9-m) long transition section for placement of the ATLAS tracks. From west to east, the 14-in. (356-mm) thick aggregate section was named Section 1, whereas the 8-in. (203-mm) thick aggregate section was named Section 3 consistently. Each section was 15-ft (4.6-m) long and was separated from adjacent sections by 10-ft (3.1-m) long transition zones. At either end of the cell, 10-ft (3.1-m) long speed stabilization zones were constructed to ensure uniform speed of loading on each section. As already mentioned, Cell 5 was constructed over a subgrade of $IBV = 6\%$; therefore, the aggregate layer thicknesses for the three sections were 10, 8, and 6 in. (254, 203, and 152 mm), respectively. The three sections for Cell 6 were constructed to similar thicknesses, using different large-size aggregate materials.

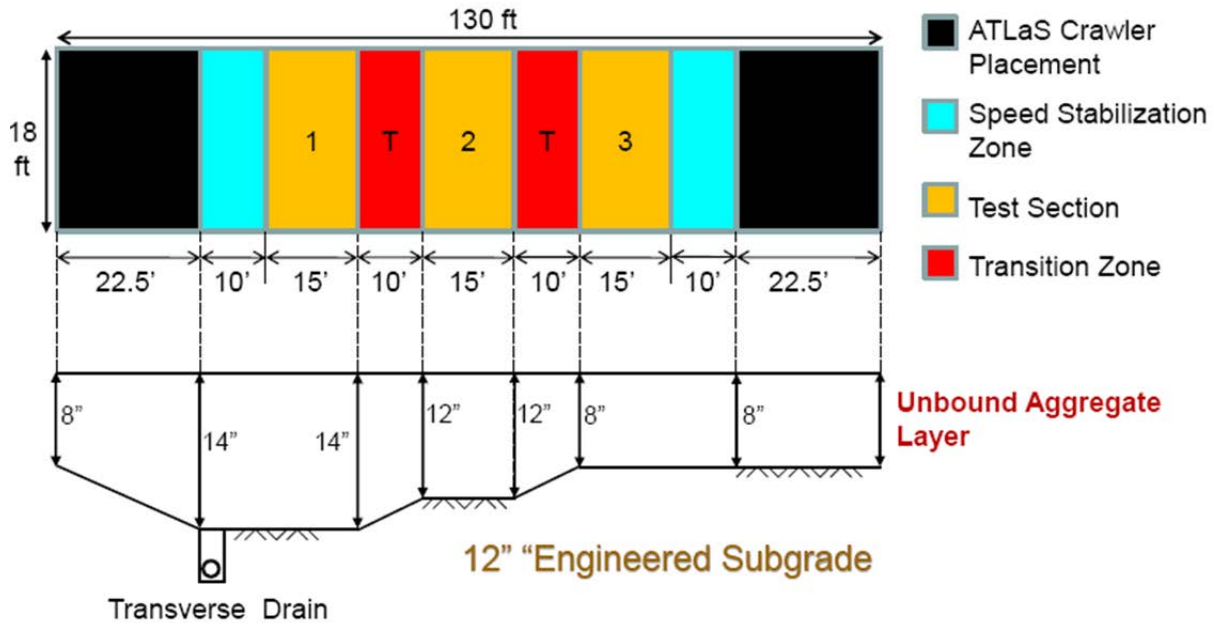


Figure 3.7. Plan view (on top) and cross-sectional details of representative full-scale pavement test sections.

3.6 SUBGRADE CHARACTERIZATION

The first step in construction of the full-scale test sections involved laboratory characterization of the subgrade soil to quantify the change in IBV with moisture content, and ultimately determine the target moisture content in the field to achieve an engineered subgrade of desired IBV. This was particularly important as the primary objective was to evaluate the effects of aggregate physical properties on pavement working platform performance over a uniformly weak, prepared subgrade. This would be possible only by eliminating subgrade variability to the maximum possible extent. Twelve boreholes, each 48 in. (1.2 m) deep, were excavated covering the entire area of the test strips, and soil samples were collected using plastic bags at 6-in. (15-cm) intervals to assess variability in the subgrade profile.

Visual classifications of the soil samples were first conducted, and four sub-groups were developed by merging samples with similar color, texture, and odor. Later, each sub-group was classified in the laboratory following the Unified as well as AASHTO classification methods. Several laboratory tests were then conducted to characterize the physical and mechanical behavior of individual sub-groups. All four sub-groups were classified as low-plasticity clayey silt (CL-ML) following the Unified classification system. Table 3.4 summarizes the soil classification, Atterberg limits, and moisture-density characteristics of the individual sub-groups under standard compaction conditions.

Table 3.4. Laboratory Classification of Preliminary Subgrade Soil Groups Identified

Physical Property	Group 1	Group 2	Group 3	Group 4
Unified Classification	CL-ML	CL-ML	CL-ML	CL-ML
AASHTO Classification	A-4	A-4	A-4	A-4
Liquid Limit (%)	21	22	20	22
Plasticity Index (%)	6.0	7.0	5.0	6.0
Optimum Moisture Content (%)	10.5	10.5	10.2	11.6
Maximum Dry Density (pcf)	124.5	123.6	126.6	119.7

Because they had similar physical and mechanical characteristics, the four subgroups were merged, and a representative group (Group 3) was used as the reference for moisture adjustment during the field construction. The selection of Group 3 as the representative soil group was primarily based on the relative frequency of collected soil samples belonging to this group. Figure 3.8 shows the moisture-density and IBV characteristics of the representative soil group as determined in the laboratory.

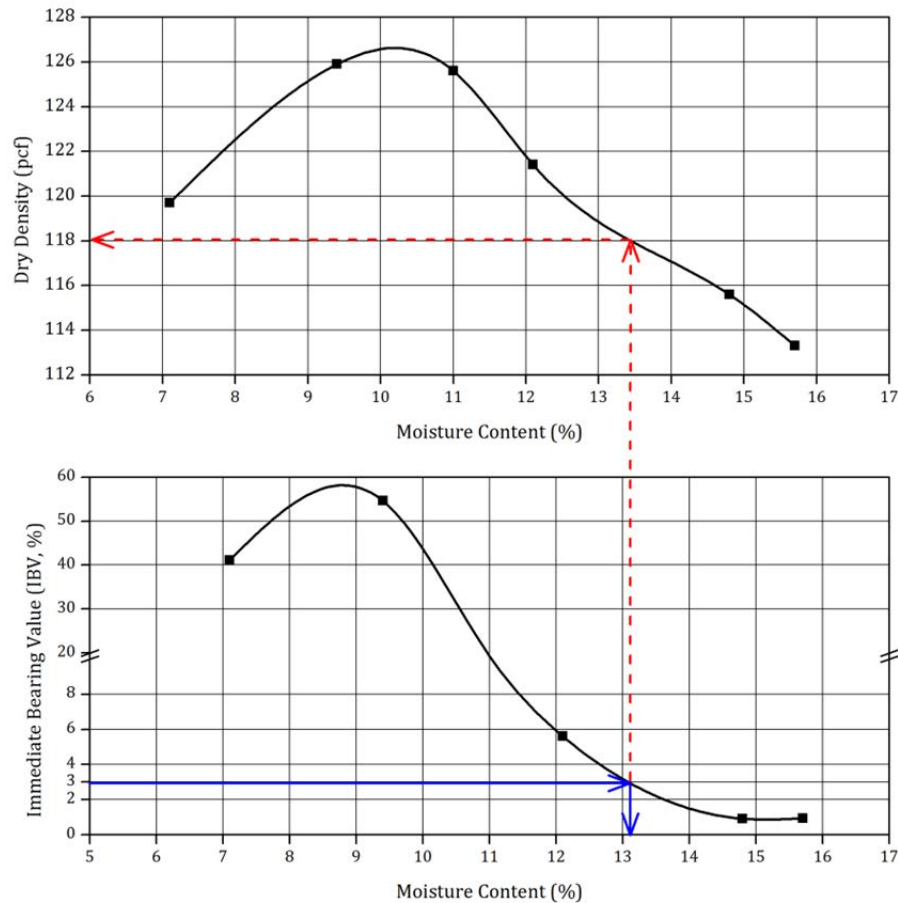


Figure 3.8. Subgrade moisture-density and IBV characteristics (with IBV = 3 Conditions highlighted).

3.7 ENGINEERING SUBGRADE STRENGTH THROUGH MOISTURE ADJUSTMENT

Because the goal was to evaluate unsurfaced pavement performance over weak subgrades, the top 12 in. (305 mm) of the subgrade layer was engineered through tilling and moisture addition to achieve a uniform IBV of 3% (6% for Cell 5, and 1% for Cell 6). The moisture content corresponding to the target IBV (as illustrated in Figure 3.8 for IBV = 3%) was used as a starting point to determine the quantity of water to be added to the test cells. In-place IBV profile was determined using the empirical relationship proposed by Kleyn et al. (Kleyn et al. 1982) to correlate the IBV with the penetration rate of a dynamic cone penetrometer (DCP).

$$\text{LOG}(CBR) = 0.84 - 1.26 \times \text{Log}(PR) \quad (3.1)$$

where PR is the DCP penetration rate (in. /blow).

This procedure was repeated until the in-place IBV for the top 12 in. (305 mm) of the subgrade (as determined from Equation 3.1) was reasonably close to the target value. Figure 3.9 shows the process of subgrade tilling, moisture addition, compaction, and DCP testing on the engineered subgrade layer. Figure 3.10 shows an example in-place subgrade IBV profile determined from DCP testing, for a test cell subgrade of target IBV = 3%. As seen from Figure 3.10, the subgrade tilling and moisture addition proved to be an effective procedure for achieving a uniform subgrade of controlled IBV.

After final compaction of the layer, uniformity of subgrade compaction was verified using different devices such as the Dynatest[®] Light Weight Deflectometer (LWD) and Humboldt[®] Soil Stiffness Gauge (GeoGauge[™]), as well as a Troxler[®] Nuclear Density Gauge. Details on operation of this equipment and important test results have been presented elsewhere (Mishra 2011).

3.8 AGGREGATE PLACEMENT AND COMPACTION

After engineering the subgrade to the target IBV, aggregate layers were constructed by placing the material in two lifts and targeting a relative compaction of 95% with respect to the MDD values determined under standard compaction conditions. Compaction of each layer was checked using a nuclear gauge, and moisture was added to the aggregate as necessary, to aid the compaction process. Owing to weak subgrade conditions, it was not always possible to achieve the target value of 95% relative compaction. In such cases, the compaction process was continued until no significant increase in density was noticed from three consecutive passes of a vibratory compactor. A summary of the as-constructed moisture contents and dry densities of compacted aggregate layers, determined from nuclear gauge testing, is given in Table 3.5. Figure 3.11 shows the achieved relative compaction values for individual test sections in Cells 1 through 5. All test sections in Cells 1, 2, and 5 could achieve relative compaction levels of 95%, whereas those in Cells 3 and 4 showed lower achieved compaction levels. This could have been a result of the significantly lower in-place moisture contents for Cells 3 and 4 (see Table 3.5) compared with the laboratory-determined OMC values (presented in Table 3.3). Compaction of the capping (CA-6) layer in Cell 6 was carried out following IDOT subbase Type B material specifications (compacted to the satisfaction of the engineer). The achieved in-place moisture and density of the capping layer are listed in Table 3.5.



(a)



(b)



(c)



(d)

Figure 3.9. (a) Subgrade tilling, (b) wetting, (c) compaction, and (d) field IBV measurement.

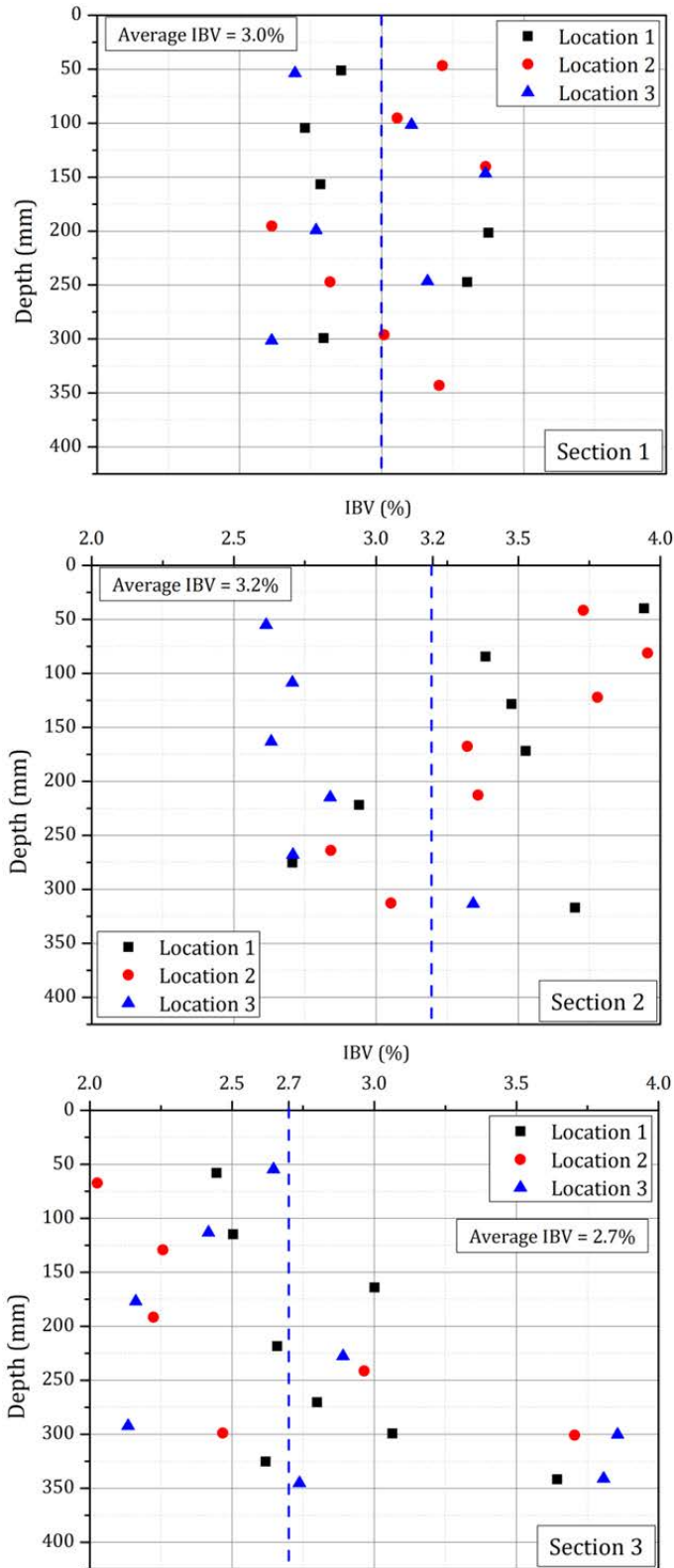


Figure 3.10. Example of in-place subgrade IBV profile determined from DCP testing for a test cell with target IBV = 3%.

Table 3.5. In-Place Achieved Moisture-Density Values for Compacted Aggregate Layers

Cell Number	Moisture Content (%)			Dry Density (pcf)		
	Section 1	Section 2	Section 3	Section 1	Section 2	Section 3
1	7.6	7.3	6.9	129.7	129.3	131.2
2	3.6	3.5	3.0	119.9	122.9	125.5
3	6.1	6.1	5.8	129.8	126.3	129.7
4	3.6	4.2	4.1	127.4	129.8	132.4
5	3.6	4.0	3.6	124.7	129.2	124.1
6	2.6	2.9	2.6	120.3	112.4	117.4

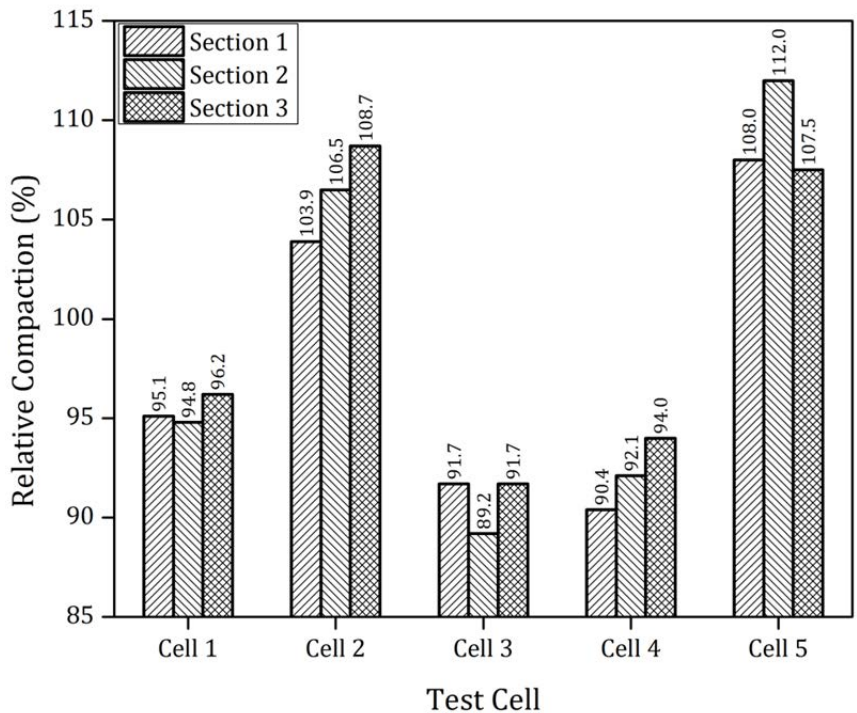


Figure 3.11. Relative compaction (ASTM D 698) levels achieved for aggregate sections.

3.9 SUMMARY

This chapter summarized the construction of full-scale construction platform test sections for accelerated pavement testing. Selection of aggregate materials for constructing the test sections was described, followed by laboratory characterization of the selected materials. Two of the aggregate materials (materials 2 and 4) comprised different amounts of fines when compared with the initially reported values from the aggregate sources. This resulted in a modification of the originally planned material comparisons to evaluate the effects of individual test factors. Results from repeated load triaxial testing of the aggregates were presented and will be used later in Chapter 4 to explain observed trends in test section performance under loading. Finally, this chapter presented details on the subgrade characterization, moisture control, and aggregate placement for construction of the full-scale pavement working platform test sections.

CHAPTER 4 ACCELERATED TESTING AND PERFORMANCE MONITORING

4.1 INTRODUCTION

This chapter presents findings from the accelerated pavement testing and performance monitoring of full-scale pavement working platform test sections. As discussed in Chapter 3, six different full-scale construction platform test cells were constructed at the University of Illinois ATREL facility representing different combinations of the aggregate material quality and subgrade strength. The test sections were subsequently loaded using an Accelerated Transportation Loading Assembly (ATLAS) to apply channelized traffic and simulate the movement of heavy trucks and construction vehicles. Rut accumulation in the pavement sections under loading was monitored through surface profile measurements, as well as ground-penetrating radar (GPR) scanning. After loading the test sections to failure, transverse trench sections were excavated across the wheel paths to obtain visual confirmation of the rut accumulation in aggregate and subgrade layers. Effects of different aggregate physical properties on the performance of construction platform test sections were then evaluated through analyses of different mechanisms contributing to failure.

4.2 TEST SECTION LOADING AND PERFORMANCE MONITORING

Design and construction of the full-scale unsurfaced pavement test cells representing different combinations of aggregate physical properties was presented in Chapter 3. Each test cell comprised three sections, numbered from west to east in an increasing order, Sections 1, 2, and 3, respectively. For Cells 1 through 5, the three different sections were characterized by different aggregate layer thicknesses constructed over a subgrade of controlled IBV. However, for Cell 6, the three sections were constructed to equal thicknesses using three different large-size aggregate materials. After construction, the test sections were loaded to failure by applying a 10-kip (44.5-kN) wheel load through a super-single tire (455/55R22.5) at a tire pressure of 110 psi (758 kPa). The tire nomenclature denotes its dimensions and type in the form of AAA/BBXCC.C, where the first number (455) is the tire width from wall-to-wall in mm; the second number (55) is the side wall height given as a percentage of the tire width (250 mm for the tire in consideration); the letter 'R' indicates a radial tire; and the third number (22.5) is the rim diameter in inches.

The development of rutting with load application for each test section was monitored through surface profile measurements using a digital caliper. Average surface profile for each test section was calculated using two measurements separated by a distance of 5 ft (152 cm), located 5-ft (152-cm) away from the section boundaries on either side. Since the profile of a pavement working platform is much more variable compared with that of a pavement with a bound surface layer, it was important to take several adjacent measurements to develop the average surface profile around a particular point. The surface profile was measured for a distance of up to 4 ft (1.2 m) on either side of wheel path centerline.

Rut depths were calculated through subtraction of the original constructed pavement profile (corresponding to zero load application) from the deformed profiles at different stages of loading. Rut depth in this research project was defined as the deflection of any point on the pavement surface from its original profile. Therefore, points adjacent to the wheel path undergoing upward heaving were represented by negative rut depths indicating the heave amounts. Trafficking of the test sections was continued up to a total rut depth of approximately 4 in. (102 mm) in most cases since the ATLAS wheel could tolerate a

maximum vertical movement of up to 4 in. (102 mm) into the rutted pavement surface before the internal vertical LVDT in the actuator of the wheel carriage assembly stroked out. However, this depth varied depending on the ATLAS track placements over individual test cells, and some sections could be tested to rut depths greater than 4 in. Transverse GPR scanning of the test sections at a different number of load applications was also used for distinguishing between rutting in the subgrade and aggregate layers. Figure 4.1 shows loading of the test sections and the surface profile measurement using a digital caliper.

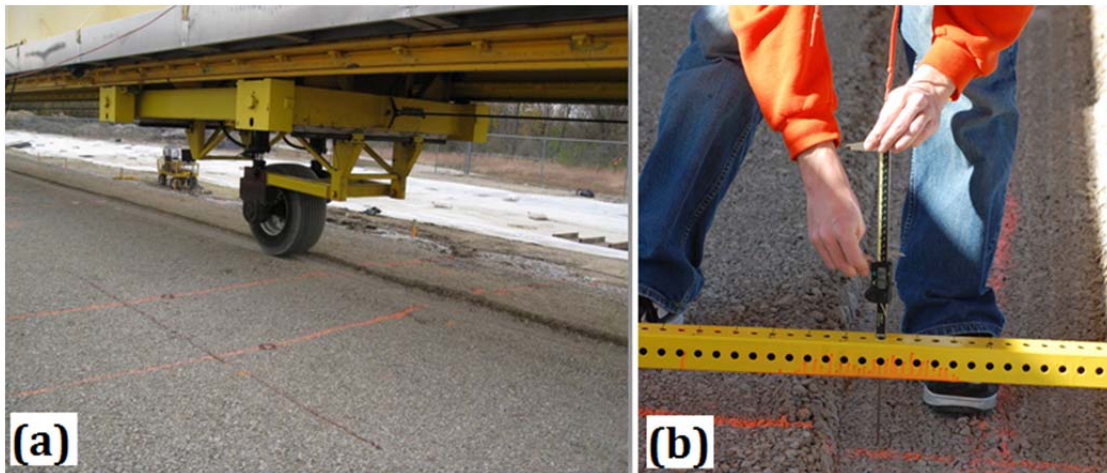


Figure 4.1. Photos showing unidirectional accelerated pavement testing and rut measurement.

4.3 EFFECT OF MOISTURE CONDITIONS ON TEST SECTION PERFORMANCE

To evaluate the effect of moisture conditions on aggregate behavior, Cells 1 through 5 were loaded to failure under as-constructed near-optimum and flooded moisture conditions. The pavement sections were constructed to be approximately 18 ft (5.5 m) wide to accommodate loading along two different wheel paths (see Figure 4.2) separated by a distance of 8 ft (2.44 m). The pavement sections were first tested under near-optimum aggregate moisture conditions (north wheel path) before artificial flooding and loading along the second (south) wheel path. Flooding of the test sections was achieved using perforated water sprinklers until excessive water was observed seeping through the boundaries of the aggregate sections. Both wheel paths were separated from the pavement edge by a distance of 5 ft (152 cm) to eliminate edge effects induced by the unsupported aggregate boundaries.

A minimum time interval was maintained between artificial flooding and loading of the pavement sections to avoid material attrition through splashing and development of excess pore water pressures. Because of inaccuracies associated with layer boundary identification using GPR in the presence of excessive moisture, transverse GPR scanning of the test sections was not conducted under flooded conditions. After testing each pavement section to failure at near-optimum and flooded conditions, transverse trenches were excavated across the wheel paths for visual identification of subgrade and aggregate layer rutting. Cell 6, which was constructed by placing a 12-in.-thick large-size aggregate layer over a subgrade of IBV = 1% and subsequently capped by a 6-in. CA-6 layer, was not tested under flooded conditions. Instead, the south wheel path of the Cell 6 was reinforced by placement of a woven geotextile at the subgrade-large-size-aggregate layer interface. Therefore,

comparison of rut accumulations along the two wheel paths for Cell 6 would highlight the effectiveness of geotextile reinforcement in pavement working platforms constructed over very weak subgrades.

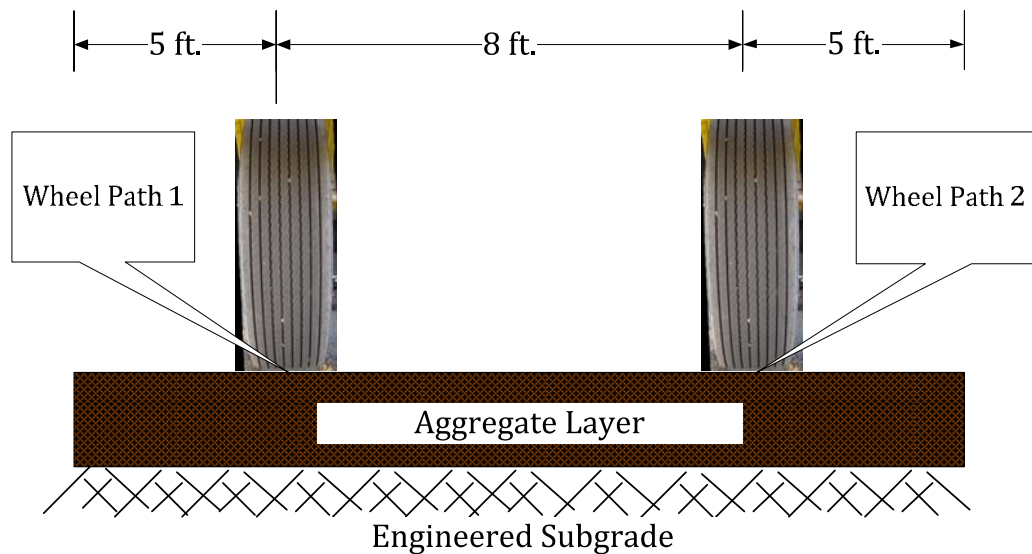


Figure 4.2. Trafficking wheel path locations 1 and 2 separated by 8 ft.

Accelerated testing of the full-scale construction platform sections was conducted between October 2010 and May 2011. Cells 1, 2, 4, 5, and 6 were tested between October and December 2010. However, winter weather conditions prevented Cell 3 tests from being finished in 2010. Therefore, Cell 3 was tested in May 2011 after the effects of spring thaw. Performance trends observed from loading of the test cells at near-optimum and flooded conditions are presented in the sections below.

4.4 CELL 1: UNCRUSHED GRAVEL WITH HIGH AMOUNTS OF NONPLASTIC FINES

This section presents analyses of probable rut mechanisms contributing to failure of the uncrushed gravel pavement sections constructed over an engineered subgrade of IBV = 3%. As explained in Chapter 3, this test cell (Cell 1) was constructed using an uncrushed gravel material containing high amounts of nonplastic fines. The test cell comprised three sections of aggregate layer thicknesses: 14, 12, and 8 in. (356 mm, 305 mm, and 203 mm) separated by 10-ft (3.1-m) long transition zones.

4.4.1 Performance Under Near-Optimum Conditions

Figure 4.3 presents surface profiles of the three test sections after application of an increasing number of load passes along the north wheel path (near-optimum aggregate moisture conditions). Section 1 shown in Figure 4.3a performed the worst and exhibited extensive heaving adjacent to the wheel path leading to failure after only 47 load applications. Section 2 (Figure 4.3b) performed better than Section 1, and could withstand 160 load applications before undergoing shear failure. Moreover, the surface heave for Section 2 was less severe compared with Section 1. It should be noted that rut accumulation accompanied by surface heaving adjacent to the wheel path is often considered to be an indicator of shear flow within the unbound granular layer (Dawson and Kolisoja 2005). Therefore, the deformed surface profiles of Sections 1 and 2 indicated failure of the

aggregate layer within itself. However, as shown in Figure 4.3c, Section 3 (8-in.-thick aggregate layer) could support a significantly higher number (400) of load applications before undergoing shear failure or developing excessive surface heave. This was in contradiction with the common assumption of thicker aggregate layers ensuring better resistance to permanent deformation. The significantly better performance of Section 3 (8-in.-thick aggregate) compared with the other two sections was clearly evident after 400 load applications. Therefore, loading of this section was stopped at this point, even though the total rut accumulation for the section was approximately 2 in. (50 mm).

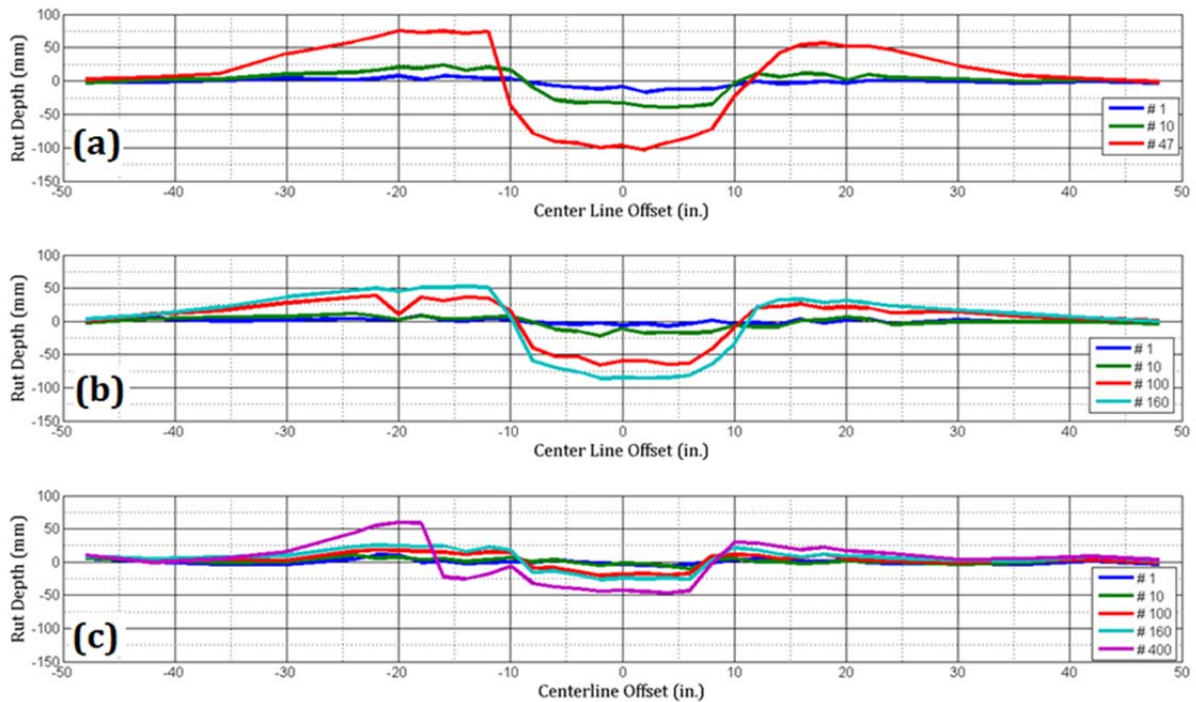


Figure 4.3. Rut developments in uncrushed gravel sections: (a) 1 (14-in.-thick aggregate layer), (b) 2 (12-in.-thick aggregate layer), and (c) 3 (8-in.-thick aggregate layer) resulting from unidirectional ATLAS loading under near-optimum aggregate moisture conditions (1 in. = 25.4 mm).

An investigation of aggregate layer moisture conditions was conducted to eliminate the possibility of excessive moisture in Section 1 leading to rapid rut accumulation. Aggregate samples were collected from different depths along the wheel path to determine the moisture content profiles in the three sections (see Table 4.1). As shown in Table 4.1, the moisture content profiles of the aggregate layers were uniform across the three test sections. This resulted in moisture content discrepancy being ruled out as a possible mechanism contributing to rapid failure of the thick uncrushed gravel sections. A close examination of GPR scans and layer boundaries obtained from excavated trench sections was next pursued to identify the rutting mechanisms.

Table 4.1. Cell 1: Moisture Content Investigation Along Wheel Path

Point	Location	Aggregate Layer Moisture Content (%)
1	Section 1, West	5.6
2	Section 1, East	5.9
3	Section 2, West	5.5
4	Section 2, East	5.2
5	Section 3, West	5.3
6	Section 3, East	5.7

Figure 4.4 shows the cross-section of the excavated trench (Figure 4.4b) alongside the GPR scan (Figure 4.4a) and the surface rut profile (Figure 4.4c) for the same test section (Section 1 of Cell 1). The yellow line (circled on top) in Figure 4.4b shows the aggregate surface, whereas the red line (circled at bottom) shows the subgrade interface. From the excavated trench section, it was clear that the heave on the surface was much higher than the heave at the subgrade interface. Also, the depression in the subgrade (shown by the black trace on the photograph in Figure 4.4b) was offset from the surface rut observed under the wheel path. A similar trend was observed from the GPR scan results (see Figure 4.4a) and indicated shear flow of material resulting in a lateral offset of the subgrade depression from the wheel path. Therefore, shear movement within the aggregate layer was the primary mode of failure associated with performance of this uncrushed gravel section.

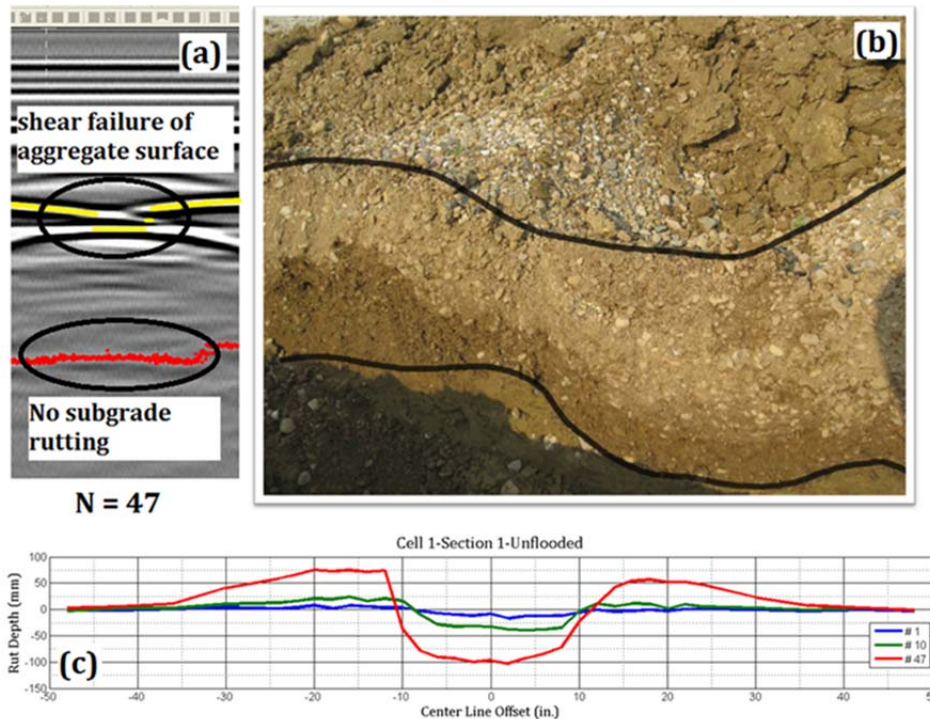


Figure 4.4. (a) GPR scan, (b) excavated trench, and (c) surface rut profile of the 14-in. (356-mm) thick uncrushed gravel aggregate section (1 in. = 25.4 mm).

Figure 4.5 shows the deformed profile of the 12-in.-thick uncrushed gravel in Section 2. Similar to the 14-in.-thick aggregate section, the GPR scan of Section 2 clearly showed a much larger rutting in the aggregate (shown by the top yellow line) compared with the subgrade (bottom red line). However, it should be noted that the subgrade rutting in Section 2 was more significant than that in Section 1. Also, looking at the cross-sectional profile from the excavated trench, the subgrade rutting in Section 2 was more defined than that in Section 1. This was primarily because of a thinner aggregate layer that existed in Section 2 and the lack of adequate aggregate depth for the development of a complete shear surface within the layer. As a result, the depression in the subgrade for Section 2 was less offset from the wheel path compared with that in Section 1. However, the aggregate layer was still the primary contributor to the failure of the section.

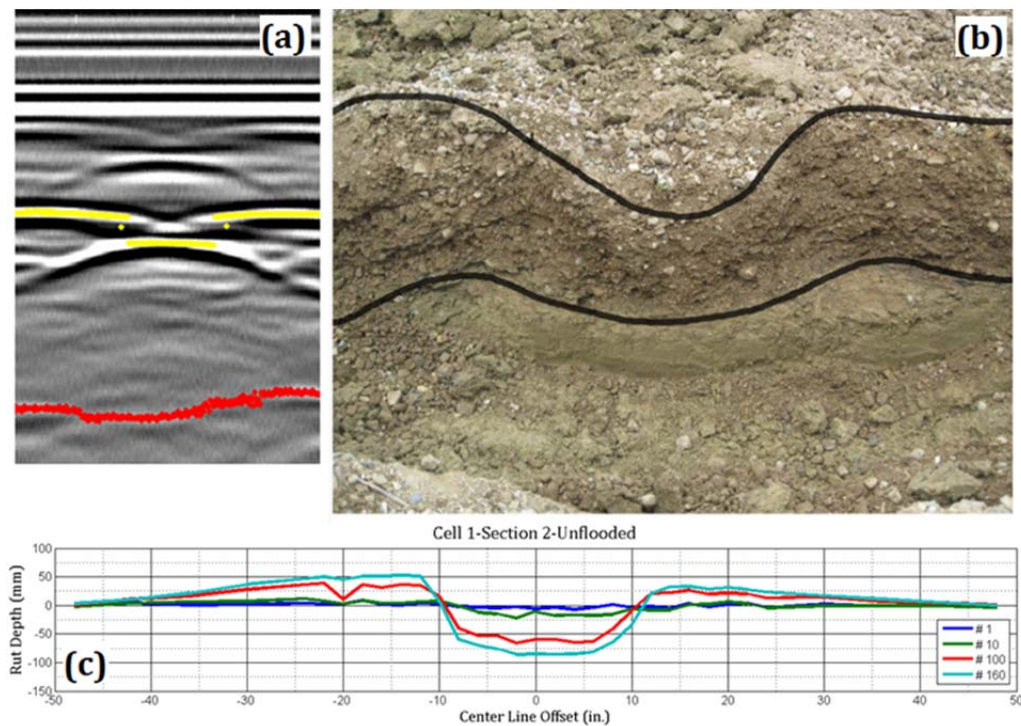


Figure 4.5. (a) GPR scan, (b) excavated trench, and (c) surface rut profile of the 12-in. (305-mm) thick uncrushed gravel aggregate section (1 in. = 25.4 mm).

Figure 4.6 shows similar profiles for the 8-in.-thick uncrushed gravel layer in Section 3. The absence of significant heave development at the subgrade interface can clearly be noticed from Figure 4.6b. Moreover, the lack of significant surface heave development on the surface (see Figures 4.6b, and 4.6c) implied no significant material movement within the aggregate layer. The subgrade deformation in Section 3 appeared to be less pronounced than Sections 1 and 2. This observation was in contradiction with common intuition regarding thick aggregate layers ensuring better pavement performance, and was attributed to the significantly higher subgrade moduli for Section 3 compared with Sections 1 and 2 as determined from LWD and GeoGauge™ measurements (see Figure 4.7). Close inspection of the in-place subgrade IBV profile as determined from DCP testing also revealed stronger subgrade conditions for Section 3 compared with Sections 1 and 2 (see Figure 4.8).

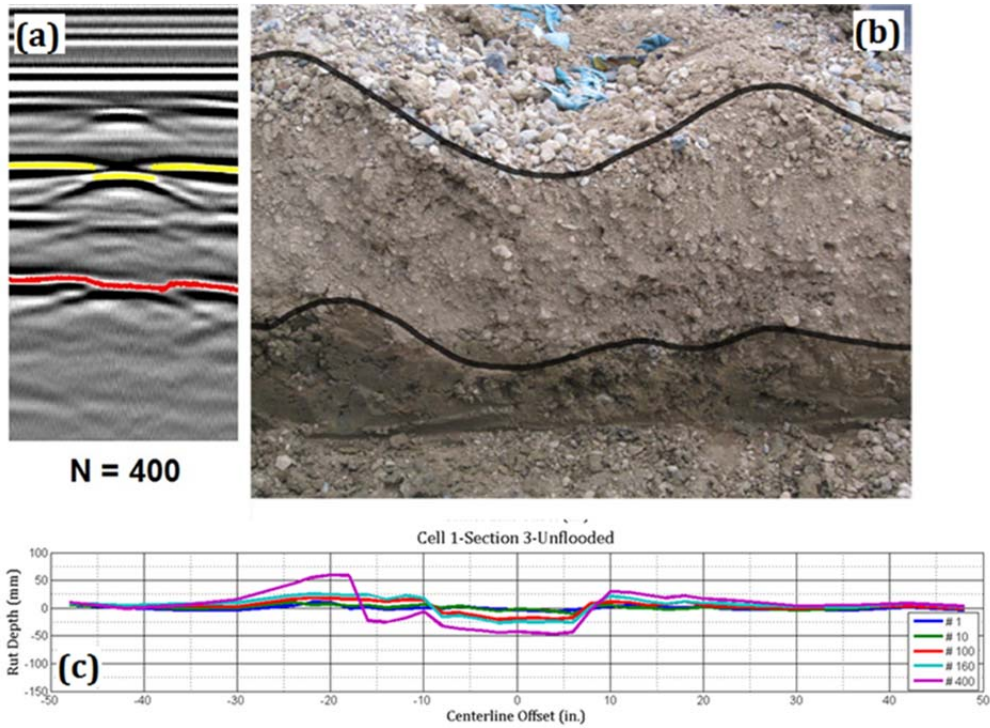


Figure 4.6. (a) GPR scan, (b) excavated trench, and (c) surface rut profile of the 8-in. (203-mm) thick uncrushed gravel aggregate section (1 in. = 25.4 mm).

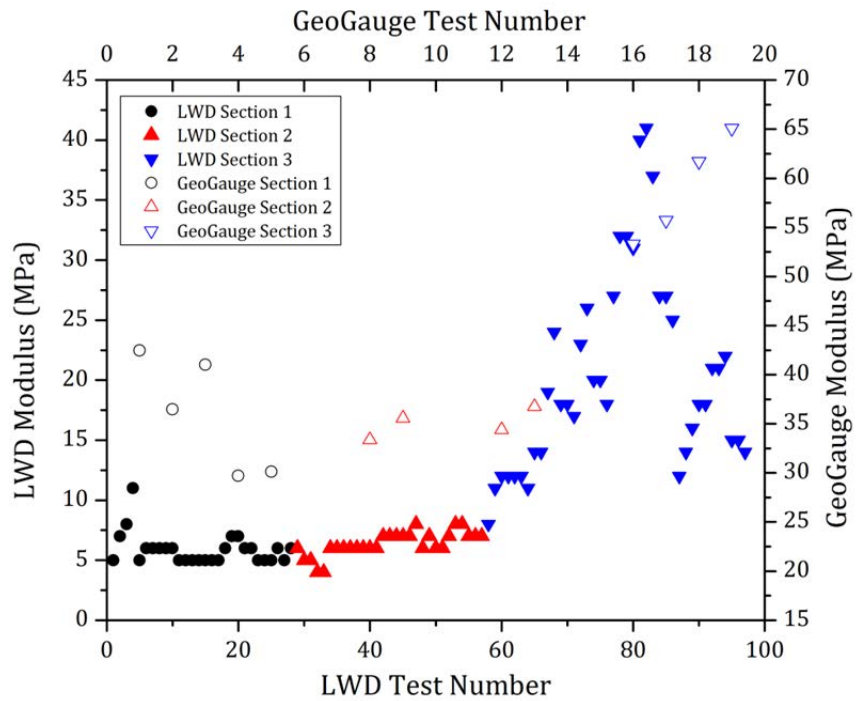


Figure 4.7. Measured field moduli for Cell 1 indicating stronger subgrade constructed in Section 3 when compared with Sections 1 and 2.

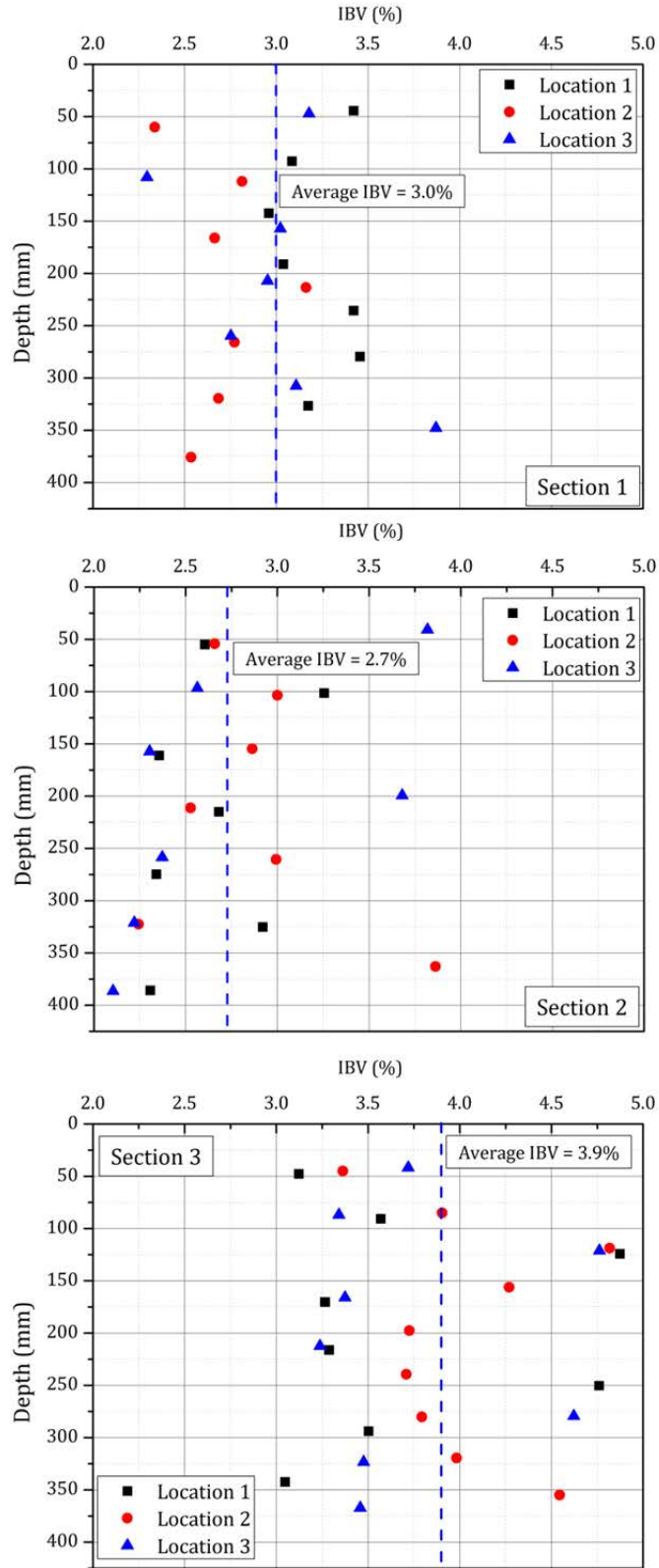


Figure 4.8. DCP measured subgrade IBV profiles for Cell 1 showing stronger subgrade conditions in Section 3.

The stronger subgrade conditions corresponding to Section 3 of Cell 1 resulted in significantly lower subgrade deformations when compared with Sections 1 and 2. Failure patterns from trafficking the test sections under near-optimum aggregate moisture conditions indicated a definite internal shear failure mechanism of the uncrushed gravel layer. This field observation was reinforced by laboratory test results comparing the permanent deformation behavior of different aggregate types (refer to Figure 3.4), which clearly showed unstable behavior of the uncrushed gravel material when compared with crushed aggregates.

4.4.2 Performance Under Flooded Conditions

To evaluate the effects of excessive moisture conditions on pavement working platform performance, the uncrushed gravel test sections in Cell 1 were artificially flooded and tested along a second (south) wheel path separated from the first by a distance of 8 ft (2.4 m). The accumulated rut amounts were recorded through surface profile measurements after different number of load applications. Figure 4.9 shows the accumulations of permanent deformation in Sections 1, 2, and 3 upon testing under flooded conditions. Because of differences in ATLAS track elevations, different test sections could be tested to different rut depths before the vertical LVDT in the ATLAS wheel actuator stroked out.

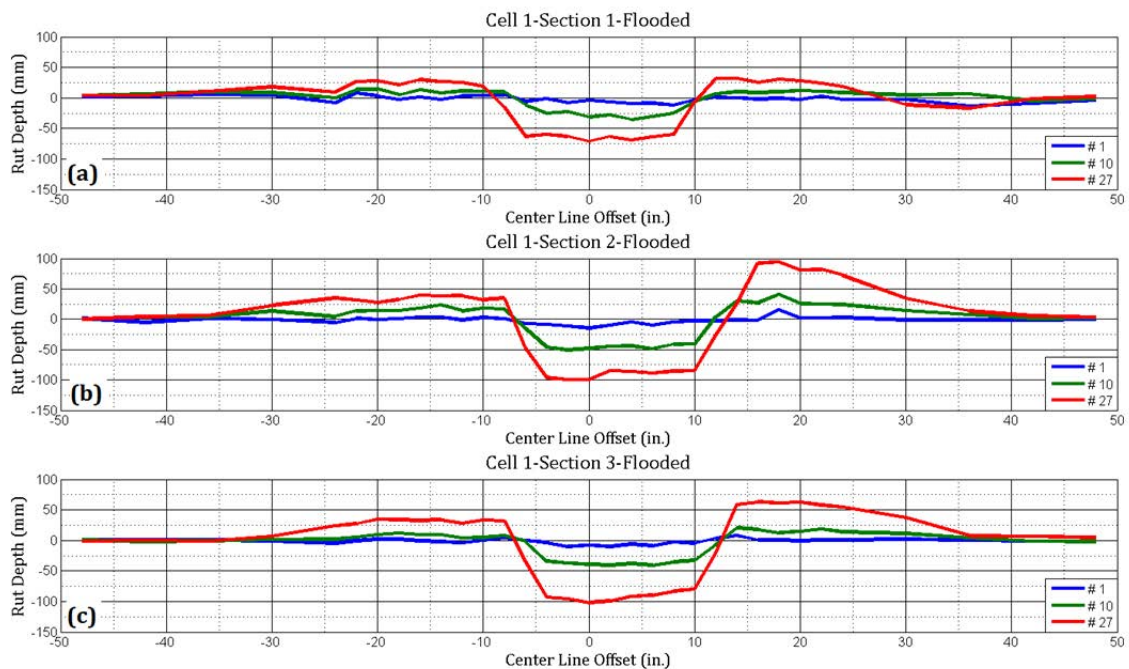


Figure 4.9. Rut developments in uncrushed gravel sections (a) 1 (14-in.-thick aggregate layer), (b) 2 (12-in.-thick aggregate layer), and (c) 3 (8-in.-thick aggregate layer) resulting from unidirectional ATLAS loading under flooded conditions (1 in. = 25.4 mm).

The test section performances under flooded conditions were significantly different from those under near-optimum aggregate moisture conditions. All the three test sections showed rapid permanent deformation accumulation and failed after only 27 load applications. It is important to note from Figure 4.9 that the amount of surface heave in Section 1 (see Figure 4.9a) under flooded conditions was significantly lower than that under the near-optimum moisture conditions indicating a somewhat lower degree of shear flow

within the aggregate layer under flooded conditions. The amounts of surface heave in Sections 2 and 3 (see Figures 4.9b and 4.9c) were significantly higher than that in Section 1. Also, Section 3, which had the thinnest (8-in.) aggregate layer, rutted the most after 27 load applications, which was expected because of the wetting of the subgrade, even though Section 3 had the highest as-constructed subgrade moduli for the near-optimum conditions.

Examination of transverse trench sections revealed a different mechanism contributing to failure of the uncrushed gravel test sections under flooded conditions. Figure C-1 in Appendix C shows the deformed layer boundaries for the aggregate surface as well as the aggregate-subgrade interface after testing under flooded conditions. The subgrade deformation for Section 1 (see Figure C-1a) was more pronounced for the flooded case when compared with the near-optimum aggregate moisture conditions (see Figure 4.4b). This resulted from ingress of excessive moisture from the aggregate layer weakening the subgrade significantly and leading to failure caused by excessive subgrade movement.

4.5 CELL 2: CRUSHED LIMESTONE WITH LOW AMOUNTS OF PLASTIC FINES

The effect of low amounts of plastic fines on the performance of this crushed limestone material was evaluated through accelerated testing of full-scale construction platform test sections constructed over an engineered subgrade of IBV = 3%. As already mentioned, the aggregate material used in this test cell contained a significantly lower amount of fines (~5%) compared with the originally reported values (~12%) from the aggregate source and was therefore categorized as a low fines material with moderately plastic (PI = 5.7) fines. As observed from the laboratory testing of aggregates during Phase I of this research project, the effect of fines plasticity on aggregate behavior was not apparent at low fines contents. Therefore, amount of fines in the aggregate matrix was expected to be the primary physical characteristic governing the performance of this particular test cell. It is also important to note that the crushed limestone in Cell 2 exhibited unstable matrix behavior under standard compaction conditions.

4.5.1 Performance at Near-Optimum Moisture Conditions

Performance of the test cell under near-optimum aggregate moisture conditions was monitored through loading and surface profile measurements along the north wheel path. GPR scanning of this test cell could not be conducted because GPR equipment was not available at the time of trafficking. Therefore, the mechanisms contributing to failure of this test cell were analyzed using surface profile measurements and excavated trench sections only.

Figure 4.10 shows the excavated trench section and surface rut profile of Section 1 (14-in.-thick aggregate layer) in Cell 2. As seen in the figure, this particular test section failed after only 52 load applications by accumulating rut depths up to 4 in. (100 mm) accompanied by significant heaving adjacent to the wheel path. As already mentioned, development of significant heave adjacent to the wheel path is often an indicator of shear movement within the aggregate layer and presents the possibility of internal shear failure of the crushed limestone layer. Close inspection of the excavated transverse trench sections showed no significant deformation at the subgrade interface (see Figure 4.10a) with the aggregate-subgrade interface remaining essentially horizontal even after loading of the test section to failure.

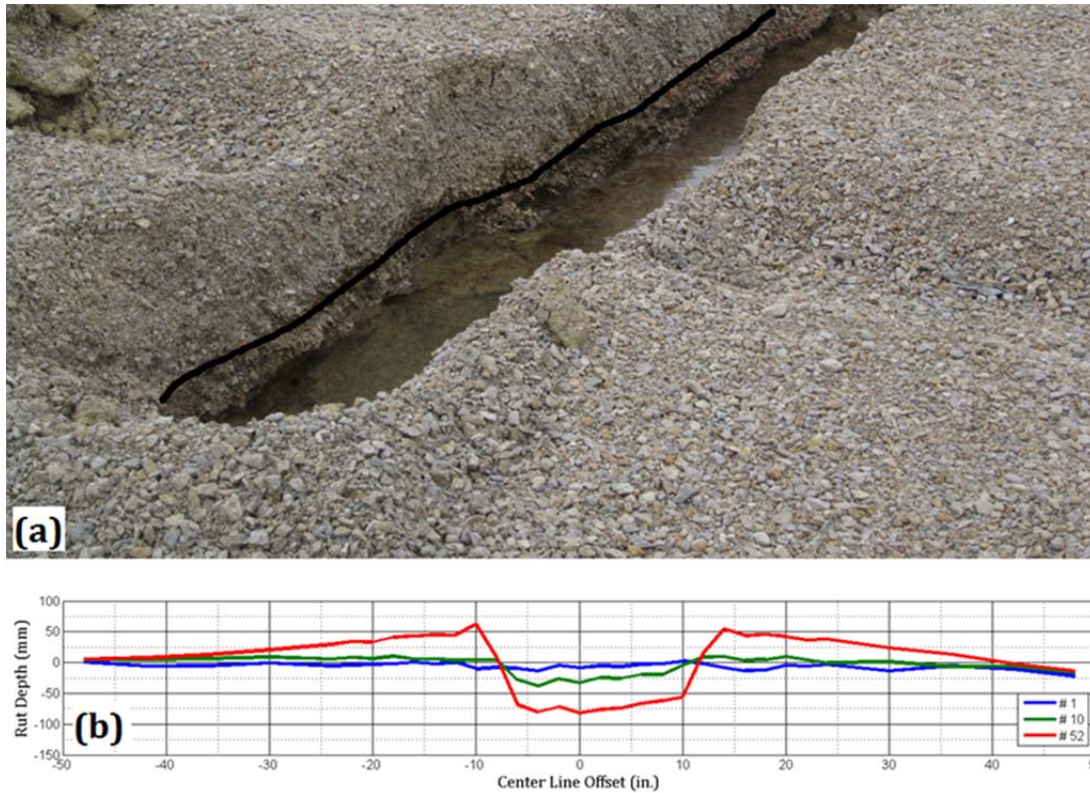


Figure 4.10. (a) Excavated trench and (b) surface rut profile of the 14-in.-thick crushed limestone section in Cell 2 (1 in. = 25.4 mm).

This behavior was in contradiction to the commonly observed trends of crushed aggregate layers resisting internal shear movement as a result of improved particle-to-particle interlock compared with uncrushed aggregates. It is important to note at this point that the crushed limestone material used in Cell 2 showed unstable matrix behavior under standard compaction conditions because of significantly low fines contents, and it could not be tested in the laboratory for permanent deformation and resilient modulus characteristics. Moreover, the material showed significantly low IBV values (18-19%) under standard compaction conditions. Laboratory test results therefore supported the hypothesis of shear movement within the aggregate layer under standard compaction densities resulting from the unstable matrix structure.

Figures 4.11, and 4.12 present the deformed profiles of Sections 2 (12-in.-thick aggregate layer) and 3 (8-in.-thick aggregate layer), respectively, upon testing under near-optimum aggregate moisture conditions. From the figures, Sections 2 and 3 could sustain 100 and 350 load applications, respectively, before accumulating significant rutting. Moreover, close inspection of the surface profiles and the excavated trench sections clearly indicated increased subgrade heaving with decreasing aggregate layer thickness. The highest subgrade heaving was noticed for the 8-in.-thick aggregate layer in Section 3.

Similar to the near-optimum loading conditions for the uncrushed gravel material in Cell 1, failure of aggregate sections in Cell 2 under near-optimum aggregate moisture conditions was also attributed to shear movement within the aggregate layer, which was also evident from the wavy nature of rut development along the wheel path. From preliminary investigation of the deformed surface profile and excavated trench sections, it was apparent that the crushed limestone material in Cell 2 experienced shear movement

within the thick aggregate layers. However, the crushed aggregate matrix resulted in adequate stress reduction at the subgrade level effectively, thus protecting the subgrade from excessive deformation under repeated wheel load applications.

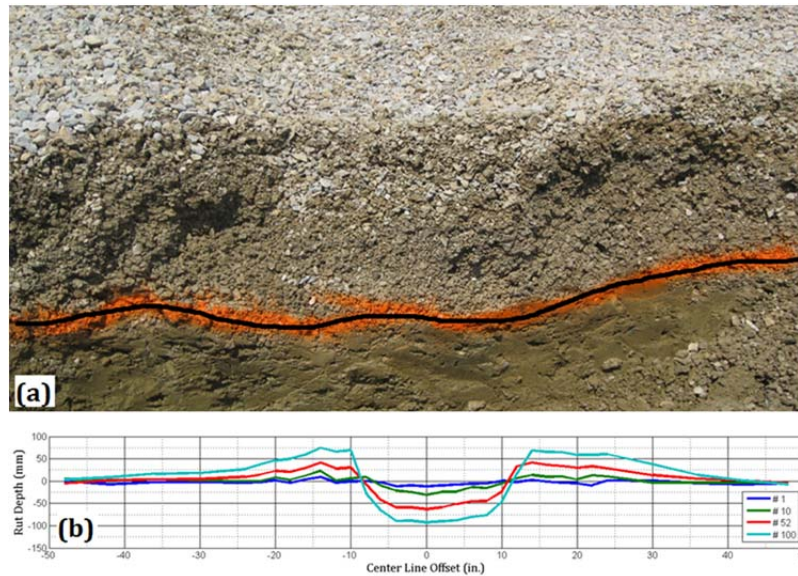


Figure 4.11. (a) Excavated trench and (b) surface rut profile of the 12-in.-thick crushed limestone section in Cell 2 (1 in. = 25.4 mm).

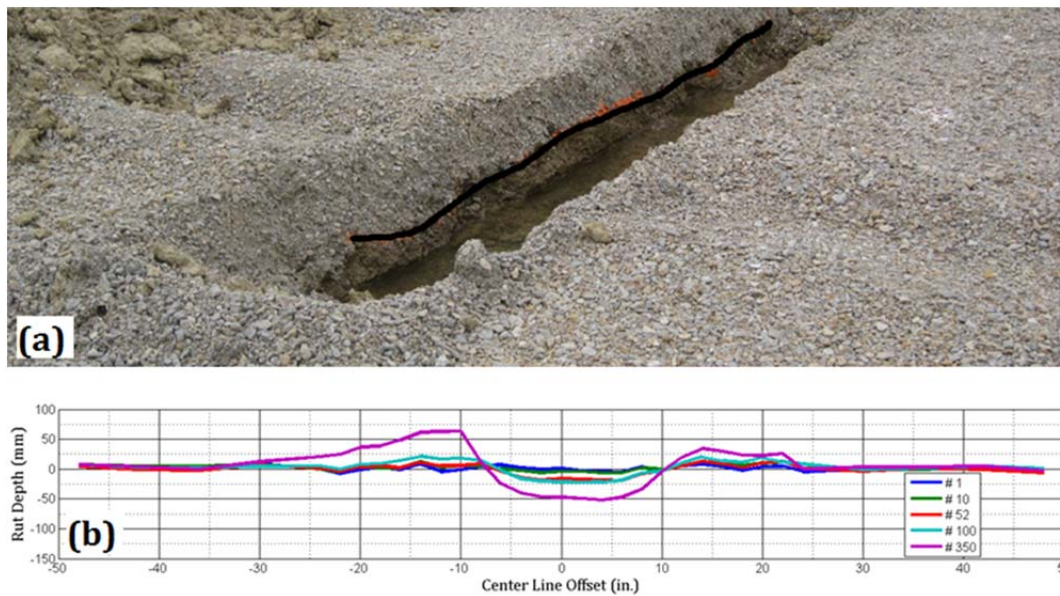


Figure 4.12. (a) Excavated trench and (b) surface rut profile of the 8-in.-thick crushed limestone section in Cell 2 (1 in. = 25.4 mm).

A further investigation of the test cell performance was conducted through analyses of the field moduli measured using LWD and GeoGauge™ on the compacted subgrade as well as aggregate layers. Figure 4.13 shows for Cell 2 the field moduli for the compacted subgrade and aggregate layers.

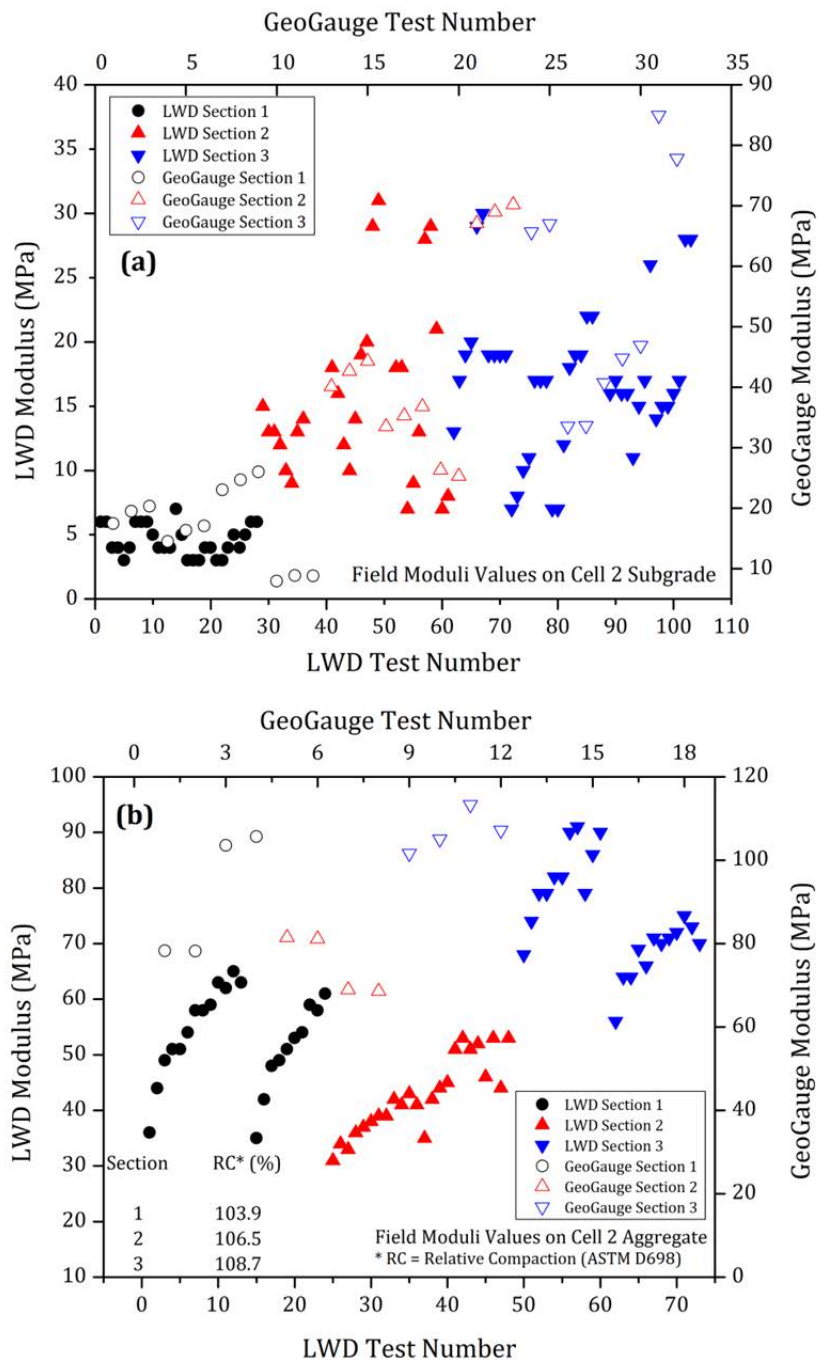


Figure 4.13. Field modulus values measured by LWD and GeoGauge™ on (a) compacted subgrade and (b) aggregate layers in Cell 2. (Sections 1, 2, and 3 correspond to aggregate layers of thicknesses 14, 12, and 8 in., respectively).

As seen in Figure 4.13a, the subgrade moduli for Sections 2 and 3 were similar in magnitude but were higher than those for Section 1 (as indicated from both LWD and GeoGauge™ results). Although the lower subgrade moduli for Section 1 could possibly be a

contributing factor resulting in rapid failure of the thickest aggregate section (Section 1) under loading, the observed difference between performances of Sections 2 and 3 could not be explained just on the basis of differences in subgrade moduli. A close inspection of the aggregate field moduli (see Figure 4.13b) revealed significantly higher moduli for Section 3 when compared with Sections 1 and 2. This could be linked to the achieved relative compaction (ASTM D 698) values for the three aggregate sections: 103.9%, 106.5%, and 108.7% for Sections 1, 2, and 3, respectively. As discussed in Chapter 3, the free-draining nature of the crushed limestone aggregate used in Cell 2 meant that the OMC and MDD values could not easily be established following the drop-hammer compaction methods. Therefore, the laboratory-determined MDD value of 115.4 pcf was not indicative of the maximum achievable densities in the field. This explained the high relative compaction values (> 100%) for all the three test sections.

The 14-in.-thick aggregate layer in Section 1 had the lowest relative compaction achieved, owing to the weaker subgrade conditions. The resulting inadequate particle interlock led to shear movement within the aggregate layer that ultimately failed after only 52 load applications. Sections 2 and 3 were both constructed over similar subgrade conditions, with the aggregate layer in Section 3 compacted to higher densities (108.7% MDD) when compared with Section 2 (106.5% MDD). Better compaction of the aggregate layer in Section 3 resulted in higher moduli (adequately captured by the LWD and GeoGauge™) and better stress dissipation with depth. Apparently, reduced stress levels at the subgrade interface resulted in Section 3 sustaining a significantly higher number of load applications (350) compared with section 2 (100) without accumulating excessive rutting.

Analysis of Cell 2 performance under near-optimum aggregate moisture conditions therefore emphasized the importance of adequate compaction for crushed aggregates with low fines. Higher relative compaction percentages for the aggregate layers could be directly linked to better performance under loading. Laboratory testing of the aggregates showed similar trends (refer to Chapter 3). Although the crushed limestone matrix with low fines (used in Cells 2 and 5) was unstable under standard compaction conditions, it performed comparable to other crushed aggregate materials with high fines, under modified compactive effort OMC and MDD conditions (refer to Figure 3.4).

4.5.2 Performance Under Flooded Conditions

Subsequent to testing under near-optimum aggregate moisture conditions, the test sections were artificially flooded and tested to failure under flooded conditions to evaluate the effect of excess moisture on pavement working platform performance. Inclement weather conditions caused testing of this cell under flooded conditions to be stopped after only 34 load applications.

Figure 4.14 shows the rut development in Cell 2 aggregate sections under flooded conditions. After 34 load applications, Section 2 (12-in.-thick aggregate layer) showed the highest rut accumulation as well as surface heave development. This was different from the trend observed in the case of Cell 1, which showed rapid failure of the thinnest aggregate layer (Section 3) under flooded conditions as a result of excessive subgrade deformations. Figure C-2 in Appendix C shows the deformed layer boundaries for the aggregate surface as well as the aggregate-subgrade interface in Cell 2 after testing under flooded conditions.

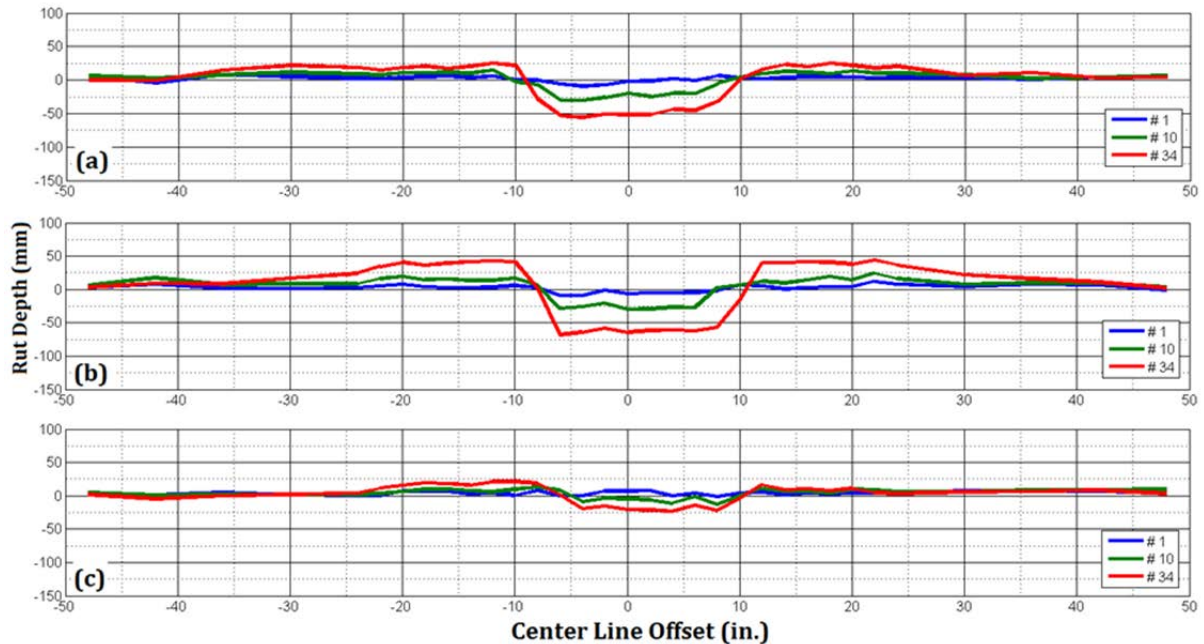


Figure 4.14. Rut developments in Cell 2 sections (a) 1 (14-in.-thick aggregate layer), (b) 2 (12-in.-thick aggregate layer), and (c) 3 (8-in.-thick aggregate layer) resulting from unidirectional ATLAS loading under flooded conditions (1 in. = 25.4 mm).

The subgrade deformation in Section 2 was clearly visible, as shown in Figure C-2b in Appendix C, whereas no significant subgrade deformation was observed for Sections 1 and 3. No logical explanation of this behavior could be deduced. However, one possible explanation could be related to inadequate flooding of Sections 1 and 3 resulting in not enough moisture wetting the subgrade to reduce the subgrade strength significantly.

An important observation can be made from the excavated trench sections shown in Figure C-2. Significant amount of subgrade intrusion into the aggregate layer was observed for all the three sections under flooded conditions. It was apparent that, owing to the low fines content and free-draining nature of the crushed limestone used in Cell 2, subgrade pumping into the aggregate layer was more significant compared with the other aggregate types.

For the crushed limestone material with low fines, degree of compaction played a significant role in governing aggregate layer behavior under near-optimum aggregate moisture conditions. The aggregate sections with lower relative compaction levels underwent internal shear failure that led to excessive rutting after relatively low number of load applications. Aggregate sections compacted to higher densities, on the other hand, sustained a significantly higher number of load applications before failing from subgrade deformation, as Section 3 did. The significant improvement in aggregate behavior under higher compactive efforts was also reflected from laboratory testing of the aggregates reported in Chapter 3. These observations lead to the conclusion that crushed aggregate materials should contain a minimum amount of fines to achieve a stable matrix structure. In the absence of sufficient fines in the void structure, the aggregate particles may become unstable under traffic loading and tend to increase movement and the permanent deformation. Higher compactive efforts can be used to somewhat improve the particle interlock in such aggregates with low fines. However, because achieving high relative compaction levels over weak subgrade conditions can often be challenging, it is

recommended that crushed aggregate with very low fines contents be avoided in construction platform applications to eliminate the possibility of internal shear failure of the aggregate cover layer. Significant subgrade intrusion into the aggregate layer was observed for all three test sections under flooded conditions. A fabric used at the subgrade interface would serve as a good separator for such low fines aggregate materials. The mechanisms contributing to pavement failure under flooded conditions were not clear for this particular test cell.

4.6 CELL 3: CRUSHED DOLOMITE WITH HIGH AMOUNTS OF NONPLASTIC FINES

The effect of high amounts of nonplastic fines on the performance of a crushed dolomite material was evaluated through accelerated testing of full-scale pavement working platform sections under near-optimum and flooded aggregate moisture conditions. As already mentioned, testing of this cell was conducted in May 2011 after the test cell had experienced winter freeze-thaw cycles. Testing took place approximately six weeks after the last freeze-thaw cycle to allow sufficient time for dissipation of any excess moisture accumulation during the spring thaw season.

The first task before loading the test cell was to assess the existing conditions of the subgrade and aggregate layers. Accordingly, DCP testing was conducted at six different locations (two locations per test section) for determination of in-place IBV profiles in the engineered subgrade and aggregate layers. Figure 4.15 shows the in-place IBV profile along the north wheel path of Section 1 (14-in.-thick aggregate layer).

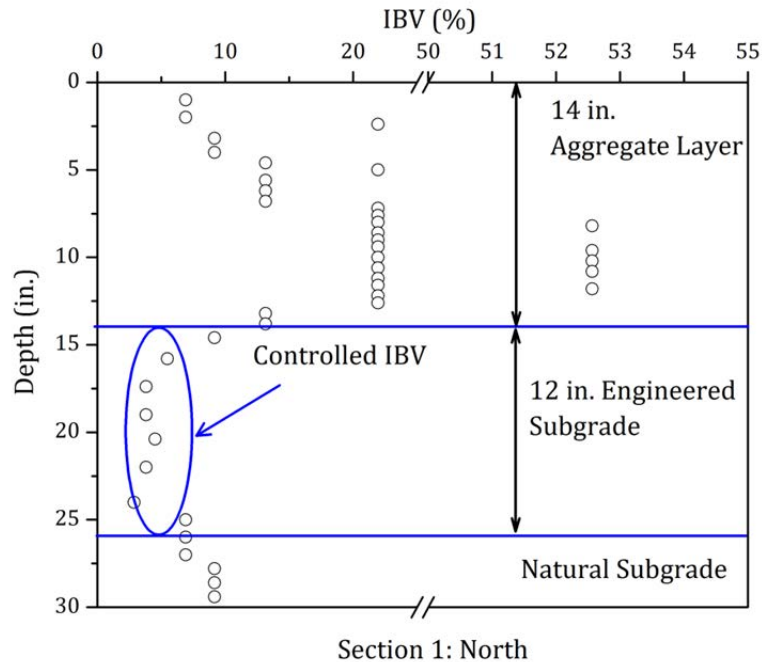


Figure 4.15. Cell 3 IBV profile with depth along the north wheel path of Section 1 (1 in. = 25.4 mm).

As shown in Figure 4.15, the subgrade IBV profile was consistently close to the as-constructed value (IBV = 3%) throughout the 12-in. depth of the engineered subgrade layer. DCP results from the other five locations showed very similar results and are presented in Appendix D. No change in engineered subgrade IBV values were observed to result from

the winter freeze-thaw cycles. The consistent IBV profile throughout the engineered subgrade layer was primarily attributed to adequate removal of excess moisture by the installed transverse and longitudinal drainage systems.

The effect of winter freeze-thaw cycles on the aggregate layer was evaluated through comparison of field modulus values for the three sections measured before and after the freeze-thaw cycles using the GeoGauge™. As shown in Figure 4.16, the aggregate layer moduli for all the three test sections after the freeze-thaw cycles were significantly higher (up to 225%) compared with the as-constructed values. This indicated significant strength gain by the crushed dolomite material after the winter. One plausible mechanism contributing to the strength gain within the crushed dolomite layer could be caused by carbonate cementation within the fines fraction (Graves 1987). Significant strength gain in high carbonate base course materials upon soaking has been reported in the literature to be a result of dissolution-precipitation of the fines fraction (Graves 1987; Graves et al. 1988).

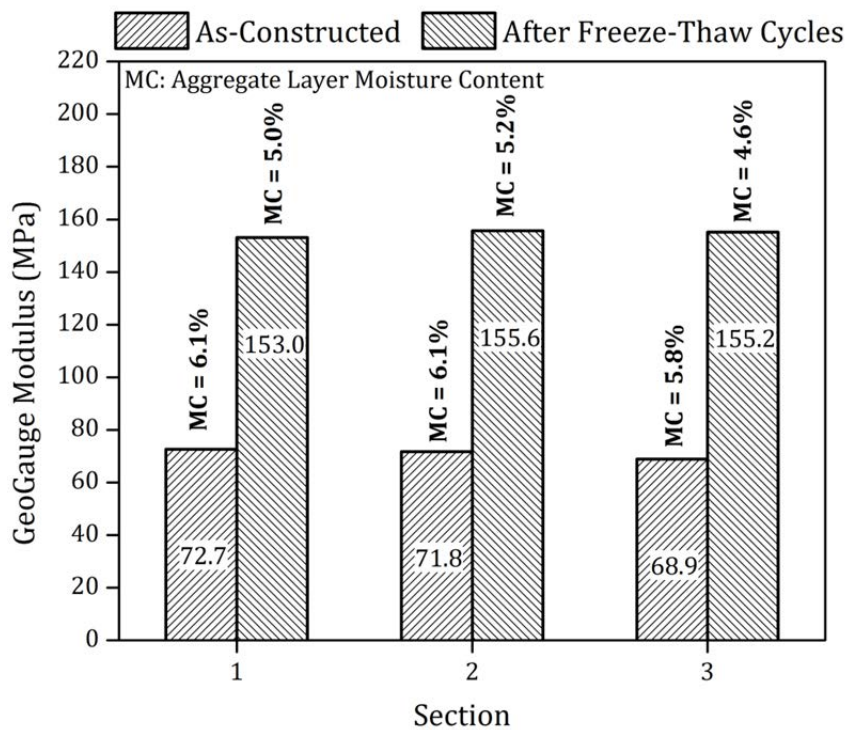


Figure 4.16, Comparisons of Cell 3 aggregate layer moduli before and after freeze-thaw cycles (Sections 1, 2, and 3 correspond to aggregate layers of thicknesses 14, 12, and 8 in., respectively).

4.6.1 Performance Under Near-Optimum Aggregate Moisture Conditions

Apparent strength gain (indicated by measured high field moduli) in the crushed dolomite material caused by freeze-thaw cycles was clearly reflected from the test section performances under loading. Figure 4.17 shows a GPR scan, excavated trench, and surface rut profile of the 14-in.-thick crushed dolomite section (Section 1) in Cell 3 upon testing under near-optimum aggregate moisture conditions.

The most important aspect to note from Figure 4.17 is the significantly higher number of load applications (700) this particular test section could sustain before only 2-in. (50-mm) rutting was accumulated. Moreover, even after 700 load applications, no surface heave was observed adjacent to the wheel path (see Figure 4.17c). This preliminary observation could

explain the absence of significant shear movement within the aggregate layer. The GPR scan (see Figure 4.17a) and excavated trench section (see Figure 4.17b) both clearly indicated that rutting of the test section was caused only by subgrade deformation.

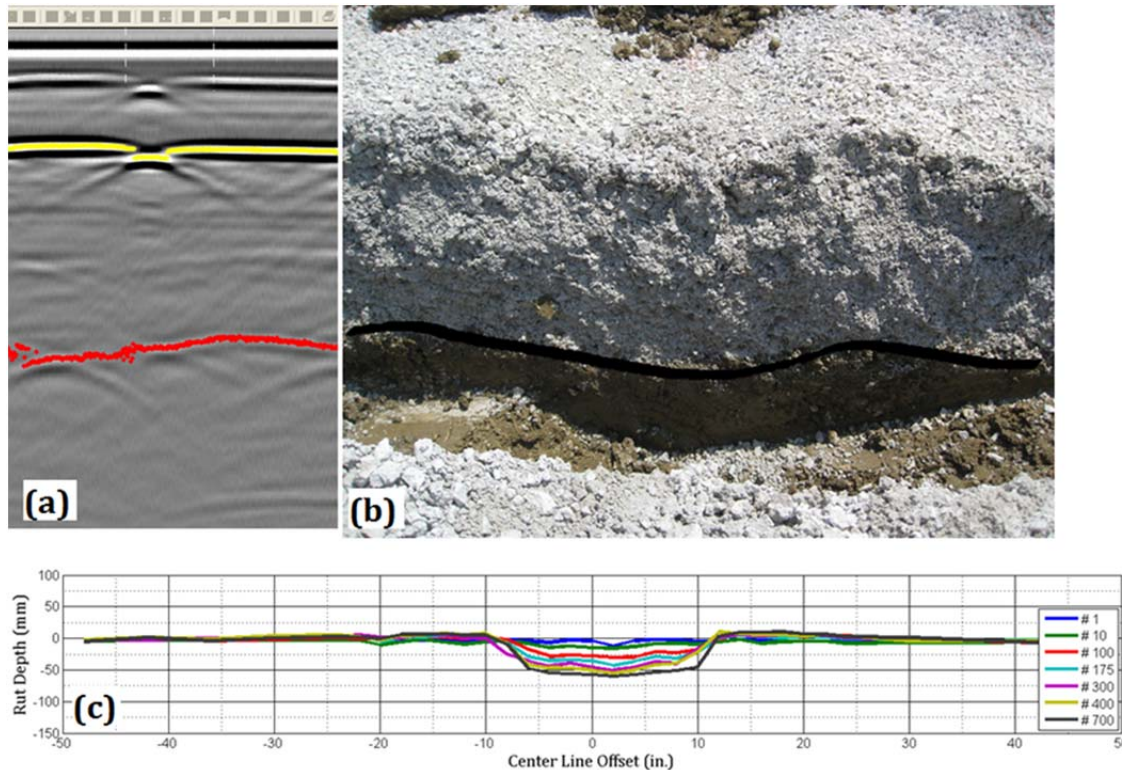


Figure 4.17. (a) GPR scan, (b) excavated trench, and (c) surface rut profile of the 14-in. (356-mm) thick crushed dolomite section in Cell 3 (1 in. = 25.4 mm).

Figures 4.18 and 4.19 show the deformed profiles for Sections 2 and 3 (12-in. and 8-in.-thick aggregate layers), respectively. Sections 2 and 3 could sustain 400 and 175 load applications, respectively, before accumulating rut depths of approximately 4 in. (100 mm). GPR scans and excavated trench sections showed subgrade deformation to be the primary mechanism responsible for failure of the test sections. As the aggregate layer thickness decreased, the subgrade was subjected to significantly higher stress levels, ultimately leading to shear failure. From the excavated trench sections (see Figures 4.18b and 4.19b), the aggregate layer clearly deformed as a flexible mat, and observed surface heaves were merely reflections of subgrade movement.

Testing of Cell 3 under near-optimum aggregate moisture conditions showed that the performance of this test cell was significantly better than the other cells, possibly as a result of carbonate cementation within the fines fraction. Another mechanism that possibly contributed to stiffening of the aggregate layer was the increased suction potentials after freeze-thaw cycles. The winter freeze-thaw cycles could have resulted in the formation of new interconnected voids within the aggregate layer, leading to increased suction potentials. The aggregate layer moisture contents after the freeze-thaw cycles were less than the as-constructed conditions (see Figure 4.16), which supports the argument of improved suction potentials. No significant shear movement within the aggregate layer was observed, and subgrade rutting was the primary mechanism contributing to pavement failure.

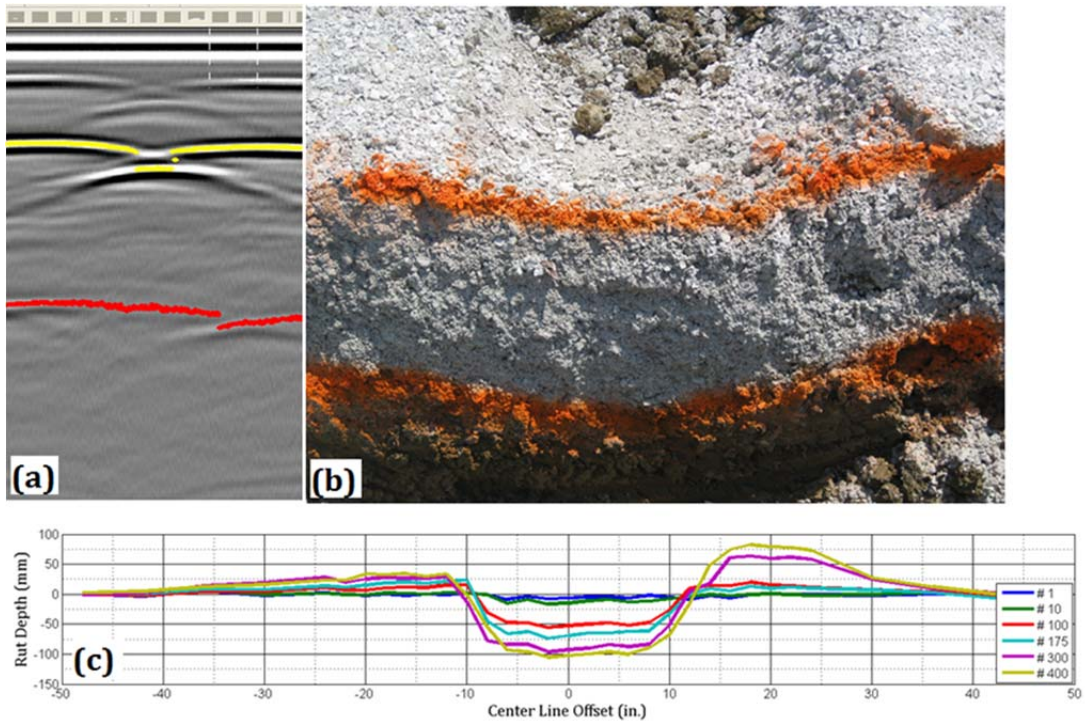


Figure 4.18. (a) GPR scan, (b) excavated trench, and (c) surface rut profile of the 12-in. (305-mm) thick crushed dolomite section in Cell 3 (1 in. = 25.4 mm).

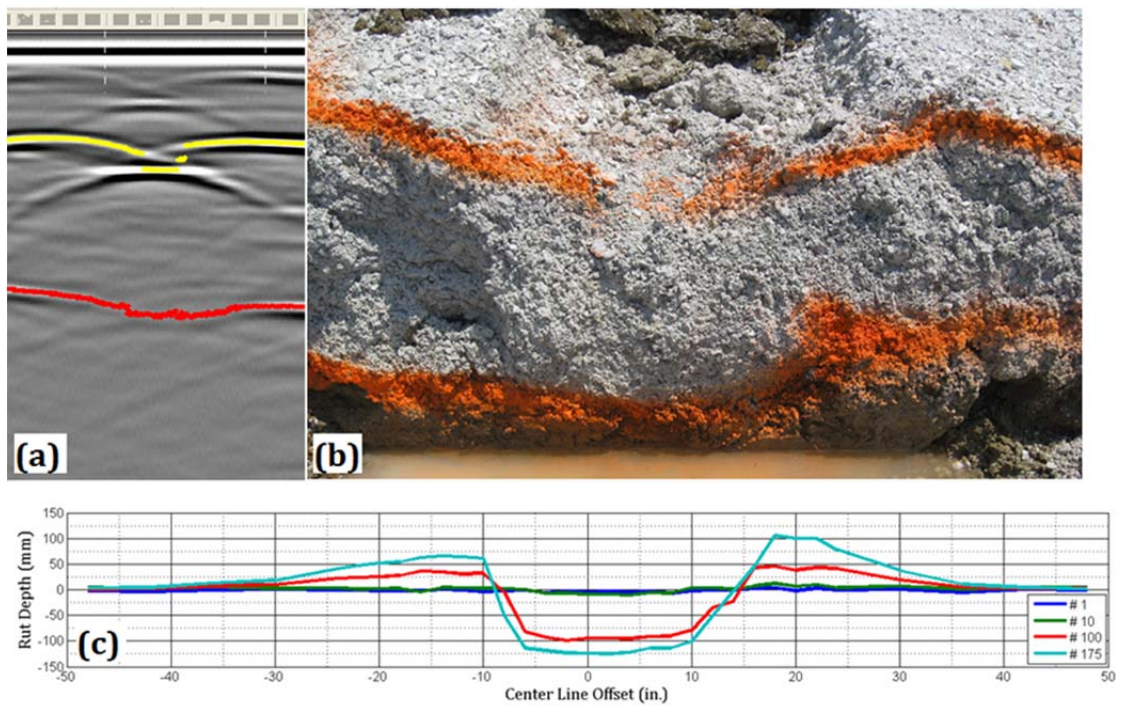


Figure 4.19. (a) GPR scan, (b) excavated trench, and (c) surface rut profile of the 8-in. (203-mm) thick crushed dolomite section in Cell 3 (1 in. = 25.4 mm).

4.6.2 Performance Under Flooded Conditions

Subsequent to testing under near-optimum aggregate moisture conditions, the effect of excess moisture on performance of the crushed dolomite material with high fines was studied through accelerated pavement testing under flooded conditions. Figure 4.20 shows the development of rutting in the three test sections of Cell 3 under flooded conditions.

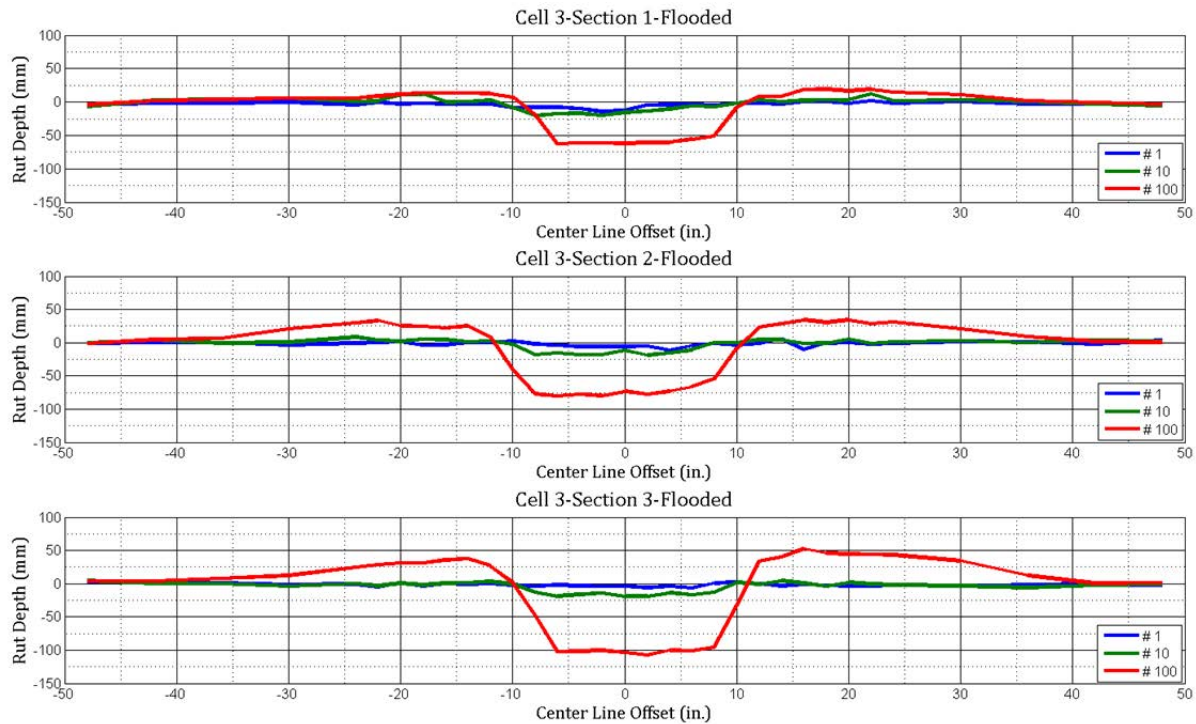


Figure 4.20. Rut developments in crushed dolomite sections in Cell 3 resulting from unidirectional ATLAS loading under flooded conditions. Sections 1, 2, and 3 correspond to aggregate layers of thicknesses 14, 12, and 8 in., respectively (1 in. = 25.4 mm).

As shown in Figure 4.20, no significant rutting was observed in the test sections for up to 10 load applications. However, upon further loading, the rutting in the sections became more apparent with the 8-in. aggregate layer in Section 3 accumulating the most rutting. An important observation can be made regarding the square nature of the rut formations shown in Figure 4.20. Carbonate cementation of the fines fraction resulted in the aggregate layer performing almost like a stiff bound layer showing punching failure from penetration into the subgrade weakened by flooding.

Figure C-3 in Appendix C shows the deformed layer boundaries as obtained from excavated transverse trenches in the three Cell 3 sections. Subgrade deformation and movement at the aggregate-subgrade interface became more apparent with decreases in the aggregate layer thickness. As observed in the case of other test cells, flooding of the test sections led to weakening of the subgrade, which failed by undergoing excessive deformation.

4.7 CELL 4: CRUSHED LIMESTONE WITH HIGH AMOUNTS OF NONPLASTIC FINES

The effect of high amounts of nonplastic fines on the performance of a crushed limestone aggregate was evaluated through accelerated pavement testing of construction platform sections under near-optimum and flooded aggregate moisture conditions. As already mentioned, the crushed limestone used in this cell (Cell 4) had higher fines contents (~10%) compared with those initially obtained during preliminary survey of potential aggregate sources and was therefore classified as a high fines material. Like the uncrushed gravel used in Cell 1, the crushed limestone material in Cell 4 also comprised high amounts of nonplastic fines. Therefore, comparative analyses of Cell 1 and Cell 4 performances would emphasize the effect of aggregate shape and angularity.

4.7.1 Performance at Near-Optimum Moisture Conditions

Figure 4.21 shows the final deformed profile for the 14-in. (356-mm) thick aggregate section in Cell 4. The test section could sustain 168 load applications before accumulating rut depths of approximately 4 in. (100 mm). Moreover, no surface heave was observed adjacent to the wheel path. The GPR scan and excavated trench sections clearly indicate a more defined subgrade deformation pattern compared with those observed in Cell 1 (see Figures 4.21a and 4.21b). Moreover, the subgrade depression was directly underneath the surface rut, indicating no significant shear movement within the aggregate layer—a result of improved particle-to-particle interlock. The apparent basin shape of the deformed subgrade (see Figure 4.21b) was attributed to the superior load spreading abilities of the crushed aggregate base course.

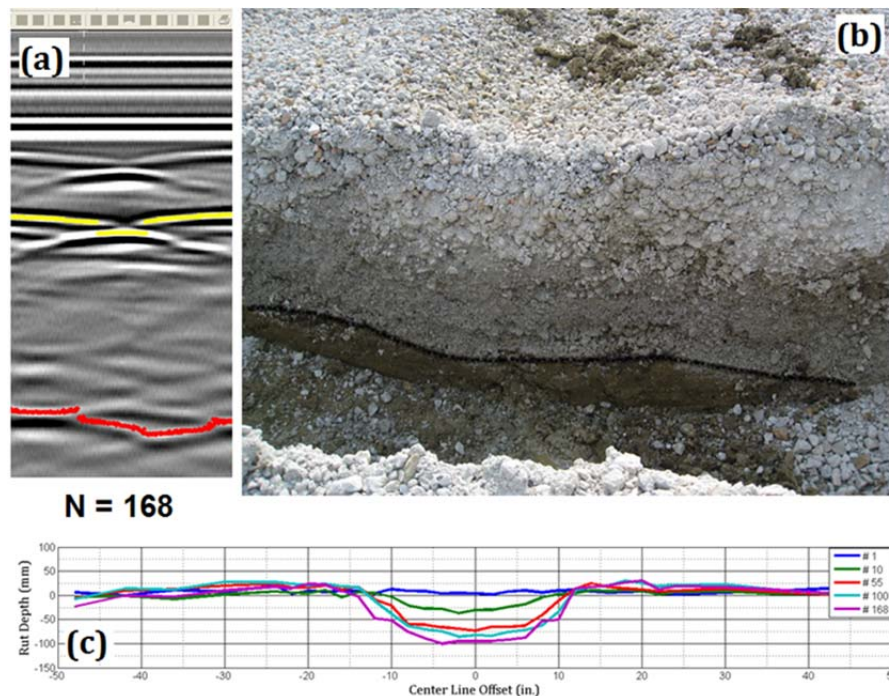


Figure 4.21. (a) GPR scan, (b) excavated trench, and (c) surface rut profile of the 14-in. (356-mm) thick crushed limestone section in Cell 4 (1 in. = 25.4 mm).

Figure 4.22 shows the final deformed profile of Cell 4 Section 2 (12-in.-thick aggregate layer). Unlike Section 1, this section showed significant heaving adjacent to the wheel path after 55 load applications (see Figure 4.22c). Moreover, as can be seen from the GPR scan, the subgrade deformation is offset from the wheel path, and hence shows the possibility of shear flow of the material. Close inspection of as-constructed moisture contents of the subgrade layer explained the excessive surface heave development in Section 2. Average moisture contents for the engineered subgrade layer in Sections 1, 2, and 3 were 13.1%, 15.2%, and 13.3%, respectively. As discussed in Chapter 3, a moisture content of approximately 13% was targeted for preparing an engineered subgrade of IBV = 3%. However, as shown in Figure 3.8, the IBV value for the subgrade soil decreases rapidly with increasing moisture contents; note that a moisture content of 15% corresponds to IBV values of less than 1%.

The significantly weaker subgrade conditions (owing to the higher moisture contents) under the 12-in.-thick aggregate layer in Section 2 resulted in failure of this section. The aggregate-subgrade layer interface observed from the excavated trench (see Figure 4.22b) clearly showed significant subgrade movement, and the surface heave observed was a direct reflection of subgrade heave.

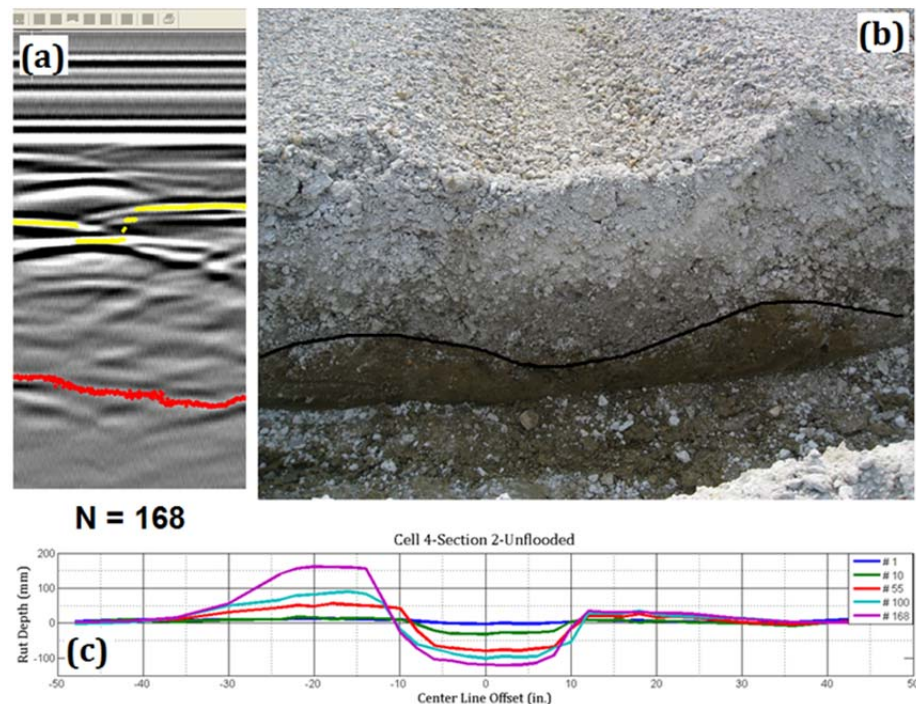


Figure 4.22. (a) GPR scan, (b) excavated trench, and (c) surface rut profile of the 12-in. (305-mm) thick crushed limestone section in Cell 4 (1 in. = 25.4 mm).

Figure 4.23 presents the deformed layer profiles for the 8-in.-thick aggregate layer in Section 3 of Cell 4. As apparent from the GPR scan and the trench sections (see Figures 4.23a and 4.23b), the subgrade deformation underneath the wheel path was clearly visible, and the surface heave noticed was primarily a reflection of the subgrade deformation.

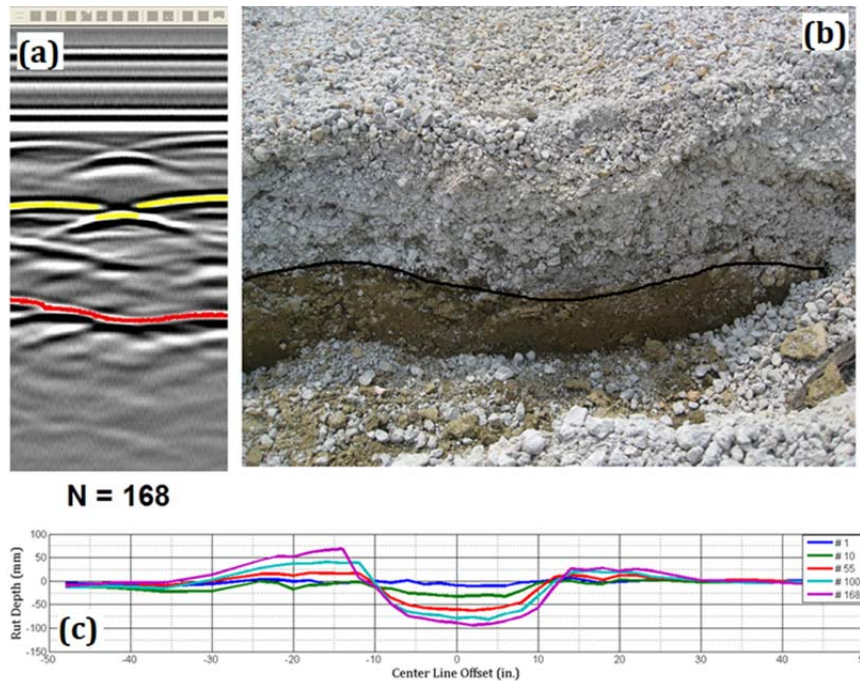


Figure 4.23. (a) GPR scan, (b) excavated trench, and (c) surface rut profile of the 8-in. (203-mm) thick crushed limestone section in Cell 4 (1 in. = 25.4 mm).

4.7.2 Performance Under Flooded Conditions

Figure 4.24 shows the development of rutting in Sections 1, 2, and 3 under flooded conditions for the crushed limestone with high amounts of nonplastic fines. The layer interface boundaries as observed from excavated transverse trenches are shown in Figure C-4 in Appendix C.

As indicated in Figures 4.24 and C-4, both Sections 1 and 3 underwent subgrade failure and showed significant heaving at the aggregate-subgrade interface, which was ultimately reflected on to the surface. After 97 load applications, Section 1 showed the highest rut accumulation (approximately 6-in.). This may have been caused by the combined effect of excess moisture and high amounts (10%) of fines in the aggregate matrix. Section 3 (8-in.-thick aggregate layer) showed the highest amount of subgrade movement, which was attributed to the higher stress levels at the subgrade interface underneath the thinnest aggregate layer.

From testing under near-optimum as well as flooded aggregate moisture conditions, the primary mechanism contributing to the pavement failure in Cell 4 was subgrade rutting. The crushed limestone with high fines did not undergo internal shear movement. Layer thickness was the primary factor governing pavement performance, with Section 3 (203-mm aggregate layer) failing first from inadequate stress dissipation at the subgrade interface. Section 1 (14-in. aggregate layer) performed consistently better than Section 3 (8-in. aggregate layer) under near-optimum aggregate moisture conditions. Section 1 showed the highest rut accumulation under flooded conditions, which may have been the result of the combined effect of excess moisture and high amount of fines in the aggregate layer. Section 2 (12-in.-thick aggregate layer) showed the highest surface heave at near-optimum conditions. This was attributed to significantly weaker subgrade conditions. The performance of Section 2 under flooded conditions could not be explained. This could possibly be related to the slightly better subgrade conditions in Section 2 along the flooded

wheel path, or local variations in the particle size distribution of the constructed aggregate layer with respect to Sections 1 and 3.

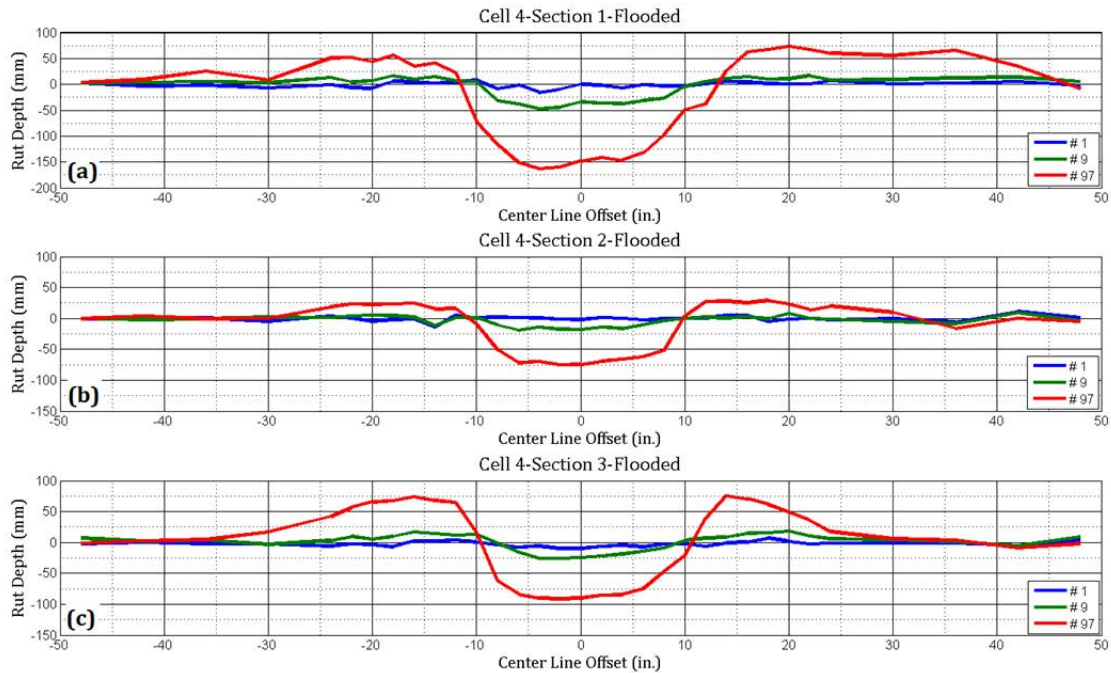


Figure 4.24. Rut developments in Cell 4 sections resulting from unidirectional ATLAS loading under flooded conditions. Sections 1, 2, and 3 correspond to aggregate layers of thicknesses 14, 12, and 8 in., respectively (1 in. = 25.4 mm).

4.8 CELL 5: CRUSHED LIMESTONE WITH LOW AMOUNTS OF PLASTIC FINES

Cell 5 was constructed using the same material as in Cell 2 (crushed limestone with low amounts of plastic fines) over a subgrade IBV of 6%, and comprised aggregate layers of thicknesses 10, 8, and 6 in. (254, 203, and 152 mm) for Sections 1, 2, and 3, respectively. The primary objective of including this test cell was to evaluate the effects of better subgrade conditions on thickness design and performance of aggregate working platforms.

4.8.1 Performance at Near-Optimum Moisture Conditions

Figure 4.25 shows GPR scan, excavated trench, and surface profile of Section 1 (10-in.-thick aggregate layer) in Cell 5 tested under near-optimum aggregate moisture conditions. From the figure, Section 1 could sustain 478 load applications without significant rut accumulation or development of surface heave. Moreover, a close examination of the GPR scan (Figure 4.25a) and excavated trench section (Figure 4.25b) clearly indicated the absence of any subgrade shear failure. The rutting observed on the surface was probably from aggregate compaction/consolidation and subgrade movement that could not be visually identified from the trench sections.

Figure 4.26 shows the deformed layer profiles for Section 2 (8-in.-thick aggregate layer) in Cell 5. As shown in the figure, no significant heaving of the surface was observed up to 100 load applications. However, upon further loading, the surface heave became more apparent. The GPR scan and excavated trench sections showed clearly defined subgrade deformation under the wheel path. Moreover, the surface heave was a reflection of

subgrade movement. This failure mechanism was much more apparent in Section 3 (6-in.-thick aggregate section), as shown in Figure 4.27.

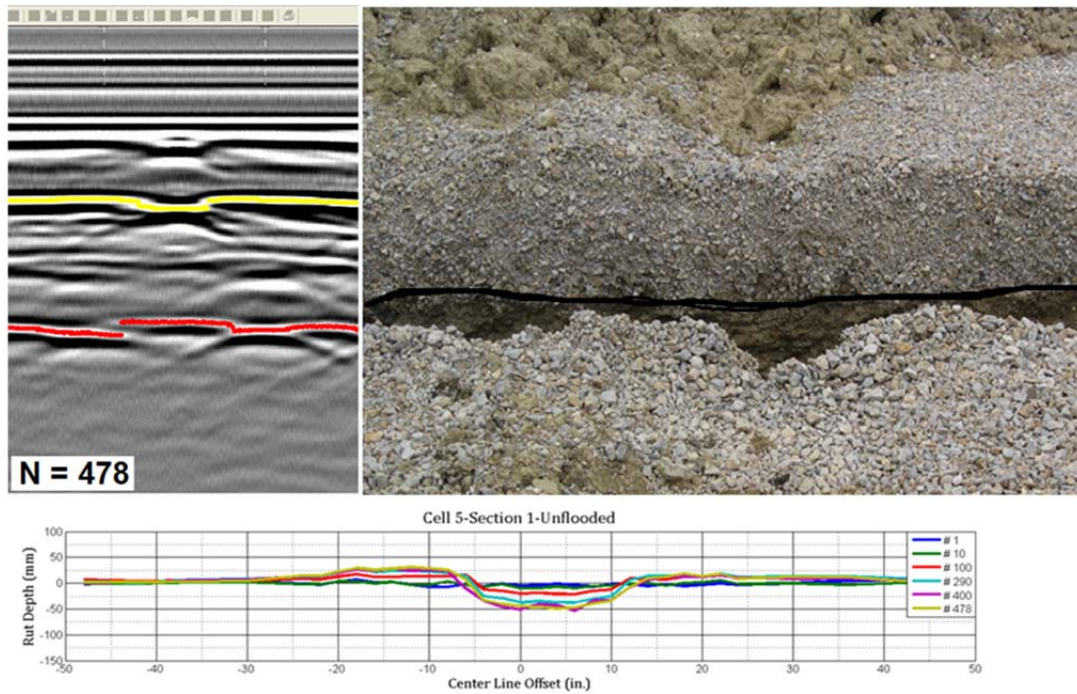


Figure 4.25. (a) GPR scan, (b) excavated trench, and (c) surface rut profile of the 10-in. (254-mm) thick crushed limestone section in Cell 5 (1 in. = 25.4 mm).

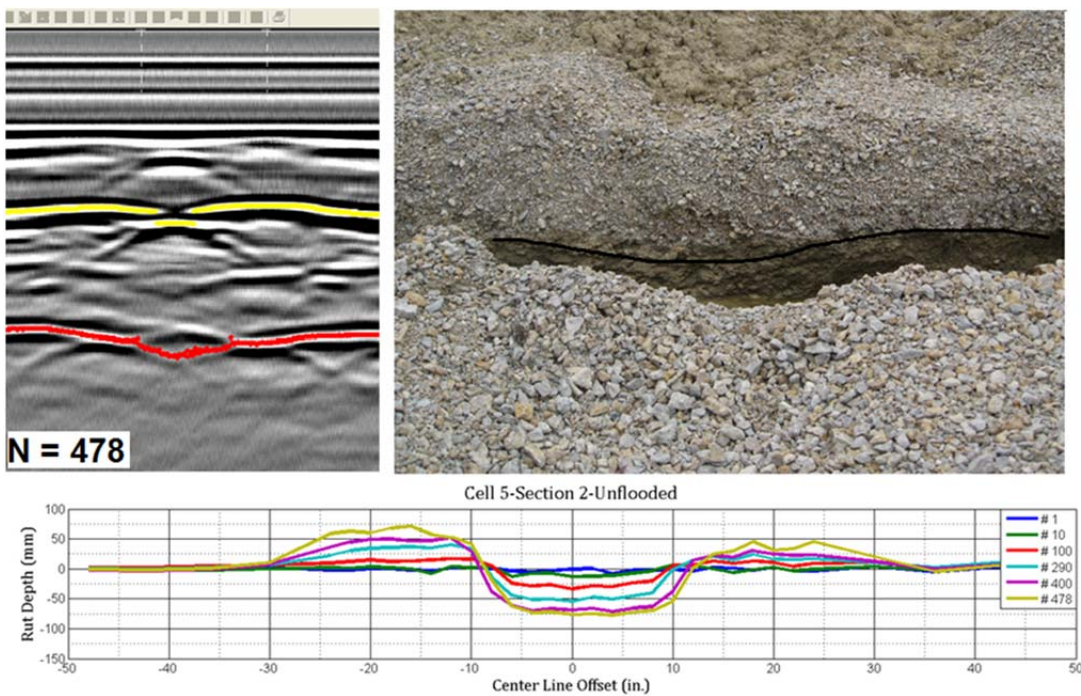


Figure 4.26. (a) GPR scan, (b) excavated trench, and (c) surface rut profile of the 8-in. (203-mm) thick crushed limestone section in Cell 5 (1 in. = 25.4 mm).

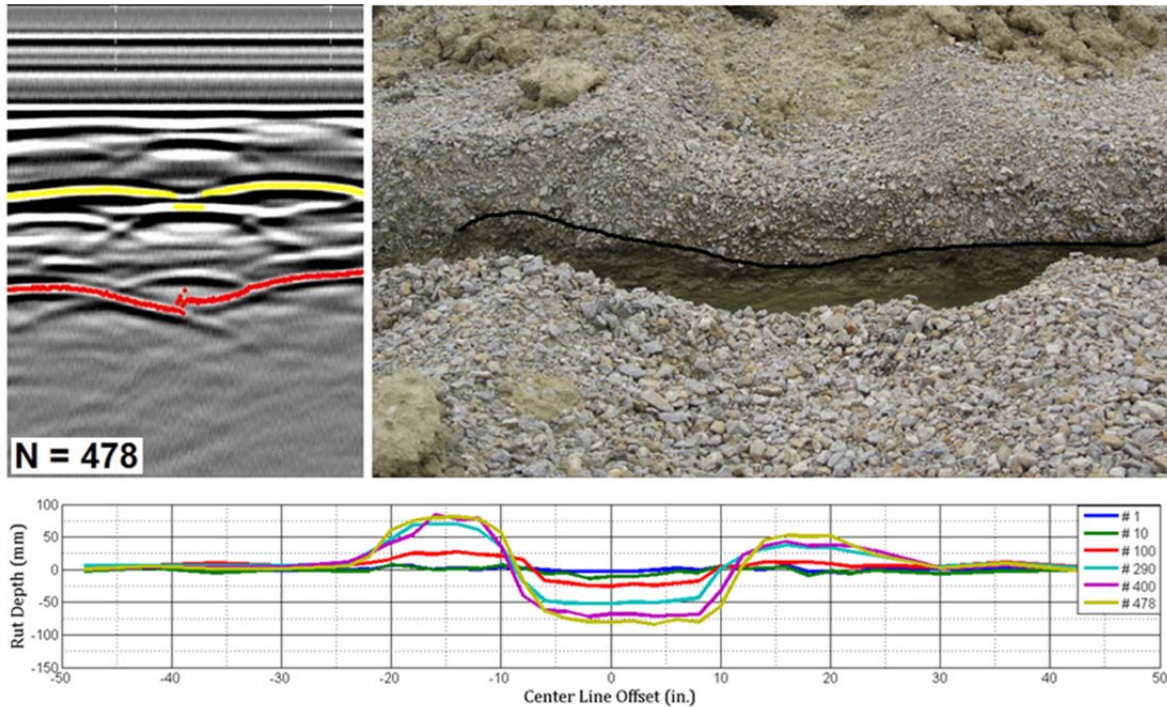


Figure 4.27. (a) GPR scan, (b) excavated trench, and (c) surface rut profile of the 6-in. (152-mm) thick crushed limestone section in Cell 5 (1 in. = 25.4 mm).

The improvement in rutting performance achieved from better subgrade support was clearly evident for Cell 5. Close examination of GPR scans and excavated trenches for the three test sections identified the different modes contributing to failure. Section 1 performed the best without undergoing shear failure even after 478 load applications. The rutting in Section 1 was probably from compaction/consolidation of aggregate and subgrade deformations that could not be visually identified from the excavated trench sections. The subgrade rutting pattern became clearly evident as the aggregate layer thickness decreased and no significant shear movement within the aggregate layer was observed. For Sections 2 and 3, rapid heaving of the aggregate surface was observed after 100 load applications.

4.8.2 Performance Under Flooded Conditions

Figure 4.28 shows the development of rutting in the three test sections of Cell 5 under flooded conditions. The test section performances under flooded conditions clearly showed the effect of excessive moisture on pavement performance, particularly for thin aggregate layers. Section 3 (6-in.-thick aggregate layer) showed rapid permanent deformation accumulation and developed significant surface heave after 125 load applications. Test section performance was significantly better for the thick aggregate sections with Section 1 (10-in.-thick aggregate layer) sustaining 216 load applications with much less rutting accumulated.

Examination of transverse trench sections revealed subgrade deformation to be the primary mechanism contributing failure of the test sections under flooded conditions. Figure C-5 in Appendix C shows the deformed layer boundaries for the aggregate surface as well as the aggregate-subgrade interface after testing under flooded conditions. As seen from the excavated trench sections, flooding of Cell 5 reduced the subgrade strength; therefore, the pavement sections failed at a lower number of load applications compared with the near-

optimum aggregate moisture conditions. However, the modes of failure for the three aggregate sections were similar to those under near-optimum aggregate moisture conditions. Section 1 (10-in.-thick aggregate layer) did not show any significant heave development adjacent to the wheel path, whereas progressively increasing heaving was observed for Sections 2 and 3 having 8-in.- and 6-in.-thick aggregate layers, respectively. The highest surface heave was observed for Section 3, which had the highest subgrade stress levels underneath the 6-in. (152-mm) thick aggregate layer. The subgrade strength was significantly reduced as a result of flooding; higher stresses applied on the weak subgrade resulted in subgrade shear failure accompanied by surface heave development.

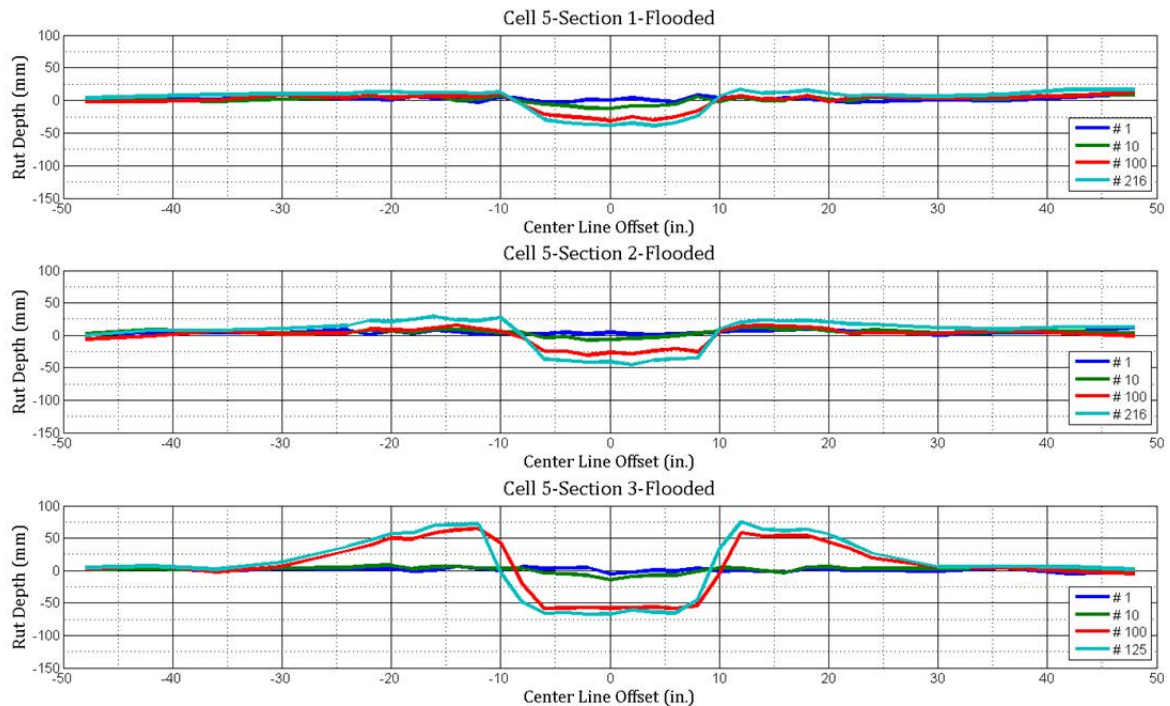


Figure 4.28. Rut developments in crushed limestone sections in Cell 5 resulting from unidirectional ATLAS loading under flooded conditions. Sections 1, 2, and 3 correspond to aggregate layers of thicknesses 10, 8, and 6 in., respectively (1 in. = 25.4 mm).

4.9 CELL 6: LARGE-SIZE AGGREGATE APPLICATIONS FOR CONSTRUCTION PLATFORMS

As already mentioned in Chapter 3, Cell 6 was constructed over a subgrade of IBV = 1% by placing a 12-in. layer of large-size aggregate material, which was subsequently capped by placing a 6-in. layer of dense-graded CA-6 material. The three sections in Cell 6 comprised large-size aggregate materials obtained from the following three different sources: (1) D6 rockfill for subgrade, primary crusher run (largest in size); (2) D3 aggregate subgrade gradation #1 (intermediate size); and (3) rip rap gradation #1 (the smallest size among the three large-size aggregate materials). The primary objective behind construction and testing of Cell 6 was to evaluate the performances of different types of large-size aggregate materials in construction platform applications, which would ultimately aid the development of material specifications defining the types and properties of large-size

aggregate materials for unbound aggregate layer applications. The effectiveness of geotextile reinforcement alongside large-size aggregate materials for construction platform applications was evaluated by placing a geotextile at the subgrade/large-size aggregate layer interface along the south wheel path. By comparing rut accumulations along the north and south wheel paths in Cell 6, the goal was to investigate and identify the reinforcement and separation benefits of the geotextile used at the subgrade/large-size aggregate layer interface.

4.9.1 North Wheel Path: Unreinforced

Figure 4.29 shows the rut accumulations in Sections 1, 2, and 3 of Cell 6 under unreinforced (no geotextile) conditions. Interestingly, after 63 passes of the 10-kip single wheel load, the intermediate-size D3 aggregate (Section 2) had the highest 4-in. rut accumulation when compared with the 2-in. rut depth observed for the smallest-size rip rap (Section 1). The largest size D6 rockfill primary crusher run material (Section 1) performed the best among the three large-size aggregate materials and accumulated only 1-in. of rut after 63 passes.

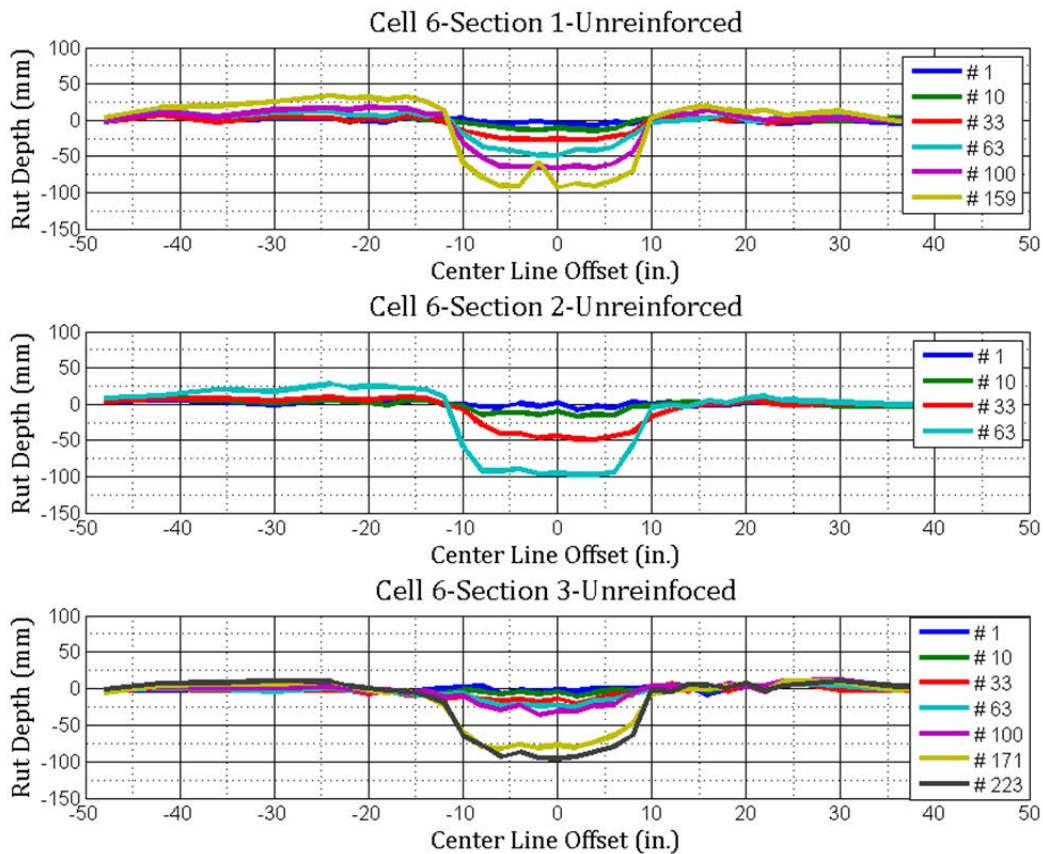


Figure 4.29. Rut developments in Cell 6 test sections resulting from unidirectional ATLAS loading under unreinforced (no geotextile) conditions. Sections 1, 2, and 3 correspond to rip rap gradation # 1, D3 aggregate-subgrade gradation # 1, and D6 rockfill for subgrade-primary crusher run, respectively (1 in. = 25.4 mm).

Significantly improved performance for the D6 rockfill material (Section 3) was most likely caused by the bridging of large aggregates across the 12-in. engineered subgrade layer. Similarly, the improved performance of the smallest rip rap in Section 1 was probably the result of dense packing of the large-size aggregate material matrix. For the D3 aggregate in Section 2, a rapid increase in rutting rate (from 2 in. to 4 in.) was observed between load application numbers 33 and 63. None of the sections in Cell 6 showed significant heave development adjacent to the wheel path. This indicated the absence of significant shear movement within the aggregate layer. Subgrade deformation was the primary mechanism contributing to the failure of the test sections. Excavation of transverse trenches clearly showed subgrade intrusion into the large-size aggregate material layers.

4.9.2 South Wheel Path: Geotextile Reinforced

Figure 4.30 shows the rut accumulation in Sections 1, 2 and 3 of Cell 6 when tested along the geotextile-reinforced wheel path. As mentioned earlier, a woven geotextile was placed over the engineered subgrade layer before placing the large-size aggregate material along the south wheel path. When the geotextile was placed over the subgrade, the wheel path trafficking performances were greatly improved in all the test sections; the number of load passes needed for the same rut depths increased for almost up to three folds. Section 2 sustained 159 load applications before accumulating approximately 4 in. of rutting compared with 63 load applications in the unreinforced case because of the more-uniform load distribution (see Figure 4.30). Unlike the unreinforced wheel path, no sudden increase in the rut depth with increased number of load applications was noticed. Excavation of transverse trench sections indicated the effectiveness of the geotextile in separation and, hence, mitigating the contamination of the large-size aggregate layer caused by subgrade intrusion.

4.10 SUMMARY OF TEST SECTION PERFORMANCE

This chapter reported results from accelerated pavement testing, and performance analyses of full-scale pavement working platform test sections constructed in this research study. Six different pavement working platform test cells were constructed using different combinations of aggregate physical properties, and were loaded to failure at near-optimum and flooded aggregate moisture conditions. Different mechanisms contributing to failure of the test sections were investigated by analyzing results from surface rut profiles, GPR scans, and excavated trench sections.

Significant differences in aggregate qualities led to different mechanisms of rut accumulation in the pavement working platform test sections. The uncrushed gravel in Cell 1 showed excessive shear movement within the aggregate layer, whereas the crushed aggregate sections in Cells 3, 4, and 5 failed primarily as a result of subgrade rutting. The crushed limestone material with low fines used in Cell 2 showed unstable matrix behavior under standard compaction conditions. This led to internal shear failure of Section 1 (14-in.-thick aggregate layer) in Cell 2. However, at higher relative compaction levels, the material showed adequate performance, and no significant shear movement within the aggregate layer was observed. Excessive subgrade deformation was the primary mechanism contributing to failure of the pavement sections under such conditions.

The effect of stronger subgrade conditions on unsurfaced pavement performance was clearly evident from the significantly higher number of load applications sustained by Cell 5 before failure. Cell 5 was constructed using the same aggregate material as in Cell 2, and it did not exhibit any significant shear movement within the aggregate layers, with failure of the test sections being primarily attributable to subgrade shear.

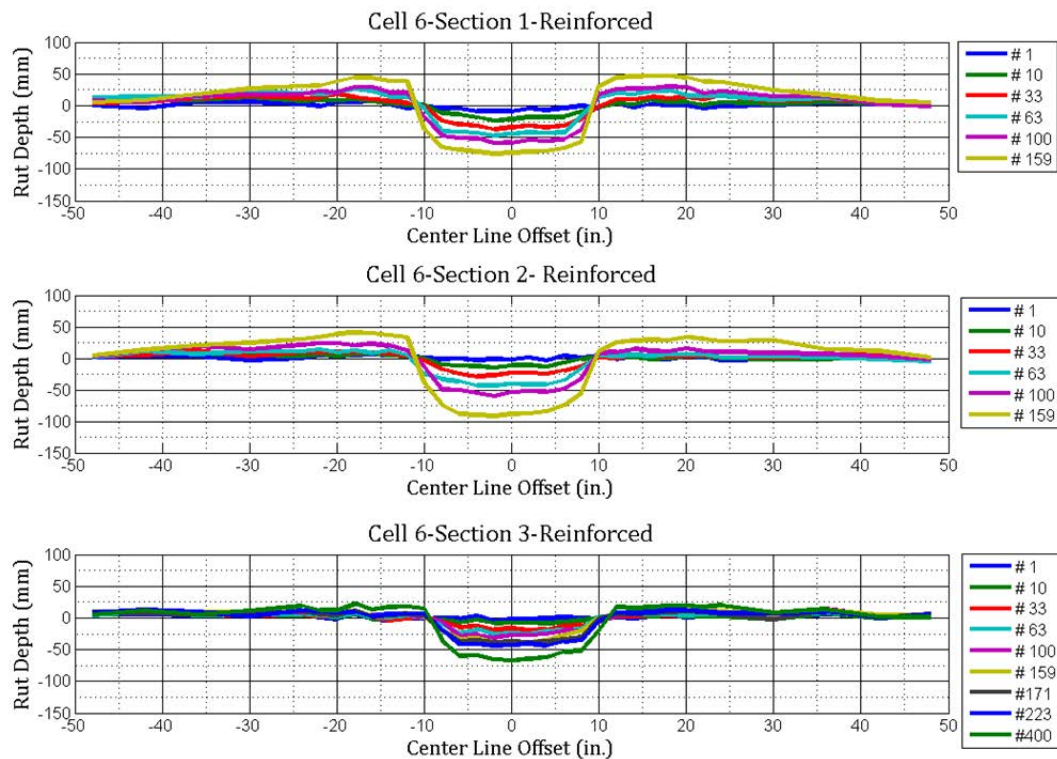


Figure 4.30. Rut developments in Cell 6 test sections resulting from unidirectional ATLAS loading under geotextile-reinforced conditions at the subgrade interface. Sections 1, 2, and 3 correspond to rip rap gradation # 1, D3 aggregate-subgrade gradation # 1, and D6 rockfill for subgrade-primary crusher run, respectively (1 in. = 25.4 mm).

Test Cell 3, constructed using a crushed dolomite material with high amounts of nonplastic fines, was subjected to over-the-winter effects, i.e., freeze-thaw cycles, which resulted in significant strength gain. This strength gain was attributed to carbonate cementation of the fines fraction and improved suction characteristics resulting from freeze-thaw cycles. The improved strength and modulus characteristics were apparent from the change in aggregate layer moduli measured using a GeoGauge™ before and after the freeze-thaw cycles (aggregate moduli increased by up to 225%). The resulting stiffer aggregate layers sustained a much higher number of load applications without undergoing significant rutting.

Test section failures under flooded conditions were primarily attributable to excessive shear movements observed in the subgrade layer. Ingress of moisture upon flooding significantly reduced the subgrade strength for all the test cells and ultimately caused more rapid subgrade deformations resulting from ATLAS loading.

Testing of Cell 6 comprising three different large-size aggregate materials under unreinforced and geotextile-reinforced conditions clearly highlighted effectiveness of the geotextile in uniform dissipation of stresses as well as in separation and mitigation of subgrade intrusion into the large-size aggregate layer.

CHAPTER 5 DISCUSSION AND RECOMMENDATIONS

5.1 SUMMARY OF RESEARCH SCOPE

The ultimate objective of this research project was to incorporate aggregate material quality aspects into the thickness designs of aggregate layers for pavement working platform applications through modification of the design curve presented in Figure A-2 of the IDOT SSM.

The first phase of the study (Tutumluer et al. 2009) characterized in the laboratory the strength, stiffness, and deformation behaviors of three different aggregate types commonly used in Illinois for construction platform applications. The aggregate physical properties (test factors) used as material quality indicators were particle shape, texture and angularity, amount of fines (material finer than 0.075 mm or passing sieve No. 200), plasticity of fines (measured on material finer than 0.425 mm or passing sieve No. 40), and compaction (moisture-density) conditions. Through completion of a factorial laboratory test matrix, the researchers evaluated individual effects of the test factors on aggregate strength, (resilient) modulus, and permanent deformation behaviors. Important findings from laboratory testing of aggregates resulted in the development of several tentative correction factors for use alongside Figure A-2 of the IDOT SSM.

Phase II of the study documented in this report was carried out to validate the initial recommendations based on the Phase I laboratory test results. Six different full-scale pavement working platform test cells were constructed representing different combinations of aggregate type and quality, as well as subgrade conditions. The test cells were subsequently loaded to failure thorough unidirectional application of a 10-kip single wheel load; performance under loading was monitored through surface profile measurements and transverse GPR scanning. Important performance trends observed from accelerated testing of the full-scale test sections were reported in Chapter 4, and different mechanisms contributing to the failure of individual cells were highlighted.

This chapter analyzes the test section performances in light of potential modifications to the design curve for aggregate cover layer thickness used by IDOT. Performance trends reported by Heckel (2009) from controlled loading conditions in a test loop were used as a basis of reference for comparing the rut depths in individual test sections. The primary objective was to examine the validity of tentative correction factors recommended from Phase I of the research study (shown in Table 2.1). Through combined analyses of laboratory and field test results, important recommendations are made regarding material specification and construction protocols for inclusion in the IDOT SSM.

5.2 MODIFICATION OF DESIGN CURVE FOR AGGREGATE COVER LAYER THICKNESS

Table 5.1 summarizes the aggregate material designations, the constructed, and the as-recommended layer thicknesses from the current IDOT SSM, along with the tentative correction factors and the in-place moisture-density data for the aggregate layers tested during this project.

Table 5.1. Summary of Test Section Configurations Along with Recommended Thicknesses

Cell	Aggregate Type	Subgrade IBV (Target)	SSM Recommended Thickness (in.)	Thickness using Phase I Factors (in.)		Section Thickness (in.)	Relative Compaction (%)*	In-Place Moisture (%)
				Dry	Wet			
1	Uncrushed Gravel: High Amounts of Nonplastic Fines	3	12	13	18.8	14	95.1	7.6
						12	94.8	7.3
						8	96.2	6.9
2	Crushed Limestone: Low Amounts of Plastic Fines			7.7	9.6	14	103.9	3.6
						12	106.5	3.5
						8	108.7	3.0
3	Crushed Dolomite: High Amounts of Nonplastic Fines			9.6	13.4	14	91.7	6.1
						12	89.2	6.1
						8	91.7	5.8
4	Crushed Limestone: High Amounts of Nonplastic Fines			9.6	13.4	14	90.4	3.6
						12	92.1	4.2
						8	94.0	4.1
5	Crushed Limestone: Low Amounts of Plastic Fines	6	8	5.1	6.4	10	108.0	3.6
						8	112.0	4.0
						6	107.5	3.6

*With Respect to ASTM D 698 Maximum Dry Density

As listed in Table 5.1, the IDOT recommended aggregate cover thickness over a subgrade of IBV = 3% is 12 in. (from Figure A-2 of the IDOT SSM). Therefore, the 12-in.-thick aggregate layers in Cells 1 through 4 could be treated as control sections for comparing the accumulated ruts with IDOT-specified threshold values. Moreover, the modified aggregate cover thicknesses calculated using the preliminary correction factors recommended from Phase I of the research project are also listed in Table 5.1. As shown in the table, application of the preliminary correction factors (listed in Table 2.1) resulted in a reduction in aggregate layer thicknesses for Cells 2 through 5 (incorporating crushed aggregates) for the dry or optimum moisture conditions, whereas the recommended aggregate layer thickness increased (to 13 in.) for Cell 1 constructed with the uncrushed gravel material with high amounts of nonplastic fines. Ideally, for validating the correction factors recommended based on the laboratory test results in Phase I, the measured rut depths for different aggregate layer thicknesses should be compared with the IDOT-specified threshold value (0.5 in.) for permissible rutting in a pavement working platform under construction traffic.

Accordingly, Table 5.2 lists the measured rut depths for different test sections in Cells 1 through 5 under near-optimum and flooded aggregate moisture conditions after 1, 10, and 100 applications of unidirectional ATLAS loading. Comparisons of the accumulated rut amounts after different numbers of load applications with the IDOT-recommended threshold values would establish the applicability of the correction factors approach for appropriate thickness designs of aggregate cover layers. The following observations and conclusions can be made regarding the measured rut depths after 1, 10, and 100 load applications for the different full-scale test sections.

Table 5.2. Maximum Rut Depths in Different Test Sections After 1, 10, and 100 Load Applications

Cell	Section Thickness (in.)	Rut Depth (mm)					
		N = 1		N = 10		N = 100	
		Near-Optimum	Flooded	Near-Optimum	Flooded	Near-Optimum	Flooded
1	14	16.8	7.8	39.4	35.4	N/A	N/A
	12	7.4	14.4	22.1	50.6	66.2	N/A
	8	6.2	10.0	10.2	40.7	19.9	N/A
2	14	14.0	8.9	38.0	30.5	N/A	N/A
	12	11.7	9.3	30.8	29.7	92.6	N/A
	8	8.1	1.3	6.5	13.4	21.8	N/A
3	14	11.7	14.4	15.7	20.7	30.3	62.8
	12	8.3	11.8	16.0	18.8	55.6	80.6
	8	6.9	6.5	10.8	19.1	99.1	107.6
4	14	-8.0*	15.6	36.7	47.0	85.7	163.6**
	12	2.5	13.9	31.5	19.1	101.1	75.1**
	8	10.9	9.9	32.9	26.2	81.6	91.1**
5	10	7.2	3.5	9.9	12.5	21.2	31.4
	8	7.8	-0.3	13.2	7.2	32.9	30.4
	6	2.8	5.5	13.9	13.7	25.1	58.6
* No clear rutting was observed. The negative value indicates surface heave							
** Surface profile measured after 97 load applications							

No consistent trend in the effects of material quality or moisture conditions on measured rut depths was observed after the first load application (N = 1). This was clearly evident from instances of higher rut depths under near-optimum aggregate moisture conditions compared with flooded conditions. This discrepancy was probably a result of particle rearrangement in the unbound aggregate surface layer under initial load applications. However, the effects of material quality and moisture conditions on performance became gradually apparent with an increase in the number of load applications. Because of internal shear movement of the aggregate layer under near-optimum moisture conditions, the 14-in.-thick sections (Section 1) in Cells 1 and 2 could not be tested to 100 load applications. Similarly, under flooded conditions, several test sections failed by accumulating rut amounts greater than 4 in. Rut depths corresponding to such sections are listed as N/A in Table 5.2.

The measured rut depths in most of the test sections exceeded the IDOT SSM threshold value of 13 mm (0.5 in.) after only 10 load applications. This was observed for near-optimum as well as flooded aggregate moisture conditions. The exception was that the 8-in.-thick sections of Cells 1 and 2 yielded 10.2-mm and 6.5-mm permanent deformations, respectively (see Table 5.2), after 10 load applications as a result of the much stronger subgrade IBV values achieved during construction (for Cell 1) and better compaction of aggregate layer (for Cell 2), as discussed in Chapter 4. Upon testing all sections to 100 load applications, the measured ruts often exceeded 2 in. (50 mm), with certain sections accumulating nearly 4-in. rutting. Therefore, evaluating the effect of aggregate material type and quality on pavement working platform performance was not possible using the IDOT-specified threshold rut depth of 0.5 in. (13 mm) as a reference. However, upon careful

analyses of aggregate and subgrade layer construction conditions, as well as taking into account the laboratory aggregate test results from the Phase I study, the effects of different aggregate physical properties on construction platform performance could still be identified.

For example, all three test sections in Cell 5 (subgrade IBV = 6%) consistently accumulated lower rut amounts when compared with the other test cells after 100 load applications. This was a clear indication of improved performance resulting from better subgrade conditions. A comparison of the aggregate layer compaction information presented in Table 5.1 indicates that the test sections in Cells 2 and 5 (both constructed using material 2) were compacted to similar densities. However, the better subgrade conditions in Cell 5 (IBV = 6% compared with IBV = 3% for Cell 2) provided stronger platforms for compaction of the aggregate layers, which ultimately resulted in lower rut depths. Unlike the 14-in. aggregate layer in Cell 2, none of the layers in Cell 5 showed internal shear movement. For the same aggregate material type, stronger subgrade conditions consistently resulted in significantly improved test section performances. This can clearly be established by comparing the maximum rut depths for the test sections in Cells 2 (subgrade IBV = 3%) and 5 (subgrade IBV = 6%). For the stronger subgrade conditions in Cell 5, lower rut depths were observed even for sections with reduced aggregate layer thicknesses when compared with Cell 2.

As discussed in Chapter 4, the crushed dolomite sections in Cell 3 performed significantly better than the other test cells constructed over similar subgrade conditions. Improved performance of Cell 3 was attributed to the possible carbonate-cementation mechanism within the dolomite fines upon prolonged exposure to moisture during winter freeze-thaw cycles. Although the test sections in Cell 3 could sustain a high number of load applications (700 load applications for Section 1) without undergoing shear failure, the accumulated rut amounts were higher than 0.5 in. after only 10 load applications. Therefore, limiting the surface rut accumulation to below 0.5 in. was not possible for any test section constructed over a subgrade of IBV = 3%. This leads the researchers to believe that the permissible rut depth criterion specified by the IDOT SSM under construction traffic loading may be difficult to control in the field if construction traffic is not limited accordingly. Such a criterion could be satisfied only for a low number of load applications (fewer than 10) with significantly strong subgrade conditions as demonstrated for Cell 5. Heckel (2009) reported approximately 60 equivalent load passes, which were required to supply material to pave a 6-in.-thick HMA lift over 1,000 ft of a 24-ft-wide roadway. Because of the need for such a high number of load passes, considered together with the current study findings on the rutting performances of full-scale aggregate construction platform test sections, the 0.5-in. rut depth criterion in the IDOT SSM may often become impractical if not impossible to satisfy.

Owing to different mechanisms as well as factors contributing to the high permanent deformation accumulations in the test sections, increasing/decreasing or adjusting the aggregate cover layer thicknesses using correction factors may not be the most efficient approach to ensure adequate subgrade stability under construction traffic. For example, an uncrushed gravel material with high amounts of fines will not perform satisfactorily in the field even though its layer thickness is increased using the correction factors, as listed in Table 5.1 with the 13-in. corrected thickness in this study. This is because such poor-quality aggregate cover material tends to fail internally as a result of low shear resistance, and a much thicker layer of this failing material will not prevent excessive rut accumulation on the surface. Similarly, wet of optimum construction conditions are expected to produce excessive permanent deformations, as listed in Table 5.2 from the current study findings. Accordingly, an 18.8-in.-thick gravel layer constructed in wet (or flooded) conditions, as listed in Table 5.1, will not necessarily outperform a 13-in.-thick gravel layer with high amounts of fines. In fact, they will both fail during the working platform construction stage.

Therefore, applying the correction factors to the original thickness from Figure A-2 of the IDOT SSM is not a viable option for such uncrushed gravel materials with high fines.

The applicability of the correction factors recommended from the laboratory test results in Phase I to the crushed limestone and dolomite materials used in the state of Illinois is probably more feasible when compared with the gravel materials. Further, the data in Table 5.1 suggest there might be room to reduce crushed stone aggregate layer thicknesses and economize the use of crushed aggregates for working platform aggregate cover designs. Even though much thicker crushed stone layers were actually constructed in the test sections for dry or near-optimum conditions than those recommended by the applied correction factors from Phase I (see Table 5.1), surface ruts in excess of the 0.5-in. allowed by the IDOT SSM were still generated in fewer than 10 load applications. This fact alone suggests that specifications for material selection and construction protocols should be revised and incorporated into the IDOT SSM to ensure adequate performance of construction platforms. This can be accomplished through consideration of improved material quality aspects as well as more realistic wheel load coverages and/or threshold rut depths in the field under construction traffic.

In summary, the correction coefficients listed in Table 2.1 may not represent the best approach for ensuring adequate performance of pavement working platforms constructed using different aggregate material types. Although the detrimental effects of some of the factors studied in this research project on aggregate performance were clearly apparent from the laboratory test results in Phase I, not all hypotheses drawn from the laboratory testing could be verified through accelerated pavement testing. Accordingly, based on the laboratory and field test results from the two phases of this research study, the researchers propose the following for inclusion in the IDOT SSM.

5.3 RECOMMENDATIONS FOR MODIFICATION OF IDOT SSM

5.3.1 Aggregate Type

Laboratory and field test results both indicated aggregate angularity to be the most important factor governing aggregate layer behavior. These findings are in agreement with results reported by Barksdale and Itani (1989). Therefore, the researchers recommend prohibiting the use of uncrushed gravel (irrespective of the fines content) for construction platform applications. Although the current research study evaluated the performance of an uncrushed gravel material with high amounts of nonplastic fines, Heckel (2009) studied the performance of an uncrushed gravel material with moderate amounts (~7%) of plastic fines. From monitoring the performance of several test sections under controlled loading, Heckel reported significantly poor performance for the uncrushed gravel material compared with crushed aggregates.

The uncrushed gravel material tested in this research study (Cell 1) exhibited significant shear movement within the aggregate layer. Therefore, subgrade deformation was not the primary factor contributing to pavement failure under such conditions. Moreover, lack of adequate compaction was not believed to be the reason behind inadequate performance of the uncrushed gravel test sections. This was based on the observation that the uncrushed gravel material accumulated significantly higher amounts of permanent deformation in the laboratory compared with the crushed aggregates, even under modified (ASTM D 1557) compaction conditions.

Heckel (2009) suggested the use of uncrushed gravel as a capping layer over large-size aggregates (e.g., primary crusher run). However, because the performance of uncrushed gravel in capping layer applications was not evaluated during this project, the researchers do not have sufficient information to validate or contradict Heckel's recommendations.

Both the laboratory and field test results from the two phases of this research project highlighted the importance of fines content (material finer than 0.075 mm or passing No. 200 sieve) for ensuring stability of a crushed aggregate matrix. At very low fines contents (often ~4%), the crushed aggregate particles tend to move with respect to each other, resulting in a less stable matrix for higher permanent deformations that can ultimately lead to shear failure. This was particularly evident for the crushed limestone with ~5% fines used in Cells 2 and 5, which showed unstable matrix behavior under standard compaction conditions. Although improved test section performances were observed under higher relative compaction levels, it is important to note that such high compaction levels may not be easy to achieve over weak subgrade conditions. Therefore, there is a minimum amount of fines required in a crushed aggregate material for use in pavement applications. Current IDOT specifications prescribe fines contents between 4% and 12% for aggregate materials satisfying the CA-6 requirements. However, on the basis of the laboratory and field test results, it is recommended that the minimum amount of fines required for crushed aggregates be increased to 6% from the current specified value of 4%. Because uncrushed aggregate matrices often comprise lower amount of voids compared with crushed aggregates, stability of the aggregate matrix can potentially be achieved at lower fines contents. Therefore, the current lower limit of 4% may be retained for uncrushed aggregate materials. However, because of inadequate performance of uncrushed gravel aggregates in the laboratory as well as in the field, the researchers in the current study recommend prohibiting its use for construction platform applications.

5.3.2 Compactive Effort

The level of relative compaction or compactive effort was found to have a significant effect on the performance of full-scale aggregate sections tested under loading. For example, a 3% difference in the achieved relative compaction levels with respect to laboratory-determined maximum dry densities was found to have a significant effect on the failure mechanism of test sections in Cell 2. It is therefore recommended that the IDOT SSM be revised to specify minimum required compaction levels for all aggregate materials used in subgrade applications. Type B subbase materials (compacted to the satisfaction of the engineer) should be removed from the list of aggregate types allowed in construction platform applications. All aggregate-improved subgrade sections should be compacted to at least 95% of the laboratory-determined maximum dry densities under standard compactive effort.

Achieving adequate compaction levels is particularly important for crushed aggregate materials with low amounts of fines. Because of insufficient packing of the voids by fines, such aggregate types may exhibit unstable matrix behavior unless compacted to very high densities. In cases where weak subgrade conditions limit aggregate compaction levels, diskings or tilling of the subgrade layer should be performed to achieve uniform distribution of the subgrade moisture.

5.3.3 Construction Lift Thickness

Construction lift thickness influenced the achieved compaction levels in the individual aggregate test sections over the weak subgrade layers. For example, Section 3 (8-in.-thick aggregate layer) in Cells 1 through 4 constructed over a subgrade of IBV = 3% achieved consistently higher levels of relative compaction compared with Sections 1 and 2 (see Table 5.1). This was primarily the result of the lower construction lift thicknesses used in Section 3 (compacted in two layers of 4-in. thickness). Higher compaction levels often resulted in higher aggregate layer moduli (as determined from LWD and GeoGauge™), which ultimately led to lower stress levels at the subgrade interface.

It is therefore recommended to limit the aggregate layer lift thickness for subgrade applications to a maximum of 4 in. This is particularly important for subgrades with IBV values less than 6%. For subgrades with IBV values greater than 6%, slightly higher lift thicknesses may be allowed because the subgrade is likely to provide sufficient support for compaction of the overlying aggregate layer. Nevertheless, the lift thickness for aggregate layers in construction platform applications should be limited to a maximum of 8 in.

5.3.4. Curing Time for Aggregate Layers

As observed in the case of Cell 3, the crushed dolomite material with high amounts of nonplastic fines performed significantly better as a result of the possible carbonate-cementation mechanism upon prolonged exposure to moisture. Anecdotal evidence as well as communication with field engineers also indicated a potential for strength gain with time for crushed limestone and dolomite materials with high fines contents. This was further reinforced by the significant increase in aggregate layer modulus for Cell 3 after freeze-thaw cycles as measured by the GeoGauge™.

It is therefore recommended that, whenever possible, aggregate layers constructed with these aggregate types be allowed to cure for at least 48 hours before construction equipment is allowed on top of it. The strength gain resulting from carbonate cementation of the fines fraction may permit a reduction in the aggregate layer thicknesses compared with the thickness values currently recommended by the IDOT SSM.

5.3.5 Effects of Moisture Conditions

Although slight moisture increases beyond optimum moisture content were found to have a significant effect on the performance of aggregate specimens in the laboratory (as discussed in Phase I of the study), field sections when tested under flooded (saturated) conditions failed primarily from excessive subgrade deformations. This was attributed to the ingress of excess moisture into the subgrade leading to significant weakening of the subgrade. In such cases, the aggregate layer thickness played a secondary role as far as governing pavement performance was concerned.

Therefore, increasing the aggregate cover layer thickness with a moisture correction factor (C_{Moisture}) may not be effective in ensuring adequate performance under flooded conditions. Because working platform performance under flooded conditions is governed primarily by subgrade strength, changing the aggregate layer thickness by 2-3 in. will not necessarily ensure adequate performance. It is therefore recommended that sufficient time be allowed for the aggregate layers to dry in the event of rain during construction operations. Where applicable, installation of subsurface drainage systems is likely to improve construction platform performance significantly.

Moreover, controlling the moisture content of the aggregate layer during placement is also likely to help, especially for aggregate materials with high fines contents. Both laboratory and field testing indicated that excessive moisture conditions had a more severe effect on aggregate materials with high fines.

5.3.6 Realistic Construction Traffic Coverage and/or Allowable Rut Depth for Aggregate Construction Platforms

The current IDOT SSM requires the finished subgrade to have a minimum IBV of 6.0 if untreated, or 10.0 if treated, and a maximum rut depth of 0.5 in. under construction traffic. This requirement was established earlier and implemented in the 1982 version of the SSM for determining when an aggregate cover would be needed as a treatment option (1) to prevent excessive subgrade sinkage under construction equipment and (2) to provide adequate support for compacting pavement layers to be constructed. A maximum rut depth

of 0.5 in. is also specified in Section 301.04 of the IDOT Standard Specifications for Road and Bridge Construction (January 1, 2012, version) as a requirement for the finished subgrade for pavement construction.

There is no specification for a realistic traffic coverage expectation and/or allowable rut depth written specifically for the constructed aggregate working platform. In the SSM, this constructed aggregate working platform is often considered the finished subgrade when the 0.5-in. rut depth criterion is enforced. However, depending on the next layer to be constructed as part of the pavement construction, allowable rut depth (and therefore realistic construction coverage, i.e., low or high number of truck passes) must be properly specified. For example, if a granular subbase or base is to be constructed as the next pavement layer, a rut depth higher than 0.5 in. may be allowed or tolerated, whereas in the case of a hot mix asphalt layer to be constructed as the next pavement layer, construction traffic may need to be limited similar to the finished subgrade not to cause greater than 0.5-in. rut depth.

REFERENCES

- Allen, J. The Effect of Non-constant Lateral Pressures of the Resilient Response of Granular Materials. PhD Dissertation, University of Illinois at Urbana-Champaign, Urbana, IL, 1973.
- Allen, J.J., and Thompson, M.R. "Resilient Response of Granular Materials Subjected to Time Dependent Lateral Stresses." Transportation Research Record 510, 1974, Transportation Research Board, National Research Council, Washington, DC, pp. 1-13.
- Barksdale, R. D. "Laboratory Evaluation of Rutting in Base Course Materials." Proceedings of the 3rd International Conference on Structural Design of Asphalt Pavements, 1972, pp. 161-174.
- Barksdale, R.D., and Itani, S.Y. "Influence of Aggregate Shape on Base Behavior." Transportation Research Record 1227, 1989, Transportation Research Board, National Research Council, Washington, DC, pp. 173-182.
- Dawson, A. R., and Kolisoja, P. "Permanent Deformation." Technical Report, ROADEX II Final Report, Road Scanners, Rovaniemi, Finland, 2005.
- Garcia, G., and Thompson, M. R. "Working Platform Requirements for Pavement Construction: A White Paper Prepared for the Technical Review Panel." Project IHR-R30: Upgrade Subgrade Stability Manual, Illinois Cooperative Highway and Transportation Research Program, April 2003.
- Graves, R. E. Strength Developed from Carbonate Cementation in Silica/Carbonate Systems as Influenced by Cement-Particle Mineralogy. MS Thesis, University of Florida, Gainesville, FL, 1987.
- Graves, R. E., Eades, J. L., Smith, L. L. "Strength Developed from Carbonate Cementation in Silica/Carbonate Base Course Materials." Transportation Research Record 1190, 1988, Transportation Research Board, National Research Council, Washington, DC, pp. 24-30.
- Gray, J. E. "Characteristics of Graded Base Course Aggregates Determined by Triaxial Tests." Engineering Research Bulletin No. 12, 1962, National Crushed Stone Association.
- Heckel, G. "Aggregate Subgrade Thickness Determination." Final Report: Experimental Features Project IL 03-01, Physical Research Report # 154, Illinois Department of Transportation, Springfield, IL, 2009.
- Hicks, R.G., and Monismith, C.L. "Factors Influencing the Resilient Properties of Granular Materials." Transportation Research Record 345, 1971, Transportation Research Board, National Research Council, Washington, DC, pp. 15-31.
- Illinois Department of Transportation (IDOT). "Subgrade Stability Manual." Bureau of Materials and Physical Research, Springfield, IL, March 1982, 66 pp.
- Illinois Department of Transportation (IDOT). "Subgrade Stability Manual." Bureau of Bridges and Structures, Springfield, IL, May 1, 2005, 27 pp. (http://www.dot.il.gov/bridges/pdf/subgrade_stability_manual.exe)

- Illinois Department of Transportation (IDOT). "Standard Specifications for Road and Bridge Construction." Adopted January 1, 2012. (<http://dot.state.il.us/desenv/stdspecs12.html>)
- Jorenby, B. N., and Hicks, R. G. "Base Course Contamination Limits." Transportation Research Record 1095, 1986, Transportation Research Board, National Research Council, Washington, DC, pp. 86-101.
- Kleyn, E. G., Maree, J. H., and Savage, P. F. "The Application of a Portable Pavement Dynamic Cone Penetrometer to Determine In Situ Bearing Properties of Road Pavement Layers and Subgrades in South Africa." In Proceedings of the 2nd European Symposium on Penetration Testing, Amsterdam, 1, National Institute for Transport and Road Research, 1982, pp. 277-282.
- Lekarp, F., Isacsson, U., and Dawson, A. "State of the Art. I: Resilient Response of Unbound Aggregates." Journal of Transportation Engineering, ASCE, Vol. 126, No. 1, 2000, pp. 66-75.
- Mishra, D. Aggregate Characteristics Affecting Response and Performance of Unsurfaced Pavements on Weak Subgrades. PhD Dissertation, University of Illinois at Urbana-Champaign, Urbana, IL, December 2011.
- Raad, L., and Figueroa, J. L. "Load Response of Transportation Support Systems." Journal of Transportation Engineering Division, ASCE, Vol. 106, No. TE1, January, 1980.
- Rowshanzamir, M. A. Resilient Cross-Anisotropic Behavior of Granular Base Materials Under Repetitive Loading. PhD Dissertation, University of New South Wales, School of Civil Engineering, Australia, 1995.
- Seyhan, U., and Tutumluer, E. "Anisotropic Modular Ratios as Unbound Aggregate Performance Indicators." Journal of Materials in Civil Engineering, ASCE, Vol. 14, No. 5, September/October, 2002, pp. 409-416.
- Thompson, M.R., and Elliott, R.P. "ILLI PAVE-Based Response Algorithms for Design of Conventional Flexible Pavements." Transportation Research Record 1043, 1985, Transportation Research Board, National Research Council, Washington, DC, pp. 50-57.
- Thompson, M. R., Kinney, T. C., Traylor, M. L., Bullard, J. R., and Figueroa, J. L. "Subgrade Stability." Final Report, Project IHR 605, Illinois Cooperative Highway and Transportation Research Program, Department of Civil Engineering, University of Illinois at Urbana-Champaign, Urbana, IL, 1977.
- Tutumluer, E. Predicting Behavior of Flexible Pavements with Granular Bases. PhD Dissertation, Georgia Institute of Technology, Atlanta, GA, 1995.
- Tutumluer, E., and Barksdale, R. D. "Behavior of Pavements with Granular Base: Prediction and Performance." Proceedings of the UNBAR4 Symposium, Nottingham, UK, 1995, pp. 173-183.
- Tutumluer, E., and Seyhan, U. "Effects of Fines Content on the Anisotropic Response and Characterization of Unbound Aggregate Bases." Proceedings of the 5th International Conference on Unbound Aggregates in Roads (UNBAR5), Unbound Aggregates in Road Construction, Edited by A.R. Dawson and A.A. Balkema, University of Nottingham, UK, 2000, pp. 153-161.

- Tutumluer, E., Thompson, M. R., Garcia, G., and Kwon, J. "Subgrade Stability and Pavement Foundation Requirements." In Proceedings of the 15th Colombian Symposium of Pavement Engineering, Melgar, Colombia, March 9-12, 2005.
- Tutumluer, E., Mishra, D. and Butt, A. A. "Characterization of Illinois Aggregates for Subgrade Replacement and Subbase." Research Report ICT-09-060, Illinois Center for Transportation, Rantoul, IL, 2009.
- van Niekerk, A.A. Mechanical Behavior and Performance of Granular Bases and Sub-Bases in Pavements. PhD Dissertation, Delft Technological University, Delft, The Netherlands, 2002.

**APPENDIX A MECHANISTIC EVALUATION OF PAVEMENT
LAYER RESPONSE DURING CONSTRUCTION**

INTRODUCTION

Unsurfaced pavements or “unpaved roads” constitute a major portion of the road network in any country. In the United States (US), over 1.6 million miles of roads are unpaved (53% of total road miles) (Skorseth and Selim 2000). Moreover, in under-developed to developing countries, unpaved roads constitute even a larger portion of the total road network. These pavement systems lack any bound (or paved) surface layer and the surface is usually made up of a well-compacted aggregate layer. Besides rural and forest routes, a common instance of unsurfaced application is seen in pavement “working platform” constructions. Working platforms are usually constructed by “capping” the soft subgrade with an unbound aggregate layer, which provides sufficient stability and support for equipment mobility during paving operations. The absence of a bound surface layer in these pavement systems and direct application of heavy traffic loads result in very high stress levels in the unbound aggregate layers. The primary function of unbound aggregate layers in unsurfaced pavements is to protect the soft subgrade. Through inter-particle contacts load is transferred and distributed to ensure that sufficiently low stresses are applied on weak, low load bearing subgrade soils. Note that it is imperative for these aggregate layers to have adequate load resistance, i.e., strength, against internal shear failure.

Conventional design approaches for unsurfaced pavements are often based on the philosophy of “protecting the subgrade.” In such methods, the thickness of the aggregate layer is designed to protect the subgrade from excessive stress levels due to the imposed wheel loads. However, these design methodologies seldom distinguish between different material qualities that may be used for construction of the unbound aggregate layers. Yet, the layer performance is greatly influenced by aggregate type, quality and physical properties. Some of the factors most commonly recognized as affecting unbound aggregate layer behavior include: particle shape and surface texture, type and amount of fines, achieved in-place density and moisture content in relation to required compaction level (Allen 1973; Jorenby and Hicks 1986; Lekarp et al. 2000; Thompson and Smith 1990). Quantifying the relative effects of aggregate physical properties on performance would greatly enhance safe, efficient and sustainable designs of unsurfaced pavement systems.

OBJECTIVE AND SCOPE

The main objective of this paper is to identify the effects of different aggregate physical properties on the response and performance of unsurfaced pavements. The mechanistic response and performance requirements are evaluated through resilient modulus (M_R), a key material property input in mechanistic layered analysis, and permanent deformation or rutting, respectively. Aggregate physical properties considered in this study include particle shape and surface texture, type and amount of fines and compaction (moisture-density) conditions. Three different aggregate types (crushed limestone, crushed dolomite and uncrushed gravel) were tested in the laboratory for strength, modulus and deformation characteristics at different factorial combinations of the above aggregate physical properties. Stress-dependent material characterization models developed from the laboratory M_R test results were used in a nonlinear axisymmetric finite element program (GT-PAVE) to compute vertical compressive stresses on top of the subgrade for typical unsurfaced pavement structures. Adequacy of the aggregate layer for subgrade protection is assessed using the concept of Subgrade Stress Ratio (SSR) (Thompson et al. 1977). Moreover, susceptibility of the aggregate layer to rutting is also evaluated through repeated load triaxial testing of aggregate specimens. Finally, the significance of different aggregate

physical properties affecting modulus and permanent deformation behavior is presented as obtained from the statistical correlations established between the aggregate properties and the M_R and permanent deformation model parameters.

LABORATORY TEST PROGRAM

Three different aggregate types (crushed limestone, crushed dolomite, and uncrushed gravel) were studied in the laboratory to quantify individual effects of aggregate physical properties on mechanistic response and performance. A laboratory test matrix was designed to study the effects of aggregate shape (including flatness and elongation, texture and angularity from imaging based evaluation), type of fines (plastic vs. nonplastic), amount of fines (ranging in increments from low to high), and moisture condition (relative to the optimum compaction conditions) on aggregate layer performance. Ranges were established for the above properties to encompass different possible material combinations allowed by local transportation agencies for use in pavement applications. These physical properties were systematically varied within the pre-determined ranges to primarily evaluate the effects on strength, resilient modulus (M_R), and permanent deformation behavior of the aggregates. Different values assigned to the individual properties being evaluated, are listed below.

- Fines content (material passing No. 200 sieve, or finer than 0.075 mm): 4 levels (4%, 8%, 12%, and 16%)
- Plasticity of Fines (measured on material finer than 0.425 mm or No. 40 sieve size): 2 levels (Plasticity index, PI = 0 and PI = 8 to 10)
- Moisture Content: 3 levels (90% of W_{opt} , W_{opt} , and 110% of W_{opt} , where W_{opt} is the optimum moisture content determined using the standard compactive effort specified in AASHTO T 99)

Effect of particle size distribution on the typical dense graded aggregate base/subbase materials having a maximum top size of 25 mm (1 in.) was not the primary focus in this study. Instead, the emphasis was given to preparing samples at one engineered well-graded gradation established through sieving and size separation of individual aggregate stockpiles. Detailed discussion on the development of the laboratory test matrix for this engineered gradation can be found elsewhere (Mishra et al. 2010; Tutumluer et al. 2009). The compaction densities targeted were selected from the moisture-density curves for the particular combination of fines content and plasticity.

Resilient Modulus and Permanent Deformation Testing

To evaluate the effects of individual aggregate physical properties on resilient modulus (M_R) and permanent deformation behavior, the three aggregate types were tested in the laboratory at different property factorial combinations. Each aggregate specimen was prepared targeting pre-determined engineered gradations through proportional blending of different size particles. As it was not feasible to blend multiple specimens corresponding to each individual combination of the aggregate physical properties, only one specimen was prepared representing each factorial property combination. Note that preliminary laboratory trials showed excellent repeatability and low coefficients of variations for test results under controlled gradation conditions. Resilient modulus tests were performed following the standard AASHTO T 307-99 procedure. Accordingly, cylindrical test specimens (152 mm or 6 in. in diameter by 152 mm or 6 in. in height) were first conditioned by applying 1,000 (three log cycles) haversine load pulses at 103 kPa (15 psi) in the axial direction at an all-round confining pressure of 103 kPa (15 psi). The sample stress-strain response during this shakedown stage was used as an indicator of the material's permanent deformation

behavior. Resilient modulus tests were subsequently performed on the conditioned samples by pulsing in the axial direction under the 15 different stress states specified in the AASHTO T 307 procedure. Figure 1 presents two typical M_R test results obtained from the laboratory tests. The two curves in Figure 1 show the moduli values for crushed dolomite specimens with 4% and 16% nonplastic fines, respectively, both tested at their optimum moisture contents or W_{opt} (AASHTO T 99).

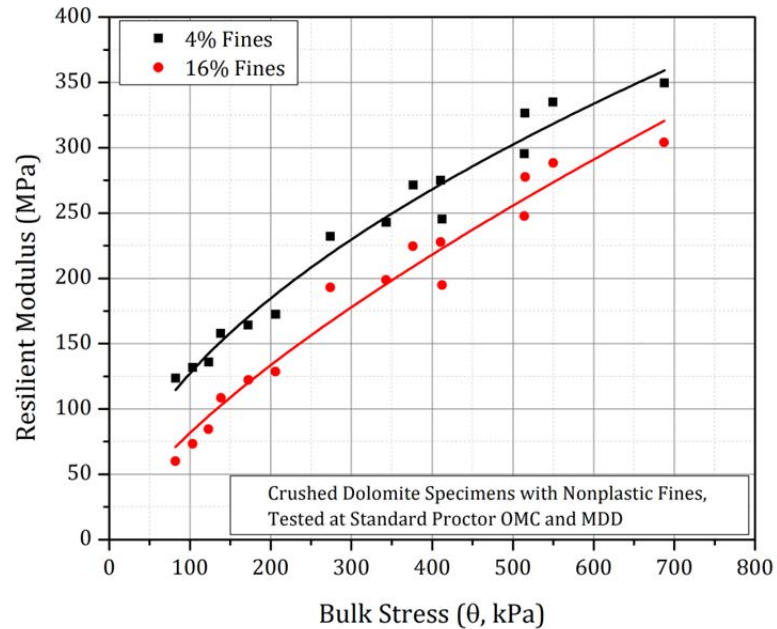


Figure 1 Resilient modulus values for crushed dolomite with nonplastic fines at W_{opt}

MATERIAL CHARACTERIZATION

Numerous models have been developed by researchers over the years through combination of applied stress states and material properties to capture the nonlinear, stress-dependent M_R behavior of unbound aggregate materials. Among the most common models used for expressing the stress dependent M_R results of unbound aggregate materials are the K- θ Model (Hicks and Monismith 1971), and the recent Mechanistic-empirical Pavement Design Guide (MEPDG) Model (www.trb.org/mepdg). The K- θ model simply correlates the resilient modulus to bulk stress (first stress invariant) without considering the applied shear stress levels, and can be used to model the stress hardening behavior of unbound aggregate materials. The MEPDG model, on the other hand, incorporates shear stress effects, and can model the stress hardening as well as stress softening behavior of geomaterials (MEPDG 2004; Thompson et al. 1998). Equations 1 and 2 show the K- θ and MEPDG resilient modulus models, respectively.

$$M_R = K \left(\frac{\theta}{P_o} \right)^n \quad (1)$$

$$M_R = k_1 p_a \left(\frac{\theta}{p_a} \right)^{k_2} \left(\frac{\tau_{oct}}{p_a} + 1 \right)^{k_3} \quad (1)$$

where

M_R = Resilient modulus;

$\theta = \sigma_1 + \sigma_2 + \sigma_3$ = Bulk stress (first stress invariant);

p_0 = Unit pressure (1 kPa or 1 psi);

σ_1 = Major principal stress

σ_2 = Intermediate principal stress = σ_3 for M_R test on cylindrical specimens;

σ_3 = Minor principal stress or confining pressure in the triaxial tests;

$\tau_{oct} = \frac{1}{3} \sqrt{(\sigma_1 - \sigma_2)^2 + (\sigma_2 - \sigma_3)^2 + (\sigma_3 - \sigma_1)^2}$ = Octahedral Shear Stress

= $\frac{\sqrt{2}}{3} (\sigma_1 - \sigma_3)$ for cylindrical specimens in triaxial tests

p_a = Normalizing stress (atmospheric pressure = 101.325 kPa) ;

K, n, k_1, k_2, k_3 = Model parameters obtained from regression analysis.

Results from M_R testing of different aggregate materials were used to develop both the simple K- θ and the more advanced MEPDG models. Moreover, permanent deformation test results from the initial conditioning stage of the M_R tests were used to develop a commonly used phenomenological model, $\varepsilon_p = AN^b$ proposed by Monismith (Monismith et al. 1985), where ε_p is the permanent strain, and N is the number of load cycles. Table 1 lists the typical M_R and ε_p characterization model parameters determined from laboratory testing of the three aggregate types, tested at optimum moisture (W_{opt}) conditions.

Table 1 Typical material characterization model parameters at W_{opt}

Aggregate Type	Aggregate Properties		Resilient Modulus					Permanent Deformation	
			$M_R = K \left(\frac{\theta}{p_o} \right)^n$		$M_R = k_1 p_a \left(\frac{\theta}{p_a} \right)^{k_2} \left(\frac{\tau_{oct}}{p_a} + 1 \right)^{k_3}$			$\epsilon_p = AN^b$	
	Plasticity Index (PI)	Fines Content (%)	K (kPa)	n	k ₁ (kPa)	k ₂	k ₃	A (x10 ⁻³)	b
Crushed Dolomite	Nonplastic	4	11217	0.529	1339	0.622	-0.359	0.631	0.187
		8	14679	0.490	1475	0.598	-0.418	0.526	0.183
		12	11772	0.493	1188	0.586	-0.364	0.924	0.216
		16	2217	0.767	814	0.908	-0.550	1.483	0.281
	Plastic	4	11704	0.532	1438	0.654	-0.472	0.959	0.150
		8	13070	0.498	1349	0.587	-0.348	0.740	0.156
		12	Specimen Failed During Testing						
	16	5634	0.562	758	0.595	-0.129	1.922	0.252	
Crushed Limestone	Nonplastic	4	12658	0.522	1455	0.609	-0.340	0.454	0.172
		8	11003	0.533	1343	0.639	-0.416	0.507	0.171
		12	12495	0.508	1345	0.591	-0.322	0.552	0.180
		16	11559	0.508	1239	0.581	-0.283	0.860	0.174
	Plastic	4	Specimen Failed During Testing						
		8	11724	0.523	1380	0.640	-0.455	0.640	0.168
		12	13449	0.464	1182	0.547	-0.322	1.104	0.163
	16	11000	0.502	1151	0.585	-0.323	1.096	0.170	
Uncrushed Gravel	Nonplastic	4	7852	0.547	1001	0.608	-0.236	0.013	0.582
		8	6616	0.552	874	0.634	-0.317	0.953	0.149
		12	1766	0.759	611	0.857	-0.380	1.503	0.187
		16	Specimen Failed During Testing						
	Plastic	4	4880	0.620	893	0.727	-0.414	0.944	0.149
		8	3591	0.660	788	0.761	-0.392	1.077	0.154
		12	1816	0.743	584	0.841	-0.380	1.463	0.167
	16	2185	0.703	591	0.825	-0.473	2.051	0.156	

M_R model parameters serve as essential layer inputs for mechanistic-empirical (M-E) pavement analysis and design procedures, such as in the Level 1 analysis of the hierarchical MEPDG material property assignments, and they can be linked to aggregate physical properties. As shown in Table 1, the effects of type and amount of fines were different on different material characterization model parameters. The most significant effect was noticed on the K parameter of the K- θ model, with the value ranging from 1766 kPa to 14,679 kPa. The n parameter varied between 0.464 and 0.767. High values for the K parameter usually corresponded to low values for the n parameter. These results are in agreement with findings by Rada and Witczak (1981), who reported an inverse power relationship between K and n, where an increase in the K parameter was often accompanied by a reduction in the n parameter. In their comprehensive study of granular material M_R test results, Rada and Witczak (1981) reported higher K values of the K- θ model for “higher quality” granular materials such as crushed stone. As shown in Table 1, for the current study the highest values for the K parameter (at W_{opt}) were obtained for the crushed dolomite with 8% nonplastic fines, whereas the two lowest K values were determined for the uncrushed gravel with 12% nonplastic (1766 kPa) and plastic (1816 kPa) fines. As a crushed dolomite with 8% fines is usually expected to perform better than an uncrushed gravel with 12% fines (Mishra et al. 2009), test results from the current study

confirm the trend of higher K values for “better quality” aggregates. Variation in the k_1 parameter (MEPDG model) was not as pronounced as the K parameter (K- θ) model.

From statistical analyses of laboratory M_R test results on various aggregate materials, Rada and Witczak (Rada and Witczak 1981) proposed a functional relationship between K and n, with a coefficient of determination (R^2) of 0.68. In comparison, the K-n relationship obtained from the current laboratory study can be seen in Figure 2 with a coefficient of determination (R^2) of 0.92. It should be noted test results from all the three aggregate types (limestone, dolomite, and uncrushed gravel) studied during the current research project have been plotted in Figure 2. The significant increase in R^2 value over that reported by Rada and Witczak was primarily achieved through elimination of inter-laboratory, inter-equipment and inter-operator variabilities. The primary objective behind presenting the relationship between K and n, and establishing the improved correlation between the two model parameters, is to emphasize the importance of laboratory testing under controlled gradation conditions. By showing the improved correlation between K and n, the authors intend to emphasize the consistency of laboratory test results from the current study. This justifies the comparison of individual test results in the subsequent sections of the paper, and eliminates any doubts regarding variations in test results induced from different test procedures, and gradation changes. Moreover, existence of such a strong K- θ model parameter relationship can be particularly useful in pavement structural evaluation and layer moduli estimation through Falling Weight Deflectometer (FWD) based backcalculation algorithms. The functional relationship between model parameters can be used to reduce the number of variables, in the backcalculation scheme and thus will enhance the efficiency of the algorithm. Further, development of such functional relationships for locally available materials can greatly assist transportation agencies in pavement structural condition assessment and design of overlays.

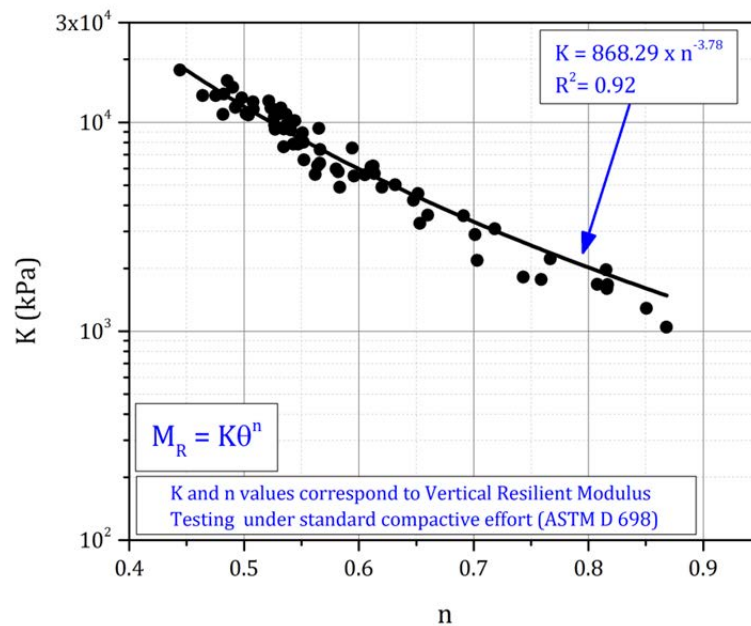


Figure 2 Relationships between K and n parameters of the K- θ model developed by the current study

FINITE ELEMENT ANALYSES OF UNSURFACED PAVEMENTS

Unbound aggregate material characterization models developed from the laboratory tests were used in a nonlinear axisymmetric finite element (FE) program GT-PAVE to predict effects of the varying M_R behavior on mechanistic response of typical two-layered, aggregate base and subgrade, unsurfaced pavement sections (Tutumluer 1995; Tutumluer and Barksdale 1995). The GT-PAVE FE program utilizes isoparametric 8-node quadrilateral elements to analyze flexible pavement structures consisting of linear or nonlinear elastic layers. Details on the nonlinear solution technique used in GT-PAVE are described elsewhere (Tutumluer 1995; Tutumluer and Barksdale 1995).

All aggregate materials which were considered in the full factorial matrix of physical properties established the FE analysis inputs for GT-PAVE runs. The unsurfaced pavements analyzed consisted of aggregate layer thicknesses of 203, 305, and 356 mm (8, 12 and 14 in.) placed over a soft subgrade soil with a target California Bearing Ratio (CBR) of 3%. Note that this is also a typical pavement working platform construction application commonly encountered in reality. Accordingly, the subgrade was assigned a constant modulus of 31 MPa (4.5 ksi), which corresponded to an unconfined compressive strength (Q_u) of approximately 158 kPa (23 psi) based on data from typical fine-grained soils in the state of Illinois. The GT-PAVE FE mesh included 600 elements (30 rows and 20 columns) to model the two-layer pavement structure with proper consideration given to boundary conditions in the selection of mesh size (Tutumluer 1995; Tutumluer and Barksdale 1995). The single wheel load of 44.5 kN (10 kip) was applied as a uniform pressure of 758 kPa (110 psi) over a circular area of radius 137 mm (5.4 in.). The Poisson's ratios for unbound aggregate and subgrade layers were taken as 0.35 and 0.45, respectively. Figure 3 shows a typical two-layer unsurfaced pavement structure analyzed using GT-PAVE.

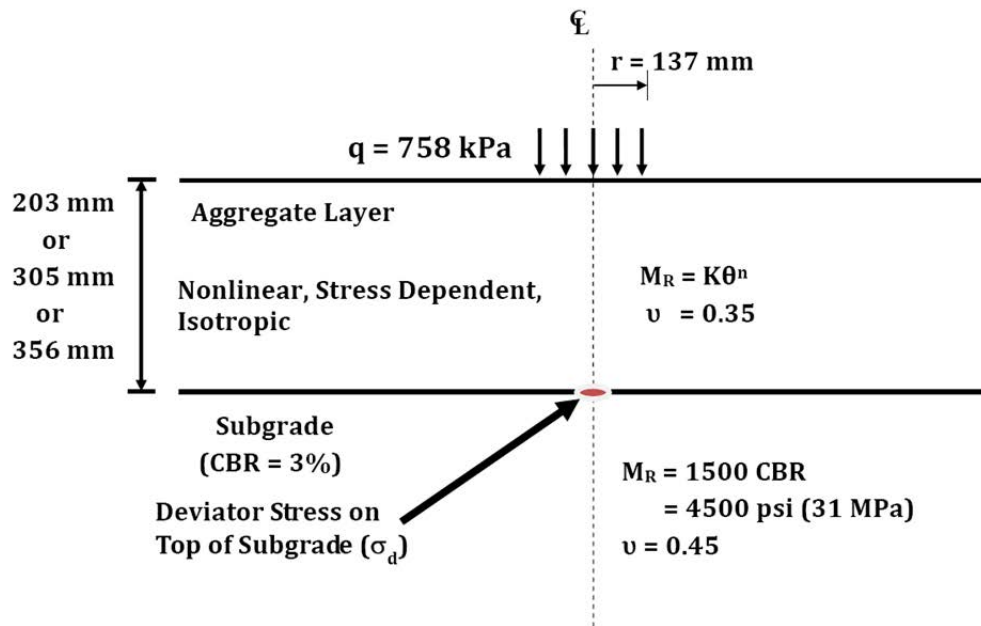


Figure 3 Schematic of a typical two-layer system analyzed using GT-PAVE

GT-PAVE FE ANALYSIS RESULTS

Vertical deviator stress on top of subgrade (σ_d) was taken as the critical pavement response of interest. Rutting potential of the subgrade was assessed by calculating the Subgrade Stress Ratio (SSR), defined as the ratio of this vertical compressive stress on the subgrade (σ_d) and the subgrade unconfined compressive strength Q_u . The SSR value was established by Thompson (Thompson et al. 1977) as a better indicator of subgrade rutting potential in comparison to the vertical strain on top of subgrade which is commonly used for controlling subgrade rutting. Accordingly, the approach for designing unsurfaced pavements is based on limiting the allowable SSR to 0.6 to 0.7 in order to prevent rutting of the subgrade (Garcia and Thompson 2003). For unsurfaced pavements and construction platforms that are characterized by lower number of load applications and lower serviceability standards, the threshold value of SSR can be set to a higher value (of the order of 0.75) (Thompson et al. 1977).

The SSR values calculated from the GT-PAVE analyses of the pavement sections were used to assess the adequacy of the aggregate layer for limiting subgrade rutting. The effects of individual aggregate physical properties on the computed SSR values were studied to identify factors that govern load spreading ability of aggregate layers and their effects on subgrade rutting potential. Figure 4 shows the change in the SSR values with nonplastic fines content for a 305-mm (12-in.) dolomite layer on top of the soft subgrade. The dark solid line shows the main regression trend line while the dashed lines show the typical upper and lower data scatter (see Figure 4). It should be noted that the upper and lower dashed lines in subsequent figures are for visual demonstration of data scatter for a particular fines content only, and are not intended to suggest the SSR values for a particular fines content. As discussed later, the upper and lower dashed boundaries can be used to highlight the effect of moisture on SSR values at different fines contents. As shown in Figure 4, there is a clear trend of increasing SSR values when the fine content in the aggregate matrix is increased; this may, for example, relate to aggregate material degradation due to intrusion of subgrade soil fines in the field. Since a higher SSR value indicates greater stresses are applied on top of the subgrade, the load spreading ability of the aggregate layer is clearly reduced when the amount of fines is increased.

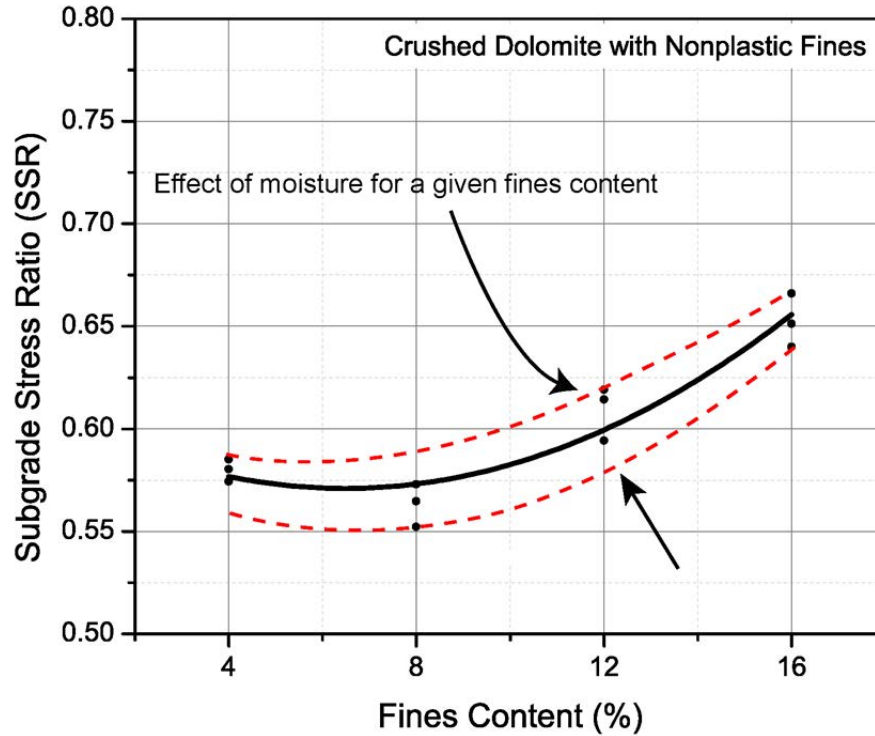


Figure 4 Subgrade Stress Ratios (SSRs) due to the 305-mm (12-in.) thick crushed dolomite layer with nonplastic fines

Another interesting observation from Figure 4 is the slight reduction in the SSR values while going from 4% to 8% fines, which may be linked to the optimum fines content as reported by researchers in the past (Seyhan and Tutumluer 2002). However, as the fines content subsequently increases beyond 8%, the SSR values increase, showing greater susceptibility of the pavement structure to undergo subgrade rutting. Interestingly, the exact same trend was found from permanent deformation testing of the dolomite samples (see Figure 5). The trend in SSR values is a reflection of the effect of fines content on the modulus of the aggregate, which results in different degrees of stress reduction at the subgrade interface. The change in behavior while going from 4% to 8% fines can be explained by the fact that at 4% fines the crushed dolomite matrix structure is not stable, and there is sufficient room for the particles to move and rearrange, therefore leading to higher deformation and lower moduli values (Mishra et al. 2010; Tutumluer et al. 2009). However, as the fines content is increased to 8%, the aggregate matrix gradually stabilizes and presents better resistance to particle movement and rearrangement. As the fines content is increased beyond 8%, all the voids in the matrix get filled, and the fines start governing the behavior of the aggregate material leading to higher deformation and lower moduli values.

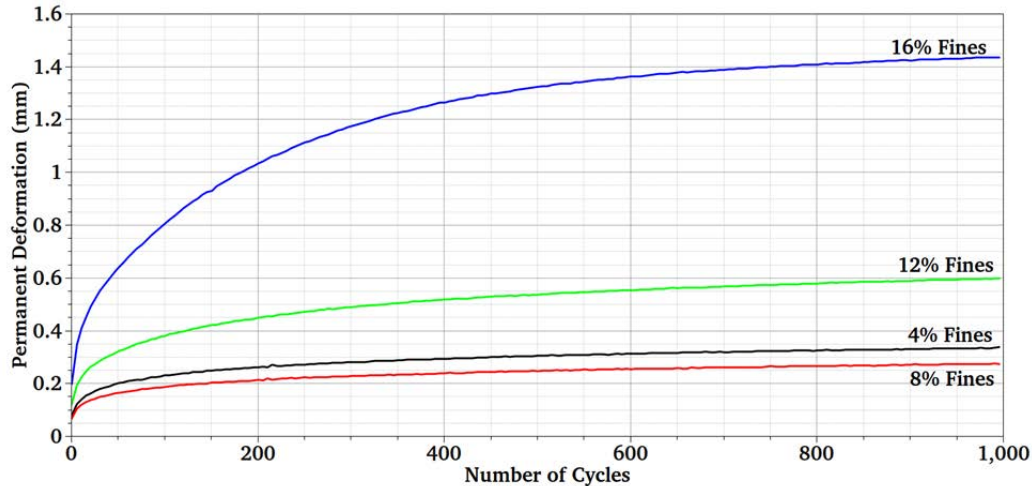


Figure 5 Permanent deformation trends for crushed dolomite with nonplastic fines at W_{opt}

These results can be used to establish a threshold value of allowable fines in aggregate layers. As the reduction in material quality is apparent (shown by higher deformation and lower modulus values) beyond a fines content of 8%, this value seems to be acting as the boundary between low and high fines categories. This observation is in complete agreement with earlier findings (Seyhan and Tutumluer 2002) that suggested 7-8% as the limit for allowable fines in unbound aggregate layers.

A distinction between crushed and uncrushed aggregate materials can be made by comparing the above findings with similar results for uncrushed gravel presented in Figures 6 and 7. Both Figures 6 and 7 indicate that there is no evidence of matrix stabilization when the fines are increased from 4% to 8%. In other words, the uncrushed gravel matrix shows deterioration in load carrying ability, as the fines content is increased beyond 4%. This can be explained by the lower voids content in the uncrushed gravel matrix that gets stabilized at relatively lower fines contents (less than 8%). This supports the argument for establishing different thresholds for allowable fines content for crushed and uncrushed aggregates (Mishra et al. 2010; Tutumluer et al. 2009).

Figures 4 and 6 can also be analyzed together for the effect of change in aggregate layer moisture content on its adequacy for subgrade protection. Both Figures 4 and 6 show that the effect of moisture content (represented by the three data points corresponding to each fines content) on aggregate modulus (and hence SSR) varies depending on whether the aggregate is crushed or uncrushed. For example, in the case of crushed dolomite with nonplastic fines (see Figure 4), the data points corresponding to different moisture contents at individual fines contents are consistently close to each other. Therefore, change in moisture does not have a significant effect on load distribution ability irrespective of the amount of fines. However, in the case of uncrushed gravel (see Figure 6), the scatter becomes wider as the fines content increases (particularly visible at 12% fines). As the fines content was increased from 12% to 16%, samples with wet of optimum moisture contents became unstable and could not be tested for M_R and permanent deformation. The scatter in the SSR values at high fines contents is even more pronounced in the case of uncrushed gravel with plastic fines (see Figure 8). This clearly proves that the effect of moisture on load carrying of the aggregate layer is dependent on particle shape (crushed vs. uncrushed), fines content, as well as plasticity of fines. Therefore, to quantify the effect of moisture content change on aggregate behavior, consideration must also be given to these other aggregate physical properties.

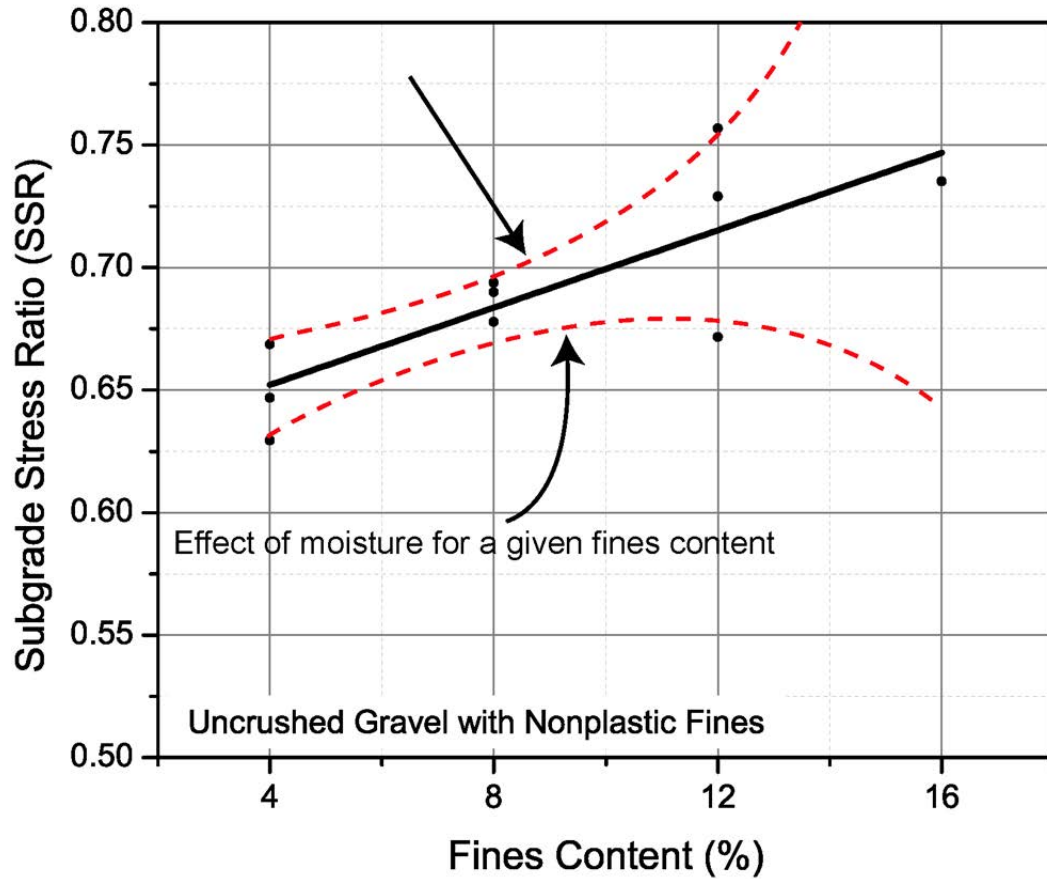


Figure 6 Subgrade Stress Ratios (SSRs) due to the 305-mm (12-in.) thick uncrushed gravel layer with nonplastic fines

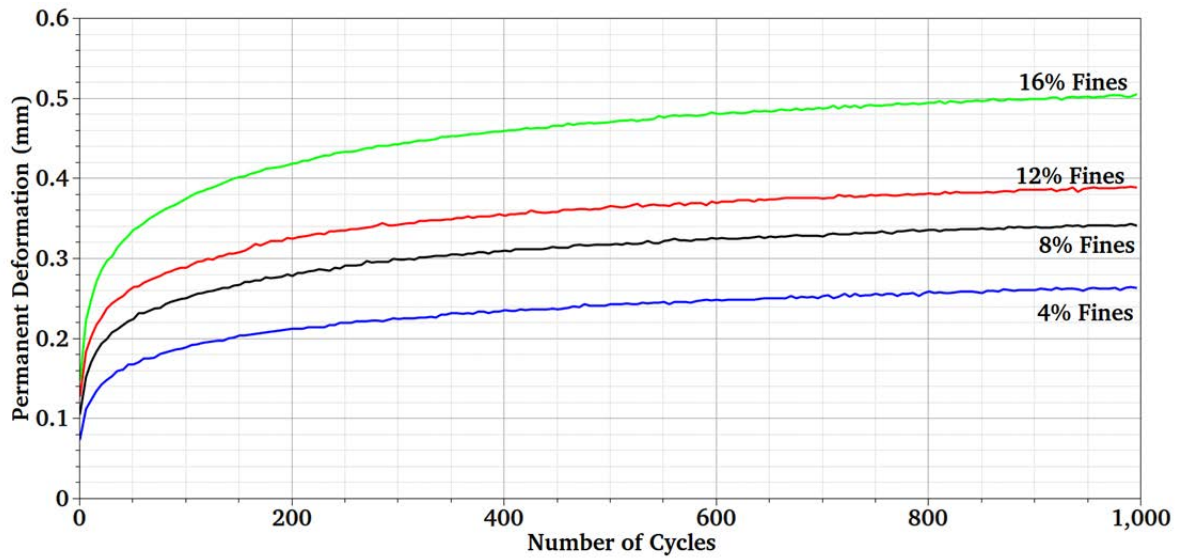


Figure 7 Permanent deformation trends for uncrushed gravel with nonplastic fines at 90% W_{opt}

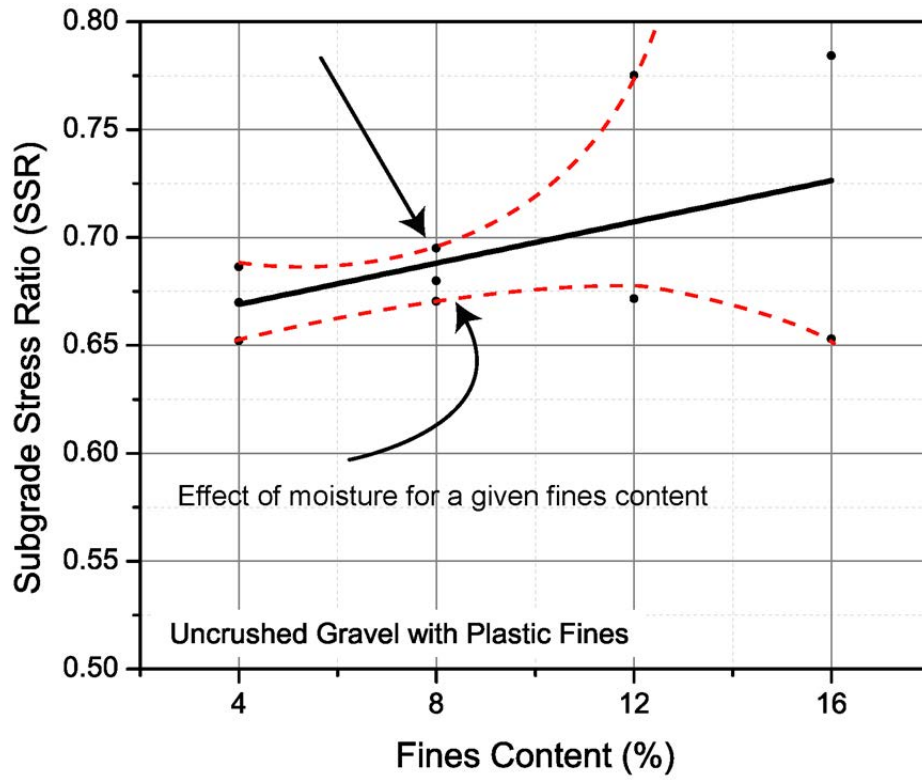


Figure 8 Subgrade Stress Ratios (SSRs) due to the 305-mm (12-in.) thick uncashed gravel layer with plastic fines

IMPORTANCE OF CONSIDERING BOTH MODULUS AND PERMANENT DEFORMATION CHARACTERISTICS

The previous section highlighted some of the similarities in the change in modulus and permanent deformation behavior of aggregates with change in physical properties. However, designing unbound aggregate layers based solely on the concept of subgrade protection can often be misleading. The effects of aggregate properties on modulus and deformation behavior of aggregates are not necessarily proportional. This can be noted by simply contrasting Figures 1 and 9. Figure 1 shows M_R curves for crushed dolomite specimens with 4% and 16% nonplastic fines tested at the optimum moisture content. Figure 9, on the other hand, shows the permanent deformation test results for the same two specimens. It can be seen that as fines content is increased from 4% to 16%, its effect on permanent deformation (increase by 400%) is much more severe than the effect on resilient modulus (decrease by 20-25%).

This issue can further be investigated by contrasting the design aspects emphasizing subgrade protection and aggregate layer rutting or shear failure. Figure 10 shows the change in SSR values with increasing unbound aggregate layer thickness for dolomite with 12% nonplastic fines and uncrushed gravel with 12% plastic fines. As expected, the subgrade stress ratio decreases as the aggregate layer thickness increases. However, for a 356-mm (14-in.) thick aggregate layer, both the dolomite with nonplastic fines and gravel with plastic fines result in acceptable SSR values (0.55 and 0.6, respectively). Therefore, judging by criteria of subgrade protection, it would appear that the pavement structure will perform adequately for both the materials leading to acceptable pavement designs.

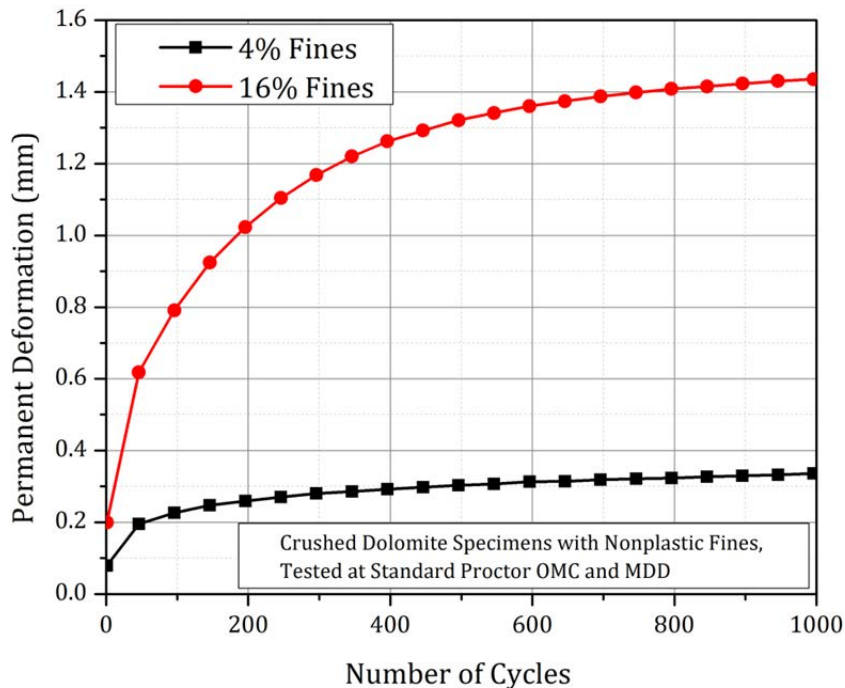


Figure 9 Permanent deformation behavior of crushed dolomite with nonplastic fines at W_{opt}

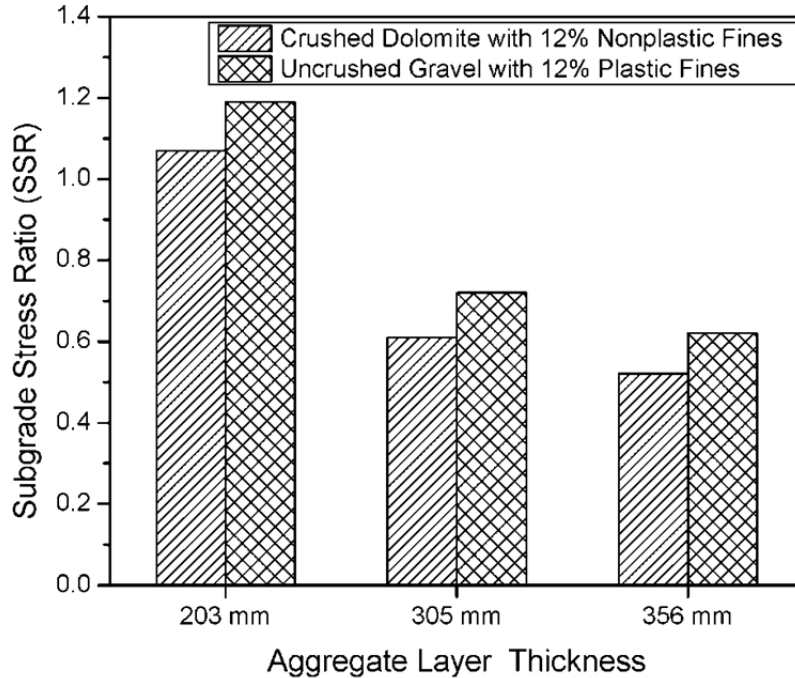


FIGURE 10 Subgrade Stress Ratios (SSRs) for crushed dolomite with 12% nonplastic fines compared to SSRs for uncrushed gravel with 12% plastic fines

However, comparing the permanent deformation behavior of the two materials reveals significantly different results. Figure 11 shows the permanent deformation test results for the same two materials. It can be seen that the uncrushed gravel with 12% plastic fines experiences shear failure at approximately 300 load applications. A pavement structure constructed with this gravel material would undergo shear failure by means of excessive rutting in the gravel layer. Therefore, protecting subgrade is not the only factor that influences performance of unsurfaced pavement systems, and due consideration should be given to aggregate type and quality and their effects on both modulus and permanent deformation behavior of the aggregate layer.

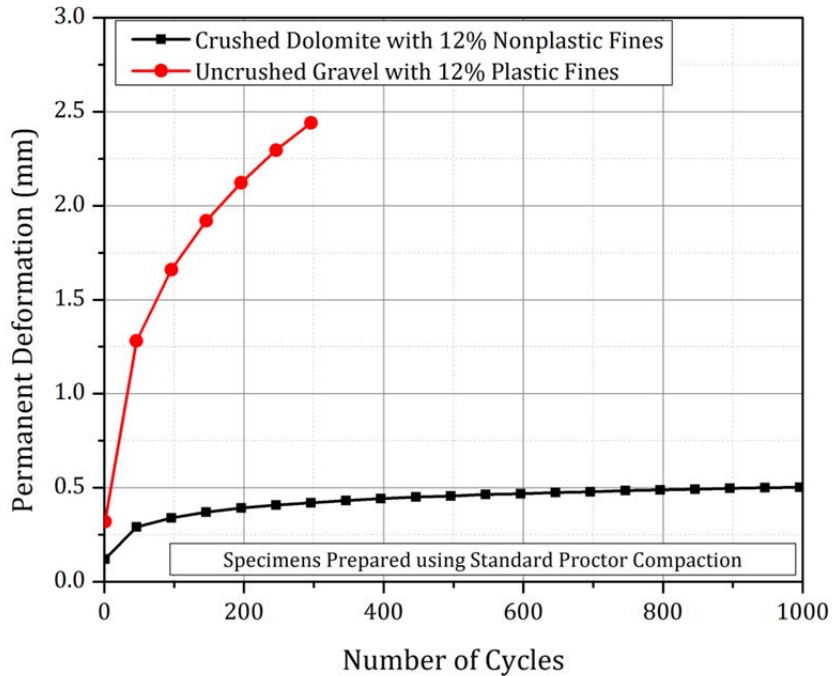


Figure 11 Permanent deformation trends of crushed dolomite with 12% nonplastic fines and uncrushed gravel with 12% plastic fines at W_{opt}

ANALYSES OF VARIANCE ON MODEL PARAMETERS

Differences in the overall aggregate physical properties studied have been shown to impact both the modulus and deformation behavior. A statistical approach for checking the significance of these different aggregate properties on mechanistic response and performance is by conducting Analyses of Variance (ANOVA) on the M_R and ϵ_p material characterization model parameters. Effects of each of the four classification variables in ANOVA, i.e., aggregate angularity, amount of fines, type of fines, and moisture condition were individually studied on the following model parameters: K , n (K - θ model), k_1 , k_2 , k_3 (MEPDG model), and A , b (phenomenological model). The statistical software package SASTM was used for analyzing the data. The effects of individual aggregate properties on any given model parameter were found to be interacting with each other. For example, the effect of amount of fines on the model parameters changed depending on the moisture condition, as well as the type of fines. This is in agreement with some of the results established in the preceding sections. Therefore, to identify the individual effects of material physical properties on the M_R and ϵ_p model parameters, each factor was considered separately as classification variables. In other words, the effect of each individual property on the model parameter was studied as averaged over all possible combinations of the other properties. The significance of each classification variable was checked at a type-I error level (α) of 0.05. Table 2 summarizes the findings from the ANOVA results. A cell marked by ' \checkmark ' means that a particular aggregate property had a significant effect on the model parameter in question, whereas a cell marked by '--' means, the effect was insignificant at $\alpha = 0.05$. Main findings from the ANOVA results are discussed below.

TABLE 2 Significance of aggregate properties affecting modulus and deformation characteristics

Aggregate Property	Resilient Modulus Models					Permanent Deformation Model	
	$M_R = K \left(\frac{\theta}{p_0} \right)^n$		$M_R = k_1 p_a \left(\frac{\theta}{p_a} \right)^{k_2} \left(\frac{\tau_{oct}}{p_a} + 1 \right)^{k_3}$			$\epsilon_p = AN^b$	
	K	n	k₁	k₂	k₃	A	b
Particle Shape	√	---	√	---	---	---	---
Compaction Moisture Condition	---	---	---	---	√	---	√
Fines Content	---	---	---	---	---	√	---
Plasticity of Fines	---	---	---	---	---	√	√
Low vs. High Fines	---	---	√	---	---	√	---

√: Significant Effect at $\alpha = 0.05$

Particle Shape

ANOVA results for particle shape (crushed vs. uncrushed) show that both K and k_1 parameters are affected significantly by particle shape. In other words, the K and k_1 values for crushed aggregates were significantly different (higher in this case) than the parameters for uncrushed gravel. This observation is in agreement with previously reported research findings (Allen 1973; Barksdale and Itani 1989; Rao et al. 2002). Unbound aggregate layers having crushed particles have been consistently found to perform superior compared to those with uncrushed particles in terms of providing a stiffer layer for load distribution. However, particle shape was not found to have a significant effect on the permanent deformation model parameters (A and b).

Fines Content

The effect of fines content (4%, 8%, 12%, and 16%) on M_R model parameters was found to be insignificant from the ANOVA results. However, fines content did have a significant effect on the “A” parameter used to characterize permanent deformation. This is in agreement with the example presented in Figure 9 which shows a drastic change in permanent deformation behavior of dolomite as the fines content is increased from 4% to 16%. The ANOVA results emphasize the point that although an increase in fines content may not lead to significant differences in the resilient modulus behavior (and hence the layer’s ability to protect the subgrade), it can still lead to unacceptable permanent deformation within the aggregate layer leading to internal shear failure.

Plasticity of Fines

Similar to the amount of fines, plasticity of fines did not have a significant effect on the M_R model parameters. However, its effect on permanent deformation model parameters (both A and b in this case) was found to be quite significant. This means, although plastic fines may not influence the stiffness of an aggregate layer significantly, they will lead to high shear deformations within the aggregate layer, resulting in excessive rutting and potential bearing capacity type shear failures at extreme conditions.

Low vs. High Fines

Based on the laboratory test results, different threshold values for fines contents were set for crushed and uncrushed aggregates, to define “low” and “high” fines contents. For crushed aggregates (dolomite and limestone), samples with up to 8% fines were categorized as having “low” fines, whereas for uncrushed gravel, samples with only up to 4% fines were categorized as “low” fines. This was based on the apparent stabilization effect around 8% fines for crushed materials, and the absence of such effect in gravel. ANOVA results show that materials with “low” vs. “high” fines exhibit significantly different k_1 and A values. This means, based on the stability of the aggregate matrix, unbound aggregate layers in the field would show significantly different modulus and permanent deformation trends. Such a classification to distinguish between aggregate matrices with low vs. high fines can be used in the development of material quality specifications used by state and national transportation agencies.

SUMMARY AND CONCLUSIONS

This paper presented relative effects of aggregate physical properties on the resilient modulus (M_R) and permanent deformation behavior of unbound aggregate layers for use in unsurfaced pavement systems. Aggregate properties studied included particle shape and surface texture, type and amount of fines, and moisture and density in relation to required compaction conditions. Material characterization models were developed for both M_R and permanent deformation trends observed from the laboratory tests. The developed stress-dependent M_R models were used in GT-PAVE nonlinear axisymmetric finite element analyses of typical unsurfaced pavement structures to predict vertical subgrade stresses as the critical pavement response. The concept of Subgrade Stress Ratio (SSR) was used to assess the adequacy of the aggregate layers for subgrade protection. Although SSR values did not relate to great differences in aggregate layer thicknesses over soft subgrade conditions for varying aggregate physical properties, aggregate layer permanent deformation trends were significantly affected by the aggregate type and quality.

These findings clearly indicated the need to consider both the resilient modulus and permanent deformation characteristics together for evaluating and selecting a certain aggregate material for satisfactory mechanistic response and rutting performance in unsurfaced pavement applications. The significance of individual aggregate properties was evaluated through a statistical Analysis of Variance (ANOVA) study for their influence on the modulus and permanent deformation model parameters. The results showed that aggregate properties had varying levels of influence on each of the modulus and permanent deformation characteristics of unbound aggregates. Aggregates with a stable matrix, i.e., not all the voids filled with fines, demonstrated improved behavior in terms of both resilient modulus and permanent deformation trends.

In conclusion, protecting the subgrade may not be the only consideration when designing rut resistant unsurfaced pavement systems, and due consideration should be given to aggregate type and quality and their effects on both modulus and permanent deformation behavior of the aggregate layer.

REFERENCES

- Allen, J. J. (1973). "The Effect of Non-Constant Lateral Pressures on the Resilient Response of Granular Materials." PhD Thesis, University of Illinois at Urbana-Champaign, Urbana, Illinois.
- Barksdale, R. D., and Itani, S. Y. (1989). "Influence of Aggregate Shape on Base Behavior." Transportation Research Record 1227, Transportation Research Board, Washington, D.C., 173-182.
- Garcia, G., and Thompson, M. R. (2003). "Working Platform Requirements for Pavement Construction." A White Paper Prepared for the Technical Review Panel, Project IHR-R30 "Upgrade Subgrade Stability Manual".
- Hicks, R. G., and Monismith, C. L. (1971). "Factors Influencing the Resilient Response of Granular Materials." Highway Research Record 345, Highway Research Board, Washington, D.C., 15-31.
- Jorenby, B. N., and Hicks, R. G. (1986). "Base Course Contamination Limits." Transportation Research Record 1095, Transportation Research Board, Washington, D.C., 86-101.
- Lekarp, F., Isacsson, U., and Dawson, A. (2000). "State of the Art. I: Resilient Response of Unbound Aggregates." Journal of Transportation Engineering, 126(1), 66-75.
- MEPDG. (2004). "Guide for Mechanistic Empirical Design of New and Rehabilitated Pavement Structures". NCHRP Report 1-37A, National Cooperative Highway Research Program, Transportation Research Board.
- Mishra, D., Tutumluer, E., and Butt, A. A. (2010). "Quantifying Effects of Particle Shape and Type and Amount of Fines on Unbound Aggregate Performance through Controlled Gradation." Transportation Research Record 2167, Transportation Research Board, Washington, D.C., 61-71.
- Mishra, D., Tutumluer, E., Kern, J., and Butt, A. A. (2009). "Characterizing Aggregate Permanent Deformation Behavior based on Types and Amounts of Fines." Proc. 8th International Conference on Bearing Capacity of Roads, Railways, and Airfields, Champaign, Illinois, 237-246.
- Monismith, C. L., Ogawa, N., and Freeme, C. R. (1985). "Permanent Deformation Characteristics of Subgrade Soils due to Repeated Loading." Transportation Research Record 537, Transportation Research Board, Washington, D.C., 1-17.
- Rada, G., and Witczak, M. W. (1981). "Comprehensive Evaluation of Laboratory Resilient Moduli Results for Granular Material." Transportation Research Record 810, Transportation Research Board, Washington, D.C., 23-33.
- Rao, C., Tutumluer, E., and Kim, I. T. (2002). "Quantification of Coarse Aggregate Angularity Based on Image Analysis." Transportation Research Record 1787, Transportation Research Board, Washington, D.C., 117-124.
- Seyhan, U., and Tutumluer, E. (2002). "Anisotropic Modular Ratios as Unbound Aggregate Performance Indicators." Journal of Materials in Civil Engineering, 14(9), 409-416.
- Skorseth, K., and Selim, A. A. (2000). "Gravel Roads: Maintenance and Design Manual", US Department of Transportation, Federal Highway Administration.
- Thompson, M. R., Tutumluer, E., and Bejarano, M. (1998). "Final Report: Granular Material and Soil Moduli Review of the Literature." COE Report No. 1, Center of Excellence for Airport Pavement Research, Department of Civil Engineering, University of Illinois at Urbana-Champaign, Urbana, Illinois.
- Thompson, M. R., and Smith, K. L. (1990). "Repeated Triaxial Characterization of Granular Bases." Transportation Research Record 1278, Transportation Research Board, Washington, D.C., 7-17.

- Thompson, M. R., Kinney, T. C., Traylor, M. L., Bullard, J. R., and Figueroa, J. L. (1977). "Subgrade Stability: Final Report". Technical Report IHR-605, Illinois Cooperative Highway and Transportation Research Program, Department of Civil Engineering, University of Illinois at Urbana-Champaign, Urbana, Illinois.
- Tutumluer, E. (1995). "Predicting Behavior of Flexible Pavements with Granular Bases." PhD Thesis, Georgia Institute of Technology, Atlanta, Georgia.
- Tutumluer, E., and Barksdale, R. D. (1995). "Behavior of Pavements with Granular Bases— Prediction and Performance." Unbound Aggregates in Roads, Proc. Fourth International Symposium on Unbound Aggregates in Roads (UNBAR4), 173-183.
- Tutumluer, E., Mishra, D., and Butt, A. A. (2009). "Characterization of Illinois Aggregates for Subgrade Replacement and Subbase", Technical Report R27-1, Illinois Center for Transportation, University of Illinois at Urbana-Champaign.

**APPENDIX B PROPERTIES OF AGGREGATE MATERIALS
USED IN CONSTRUCTION OF FULL-SCALE TEST
SECTIONS**

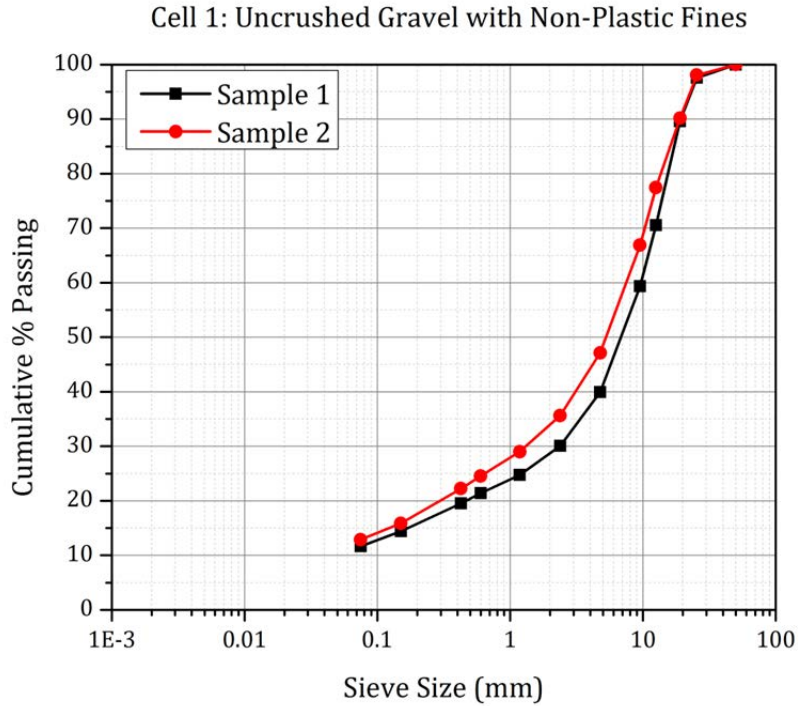


Figure B-1 Particle size distribution of the uncrushed gravel material with nonplastic fines used in Cell 1

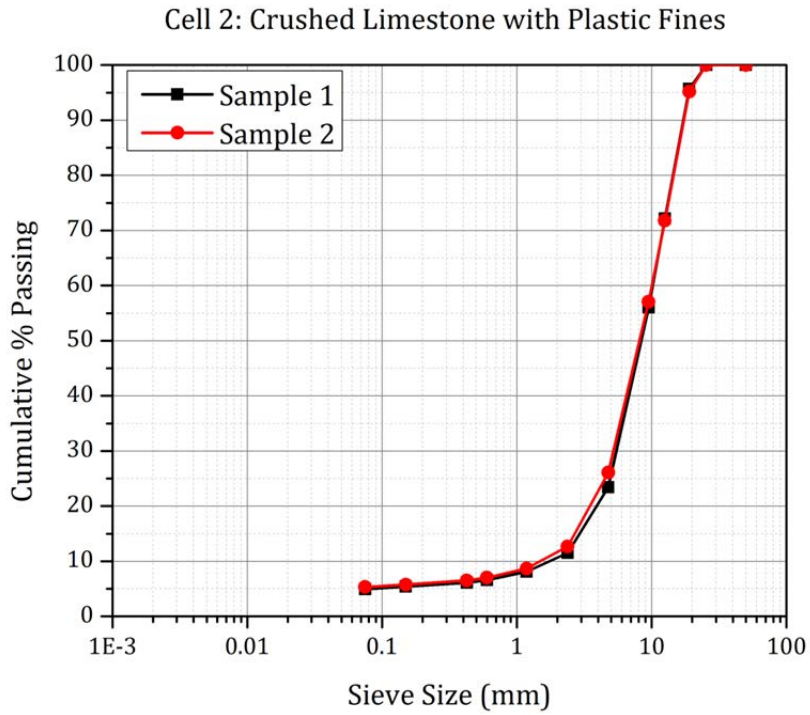


Figure B-2 Particle size distribution of the crushed limestone material with plastic fines used in Cell 2

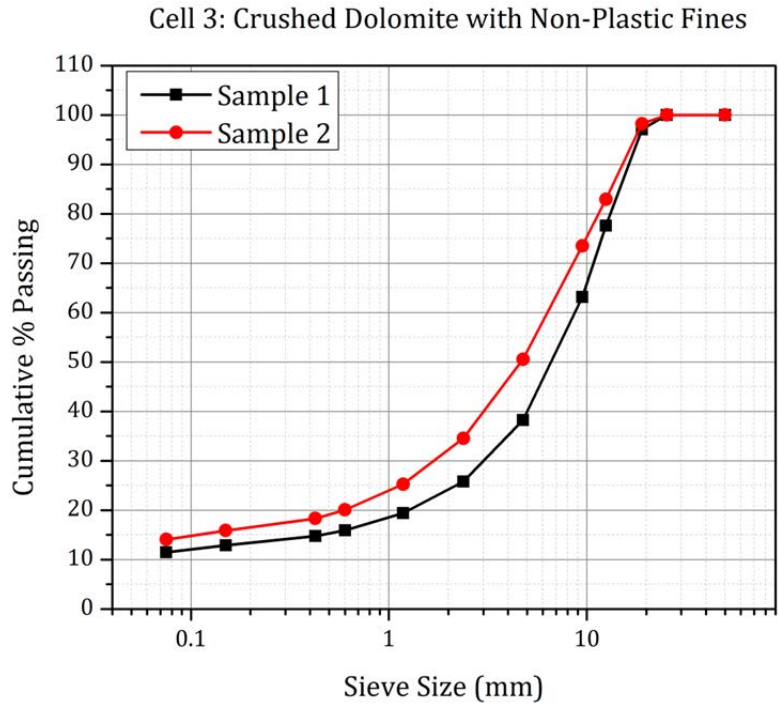


Figure B-3 Particle size distribution of the crushed dolomite material with nonplastic fines used in Cell 3

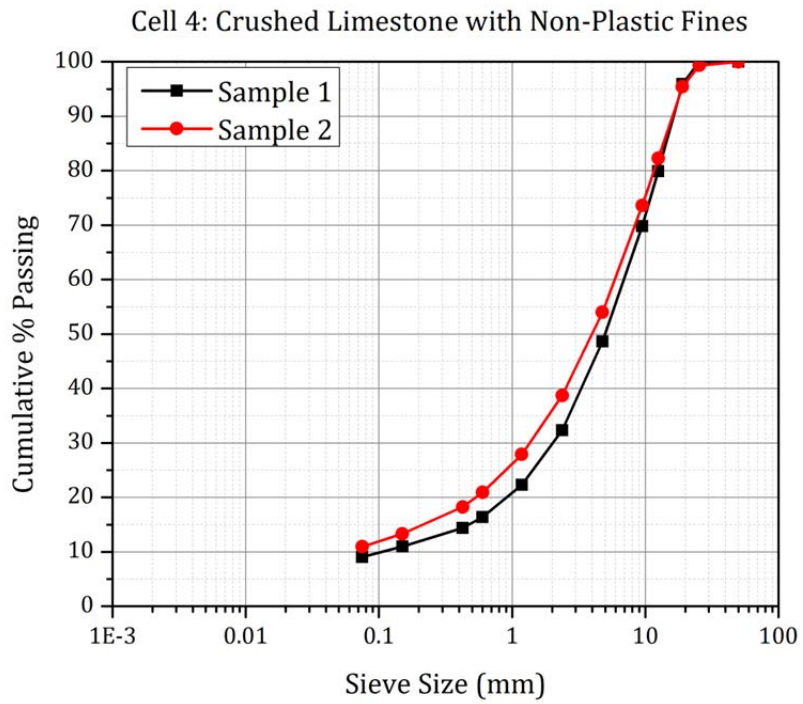


Figure B-4 Particle size distribution of the crushed limestone material with nonplastic fines used in Cell 4

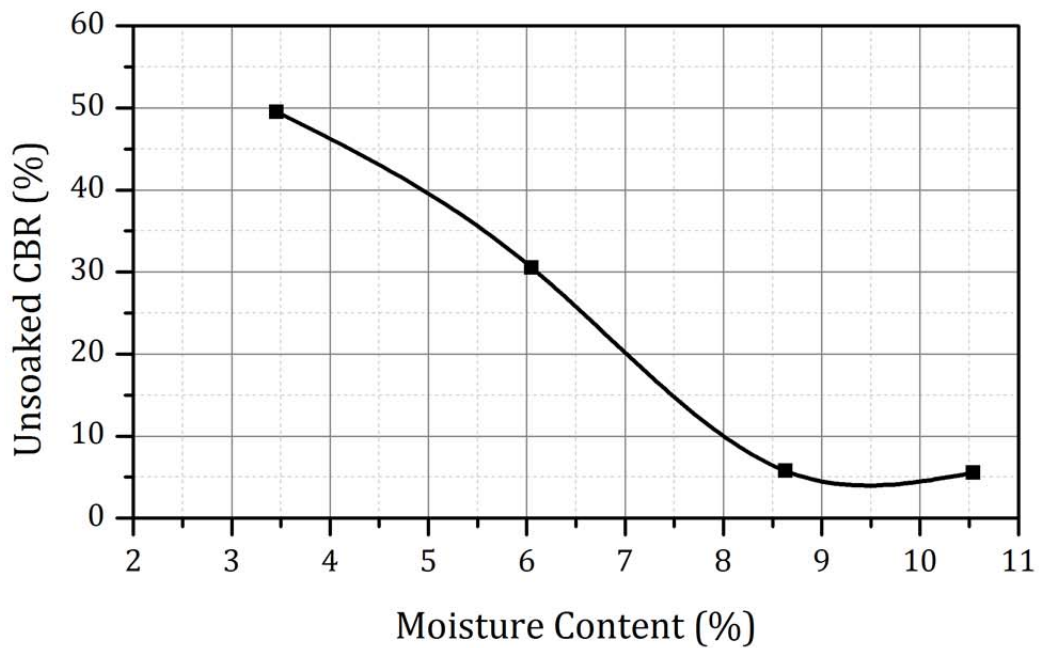
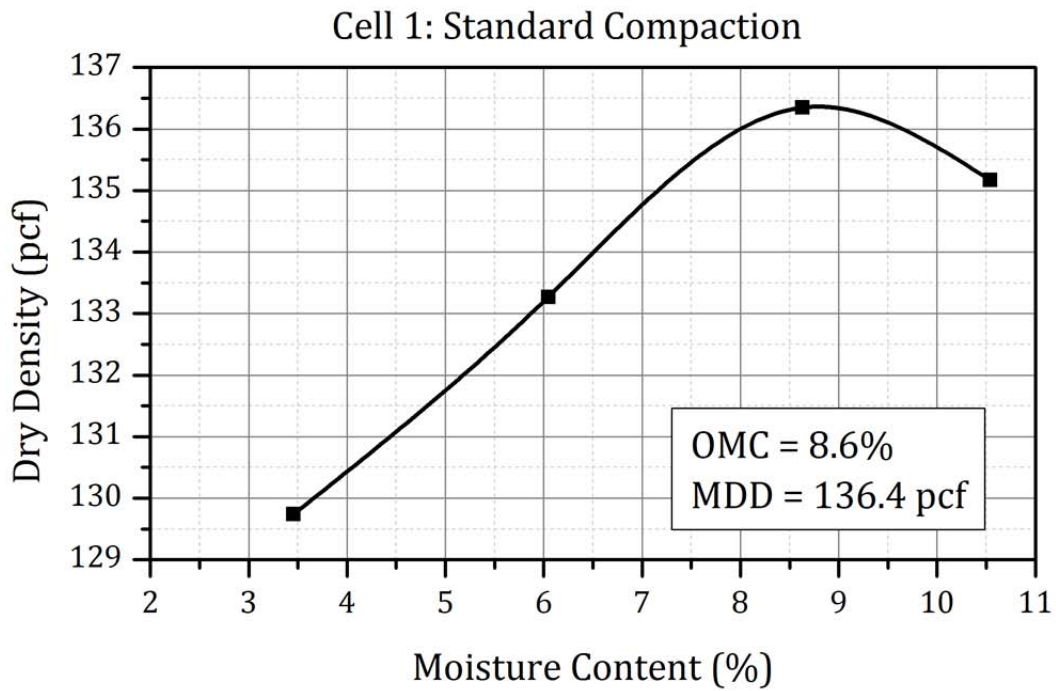


Figure B-5 Moisture-density and IBV characteristics for the uncrushed gravel material with high amounts of nonplastic fines (Cell 1) under standard compactive effort (IBV shown as "Unsoaked CBR" in the plot)

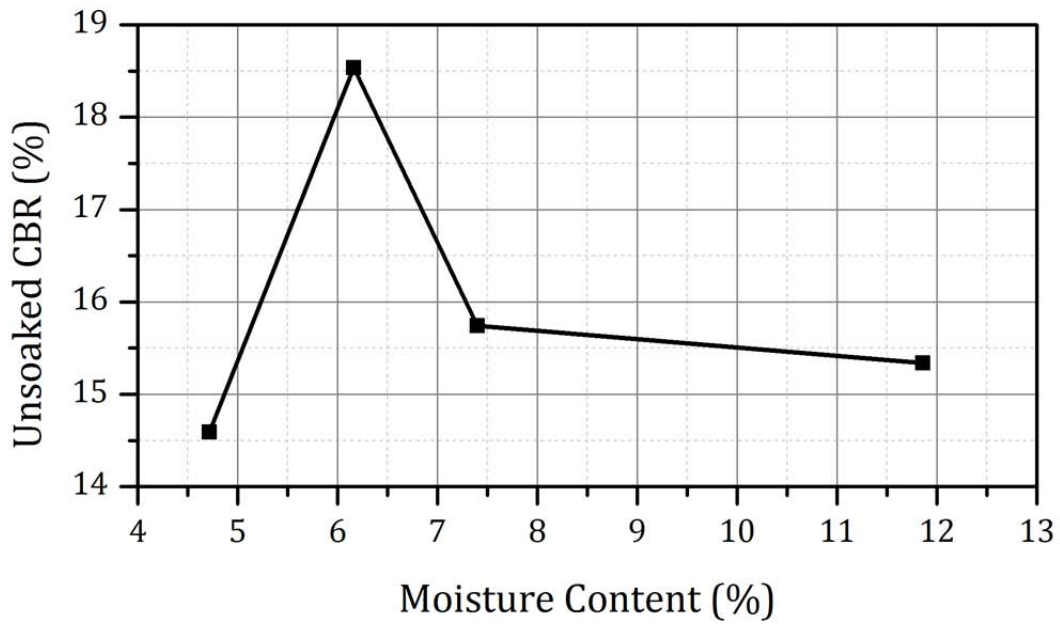
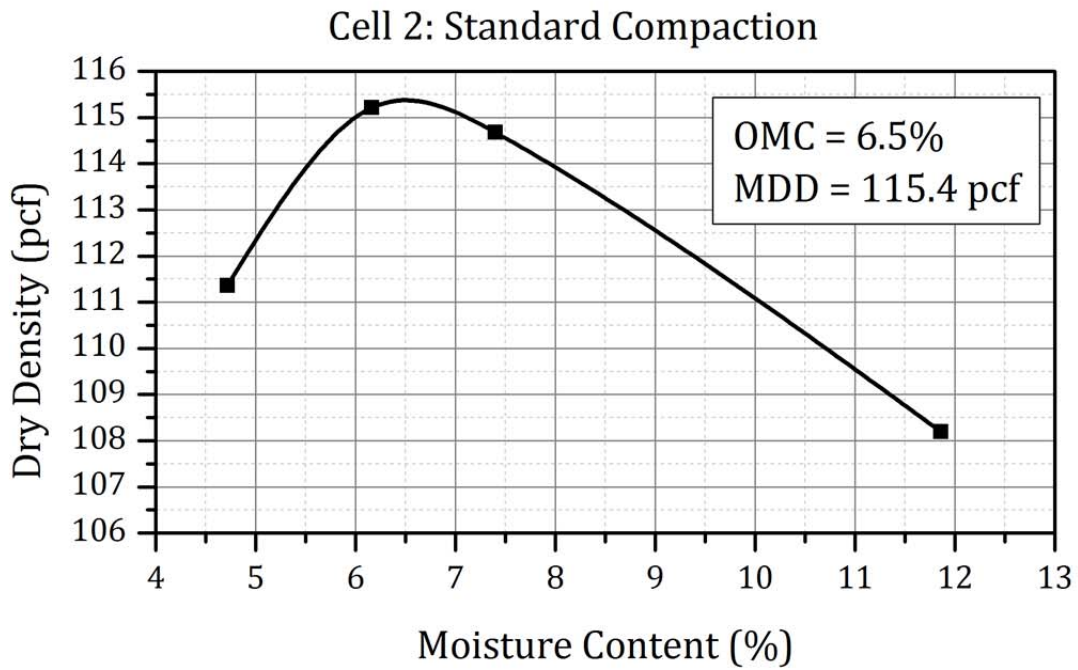


Figure B-6 Moisture-density and IBV characteristics for the crushed limestone material with low amounts of plastic fines (Cell 2) under standard compactive effort (IBV shown as “Unsoaked CBR” in the plot)

Cell 3: Standard Compaction

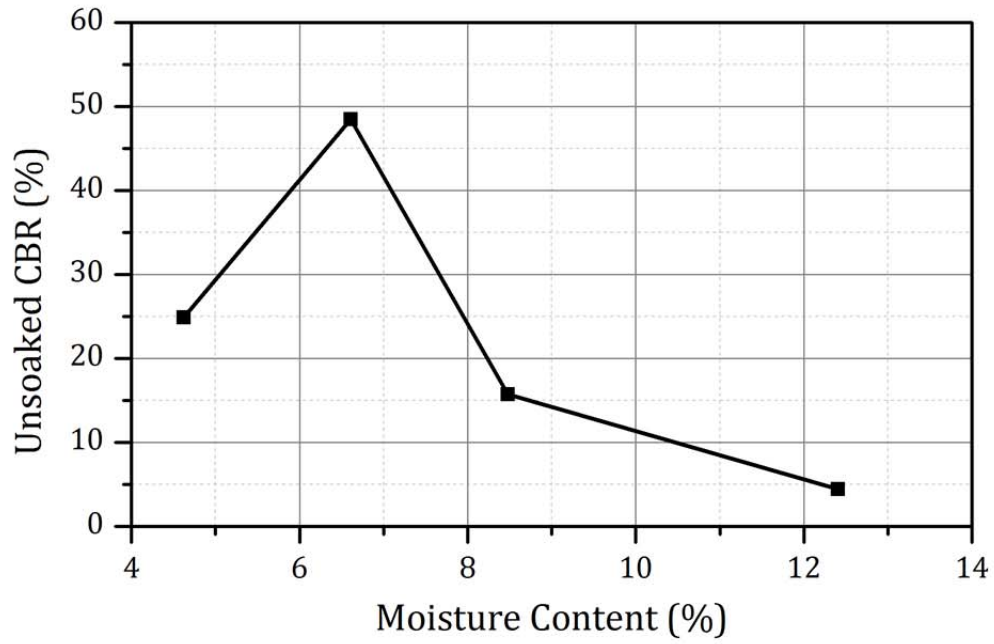
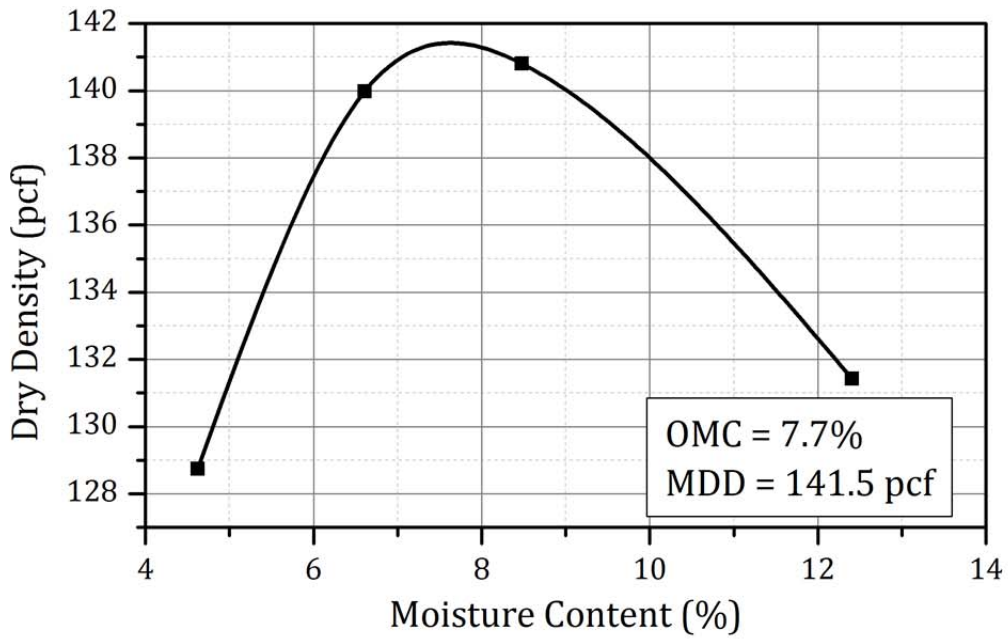


Figure B-7 Moisture-density and IBV characteristics for the crushed dolomite material with high amounts of nonplastic fines (Cell 3) under standard compactive effort (IBV shown as “Unsoaked CBR” in the plot)

Cell 4: Standard Compaction

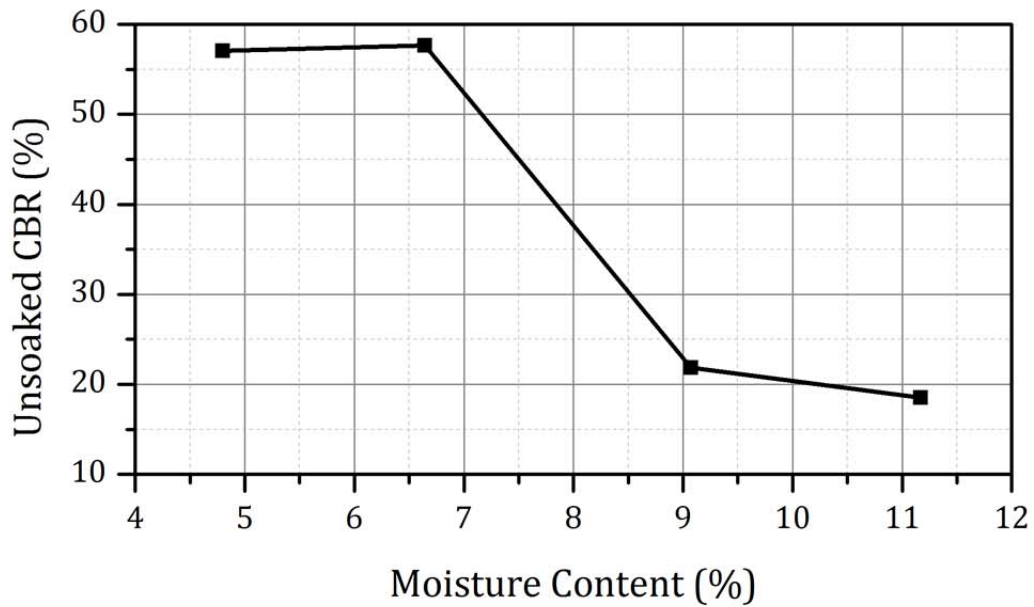
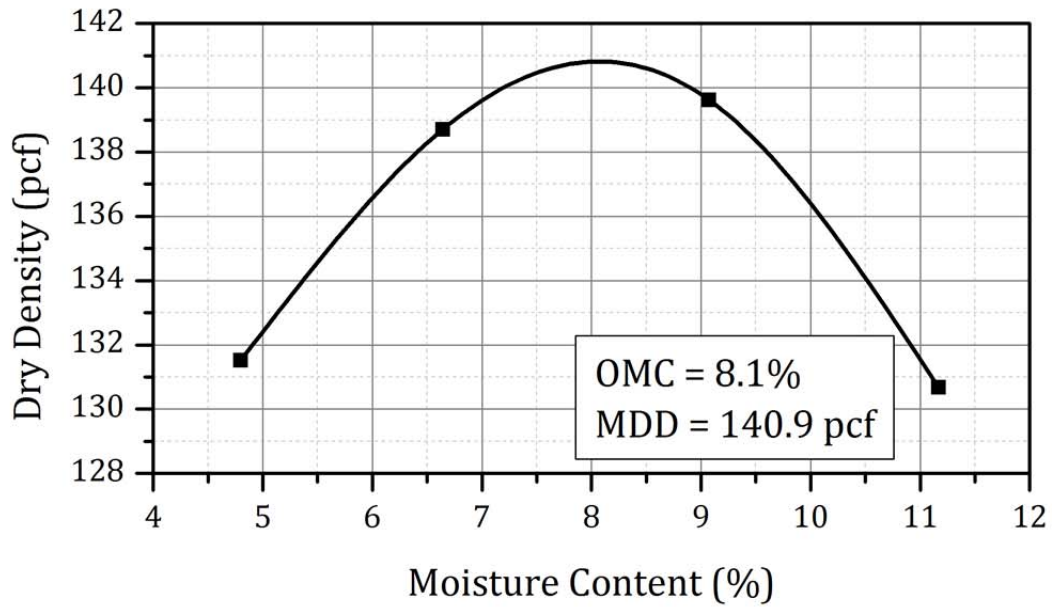


Figure B-8 Moisture-density and IBV characteristics for the crushed limestone material with high amounts of nonplastic fines (Cell 4) under standard compactive effort (IBV shown as “Unsoaked CBR” in the plot)

**APPENDIX C ACCELERATED PAVEMENT TESTING AND
PERFORMANCE MONITORING**

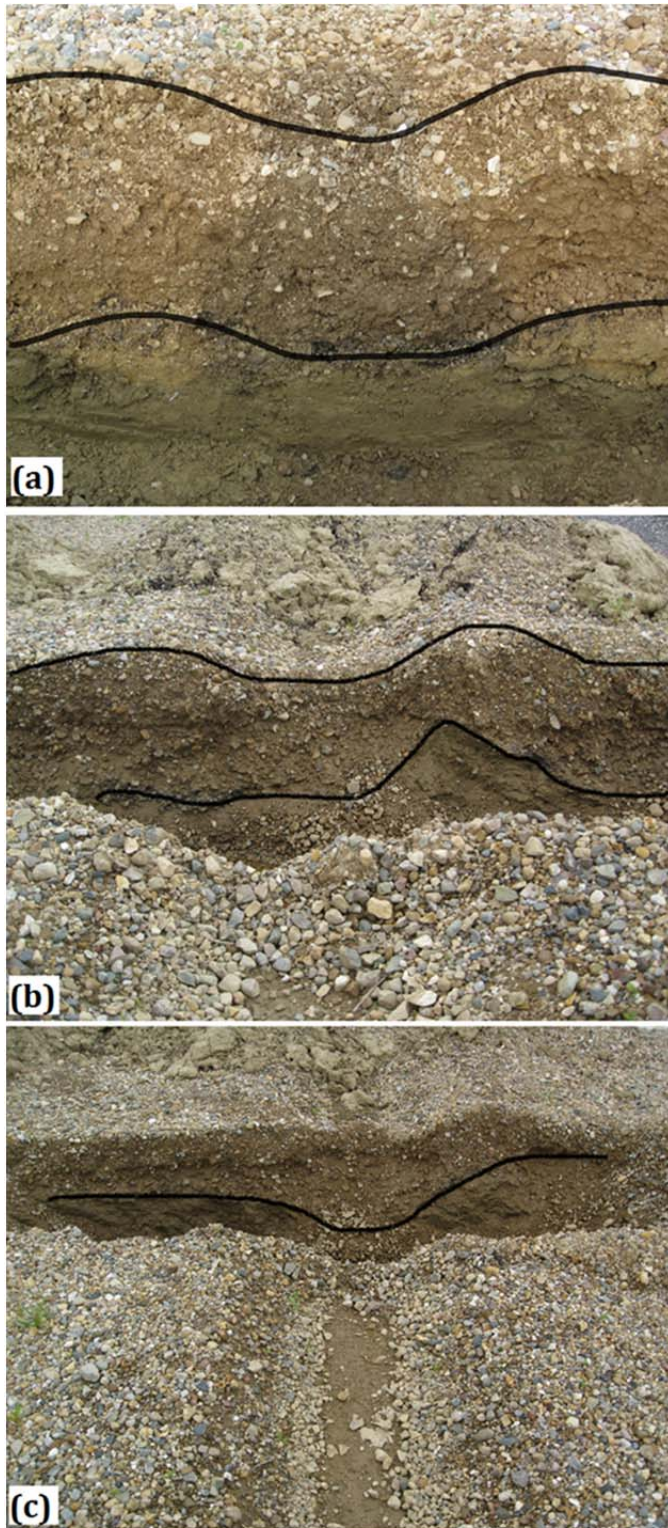


Figure C-1 Excavated trench photos showing surface and base-subgrade interface deformations in test sections (a) 1, (b) 2, and (c) 3 for Cell 1 due to loading under flooded conditions

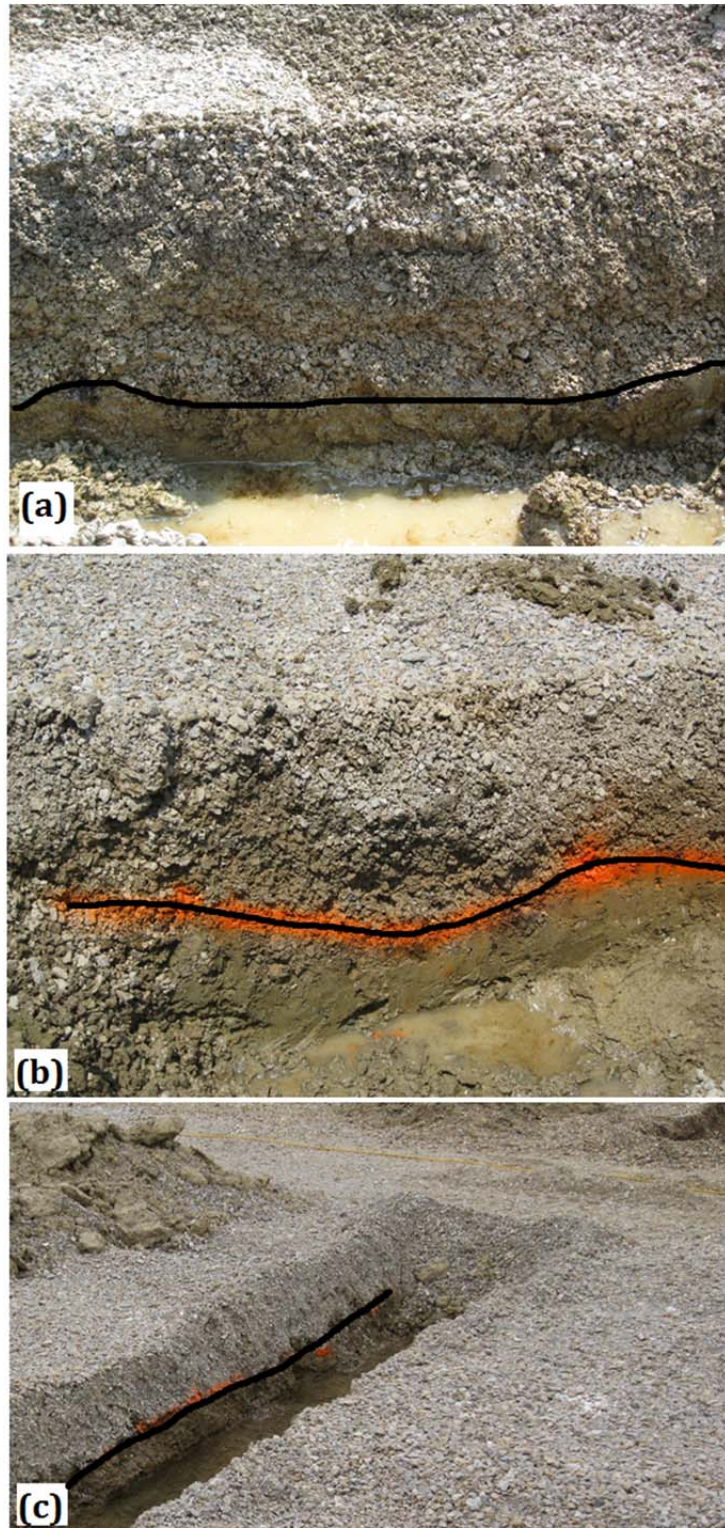


Figure C-2 Excavated trench photos showing surface and base-subgrade interface deformations in test sections (a) 1, (b) 2, and (c) 3 for Cell 2 due to loading under flooded conditions

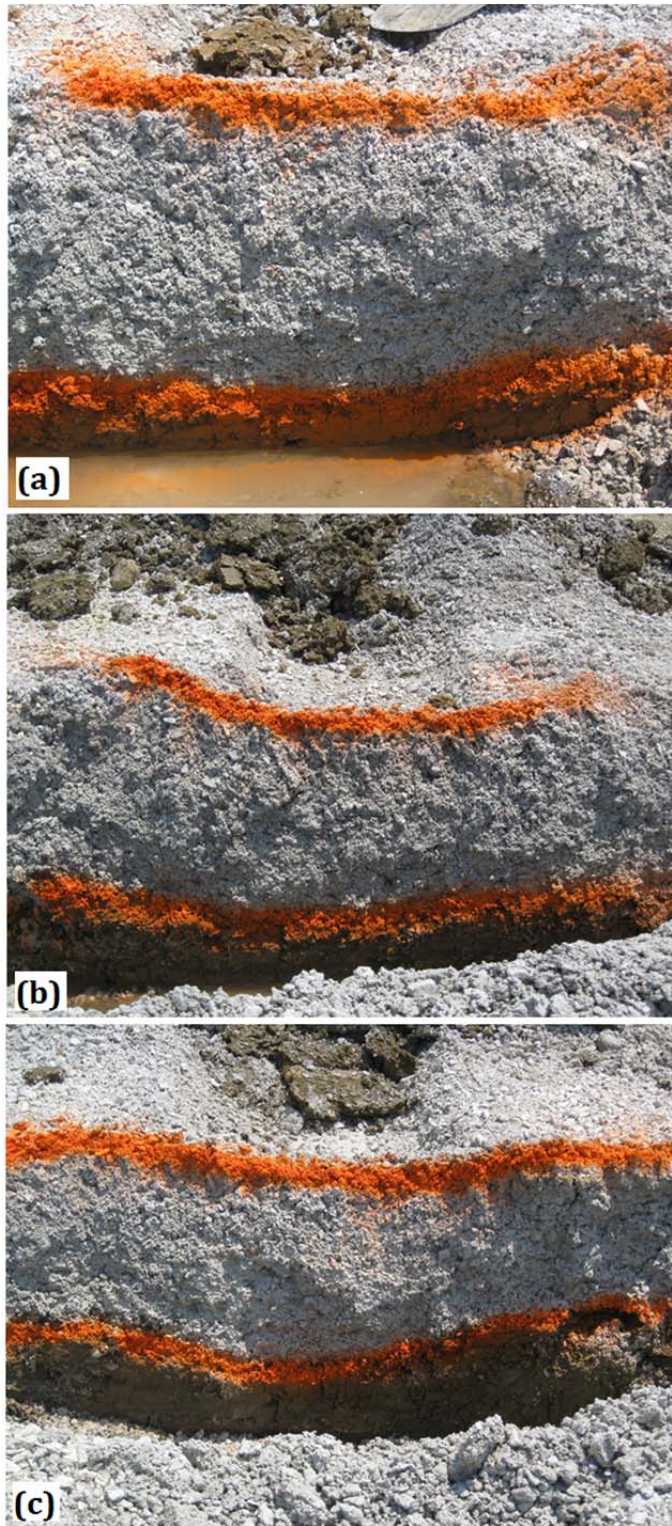


Figure C-3 Excavated trench photos showing surface and base-subgrade interface deformations in test sections (a) 1, (b) 2, and (c) 3 for Cell 3 due to loading under flooded conditions

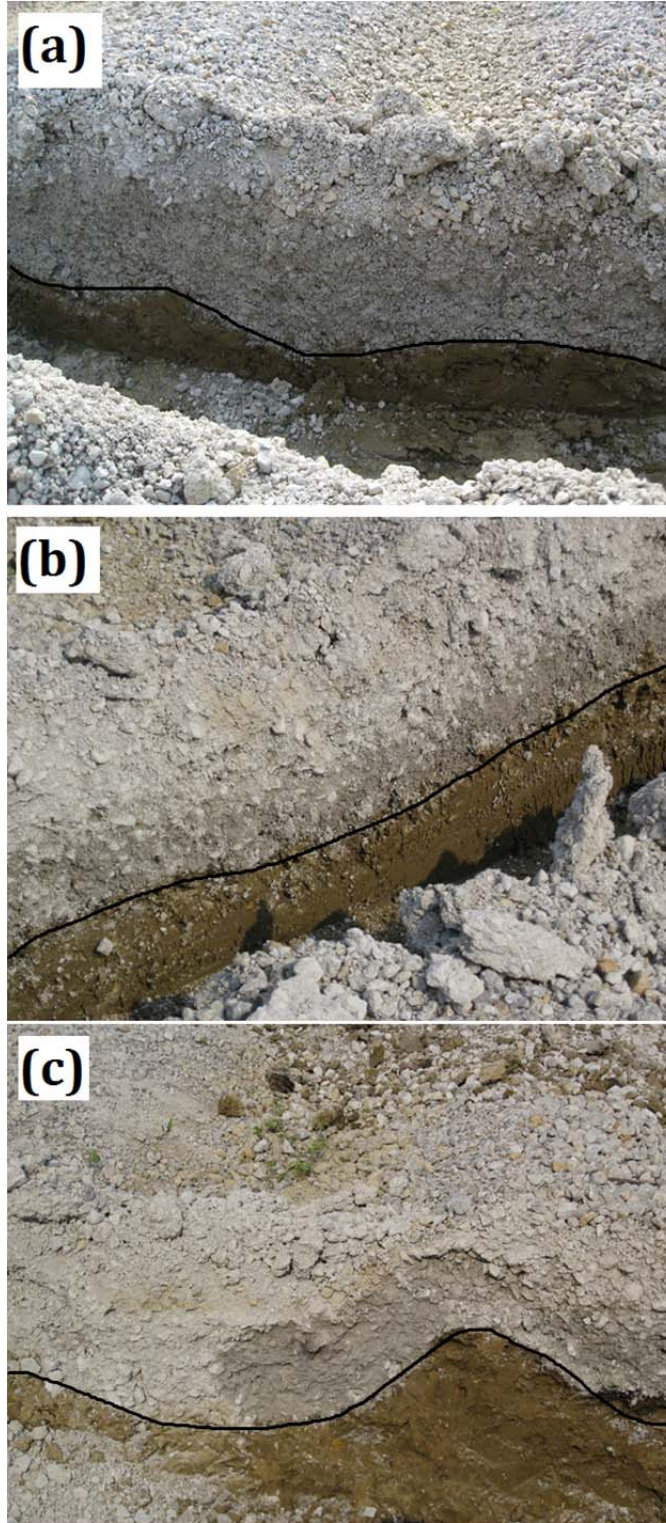


Figure C-4 Excavated trench photos showing surface and base-subgrade interface deformations in test sections (a) 1, (b) 2, and (c) 3 for Cell 4 due to loading under flooded conditions

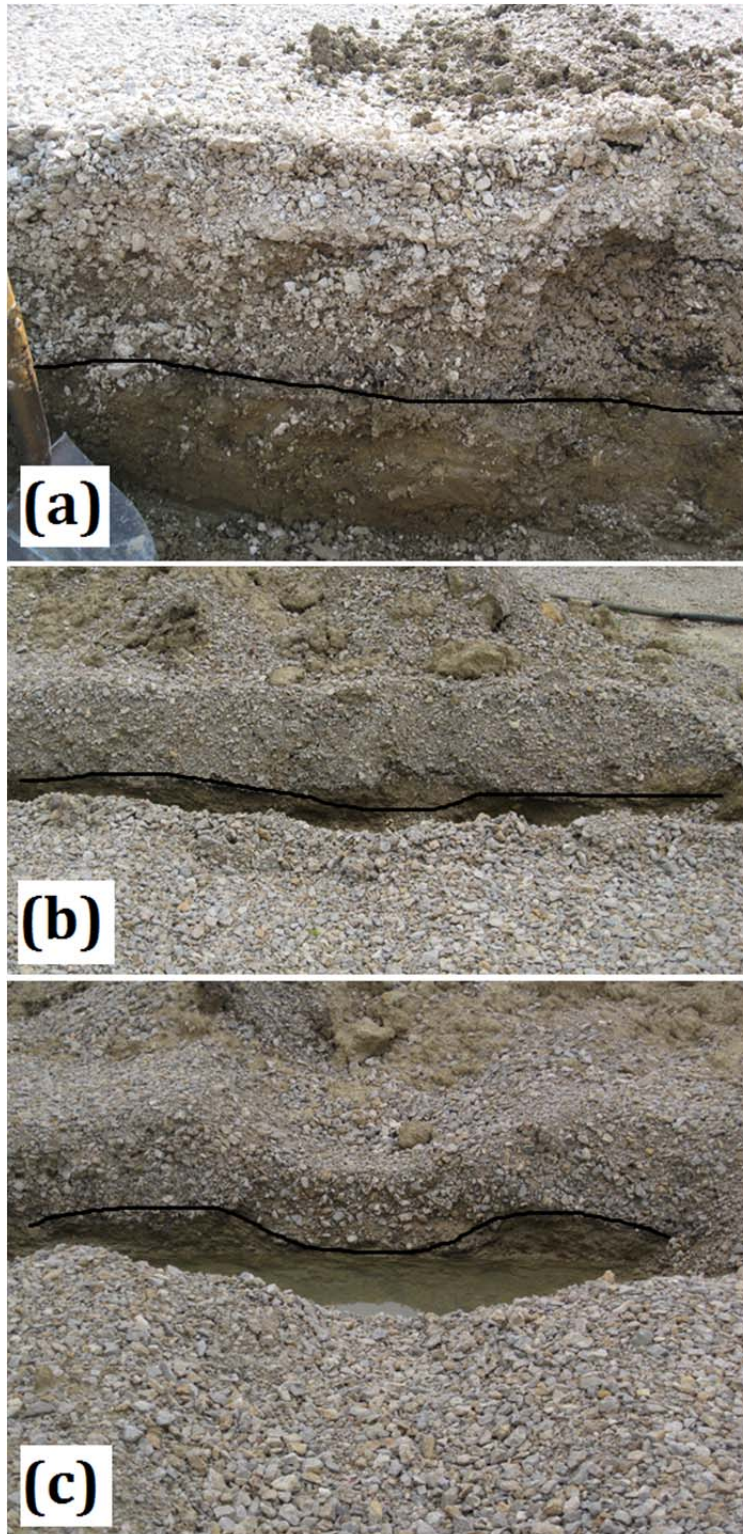


Figure C-5 Excavated trench photos showing surface and base-subgrade interface deformations in test sections (a) 1, (b) 2, and (c) 3 for Cell 2 due to loading under flooded conditions

**APPENDIX D INVESTIGATION OF FREEZE-THAW EFFECTS ON
CELL 3**

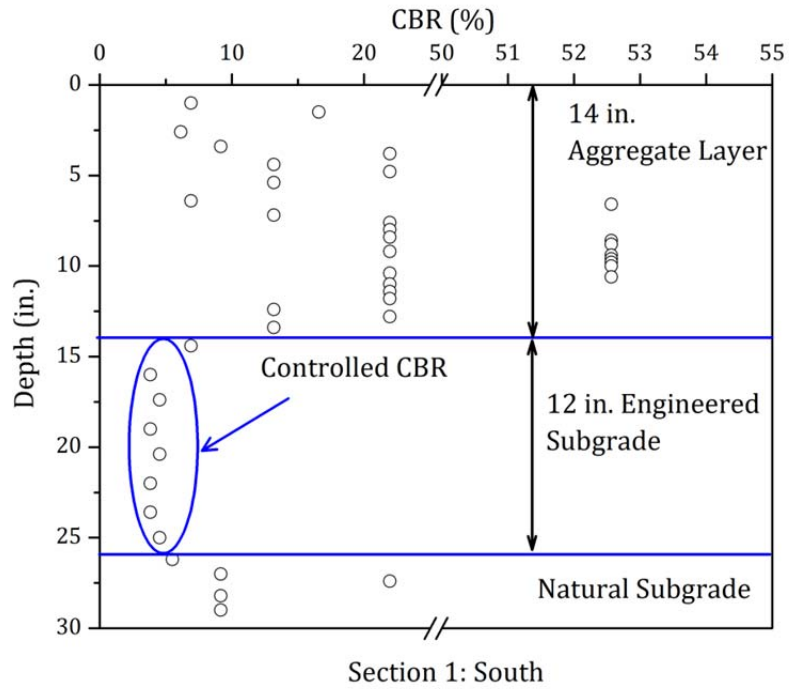


Figure D-1 IBV profile with depth along the South wheel path of Cell 3 Section 1 effort (IBV shown as “CBR” in the figure)

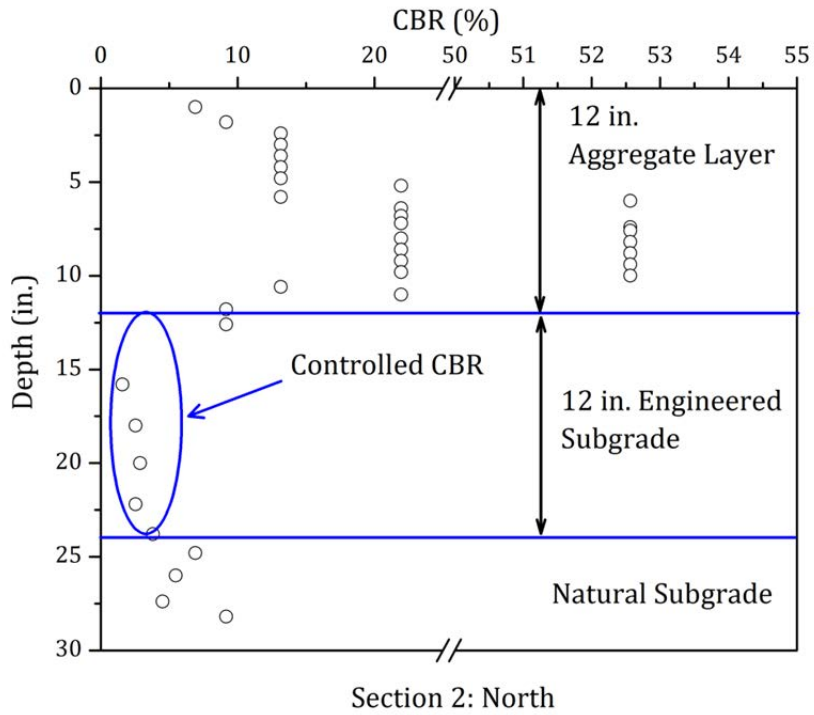
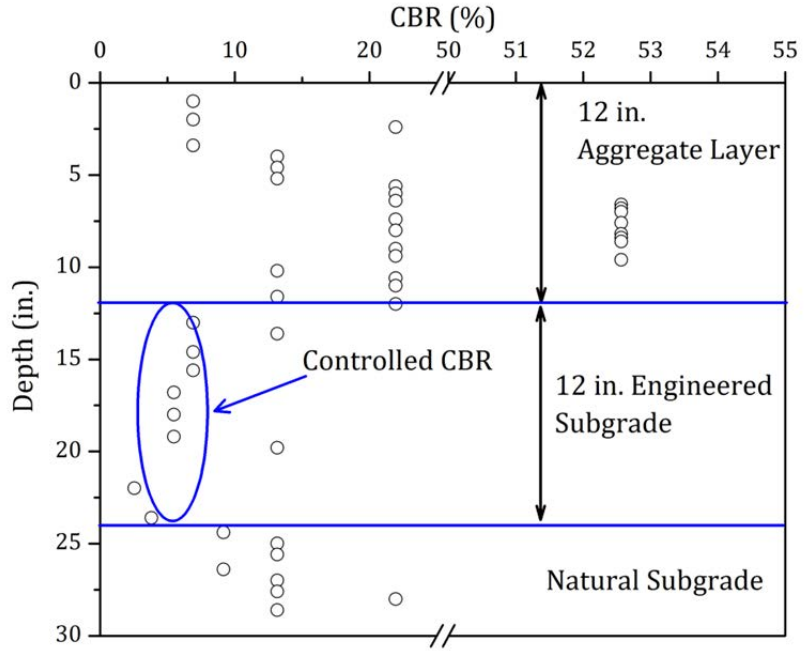
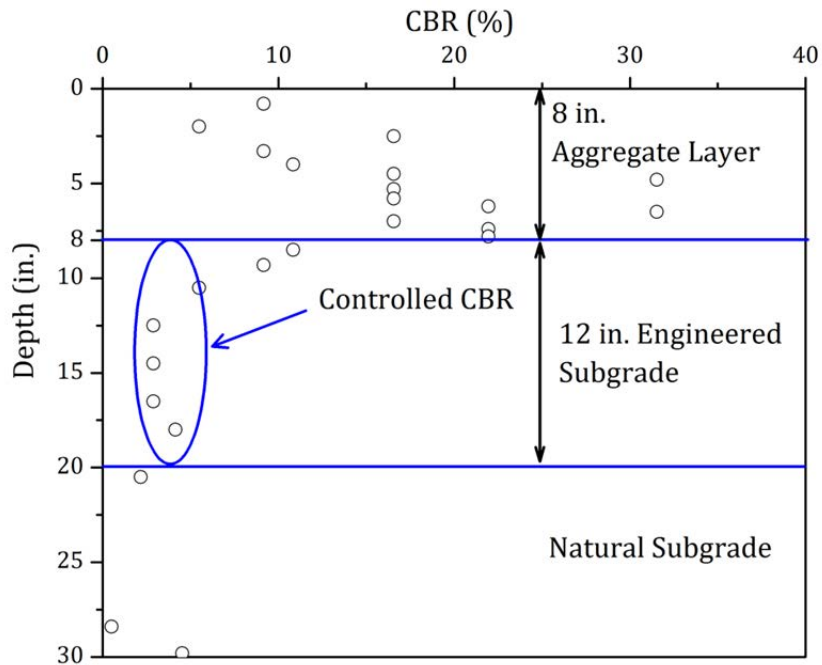


Figure D-2 IBV profile with depth along the North wheel path of Cell 3 Section 2 (IBV shown as “CBR” in the figure)



Section 2: South

Figure D-3 IBV profile with depth along the South wheel path of Cell 3 Section 2 (IBV shown as “CBR” in the figure)



Section 3: North

Figure D-4 IBV profile with depth along the North wheel path of Cell 3 Section 3 (IBV shown as “CBR” in the figure)

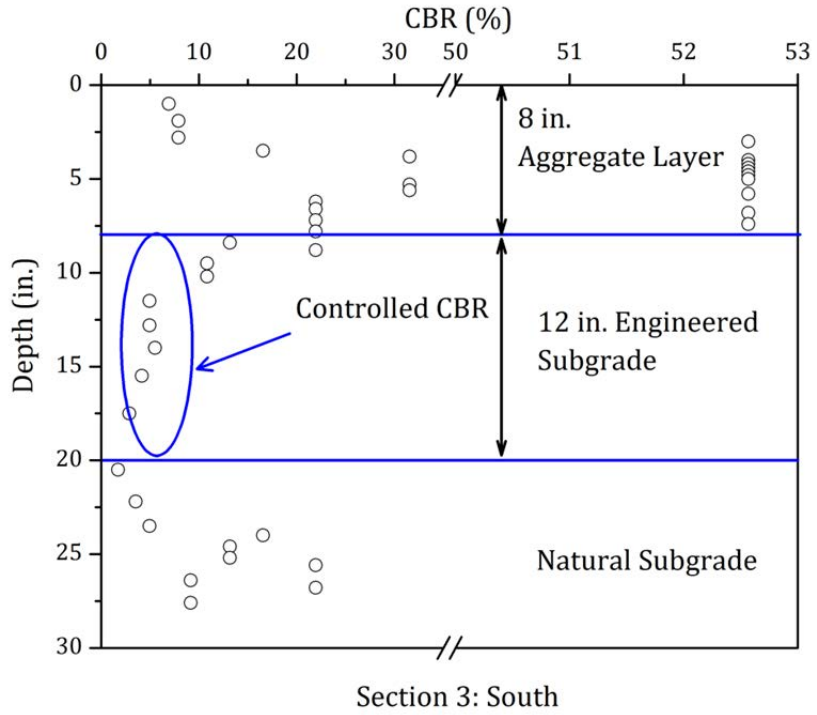


Figure D-5 IBV profile with depth along the South wheel path of Cell 3 Section 3 (IBV shown as “CBR” in the figure)

**APPENDIX E SURFACE PROFILE
MEASUREMENTS DATA**

Deflection Worksheet

11/15/2010 Cell 1 ← # of Passes 0 → Wheel Path: North

Measurements

		West						East					
		1		2		3		4		5		6	
North	48	134.65	141.94	137.88	139.11	145.72	141.75						
	42	131.83	139.86	144.05	145.5	136.69	135.88						
	36	134.25	132.27	142.59	146.79	134.95	134.77						
	30	132.99	138.38	149.24	146.32	132.94	134.09						
	24	132.57	132.89	146.34	147.15	139.14	145.24						
	22	132.46	135.09	151.59	140.04	142.32	147.76						
	20	135.03	138.95	146.43	143.23	142.31	147.39						
	18	133.42	135.33	151.17	148.14	140.43	142.59						
	16	135.33	144.3	144.26	142.21	139.53	144.45						
	14	134.13	135.67	150.72	141.4	135.25	133.31						
	12	135.19	146.57	153.49	148.49	132.08	142.55						
	10	133.73	144.52	147.8	149.68	138.27	137.65						
	8	136.58	137.16	147.96	148.66	140.27	134.34						
	6	133.93	135.22	145.03	145.18	140.53	140.3						
	4	130.79	140.17	139.55	146.32	137.16	137.75						
	2	129.14	134.79	135.38	142.7	136.11	132.63						
	0	130.91	139.39	149.28	138.01	133.42	138.57						
	2	127.69	129.72	146.72	138.82	129.37	137.66						
	4	130.75	133.9	136.68	144.26	129.19	130.7						
	6	128.97	133.91	133.2	140.69	128.33	129.51						
	8	126.92	133.88	137.21	143.04	128.17	135.24						
	10	120.31	131.08	127.89	134.59	130.34	135.96						
	12	127.78	133.88	127.68	134.35	129.91	137.55						
	14	122.65	135.96	121.73	147.63	124.61	131.66						
16	132.75	136.06	136.04	142.47	126.93	130.25							
18	132.71	137.22	128.1	133.94	134.57	132.12							
20	134.42	134.24	131.01	133.11	130.02	131.74							
22	135.56	144.6	132.47	130.92	129.22	134.56							
24	136.06	141.79	123.96	137.68	128.75	132.36							
30	140.59	142.38	136.34	136.14	126.92	135.19							
36	142.89	141.59	134.3	131.53	132.7	133.81							
42	142.98	142.97	136.74	136.6	133.66	148.86							
48	136.49	143.35	135.72	133.96	132.92	144.29							

Deflection Worksheet

11/16/2010 Cell 1 # of Passes 1 (Actually 2) Wheel Path: North

Measurements

	West ← ————— → East						
	1	2	3	4	5	6	
North	48	137.08	143.23	138.7	136.26	137.82	138.74
	42	139.34	136.91	142.86	138.38	136.24	135.33
	36	133.91	131.78	147.34	141.08	141.12	135.67
	30	128.11	135.35	148.05	144.14	133.11	140.05
	24	129.12	133.01	144.16	141.97	138.61	136.51
	22	129.83	130.66	144.54	141.74	137.97	130.35
	20	128.96	130.42	143.7	140.91	140.05	130.34
	18	129.15	134.52	140.18	141.4	139.19	145.38
	16	130.91	133.22	140.82	142.94	139.19	142.09
	14	128.33	130.29	149.71	142.8	132.91	141.56
	12	130.19	143.68	150.04	142.8	136.18	141.82
	10	129.53	140.91	150.12	141.48	136.58	139.53
	8	136.43	143.38	157.3	143.58	137.08	139.53
	6	140.53	143.38	154.83	142.55	137.74	136.51
	4	143.88	146.7	146.3	148.75	136.85	138.95
	2	142.26	145.09	144.6	138.72	133.94	138
CL	0	140.33	147.13	151.08	148.23	136	143.05
	2	142.4	148.54	141.81	149.86	134.69	142.73
	4	142.62	147.24	145.68	150.13	136.69	135.69
	6	142.6	145.08	137.83	142.58	132.52	132.1
	8	139.92	143.93	137.56	139.51	126.99	137.51
	10	126.89	134.66	132.92	137.9	126.25	135.14
	12	127.88	135.46	128.59	137.82	124.61	132.82
	14	123.34	143.84	138.18	142.3	122.29	131.24
	16	133.32	140.47	135.29	136.69	124.93	130.41
	18	131.98	139.73	134.41	133.15	129.04	135.18
	20	134.77	138.88	128.79	131.13	125.45	131.11
	22	139.93	138.86	128.74	127.64	130.66	134.58
	24	135.92	140.5	131.94	137.44	130.66	134.3
	30	141.95	141.33	130.25	137.26	127.24	140.21
	36	147.82	141.93	130.42	138.1	133.43	141.29
	42	142.64	144.14	141.13	133.94	136.77	141.61
South	48	141.53	144.07	138	136.41	139.07	144.92

Deflection Worksheet

11/16/2010 Cell 1 # of Passes 10 Wheel Path: North

Measurements

	West						East
	1	2	3	4	5	6	
North	48	136.21	145.58	140.08	142.37	136.87	139.03
	42	132.11	134.21	143.56	137.73	135.98	131.22
	36	130.86	130.48	135.05	141.77	134.82	136.02
	30	120.61	130.48	144.83	136.85	133.7	133.75
	24	116.82	123.87	138.08	132.77	134.88	128.87
	22	115.66	120.4	140.29	135.9	141.9	136.27
	20	112.51	120.89	145.28	138.59	140.8	134.29
	18	113.42	116.62	141.33	141.08	140.94	134.5
	16	111.85	120.36	140.47	138.56	134.44	139.66
	14	116.84	121.07	147.36	136.51	131.1	136.73
	12	113.2	127.46	147.46	141.21	133.36	134.32
	10	119.45	125.44	144.05	138.82	129.08	133.85
	8	151.38	141.92	161.56	139.01	139.9	134.08
	6	165.24	161.32	165.13	149.47	139.63	135.14
	4	165.99	169.88	160.96	154.88	138.64	139.38
	2	164.37	163.46	159.54	162.69	137.61	141.04
CL	0	167.72	168.5	155.23	154.51	137.15	139.31
	2	165.04	168.5	167.41	153.01	136.87	136.03
	4	171.51	171.85	158.08	156.13	134.5	136.71
	6	174.23	165.6	160.81	148.28	138.52	139.67
	8	167.35	163.55	161.52	150.75	125.84	131.78
	10	124.57	132.68	140.49	135.38	124.72	130.67
	12	113.2	127.09	138.08	140.48	134.07	132.72
	14	111.47	134.28	143.46	143.5	123.76	131.05
	16	118.4	127.53	135.47	140.36	120.63	142.41
	18	121.7	127.58	127.86	130.67	130.78	138.38
	20	128.46	137.55	122.24	128.82	127.27	131.28
	22	128.97	132.51	130.25	127.24	126.03	138.41
	24	130.33	137.6	130.21	141.21	127.4	134.07
	30	138.22	138.56	134.21	139.69	126.14	142.83
	36	143.82	142.16	131.05	136.57	131.22	137.16
	42	141.29	141.19	138.75	135.75	134.08	137.27
South	48	136.89	144.29	135.95	141.95	134.52	142.64

Deflection Worksheet

11/16/2010 Cell 1 # of Passes 47 Wheel Path: North

Measurements

	West		East			
	1	2	3	4	5	6
North	48	136.48	135.71			
	42	131.1	129.39			
	36	124.92	119.85			
	30	93.06	96.79			
	24	66.7	80.17			
	22	61.74	73.06			
	20	54.23	69.34			
	18	53.43	70.16			
	16	52.35	77.61			
	14	52.84	74.44			
	12	58.76	75.21			
	10	180.96	172.57			
	8	215.9	215.9			
	6	228.6	222.25			
	4	228.6	228.6			
	2	234.95	228.6			
CL	0	234.95	228.6			
	2	234.95	228.6			
	4	222.25	228.6			
	6	215.9	215.9			
	8	202.9	203.2			
	10	145.4	151.78			
	12	104	138.66			
	14	87.59	87.57			
	16	72.77	87.58			
	18	66.2	91.01			
	20	67.69	97.18			
	22	76.28	99.68			
	24	82.6	100.94			
	30	117.8	118.61			
	36	136.06	133.92			
	42	140.37	139.84			
South	48	140.56	141.78			

Deflection Worksheet

11/16/2010 Cell 1 # of Passes 100 Wheel Path: North

Measurements

	West		Measurements				East
	1	2	3	4	5	6	
48			137.21	140.17	135.28	133.69	
42			132.53	134.98	135.37	132.7	
36			125.39	131.41	131.69	129.66	
30			116.31	123.7	135.45	126.21	
24			107.81	112.83	126.35	126.36	
22			108.76	105.54	127.07	126.34	
20			107.49	161.91	128.19	126.37	
18			108.02	119.16	127.91	123.1	
16			108.68	115.19	127.61	126.73	
14			110.87	108.37	123.12	121.92	
12			112.92	119.18	123.01	121.85	
10			148.39	118.19	120.41	125.4	
8			190.87	186.92	146.72	146.58	
6			209.55	187.3	150.48	147.47	
4			203.2	188.41	151.53	152.2	
2			222.25	188.17	153.12	155.34	
0			215.9	190.86	154.25	155.8	
2			215.9	188.99	149.32	153.25	
4			215.9	194.77	149.3	149.03	
6			215.9	185.27	147.8	144.82	
8			188.32	174.42	121.98	122.96	
10			145.85	134.18	115.36	128.66	
12			101.75	117.58	117.76	129.07	
14			106.58	118.81	120.3	125.86	
16			104.35	121.12	119.31	124.4	
18			101.58	120.04	118.29	125.73	
20			99.97	121.36	125.52	127.11	
22			106.1	117.22	126.67	130.75	
24			107.52	128.08	127.65	130.77	
30			116.25	127.1	129.68	134.33	
36			121.78	130.22	129.61	132.01	
42			130.92	133.95	133.87	143.48	
48			134.09	134	137.94	142.22	

North



CL



South


Deflection Worksheet

11/18/2010 Cell 1 # of Passes 160 Wheel Path: North

Measurements

West ←  East

	1	2	3	4	5	6
48			136.33	134.65	135.82	134.31
42			136.72	132.39	132.92	129.54
36			124.3	122.32	131.17	125.04
30			114.4	107.65	128.58	119.74
24			104.19	96.09	126.41	111.19
22			100.29	91.26	128.58	110.51
20			110.21	88.58	124.7	115.82
18			110.32	87.41	124.71	112.17
16			96.13	88.15	124.63	112.18
14			101.11	86.86	123.75	112.36
12			110.47	88.85	117.04	112.35
10			152.72	132.61	118.96	121.08
8			228.6	188.86	151.3	154.13
6			228.6	201.48	153.29	154.47
4			228.6	209.55	155.39	159.1
2			241.3	209.55	163.08	158.84
0			241.3	215.9	159.81	160.54
2			241.3	215.9	159.53	158.02
4			241.3	209.55	155.89	152.5
6			234.95	202.39	153.25	156.07
8			228.6	180.6	137.81	119.52
10			181.28	148.43	103.19	120.02
12			117.98	103.18	111.92	120.01
14			95.14	110.06	110.04	123.21
16			102.29	110.63	118.6	123.4
18			95.45	109.24	116.73	126.26
20			93.73	107.76	115.8	128.29
22			93.98	113.39	117.65	129.16
24			93.88	121.43	120.51	129.14
30			113.2	125.82	124.46	132.33
36			118.02	125.97	128.91	134.86
42			130.3	132.55	131.27	134.86
48			134.85	135.34	135.17	140.15

North

 CL

 South

Deflection Worksheet

11/18/2010 Cell 1 # of Passes 400 Wheel Path: North

Measurements

West ←  East

	1	2	3	4	5	6
48					135.79	131.55
42					138.8	134.92
36					134	126.32
30					123.59	112.12
24					113.56	83.79
22					111.7	67.86
20					111.45	59.57
18					112.22	52.82
16					109.5	220.54
14					98.51	220.54
12					90.83	220.54
10					119.36	168.85
8					171.68	168.09
6					175.41	180.16
4					175.61	180.31
2					175.79	180.76
0					175.8	181.69
2					175.84	181.16
4					175.67	177.41
6					172.01	173.1
8					143.84	124.32
10					105.54	101.83
12					99.3	111.12
14					95.87	113.16
16					106.51	113.23
18					107.68	114.81
20					111.97	116.8
22					113.75	120.7
24					113.6	121.46
30					121.09	132.82
36					130.54	125.87
42					131.77	134.47
48					134.87	136.34

North



CL





South

Deflection Worksheet

11/19/2010 Cell 1 # of Passes 0 Wheel Path: South

Measurements

West ←  East

		1	2	3	4	5	6
North  CL  South	48	140.91	140.46	145.96	137.76	139.01	140.6
	42	142.4	134.33	139.51	140.15	136.53	136.46
	36	142.25	132.2	134.32	131.75	136.69	132.55
	30	142.28	131.59	131.15	129.65	129.18	130.62
	24	124.73	125.93	131.04	124.55	127.89	129.68
	22	137.8	137.69	130.78	127.27	127.48	129.09
	20	139.56	133.17	129.6	125.5	130.48	128.92
	18	136.37	124.33	132.02	130.03	127.07	128.41
	16	137.18	133.36	132.07	131.21	132.33	124.91
	14	134.81	132.8	134.49	131.01	129.52	129.37
	12	136.91	136.35	131.19	133.94	129.3	121.44
	10	140.28	137.73	138.37	127.68	133.76	129.53
	8	143.93	135.85	129.98	133.4	132.63	136.68
	6	135.67	134.69	133.01	139.96	136.24	127.48
	4	140.09	136.91	136.93	141.04	139.75	131.47
	2	144.14	131.81	136.03	140.63	133.57	132.34
	0	138.14	131.5	136.2	140.52	134.66	131.81
	2	138.02	137.62	141.18	146.49	137.28	128.4
	4	131.6	131.59	142.49	141.93	136.28	130.47
	6	132	132.17	131.61	135.63	134.41	130.49
	8	139.35	132.64	135.92	137.54	136.89	135.36
	10	137.27	133.98	134.91	134.13	131.17	134.91
	12	130.23	131.12	128.06	124.69	133.13	131.91
	14	126.58	133.14	121.08	116.68	137.91	133.11
	16	121.26	123.59	111.79	114.82	128.96	129.52
	18	121.04	127.63	144.46	109.16	123.14	127.67
	20	123.2	124.1	114.97	109.79	125.05	121.48
	22	123.17	122.56	115.76	110.31	127.44	118.6
	24	120.92	122.41	118.51	112.28	120.08	119.28
	30	126.75	120.33	123.12	113.09	124.51	121.65
	36	122.49	125.97	120.42	117.23	122.59	122.8
	42	123.1	123.06	122.1	122.29	127.34	130.86
	48	137.5	133.87	129.13	133.23	130.01	131.69

Deflection Worksheet

11/20/2010 Cell 1 # of Passes 1 Wheel Path: South

Measurements

West ← ————— → East

		1	2	3	4	5	6
North	48	137.83	139.84	141.75	138.82	139.02	137.83
	42	133.87	137.79	140.61	149.46	135.82	135.79
	36	132.94	129.82	134.39	129.03	133.85	134.26
	30	136.05	128.79	130.59	131.4	129.15	133
	24	135.44	131.01	128.25	137.66	133.77	133.86
	22	132.73	127.25	131.81	123.25	129.2	128.91
	20	134.06	132.26	132.15	124.47	129.38	126.64
	18	134.45	131.43	129.29	131.26	125.18	126.46
	16	135.46	132.04	131.08	125.21	131.9	126.45
	14	135.9	137.23	131.08	126.94	132.39	129.99
	12	135.41	131.48	131.12	136.21	129.91	129.07
	10	140.04	130.56	132.42	127.95	132.13	131.89
	8	135.57	134.68	132.44	128.82	131.58	129.04
	6	142.68	139.57	147.06	140.29	134.86	128.61
	4	141.17	139.03	150.53	145.02	140.67	137.46
	2	151.03	140.47	150.64	148.85	144.23	141.76
CL	0	141.18	136.06	151.67	153.77	142.22	140.08
	2	145.63	143.78	151.24	155.66	144.84	140.68
	4	144.94	136.41	146.79	145.53	142.51	135.84
	6	144.71	137.44	143.17	143.25	144.82	137.1
	8	159.59	136.68	140.74	141.61	137.31	140.13
	10	146.79	131.33	132.48	141.15	136.51	139.19
	12	127.45	132.06	128.38	130	129.88	128.72
	14	128.53	131.36	121.48	119.06	128.13	127.49
	16	125.33	124.07	118.52	111.61	129.64	127.43
	18	124.72	125.49	116.27	106.41	125.73	123.35
	20	127.04	125.21	113.53	106.86	125.63	122.25
	22	121.04	120.02	111.77	110.44	126.26	118.21
	24	129.27	119.38	112.52	112.84	119.53	118.56
	30	130.04	123.04	120.61	117.49	122.17	119.48
	36	137.87	137.78	121.53	118.79	123.54	122.38
	42	141.82	122.68	122.65	124.4	132.39	128.75
South	48	141.88	136.81	133.65	129.58	132.16	135.5

Deflection Worksheet

11/20/2010 Cell 1 # of Passes 10 Wheel Path: South

Measurements

	Measurements					
	West	1	2	3	4	5
48	136.84	136.74	142.5	139.54	137.18	140.64
42	130.44	133.58	139.6	131.74	136.35	140.84
36	127.31	127.03	128.95	129.09	131.11	139.08
30	132.46	123.9	120.96	113.05	125.79	131.14
24	128.46	121.91	113.88	133.39	125.16	128.05
22	125.81	122.21	120.08	111.37	120.12	125.52
20	121.17	124.2	117.22	110.03	120.82	120.65
18	129.28	121.99	116.69	116.86	114.63	117.4
16	125.83	117.93	115.11	112.5	120.74	118.23
14	124.6	127.65	113.97	104.51	120.81	119.95
12	126.26	124.23	121.1	116.53	118.14	124.34
10	126.09	131.11	120.36	109.99	129.06	124.68
8	125.45	134.56	115.28	113.92	129.18	124.08
6	163.83	129.67	157.22	146.8	140.22	127.35
4	166.7	160.81	184.93	185.4	173.22	166.42
2	168.15	153.69	188.11	189.81	171.81	169.25
0	170.11	161.59	183.77	188.82	175.87	169.09
2	169.11	162.98	187.21	189.62	176.75	170.07
4	172.52	161.5	185.72	187.34	177.81	164.67
6	169.64	155.18	181.86	182.83	174.93	171.28
8	167.02	154.23	174.46	182.39	171.67	171.2
10	150.57	132.99	174.38	176.33	168.62	162.18
12	127.23	121.12	117.81	127.81	124.19	155.51
14	120.39	119.21	90.08	87.08	113.49	116.84
16	112.75	114.82	89.14	83.62	109.44	113.01
18	114.03	115	91.55	81.28	112.34	113.03
20	110.22	112.66	92.17	81.03	107.41	109.98
22	110.94	113.8	93.41	82.47	106.75	102.87
24	112.9	113.11	93.74	88.19	106.74	105.35
30	119.59	118.33	108.75	98.6	116.92	107.27
36	115.48	120.34	113.26	109.06	119.43	118.25
42	131.41	124.82	119.44	122.09	129.36	131.99
48	144.65	128.52	128.77	127.58	132.68	132.97

North



CL



South

Deflection Worksheet

11/20/2010 Cell 1 # of Passes 27 Wheel Path: South

Measurements

	West						East
	1	2	3	4	5	6	
48	135.42	137.64	140.22	143.77	141.44	141.01	
42	132.8	135.55	140.42	130.88	134.37	138.27	
36	128.18	125.54	127.89	126.63	135.47	136.02	
30	118.1	119.73	112.43	102.57	120.43	126.84	
24	118.17	113.47	98.69	87.88	93.91	115.78	
22	112.11	110.27	100.64	94.61	88.75	112.89	
20	108.08	108.78	96.11	103.88	82.72	107.19	
18	106.22	112.18	101.66	96.13	82.97	104.77	
16	105.22	105.75	101.36	82.54	83.07	109.26	
14	105.1	108.8	102.92	86.07	83.11	107.53	
12	112.11	111.24	94.89	92	82.9	111.39	
10	123.31	116.51	96.85	104.55	87.99	108.78	
8	158.36	151.44	100.21	93.65	90.3	114.77	
6	203.2	193.82	194.02	174.89	189.74	144.25	
4	203.2	193.81	228.6	241.3	234.95	222.25	
2	209.55	192.28	234.95	241.3	234.95	222.25	
0	209.55	202.88	234.95	241.3	241.3	228.6	
2	209.55	192.02	228.6	228.6	241.3	222.25	
4	209.55	192.02	228.6	228.6	228.6	222.25	
6	203.16	188.81	215.9	228.6	228.6	215.9	
8	203.3	188.82	215.9	228.6	228.6	209.55	
10	137.9	146.35	215.9	222.25	222.25	203.2	
12	97.1	100.82	162.88	143.27	131.92	175.74	
14	94.84	101.62	99.3	87.95	66.82	87.77	
16	92.87	101.5	12.31	29.1	58.38	73.5	
18	84.84	102.26	36.39	29.07	58.4	70.08	
20	91.2	99.75	33.33	29.06	58.46	63.69	
22	93.24	105.12	33.28	29.01	66.64	63.7	
24	100.26	105.56	43.07	43.08	67.03	63.56	
30	161.12	109.19	95.46	72.3	98.71	73.03	
36	162.07	119.51	106.07	105.15	119.74	111.36	
42	128.93	119.54	113.94	119.61	123.97	121.29	
48	139.07	129.1	127.51	128.1	127.91	124.38	

North



CL



South

Deflection Worksheet

11/22/10 Cell 2 # of Passes 0 Wheel Path: North

Measurements

West ← —————→ East

		1	2	3	4	5	6
North	48	138.8	130.07	136	136.72	132.95	139.17
	42	133.33	121.52	132.18	129.46	131.07	128.24
	36	130.86	119.11	134.09	131.25	128.41	126.04
	30	128.04	117.34	117.03	131.88	134.67	124.81
	24	126	114.86	114.88	119.13	119.82	126.11
	22	126.86	116.09	115.53	118.37	114.23	124.45
	20	129.69	114.77	121.14	124.78	120.46	123.81
	18	131.11	116.14	117.24	121.39	120.49	127.36
	16	131.03	114.17	126	130.12	118.86	123.78
	14	129.63	114.65	145.11	120.81	120.32	130.9
	12	126.33	118.3	112.17	124.85	122.93	119.41
	10	130.64	116.31	120.07	128.14	119.23	124.56
	8	135.32	125.57	123.95	139.42	120.12	130.21
	6	135.9	130.09	124.89	143.36	121.37	135.44
	4	138.39	119.89	123.27	125.76	122.04	130.78
	2	143.06	143.68	124.54	127.04	125.61	125.53
	0	145.96	134.7	117.46	129.38	126.07	130.59
	2	150.27	142.25	132.59	120.12	124.86	132.41
	4	150.85	139.11	126.01	129.04	126.24	129.4
	6	152.7	145.79	135.57	128.59	120.31	135.84
	8	155.27	139.8	129.03	136.17	129.94	139.32
	10	149.76	148.99	134.22	128.32	126.3	129.32
	12	152.52	132.72	128.87	135.38	128.84	136.1
	14	145.89	121.36	127.74	133.35	130.66	145.12
	16	134.49	115.38	124.46	128.42	130.73	138.59
	18	131.83	118.91	127.36	122.75	127.73	130.58
	20	139.59	113.07	118.26	124.8	135.76	129.62
	22	131.28	110.08	118.06	127.57	135.08	128.77
	24	133.55	112.1	134.08	121.774	119.73	133.76
	30	133.98	112.16	126.66	123.99	125.46	130.96
	36	134.42	114.83	125.64	131.59	137.95	131.65
	42	133.72	122.57	135.19	127.42	137.66	137.48
South	48	136.77	110.03	137.28	126.75	138.45	126.63

Deflection Worksheet

11/29/2010 Cell 2 # of Passes 1 Wheel Path: North

Measurements

	Measurements					
	West					East
	1	2	3	4	5	6
48	134.88	131.23	136.34	135.19	132.73	126.25
42	129.68	137.05	141.47	134.87	126.06	126.85
36	130.75	130.17	137.82	132.84	125.85	133
30	125.84	121.27	127.38	127.44	121.04	122.09
24	130.43	121.19	121.8	120.22	122.51	123.71
22	130.42	120.88	116.05	122.24	128.09	126.69
20	125.63	124.78	117.51	125.13	120.06	127.48
18	132.5	119.38	119.85	126.08	113.75	127.26
16	128.68	115.88	117.85	130.18	120.77	125.1
14	123.97	124.47	118.07	128.92	116.55	117.61
12	124.81	119.98	119.22	124.12	124.9	126.06
10	137.16	130.57	124.59	124.87	124.18	121.88
8	139.56	137.32	126.21	136.98	119.18	122.26
6	141.24	142.79	132.11	141.81	118.63	123.78
4	146.57	139.67	135.29	137.02	119.17	128.15
2	152.94	142.6	133.19	137.39	123.58	127.36
0	157.6	140.66	130.62	139.64	123.04	132.05
2	153.17	149.75	138.4	133.64	125.98	138
4	152.58	150.78	136.56	133.76	128.95	135.01
6	154.32	150.26	139.19	137.11	129.59	137.06
8	155.08	144.85	135.27	140.07	128.88	133.27
10	151.19	142.66	131.42	129.63	124.03	136.35
12	145.63	143.05	133	135.47	123.36	129.98
14	147.03	137.02	127.6	128.87	123.48	135.14
16	148.04	128.25	125.1	129.86	129.77	131.5
18	143.33	132.53	132.38	125.35	125.5	136.91
20	141.56	120.42	127.77	124.37	132.05	125.08
22	135.77	117.51	133.75	131.05	128.05	126.23
24	130.72	121.14	129.65	123.52	125.45	137.05
30	146.07	127.38	124.2	125.68	131.29	125.21
36	139.6	120.17	135.47	130.93	126.44	138.21
42	139.48	138.11	141.39	135.08	135.89	138.65
48	149.79	140.91	135.03	138.33	138.07	138.57

North



CL



South

Deflection Worksheet

11/29/2010 Cell 2 # of Passes 10 Wheel Path: North

Measurements

West ← → East

	1	2	3	4	5	6
48	134.22	124.61	133.69	129.65	128.58	129.54
42	123.68	121.73	134.28	127.66	125.41	125.25
36	121.11	116.32	129.03	128.61	116.16	129.28
30	116.77	111.22	121.15	125.58	121.5	123.13
24	117.06	112.9	117.45	116.37	119.01	126.33
22	116.88	110.13	111.15	122.34	125.19	122.1
20	116.98	114.39	113.22	116.16	114.86	121.12
18	116.88	109.56	112.7	120.2	119.58	124.08
16	119.84	113.69	113.28	118.97	114.68	124.11
14	120.89	111.92	104.13	116.92	114.13	111.5
12	122.26	114.63	111.3	123.54	120.59	116.4
10	121.44	117.01	118.04	118.56	115.51	117.52
8	131.3	120.78	122.47	122.75	116.19	122.66
6	164.7	158.05	151.87	138.21	120.19	136.03
4	168.86	165.45	151.58	140.75	123.18	134.32
2	167.27	172.09	153.09	147.61	126.7	135.93
0	174.65	171.57	160.2	148.28	128.9	135.32
2	171.26	170.26	156.6	144.66	125.58	139.78
4	171.32	171.21	156.18	147.24	129.39	139.15
6	170.36	166.91	151.62	140.44	128.02	141.05
8	172.76	161.73	150.29	146.75	129.19	136.91
10	160.53	147.04	135.48	138.46	129.15	127.26
12	140.88	126.38	124.85	127.08	126.83	127.75
14	124.89	123.37	114.12	120.18	118.68	130.1
16	123.11	119.65	113.37	120.31	121.54	130.88
18	124.6	116.06	105.67	123.33	125.25	120.35
20	125.07	107.53	118.14	118.22	122.56	123.16
22	120.2	111.66	107.04	113.18	117.9	121.76
24	129.6	116.81	118.09	117.45	121.94	129.58
30	121.54	122.54	126.17	131.41	125.74	131.43
36	134.16	127.92	128.55	135.81	132	139.44
42	136.09	132.68	133.61	137.1	131.22	135.44
48	141.91	135.64	136.15	136.37	138.16	135.66

Deflection Worksheet

12/1/2010 Cell 2 # of Passes 52 Wheel Path: North

Measurements

	West			East		
	1	2	3	4	5	6
48	133.8	123.94	140.16	142.75	136.82	128.29
42	122.64	117.33	128.39	129.65	127.64	133.64
36	119.14	105.6	132.08	125.12	129.42	129.81
30	102.66	101.77	113.18	127.18	120.74	126.41
24	91.72	89.87	107.59	106.72	118.01	125.05
22	94.09	81.19	93.66	110.85	125.8	120.57
20	93.08	84.73	98.33	101.98	119.57	117.98
18	88.21	77.14	89.03	108.37	119.71	117.16
16	86.88	71.73	90.92	105.88	116.93	121.44
14	82.91	71.36	77.71	104.68	115.68	113.6
12	84.59	71.42	85.14	95.81	116.34	114.51
10	51.75	71.02	84.85	102.02	121.63	110.59
8	82.89	162.01	147.88	129.67	120.51	111.73
6	193.36	8.25 in	189.42	164.9	125.36	138.98
4	8 in	8.5 in	192.86	174.17	132.59	150.47
2	8.5 in	8.5 in	200.61	169.24	136.33	151.13
0	8.75 in	8.75 in	197.69	174.33	133.45	153.79
2	8.75 in	8.75 in	198.5	171.9	136.75	155.26
4	8.75 in	8.5 in	190.59	167.31	139.97	153.7
6	8.5 in	8.5 in	188.63	165.69	140.91	154.36
8	8.5 in	8 in	185.25	169.99	137.7	147.8
10	8.5 in	195.88	157.87	151.13	127.83	134.81
12	176.48	78.03	79.81	118.39	127.96	127.19
14	87.61	72.17	73.49	104.53	123.32	126.25
16	82.74	79.45	75.13	105.71	116.86	134.33
18	91.42	68.5	81.57	101.85	120.9	133.78
20	97.58	70.97	75.9	107.44	118.4	126.62
22	90.49	77.93	79	101.2	117.61	120.97
24	95.01	74.55	90.91	107.71	115.3	135.88
30	102.8	95.51	101.16	122.12	125.1	139.17
36	112.75	109.93	125.78	121.08	132.16	133.19
42	130.44	129.44	130.01	130.71	138.11	139.72
48	139.07	135.75	132.05	139.65	137.63	139.93

North



CL



South

Deflection Worksheet

12/1/2010 Cell 2 # of Passes 100 Wheel Path: North

Measurements

	West		Measurements			East
	1	2	3	4	5	6
48			128.85	137.89	127.95	130.34
42			120.65	124.85	129.45	125.3
36			113.83	118.62	122.81	127.07
30			105.87	107.35	130.05	120.26
24			85.91	95.33	117.41	117.97
22			77.81	82.15	119.82	118.35
20			73.11	81.32	113.99	114.49
18			62.87	76.44	118.79	110.94
16			61.14	75.59	109.97	103.23
14			52.22	64.41	112.01	96.83
12			40.27	64.8	116.49	92.55
10			44.42	65.46	114.01	93.89
8			161.24	157.04	118.66	103.55
6			8.25 in	191.33	119.94	141.46
4			9 in	199.08	139.65	145.81
2			9 in	201.11	135.52	156.09
0			9 in	203.35	139.12	160.12
2			9 in	203.97	141.72	159.16
4			9 in	202.37	143.82	155.33
6			8.75 in	202.15	142.77	151.09
8			8.5 in	202.38	134.72	147.2
10			182.53	172.04	133.23	128.81
12			137.85	93.34	121.51	122.22
14			35.7	88.79	118.95	117.18
16			36.19	85.58	114.9	127.69
18			37.87	82.5	118.34	116.76
20			38.02	87.4	113.01	115.46
22			41.93	85.56	119.61	119.44
24			41.91	93.87	113.58	123.03
30			78.45	97.67	122.95	136
36			108.73	121.8	134.67	131.25
42			129.56	130.78	131	134.67
48			136.74	141.2	137.23	126.34

North



CL



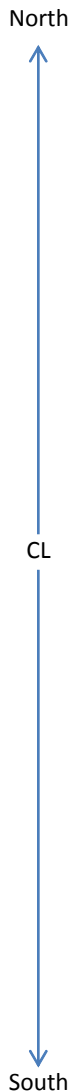
South

Deflection Worksheet

12/1/2010 Cell 2 # of Passes 350 Wheel Path: North

Measurements

	West				East	
	1	2	3	4	5	6
48					130.07	128.57
42					122.64	128.57
36					122.1	131.92
30					117.79	116.59
24					107.15	97.4
22					104.27	85.59
20					98.7	72.27
18					96.81	74.55
16					89.38	55.94
14					87.44	40.74
12					86.62	30.25
10					88.05	29.1
8					93.93	132.6
6					134.05	171.52
4					159.32	174.16
2					163.91	180.53
0					166.08	185.16
2					169.19	186.5
4					171.43	187.53
6					166.15	184.48
8					163.83	173.51
10					155.78	106.98
12					122.13	103.32
14					100.66	106.28
16					104.9	104.95
18					103.68	108.74
20					103.08	116.97
22					110.17	102.34
24					122.39	130.79
30					118.88	131.41
36					127.59	135.7
42					134	131.65
48					144.28	x



Deflection Worksheet

11/23/2010 Cell 2 # of Passes 0 Wheel Path: South

Measurements

West ← —————→ East

		1	2	3	4	5	6
North	48	136.98	150.78	143.99	134.48	140.53	144.27
	42	140.99	150.08	148.74	152.76	147.8	141.28
	36	146.24	165.39	150.26	152.45	145.39	158.24
	30	141.29	155.56	158.15	144.65	148.76	156
	24	131.68	144.61	146.49	150.87	141.08	151.17
	22	133.61	143.88	154.31	142.7	144.62	143.99
	20	134.02	152.71	152.84	146.83	150.61	144.99
	18	139.54	147.78	145.17	145.3	153.61	140.24
	16	136.64	149.55	145.24	145.65	145.24	149.65
	14	136	150.43	147.11	144.07	145.62	141.84
	12	138.04	154.47	148.7	144.66	145.93	140.3
	10	139.01	148.27	151.51	146.18	145.34	141.72
	8	138.64	150.06	148.51	141.89	140.56	146.4
	6	133.33	143.73	144.73	140.05	142.4	141.4
	4	134.98	143.22	144.84	142.86	141.19	143.64
	2	142.03	146.59	157.39	143.53	150.73	147.35
CL	0	141.64	147.59	145.98	139.84	146.58	153.72
	2	139.87	150.09	149.82	139.12	146.74	153.53
	4	144.92	152.48	146.68	143.9	144.77	143.97
	6	142.4	151.12	144.9	142.3	151.47	150.78
	8	142.42	156.32	143.6	147.68	148.42	131.58
	10	138.44	145.65	148.16	145.61	152.3	150.49
	12	140.92	140.29	147.47	141.77	150.73	153.6
	14	140.46	152.48	144.43	134.28	142.03	145.75
	16	140.45	153.88	142.23	141.73	148.85	144.82
	18	143.67	150.28	154.7	143.6	147.84	143.67
	20	145.69	148.93	144.54	145.35	149.05	145.93
	22	143.26	152.57	156.62	146.95	144.83	143.4
	24	138.42	150.91	147.4	144.75	144.17	141.86
	30	129.62	142.21	145.74	135.38	139.01	139.2
	36	125.87	138	148.48	136.22	139.04	143.09
	42	128.88	142.15	145.93	132.64	138.45	141.33
South	48	135.92	143.02	137.08	133.41	138.84	137.09

Deflection Worksheet

11/23/2010 Cell 2 # of Passes 1 Wheel Path: South

Measurements

	Measurements					
	West	1	2	3	4	5
48	131.13	144.32	133.54	140.03	137.15	139.81
42	146.95	152.35	143.33	142.04	140.66	146.54
36	140.82	154.07	149.91	149.65	138.88	154.68
30	135.55	151.03	154.15	145.98	147.01	155.34
24	129.68	141.38	146.85	145.63	143.35	148.66
22	129.67	144.76	141.77	145.41	142.45	146.25
20	134.85	144.71	143.79	139.84	142.43	138.85
18	135.01	142.86	140	143.31	139.28	142.06
16	131.56	142.82	141.9	143.61	140.33	140.55
14	131.68	147.33	141.9	143.64	140.53	140.06
12	133.42	147.34	142.82	143.63	140.74	135.98
10	137.55	148.19	143.01	143.4	141.84	144.06
8	144.95	144.46	148.49	137.48	133.23	138.53
6	138.02	150.97	152.43	150.09	140.85	143.34
4	144.98	151.04	155.47	150.89	141.25	143.59
2	150.56	152.48	155.46	147.74	138.25	145.93
0	143.66	149.2	151.34	147.48	141.08	145.31
2	142.8	150.71	150.15	149.4	139.41	145.98
4	142.94	150.68	151.19	149.54	142.98	146.43
6	142.34	152.86	149.59	146.47	143.2	150.98
8	135.56	150.43	149.25	146.46	141.61	141.08
10	135.95	141.58	144.41	136.06	144.94	149.65
12	136.64	141.68	143.18	136.29	147.74	145.28
14	143.57	141.67	143.51	134.18	137.1	147.35
16	143.05	141.9	140.06	138.99	146.64	139
18	138.34	145.8	151.66	139.03	141.22	144.79
20	139.15	146.8	141.2	140.53	143.56	142.42
22	140.75	148.42	137.54	140.98	138.55	141.59
24	135.35	146.03	140.68	136.18	136.33	143.16
30	130.06	134.43	143.33	128.3	134.05	129.88
36	130.4	131.22	132.41	135.97	131.51	134.86
42	130.23	132.62	137.71	127.88	131.53	134.91
48	132.23	135.05	133.91	137.61	134.48	133.99

North



CL



South

Deflection Worksheet

11/23/2010 Cell 2 # of Passes 10 Wheel Path: South

Measurements

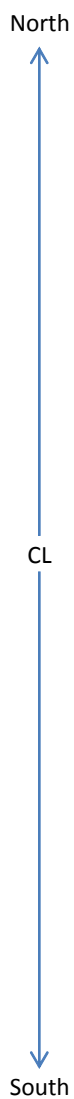
	West ← → East						
	1	2	3	4	5	6	
North	48	135.95	138.92	128.48	137.15	140.27	135.28
	42	140.14	146.73	133.31	133.86	146.19	142.27
	36	138.26	158.35	144.2	144.6	145.69	153.88
	30	130.16	143.85	145.71	140.86	149.88	152.76
	24	122.64	135.77	140.25	139.86	144.29	143.59
	22	127.3	135.54	133.33	130.86	139.97	141.83
	20	128.64	136.4	130.97	129.82	141.43	140.84
	18	129.55	136.11	129.9	131.4	139.78	135.35
	16	126.13	137.86	131.26	128.87	140.19	134.76
	14	125.68	139.91	134.12	129.35	136.55	135.82
	12	128.63	135.19	132.8	133.98	137.89	136.68
	10	157.21	136.17	132.74	131.6	138.17	129.75
	8	160.01	143.59	137.54	140.9	129.52	132.24
	6	162.56	175.04	167.38	174.35	133.87	133.19
	4	167.81	171.35	168.48	171.13	145.78	155.52
	2	168.22	171.84	168.95	173.74	151.66	152.61
CL	0	161.17	168.86	169.34	175.81	150.84	159.25
	2	165.05	174.23	171.83	175.27	154.82	157.48
	4	165.56	171.25	171.86	172.2	151.79	159.7
	6	162.17	171.23	168.92	172.17	151.66	154.94
	8	141.86	167.5	168.87	117.14	150.21	156.68
	10	132.93	142.29	139.57	141.03	150.58	153
	12	129.95	132.11	136.31	128.69	140.3	142.02
	14	133.18	134.53	135.74	123.12	135.57	140
	16	135.49	136.14	130.64	124.31	147.05	133.94
	18	136.3	138.32	132.62	126.66	141.17	140.95
	20	132.1	136.08	132.65	129.14	136.27	139.11
	22	136.03	140.08	126.65	129.13	138.89	133.08
	24	132.49	136.85	130.42	129.26	136.45	136.23
	30	125.49	131.38	135.85	129.86	135.99	130.77
	36	127.28	131.32	129.77	135.01	133.9	129.93
	42	128.28	134.63	133.96	124.68	134.4	128.06
South	48	135.42	131.18	132.5	131.68	127.86	128.75

Deflection Worksheet

11/23/2010 Cell 2 # of Passes 34 Wheel Path: South

Measurements

	West						East
	1	2	3	4	5	6	
48	145.68	141.99	136.21	136.35	144.33	136.68	
42	144.08	149.12	143.7	140.34	146.08	151.79	
36	140.49	142.27	137.62	147.76	147.75	156.08	
30	127.95	125.28	134.95	134.23	146.47	155.17	
24	115.57	123.71	131.57	117.51	143.05	141.05	
22	118.46	130.15	123.11	105.58	136.15	129.93	
20	123.35	126.43	112.11	105.81	137.99	126.01	
18	122.13	124.21	114.11	103.93	138.02	116.81	
16	122.85	129.37	110.26	101.68	136.35	122.29	
14	124.22	121.76	112.86	95.87	132.46	122.37	
12	124.13	118.8	109.79	98.5	130.3	112.89	
10	123.53	120.93	113.41	101.61	126.89	117.75	
8	172.35	174.75	144.33	142.54	132.56	116.45	
6	182.85	201.09	204.63	8.5 in	132.53	149.55	
4	189.04	200.85	200.66	8.5 in	157.41	166.34	
2	188.36	203	204.17	8 (3/8) in	161.24	168.49	
0	189.42	203.61	204.1	8.25 in	163.95	177.75	
2	190.72	203.26	202.8	8.25 in	162.41	180.66	
4	182.48	203.12	202.55	8.25 in	159	176.83	
6	180.65	203.2	201.49	8.25 in	159.84	170.93	
8	164.58	197.9	200.85	8 in	155.48	168.56	
10	123.99	156.19	164.11	161.91	152.24	157.91	
12	124.65	125.34	106.86	101.93	139.87	131.63	
14	122.72	124.38	108.11	90.36	133.25	136.04	
16	124.28	130.1	107.36	93.28	143.13	129.53	
18	120.96	122.46	114.81	101.4	138.47	137.3	
20	127.35	123.81	115.9	97.4	136.42	136.66	
22	128.87	130.86	114.73	100.72	134.16	144.5	
24	123.49	125.37	114.57	104.27	140.44	139.03	
30	130.67	127.26	125.02	112.48	134.36	131.95	
36	121.5	121.21	120.42	131.61	139.84	130.09	
42	127.58	137.42	128.89	127.53	131.79	131.26	
48	138.2	131.88	134.08	133.12	130.31	139.54	



Deflection Worksheet

Cell 3 # of Passes 0 Wheel Path: North

Measurements

West ←  East

		1	2	3	4	5	6
North	48	139.31	146.62	145.53	146.7	150.94	143.47
	42	146.58	148.04	143.77	143.85	153.35	147.08
	36	134.52	147.95	149.77	147.51	148.61	151.65
	30	138.54	146.71	148.31	139.95	147.31	150.57
	24	140.25	145.57	152.86	143.92	143.55	148.1
	22	139.35	146.58	153.12	141.48	139.98	147.01
	20	137.65	145.73	155.09	143.85	139.9	151.89
	18	138.44	151.41	153.21	147.98	140.84	154.99
	16	142.75	148.98	152.88	147.86	137.97	155.98
	14	142.9	150.75	152.79	149.46	143.95	155.36
	12	141.62	148.91	160.2	150.91	143.74	153.39
	10	141.08	154.54	159.75	149.54	140.56	154.87
	8	142.95	151.56	157.99	151.37	143.22	155.11
	6	140.78	150.06	153.68	142.78	141.22	157.57
	4	134.64	148.73	152.13	150.34	138.4	151.49
	2	139.83	146.15	147.66	142.42	138.14	149.5
CL	0	139.82	147.65	152.36	144.5	139.28	152.36
	2	135.25	145.41	152.15	150.45	137.85	153.08
	4	134.63	148.78	153.71	148.01	135.05	153.71
	6	143.15	152.46	148.7	146.03	142.43	151.03
	8	140.2	150.96	149.79	146.2	136.79	149.1
	10	135.83	148.5	150.52	140.69	141.52	151.67
	12	129.95	149.99	144.86	141.48	142.55	153.93
	14	133.89	148.81	143.49	146.04	142.33	152.89
	16	127.51	148.98	138.16	140.53	141.51	155.5
	18	132.07	144.89	146.05	142.86	146.88	154.53
	20	135.68	145.43	144.02	143.25	140.94	154.89
	22	133.09	145.84	145.16	142.65	146.7	154.53
	24	130.28	147.11	146.75	140.13	148.3	156.64
	30	132.38	144.47	145	148.82	152.86	154.43
	36	139.41	143.45	145.52	146.13	148.85	151.36
	42	141.07	136.24	138.69	149.89	142.28	150.11
South	48	141.35	136.28	142.8	147.82	142.1	142.31

Deflection Worksheet

Cell 3 # of Passes 1 Wheel Path: North

Measurements

West ←  East

		1	2	3	4	5	6
North	48	145.35	149.27	143.85	147.01	153.68	146.42
	42	145.34	147.84	150.37	145.03	153.69	156.03
	36	139.6	148.5	151.64	135.59	149.9	151.47
	30	138.57	144.7	149.81	142.73	145.43	150.96
	24	139.96	149.28	150.95	142.21	144.5	149.82
	22	130.18	150.91	149.71	144.95	138.93	149.93
	20	134.33	153.37	154.75	147.57	141.77	153.19
	18	146.41	152.77	152.69	148.57	144.63	156.46
	16	141.17	155.81	157.77	148.66	144.27	153.8
	14	142.83	151.85	150.91	151.51	140.7	158.39
	12	140.29	155.41	157.3	155.01	142.79	157.44
	10	146.12	159.96	159.22	147.01	142.96	159.55
	8	144.56	155.52	160.04	152.67	143.61	159.51
	6	145.44	154.03	158.55	154.48	140.68	160.16
	4	143.65	152.59	157.66	153	143.88	157.96
	2	140.52	150.47	155.49	150.15	140.78	153.79
	0	144.43	151.66	160.59	149.78	140.5	159.74
	2	147.88	156.16	158.21	153.92	140.95	156.77
	4	138.63	152.91	158.25	152.93	139.1	160
	6	146.97	153.08	157.48	150.96	142.11	157.41
	8	143.39	153.64	153.21	147	141.77	157.82
	10	139.64	154.83	153.47	148.73	141.02	156.81
	12	140.57	150.8	154.5	148.47	140.04	158.81
	14	138.22	148.75	152.88	142.4	141.03	155.46
	16	135.35	147.89	150.72	141.63	137.75	153.25
	18	137.45	148.4	146.99	143.11	141.08	153.32
	20	135.79	154.13	144.29	141.9	141.66	157.92
	22	139.57	148.52	146.87	142.25	138.85	157.27
	24	136.51	147.67	146.43	142.26	147.37	157.87
	30	136.19	148.67	149.68	148.08	152.39	153.14
	36	143.54	147.21	147.04	143.35	149.61	161.2
	42	144.45	145.16	141.5	149.3	142.44	149.06
South	48	148	142.25	143.74	146.32	142.7	143.3

Deflection Worksheet

Cell 3 # of Passes 10 Wheel Path: North

Measurements

West ← ————— → East

		1	2	3	4	5	6
North	48	144.8	150.05	145.35	144.91	136.57	149.78
	42	145.71	156.01	147.51	140.91	145.59	150.52
	36	142.26	146.75	148.36	136.74	136.44	153.68
	30	141.24	150.43	151.78	138.05	141.19	151.74
	24	142.75	148.44	150.32	143.55	134.48	149.75
	22	140.26	152.61	153.1	143.36	135.35	149.53
	20	146.54	157.43	155.39	146.52	137.02	150.31
	18	148.85	152.62	153.76	143.92	133.57	156.52
	16	142.71	153.44	149.49	148.77	139.82	161.81
	14	146.99	158.58	153.24	148.53	134.27	157.02
	12	152.01	156.58	156.07	150.15	133.62	156.38
	10	152.03	156.06	157.74	149.7	132.48	157.3
	8	147.26	156.14	159.99	151.03	136.34	158.23
	6	152.07	154.89	166.12	161.6	136.06	162.25
	4	153.76	158.55	166.01	155.3	144.04	161.37
	2	151.93	159.04	163.6	158.52	139.63	161.04
CL	0	156.12	160.75	168.65	158.45	145.5	164.09
	2	153.67	158.41	166.24	158.47	143.65	164.7
	4	151.95	157.46	163.54	156.03	148.25	162.11
	6	153.14	159.57	164.91	155.34	144.8	160.23
	8	150.28	156.57	164.3	154.91	142.28	156.87
	10	145.01	157.85	156.85	150.69	131.76	154.82
	12	141.59	150.36	152.88	140.7	131.5	157.48
	14	140.35	146.56	152.38	138.28	135.89	156.64
	16	139.05	152.95	146.9	136.61	129.79	152.92
	18	136.57	151.39	152.14	138.26	124.06	153.75
	20	138.78	151.73	145.5	141.12	126.73	155.29
	22	137.3	151.26	147.85	141.77	128.16	153.07
	24	140.27	152.47	147.11	143.31	143.4	153.35
	30	139.58	150.79	148.64	146.25	145.98	148.41
	36	148.81	148.74	146.36	139.18	143.8	154.45
	42	143.69	144.3	150.39	140.62	139.29	145.14
South	48	147.7	142.29	142.68	146.2	133.73	140.59

Deflection Worksheet

Cell 3 # of Passes 100 Wheel Path: North

Measurements

West ←  East

		1	2	3	4	5	6
North	48	145.04	148.27	144.37	146.2	145.28	147.79
	42	142.13	151.82	150.23	143.03	143.1	153.39
	36	146.07	144.71	150.12	137.96	137.38	147.84
	30	140.84	146.92	148.7	131.56	135.79	142.52
	24	137.87	146.91	147.31	128.33	124.13	123.48
	22	139.02	149.15	147.7	132.9	113.88	126.28
	20	132.48	151.5	149.67	136.69	114.07	126.61
	18	141.82	146.59	143.11	137.28	114.39	126.58
	16	136.75	150.48	142.73	134.66	105.52	116.18
	14	139.29	150.85	146.12	133.77	107.45	122.98
	12	140.42	150.97	146.64	135.14	111.08	124.61
	10	142.51	149.22	146.64	131.46	109.68	121.4
	8	146.43	151.78	185.17	185.39	178.92	129.84
	6	158	168.53	196.36	195.24	8 13/16 in	9 7/16 in
	4	164.58	176.14	198.55	7 7/8 in	9 1/16 in	9 11/16 in
	2	166.12	172.79	201.24	7 7/8 in	9 1/4 in	9 7/8 in
	0	167.73	175.35	201.68	7 7/8 in	9 3/8 in	9 3/4 in
	2	166.9	174.32	202.71	7 7/8 in	9 5/16 in	9 3/4 in
	4	165.37	178.19	200.51	7.75 in	9 1/4 in	9 5/8 in
	6	162.21	175.77	196.02	202.63	9 3/16 in	9 9/16 in
	8	162.72	173.73	193.13	197.68	8 15/16 in	9 7/16 in
	10	149.87	171.26	161.04	183.54	8 5/8 in	9 1/8 in
	12	135.32	149.15	143.84	121.73	181.8	184.76
	14	126.56	141.74	144.79	115.92	101.06	97.14
	16	127.36	140.37	136.94	112.79	103.17	107.28
	18	127.62	142.54	134.67	114.68	101.01	108.7
	20	130.9	143.93	141.04	115	111.96	106.37
	22	124.88	145.29	142.08	118.63	106.78	108.58
	24	129.12	141	142.61	120.59	112.62	109.36
	30	134.7	146.57	144.89	134.56	137.55	131.75
	36	142.16	150	144.88	139.02	141.75	147.69
	42	144.67	146.02	150.19	146	140.92	146.2
South	48	143.67	140.58	142.92	141.02	136.5	140.14

Deflection Worksheet

Cell 3 # of Passes 175 Wheel Path: North
 Measurements

		West ←					→ East
		1	2	3	4	5	6
North	48	145.31	147.58	144.17	145.53	138.27	148.57
	42	143.43	149.89	144.89	141.69	138.72	153.82
	36	142.16	147.71	146.74	133.38	129.16	144.8
	30	140.38	144.38	144.64	127.79	123.66	138.06
	24	136.83	145.25	138.75	130.74	99.68	109.68
	22	137.13	140.32	141.55	129.89	86.24	107.31
	20	144.28	149.79	141.51	127.92	83.13	105.03
	18	141.68	146.89	137.55	126.54	83.03	104.77
	16	137.65	149.79	136	124.95	74.39	93.91
	14	137.1	146.65	140.25	126.37	70.2	98.15
	12	141.72	143.78	142.7	125.77	72.31	96.27
	10	145.15	146.94	140.09	123.06	77.18	96.77
	8	155.06	153.7	199.12	201.99	200.06	199.72
	6	170.64	178.29	8 3/8 in	8 1/2 in	9 3/4 in	11 in
	4	171.37	181.41	8 3/8 in	8 1/2 in	9 3/4 in	11 in
	2	175.18	180.07	8 1/2 in	8 3/4 in	10 in	11 in
CL	0	175.24	183.96	8 3/8 in	8 3/4 in	10 1/4 in	11 in
	2	178.75	187.75	8 1/2 om	8 1/2 in	10 1/4 in	11 in
	4	173.68	182.69	8 1/2 in	8 1/2 in	10 in	11 in
	6	172.07	181.28	8 1/4 in	8 1/4 in	10 in	10 1/2 in
	8	173.6	181.5	8 1/4 in	8 1/4 in	10 in	10 1/4 in
	10	151.11	176.92	177.82	177.82	9 1/4 in	10 1/4 in
	12	131.54	146.96	143.1	143.1	196.28	202.6
	14	130.71	141.58	135.45	135.45	163.48	138.31
	16	129.71	141.85	134.02	134.02	113.3	95.47
	18	131.45	143.78	131.62	131.62	47.73	43.7
	20	131.69	141.55	133.79	133.79	51.85	43.7
	22	130.95	143.82	132.45	132.45	58.02	43.69
	24	129.26	148.57	133.92	133.92	76.78	73.72
	30	134.48	145.86	140.07	140.07	128.25	105.52
	36	140.26	150.27	143.06	143.06	139.56	139.61
	42	138.67	144.44	151.11	151.11	140.15	143.81
South	48	143.67	140.49	144.41	144.41	140.66	139.78

Deflection Worksheet

Cell 3 # of Passes 300 Wheel Path: North
 Measurements

	West ← ————— → East					
	1	2	3	4	5	6
North	48	147.35	143.83	146.65	147.56	
	42	149.58	150.34	149.92	135.37	
	36	141.33	142	143.34	125.25	
	30	137.9	146.32	138.45	112.97	
	24	139.48	140.82	132.12	108.09	
	22	134.7	141.42	137.6	119.97	
	20	135.32	145.94	132.48	115.66	
	18	139.43	148.21	127.07	118.58	
	16	135.52	145.17	132.47	115.82	
	14	135.56	146.16	133.11	117.68	
	12	139.07	148.83	133.63	119.48	
	10	143.03	152.72	132.6	202.95	
	8	171.39	174.73	8.75 in	9 1/2 in	
	6	175.04	187.97	8.75 in	9 1/2 in	
	4	181.88	189.27	9 in	9 1/2 in	
	2	183.01	181.28	9 1/4 in	9 3/4 in	
CL	0	184.06	194.95	9 1/4 in	9 3/4 in	
	2	185.29	196.51	9 1/4 in	9 3/4 in	
	4	186.91	188.94	9 in	9 1/2 in	
	6	179.24	190.46	9 in	9 1/2 in	
	8	182.91	188.92	8 3/4 in	9 1/2 in	
	10	154.81	160.58	189.7	203.27	
	12	132.42	144.28	132.86	144.27	
	14	126.22	144.36	130.03	123	
	16	128.95	141.08	118.37	38.55	
	18	130.05	135.89	123.72	38.54	
	20	129.14	142.81	121.68	46.4	
	22	127.22	141.23	118.58	46.4	
	24	128.57	146.14	124.22	46.38	
	30	131.13	149.74	128.57	115.93	
	36	136.39	150.36	139.11	133.26	
	42	141.33	147.92	143.97	141.01	
South	48	141.44	140.02	146.56	141.47	

Deflection Worksheet

Cell 3 # of Passes 400 Wheel Path: North

Measurements

West ← ————— → East

		1	2	3	4	5	6
North	48	142.56	147.48	141.18	146.16		
	42	144.51	148.07	147.43	131.06		
	36	141.67	143.71	138.19	134.7		
	30	136.42	140.77	131.48	124.35		
	24	136.78	137.21	128.43	121.84		
	22	134.87	144.9	130.24	117.52		
	20	143.58	146.9	125.62	105.56		
	18	136.9	145.71	122.06	113.99		
	16	136.15	147.16	118.05	114.81		
	14	135.86	140.89	127.58	115.51		
	12	135.1	145.28	130.13	114.21		
	10	141.46	139.32	195.96	115.92		
	8	161.02	150.03	203.25	8 1/2 in		
	6	183.35	190.5	9 1/4 in	9 3/4 in		
	4	184.8	191.99	9 1/2 in	10 in		
	2	186.54	194.24	9 3/4 in	10 in		
CL	0	190.12	197.86	9 3/4 in	10 in		
	2	191.77	199.05	9 3/4 in	10 in		
	4	187.3	197.34	9 1/2 in	10 in		
	6	182.74	196.64	9 1/2 in	10 in		
	8	181.14	189.59	9 in	9 3/4 in		
	10	162.31	164.17	198.09	9 in		
	12	116.07	143.93	121.21	196.69		
	14	126.46	142.59	112.94	79.07		
	16	125.13	138.93	112.43	16.8		
	18	125.05	139.15	111.15	13.76		
	20	132	141.61	111.4	17.92		
	22	123.32	143.73	109.47	23.35		
	24	126.09	144.89	115.06	25.06		
	30	136.1	148.93	129.08	111.11		
	36	143.29	148.17	137.19	129.87		
	42	140.63	144.33	143.44	143.86		

Deflection Worksheet

Cell 3 # of Passes 700 Wheel Path: North
 Measurements

	West ← ————— → East					
	1	2	3	4	5	6
North	48	147.9	148.73			
	42	144.61	148.11			
	36	143.53	147.37			
	30	139.79	144.91			
	24	137.09	143.43			
	22	137.78	144.37			
	20	138.67	144.57			
	18	132.4	144.89			
	16	135.99	143.06			
	14	139.32	140.6			
	12	137.68	143.38			
	10	140.68	145.08			
	8	138.88	175.41			
	6	188.05	199.1			
	4	191	202.14			
	2	195.66	203.03			
CL	0	198.85	8 in			
	2	197.86	8 in			
	4	195.85	202.87			
	6	200.72	202.67			
	8	191.7	201.94			
	10	186.12	189.23			
	12	130.21	142.28			
	14	126.3	137.84			
	16	122.02	135.62			
	18	118.89	138.17			
	20	127.13	139.85			
	22	126.99	139.84			
	24	130	142.96			
	30	128.94	146.04			
	36	140.26	147.6			
	42	144.07	147.13			
South	48	143.94	139.85			

Deflection Worksheet

Cell 3 # of Passes 0 Wheel Path: South

Measurements

West ←  East

		1	2	3	4	5	6
North	48	140.89	144.03	149.95	151.35	145.61	142.75
	42	139.58	143.16	145.51	152.51	135.53	132.86
	36	134.07	143.24	145.61	143.54	133.83	129.25
	30	134.49	143.84	139.87	139.57	124.61	124.62
	24	127.33	144.84	138	139.23	126.54	121.25
	22	130.34	143.96	135.01	138.08	120.6	116.24
	20	131.85	140.72	133.46	136.28	119.45	119.08
	18	132.33	141.89	129.51	136.18	118.39	120.97
	16	132.89	140.66	132.57	128.7	118.86	120.98
	14	133.29	139.72	131.7	137.1	120.54	121.04
	12	133.17	141.74	133.11	132	120.35	124.24
	10	130.59	142.35	130.39	131.15	118.8	123.38
	8	130.92	141	130.17	135.08	123.92	126.62
	6	135.86	141.07	128.07	136.1	125.35	126.63
	4	139.32	141.38	134.54	129.03	126.65	126.9
	2	139.42	140.05	132.41	133.56	128.72	127.69
CL	0	138.66	144.29	138.46	133.84	120.76	128.75
	2	142.16	143.2	134.39	128.74	124.49	117.59
	4	140.27	141.62	131.94	133.84	128.76	120.56
	6	139.67	144.53	140.76	132.35	126.43	122.21
	8	138.76	144.57	137.49	137.83	127.86	126.09
	10	141.64	143.5	135.89	125.92	127.73	131.26
	12	136.8	141.63	131.58	132.91	131.89	131.81
	14	129.59	143.36	132.98	135.45	131.5	128.35
	16	139.54	144.65	133.6	131.36	130.68	137.03
	18	135.93	142.3	132.85	134.24	133.2	138.34
	20	135.27	143.12	137.07	135.93	133.22	133.82
	22	136.51	151.65	131.98	136.88	135.88	136.54
	24	138.03	141.69	137.13	137.46	140.21	135.42
	30	138.84	145.94	140.01	136.67	139.66	145.54
	36	140.1	146.24	146.69	142.47	140.29	150.89
	42	137.78	146.93	150.27	143.03	145.12	155.72
South	48	138.96	147.93	148.49	148.51	140.26	148.72

Deflection Worksheet

Cell 3 # of Passes 1 Wheel Path: South

Measurements

West ← → East

		1	2	3	4	5	6
North	48	146.53	146.73	151.09	151.76	145.17	137.64
	42	144.32	142.25	145.02	152.59	133.7	132.43
	36	136.95	145.03	144.79	144.99	131.34	129.05
	30	136.01	142.97	144.85	141.16	127.82	125.73
	24	136.53	143.57	139.42	139.76	127.08	121.85
	22	131.01	144.71	134.04	137.6	127.65	119.92
	20	138.56	140.08	131.17	136.16	117.61	118.65
	18	137.38	140.76	135.02	138.55	127.46	120.22
	16	137.94	142.79	133.72	133.61	118.41	120.88
	14	139.99	139.68	135.34	132.4	119.6	123.7
	12	141.14	140.03	132.5	132.39	121.31	123.68
	10	143.71	145.78	122.66	134.47	124.03	121.62
	8	138.15	149.63	134.1	134.58	128.76	129.76
	6	144.09	148.36	134.26	137.29	126.85	129.13
	4	149.67	151.26	140.38	134.71	128.29	131.41
	2	151.99	156.3	140.94	136.74	130.22	133.47
CL	0	150.01	157.81	146.51	137.18	124.88	133.06
	2	142.75	151.7	135.72	137.9	126.65	127.37
	4	142.62	147.86	150.27	139.08	131.34	126.11
	6	145.73	146.41	142.71	139.32	131.04	130.65
	8	142.74	150.37	139.83	137.63	129.07	123.78
	10	146.21	143.12	141.61	126.97	130.47	123.6
	12	135.69	145.92	135.59	131.89	135.32	128.38
	14	137.51	141.53	130.05	127.44	136.06	130.25
	16	140.05	142.81	152.62	133.4	131.63	138.53
	18	135.61	141.51	136.12	132.17	139.51	137.53
	20	137.52	144.59	141.51	131	137.4	137.92
	22	137.58	147.3	139.79	133.27	139.94	139.32
	24	141.36	142.62	139.99	136.76	140.38	140.63
	30	137.55	146.71	140	132.93	144.81	147.86
	36	145.35	145.93	141.92	144.56	144.42	150.57
	42	141.8	149.27	150.5	146.56	147.45	155.05
South	48	147.71	150.55	140.71	149.42	145.32	148.52

Deflection Worksheet

Cell 3 # of Passes 10 Wheel Path: South

Measurements

	West ← ————— → East						
	1	2	3	4	5	6	
North	48	143.56	155.62	148.87	152.97	145.94	134.1
	42	137.2	140.82	138.02	152.32	136.25	131.74
	36	133.15	135.68	144.17	146.19	134.77	127.92
	30	125.21	142.47	137.79	139.93	131.7	126.01
	24	131.15	140.68	131.5	129.56	127.18	120.49
	22	132.33	139.72	131.4	133.56	124.81	118.45
	20	117.81	133.05	133.14	132.5	123.77	114.03
	18	124.04	127.68	129.74	125.22	126.03	117.26
	16	134.42	139.87	120.47	131.99	118.3	120.94
	14	134.55	138.03	133.87	132.6	119.38	120.02
	12	131.6	138.86	130.57	130.01	118.19	120.6
	10	142.15	148.57	131.85	135.07	120.26	123.55
	8	153.84	159.56	153.67	147.41	134.14	142.2
	6	153.53	158.2	149.1	146.63	146.61	142.77
	4	153.18	160.99	151.58	148.49	141.73	144.76
	2	160.39	159.59	151.69	151.3	139.54	145.09
CL	0	155.61	158.81	149.22	146.89	143.07	144.72
	2	151.41	161.43	152.67	148.02	142.53	136.88
	4	144.25	158.68	150.45	146.14	140.47	136.35
	6	150.41	145.77	150.48	144.9	141.96	140.25
	8	149.81	148.05	144.6	131.23	140.23	139.62
	10	147.86	141.25	140.67	120.75	131.91	123.34
	12	132.03	140.67	132.43	123.46	134.05	130.59
	14	135.13	137.31	128.04	131.47	126.74	124.35
	16	140.6	139.19	133.87	133.37	133.43	133.29
	18	133.49	138.29	136.21	132.43	140.2	139.84
	20	136.27	137.68	137.41	124.73	137.55	125.51
	22	136.38	129.28	138.37	133.82	136.41	136.95
	24	134.16	141.48	134.66	137.49	137.82	142.08
	30	141.79	137.22	134.21	137.18	144.11	148.2
	36	142.67	141.31	145.68	143.34	144.28	158.48
	42	141.17	148.98	146.64	139.1	147.01	158.96
South	48	148.04	149.61	147.52	143.96	143.89	146.79

Deflection Worksheet

Cell 3 # of Passes 100 Wheel Path: South
 Measurements

	West ← ————— → East						
	1	2	3	4	5	6	
North	48	143.46	149.81	155.01	148.8	148.49	132.53
	42	141.86	137.28	144.11	145.11	138.06	122.95
	36	134.35	135.18	142.74	134.19	136.29	111.07
	30	128.27	138.91	118.42	119.91	126.1	98.4
	24	125.73	135.1	116.71	100.9	116	82.4
	22	126.01	130.42	104.17	102.81	101	78.82
	20	122.77	126.68	113.31	106.65	99.33	77.24
	18	122.75	125.35	108.6	108.15	96.76	80.6
	16	122.08	124.62	111.43	106.41	88.49	79.9
	14	121.29	124.81	109.4	109.16	82.13	83.82
	12	124.52	124.75	146.61	101.74	90.03	101.18
	10	138.04	120.45	189.96	153.84	84.47	155.88
	8	184.57	126.94	8 1/4 in	8 1/4 in	111.14	9 1/4 in
	6	199.33	8 in	8 1/2 in	8 1/4 in	8 3/4 in	9 1/4 in
	4	200.03	8 in	8 1/4 in	8 1/4 in	8 1/2 in	9 1/2 in
	2	198.66	8 in	8 1/2 in	8 1/4 in	8 1/2 in	9 1/2 in
CL	0	204.02	8 in	8 1/4 in	8 1/4 in	8 1/2 in	9 1/2 in
	2	203.25	8 in	8 1/4 in	8 1/4 in	8 3/4 in	9 1/4 in
	4	197.6	205.2	8 1/4 in	8 in	8 3/4 in	9 in
	6	191.17	204.53	8 in	8 in	8 3/4 in	9 in
	8	192.28	192.39	202.24	183.47	8 1/2 in	9 in
	10	158.05	144	146.02	133.66	182.51	142.08
	12	135.81	126.61	118.54	99.86	99.53	96.04
	14	131.95	124.03	105.55	104.75	88.01	91.75
	16	120.29	126.97	98.01	98.49	77.5	85.06
	18	115.74	124.2	107.61	98.57	93.38	86.73
	20	117.54	128.2	108.86	95.69	90.25	86.96
	22	119.42	130.1	106.24	105.68	95.47	89.6
	24	119.2	131.63	102.62	109.88	93.69	94.78
	30	126.53	136.75	123.85	111.38	102.16	114.5
	36	138.74	143.57	131.9	138.95	132.5	134.34
	42	144.84	141.31	148.9	141.25	149.17	149.98
South	48	144.5	148.77	150.35	145.83	139.28	146.6

Deflection Worksheet

Cell 4 # of Passes 0 Wheel Path: North

Measurements

11/3/2010

West ←  East

		1	2	3	4	5	6
North	48	111.2	114.89	126.15	135.48	111.08	113.86
	42	100	125.02	126.15	143.33	105.22	127.78
	36	107.06	125.85	125.94	137.36	101.12	127.23
	30	120.98	130.52	132.81	138.43	105.44	122.53
	24	127.27	125.15	124.62	137.11	112.61	127.7
	22	116.24	125.31	128.39	139.67	112.83	126.06
	20	117.42	130.51	130.17	140.72	108.46	126.79
	18	126.34	127.59	133.15	141.42	106.62	129.42
	16	114.13	124.52	141.25	143.29	100.81	129.42
	14	120.33	128.23	136.17	145.42	107.16	127.85
	12	120.64	132.97	134.95	142.16	109.06	125.84
	10	123.75	146.45	135.16	140.39	111.62	133.47
	8	124.23	143.32	134.08	141.02	111.91	122.83
	6	126.89	139.07	133.19	138.65	115.64	126.54
	4	123.65	139.51	129.55	138.18	108.57	126.11
	2	123.13	137.22	129.71	137.61	108.09	124.21
CL	0	124.32	136.43	129.76	134.08	105.05	125.88
	2	121.98	136.06	133.2	133.02	109.83	116.75
	4	122.02	139.38	130.47	132	108.57	118.29
	6	121.35	141.11	129.06	132.6	106.64	122.24
	8	121.3	143.4	130.35	134.43	114.91	119.86
	10	123.47	135.03	132.97	132.46	107.9	118.63
	12	126.73	135.03	139.53	132.18	112.31	116.3
	14	131.37	136.62	134.44	130.7	113.91	125.16
	16	122.81	142.08	134.44	129.59	112.86	125.14
	18	126.92	139.5	135.2	130.25	112.05	120.19
	20	128.33	132.72	132.19	130.67	119.4	125.33
	22	126.35	130.43	131.28	129.22	125.5	121.62
	24	124.67	133.01	128.49	130.68	122.48	127.86
	30	124.89	130.65	124.31	126.33	127.9	123.49
	36	125.48	129.48	120.73	128.88	128.13	123.2
	42	125.49	139.09	137.92	137.9	128.22	128.45
South	48	128.94	139.1	135.1	135.7	126.98	126.04

Deflection Worksheet

11/3/2010 Cell 4 # of Passes 1 Wheel Path: North

Measurements

	West						East
	1	2	3	4	5	6	
48	119.64	94.93	123.31	128.23	103.73	129.61	
42	125.68	99.29	115.17	133.67	113.44	133.07	
36	99.62	110.18	118.6	127.2	112.08	137.57	
30	114.05	122.49	119.15	130.24	110.92	128.89	
24	110.63	101.48	116.61	124.62	109.28	123.07	
22	117.26	118.04	116.54	124.08	109.73	123.22	
20	117.24	112.75	117.44	129.3	108.01	128.75	
18	120.95	118.7	124.53	122.25	105.63	127.83	
16	112.77	107.46	129.07	134.42	111.3	130.83	
14	116.01	115.38	127.96	132.58	111.82	131.78	
12	120.4	127.13	127.33	131.14	111.18	128.99	
10	120.68	124.01	123.37	131.58	111.8	133.17	
8	125.91	123.16	133.56	130.66	115.72	125.71	
6	125.61	123.14	132.05	135.68	111.71	128.09	
4	128.12	126.62	132.82	135.72	115.67	131.84	
2	126.09	124.47	132.33	137.85	116.44	125.39	
0	127.72	125.21	132.25	136.67	120.82	128.43	
2	126.8	127.86	131.17	133.9	119.98	128.45	
4	128.32	117.23	132.85	133.73	122.61	124.68	
6	123.71	118.35	132.13	133.75	119.41	129.86	
8	126.92	125.38	129.52	133.68	119.41	120.51	
10	123.36	115.05	131.15	128.36	111.43	118.04	
12	122.43	116.39	129.23	124.3	105.78	118.01	
14	128.57	123.96	125.19	124.98	109.5	116.11	
16	130.99	123.62	124.33	125.78	113.23	121.24	
18	123.82	128.34	126.45	121.99	111.41	129.61	
20	128.52	115.1	127.4	125.55	127.82	119.15	
22	120.1	129.41	129.11	125.46	123.82	122.17	
24	125.74	130.01	124.33	124.54	122.71	121.93	
30	124.63	118.94	123.85	128.91	127.74	121.16	
36	119.46	116.53	123.48	121.08	129.22	124.73	
42	122.42	114.14	130.11	126.68	126.95	128.54	
48	134.92	119.58	132.02	133.58	129.28	124.36	

North



CL

South

Deflection Worksheet

11/3/2010 Cell 4 # of Passes 10 Wheel Path: North

Measurements

	West						East
	1	2	3	4	5	6	
North	48	108.41	124.9	132.29	127.26	122.47	123.95
	42	108.78	118.99	121.41	129.87	131.93	130.69
	36	115.72	132.16	124.32	131.89	135.92	136.75
	30	111.32	136.47	124.24	127.04	138.61	131.99
	24	106.14	129.88	118.82	122.28	124.14	117.23
	22	106.15	125.4	117.74	116.52	123.8	123.04
	20	114.65	124.68	115.41	122.5	138.81	132.3
	18	98.4	133.43	123.85	127.45	133.63	120.15
	16	111.04	135.44	131.04	127.07	128.78	116.51
	14	111.14	123.94	125.73	126.5	122.72	118.05
	12	112.05	132.97	126.53	126.52	123.47	115.77
	10	122.53	153.998	130.1	126.05	131.02	142.42
	8	140.87	169.12	134.04	148.38	126.97	140.19
	6	150.44	169.73	154.38	160.99	139.89	154.05
	4	150.66	168.33	160.07	166.7	141.47	147.68
	2	164.5	169.32	160.38	168.61	143.28	149.75
CL	0	149.6	172.31	161.2	165.63	146.63	150.02
	2	157.05	161.36	160.33	160.37	140.09	148.73
	4	148.38	161.25	159.7	157.86	145.12	142.03
	6	147.59	152.26	158.11	157.67	146.91	147.46
	8	140.52	133.28	153.16	158.08	145.29	129.62
	10	120.04	133.51	130.85	125.88	122.57	111.92
	12	124.56	128.61	133.56	120.27	122.54	108.39
	14	118.47	128.23	131.2	119.34	124.73	112.71
	16	121.56	126.1	127.45	116.82	130.92	117.85
	18	118.78	126.9	127.95	133.66	130.01	114.04
	20	117.66	125.79	130.28	121.35	122.23	116.82
	22	123.17	131.26	131.09	120.28	124.29	119.85
	24	117.37	127.06	126.45	128.48	126.88	118.2
	30	119.98	118.5	127.83	124.11	133.26	122.42
	36	120.91	128.14	131.52	132.18	132.24	124
	42	131.35	128.26	129.44	135.93	133.28	128.73
South	48	126.99	127.8	129.21	134.98	130.31	128.73

Deflection Worksheet

11/3/2010 Cell 4 # of Passes 55 Wheel Path: North

Measurements

West ←  East

		1	2	3	4	5	6
North	48	111.43	125.89	129.45	132.16	122.84	117.86
	42	103.61	103.17	120.24	140.18	121.84	132.36
	36	97.88	108.97	119.23	123.15	117.01	129.67
	30	104.55	107.64	105.89	103.31	114.05	113.55
	24	99.41	104.98	92.79	80.23	110.38	99.46
	22	106.76	103.25	88.74	77.65	108.54	100.13
	20	103.07	111.38	96.95	78.58	104.37	107.73
	18	102.43	110.1	83.58	77.72	109.01	92.96
	16	105.32	108.29	92.93	85.52	106.95	89.97
	14	100.63	111.68	96.88	84.32	117.06	86.02
	12	125.48	147.08	95.91	86.87	107.12	94.54
	10	144.46	168.49	99.93	90.39	103.99	152.12
	8	184.41	202.72	151.29	166.04	133.24	174.36
	6	189.13	198.37	199.1	200.26	159.35	183.92
	4	192.51	202.9	206.375	203.2	163.68	184.94
	2	196.65	202.78	209.55	209.55	167.74	183.19
CL	0	204.2	202.86	209.55	212.725	169.97	182.69
	2	192.21	196.76	209.55	209.55	169.06	183.03
	4	197.53	194.44	209.55	209.55	161.39	183.45
	6	190.72	197.71	203.87	203.27	159.83	177.07
	8	185.6	162.27	202.46	198.15	163.26	161.74
	10	148.89	130.39	161.67	135.18	127.09	132.87
	12	120.87	113.59	126.04	105.14	116.11	95.76
	14	99.45	118.93	119.35	104.58	119.49	94.73
	16	103.8	127.26	119.06	107.84	119.48	99.08
	18	122.01	116.6	113.62	99.33	122.34	104.05
	20	111.48	125.9	120.31	108.99	120.68	99.6
	22	114.39	125.96	117.18	106.84	123.1	98.76
	24	115.22	123.38	116.6	110.49	123.64	113.54
	30	111.86	115.97	127.41	118.48	130.02	119.43
	36	116.07	126.28	127.83	130.72	126.53	119.72
	42	130.96	131.23	132.1	133.44	130.41	129.6
South	48	126.01	135.18	130.8	133.66	130.09	128.91

Deflection Worksheet

11/08/2010 Cell 4 # of Passes 100 Wheel Path: North

Measurements

West ←  East

		1	2	3	4	5	6
North	48	111.64	130.39	129.95	137.25	123.04	128.16
	42	96.02	101.25	126.45	140.36	119.27	135.91
	36	102.31	106.14	116.13	116.55	126.01	133.32
	30	94.09	102.04	87.01	83.89	113.61	109.12
	24	88.95	108.67	63.95	66.79	101.07	83.35
	22	84.45	108.82	61.56	48.81	94.3	78.88
	20	104.16	102.31	58.63	48.82	94.78	65.91
	18	96.55	110.69	51.42	51.3	96.56	65.08
	16	101.94	99.91	60.07	44.74	84.62	65.02
	14	113.55	101.44	69.29	45.41	101.09	57.58
	12	121.5	156.75	65.33	96.9	86.02	71.13
	10	162.71	184.17	159.03	152.45	94.44	160.72
	8	193.02	202.43	193.39	203.3	136.64	195.25
	6	203.2	203.2	209.55	209.55	167.79	203.52
	4	203.2	209.55	215.9	223.52	173.03	202.84
	2	215.9	215.9	228.6	228.6	174.82	202.84
CL	0	215.9	209.55	234.95	231.14	187.29	202.5
	2	215.9	209.55	228.6	228.6	181.17	200.41
	4	209.55	203.2	228.6	228.6	186.36	203.6
	6	203.2	202.64	228.6	223.52	175.68	192.42
	8	197.07	193.56	203.2	204.02	189.87	169.62
	10	167.83	158.67	185.44	189.36	165	125.33
	12	136.76	103.72	121.37	96.06	140.85	89.05
	14	122.71	111.41	116.18	94.68	117.98	85.31
	16	103.31	121.79	109.28	99.81	107.62	86.11
	18	103.34	102.46	102.73	91.43	104.88	90.57
	20	107.13	103.72	114.17	101.19	117.1	88.57
	22	106.74	111.41	114.8	104.34	121.17	91.92
	24	103.21	113.01	122.85	99.9	127.09	104.31
	30	107.12	103.57	107.52	116.86	127.03	122.06
	36	116.5	115.69	120.17	123.05	136.15	122.87
	42	128.64	127.76	137.09	133.92	130.98	129.25
South	48	134.87	132.28	134.37	134.5	130.97	128.15

Deflection Worksheet

11/08/2010 Cell 4 # of Passes 168 Wheel Path: N

Measurements

	← West → East						
	1	2	3	4	5	6	
North	48	121.65	150.97	123.67	131.57	122.1	124.02
	42	111.65	114.35	128.71	131.44	116.68	122.97
	36	109.37	128.45	116.54	116.72	114.13	121.31
	30	104.34	126.86	82.47	77.16	108.11	93.73
	24	100.84	116.02	22.55	-41.08	90.54	61.36
	22	105.04	108.59	-2.55	-42.54	83.92	49.5
	20	92.25	109.02	-9.12	-41.75	82.42	49.89
	18	98.3	112.14	-7.33	-38.2	72.09	41.14
	16	110.26	111.74	-4.02	-29.7	74.65	23.96
	14	124.09	130.24	-0.18	-31.87	71.56	26.87
	12	169.62	180.31	-2.14	143.95	93.23	128.54
	10	176.83	196.74	166.19	159.84	113.91	154.17
	8	215.9	203.2	203.2	215.9	137.67	195.18
	6	215.9	228.6	241.3	238.125	180.96	209.55
	4	228.6	234.95	228.6	254	184	209.55
	2	212.725	238.125	247.65	254	190.91	212.725
CL	0	212.725	238.125	241.3	260.35	198.47	209.55
	2	212.725	234.95	247.65	260.35	198.18	215.9
	4	215.9	228.6	241.3	260.35	193.24	215.9
	6	215.9	222.25	241.3	247.65	188.62	209.55
	8	185.05	185.98	241.3	209.55	182.94	203.83
	10	176.92	182.25	196.69	95.73	160.69	179.49
	12	118.15	114.93	115.64	87.23	140.32	111.99
	14	115.76	117.63	115.86	87.54	112.07	75.16
	16	112.98	111.72	111.55	89.49	111.36	78.82
	18	106.56	106.74	113.37	89.48	104.16	73.04
	20	99.76	100.76	112.8	92.25	112.23	89.24
	22	113.06	120.18	105.89	97.92	114.06	82.22
	24	108.92	111.29	108.31	97.74	115.25	91.96
	30	111.91	109.39	107.89	118.13	130.03	118.17
	36	115.53	117.58	117.88	126.33	128.44	122.67
	42	129.15	124.47	130.62	140.62	133.16	133.87
South	48	125.16	125.67	129.83	135.81	130.59	127.27

Deflection Worksheet

11/9/2010 Cell 4 # of Passes 0 Wheel Path: South

Measurements

West ← —————→ East

		1	2	3	4	5	6
North	48	139.23	147.4	137.39	138.18	141.91	135.86
	42	142.13	145.43	140.28	136	141.76	146.76
	36	140.96	133.4	135.27	136.24	140.63	142.02
	30	112.32	131.33	135.94	137.11	134.13	142.2
	24	119.51	125.79	143.48	135.77	135.01	134.7
	22	119.09	115.14	144.17	133.78	136.45	137.8
	20	112.91	116.67	144.35	136.89	134.49	145.27
	18	121.69	121.85	142.13	137.06	135.15	140.6
	16	111.63	121.59	141.89	134.9	142.06	141.81
	14	113.87	124.11	125.34	137.25	142.63	142.35
	12	110.59	115.91	148.9	148.22	144.3	142.93
	10	112.5	121.36	148.57	147.98	144.57	144.4
	8	112.82	116.71	146.84	147.95	134.59	142.22
	6	115.71	116.13	145.05	149.73	135.39	142.2
	4	103.07	118.37	148.01	149.61	135.23	142.18
	2	106.86	117.68	144.63	149.61	132.75	142.21
CL	0	111.63	128.29	146.06	149.88	133.75	143.84
	2	112.97	113.57	146.15	153.81	135.11	145.11
	4	107.21	114.31	146.51	153.61	136.04	145.35
	6	108.35	116.84	146.41	148.3	136.01	145.33
	8	106.05	118.18	146.65	148.05	136.09	145.28
	10	99.73	113.72	146.75	153.73	136.08	145.23
	12	97.87	113.49	140.74	153.73	136.13	143.8
	14	107.01	111.22	144.17	152.13	136.11	140.38
	16	108.38	100.13	142.9	148.24	136.12	150.31
	18	104.92	100.27	136.27	144.23	136.67	149.74
	20	107.5	87.09	138.53	144.77	137.18	141.99
	22	101.11	97.7	130.27	148.86	137.18	141.32
	24	96.54	96.53	129	146.86	126.39	145.21
	30	93.83	99.96	135.45	147.4	126.37	136.49
	36	109.88	98.58	131.96	143.81	129.1	139.18
	42	124.76	125.57	141.69	155.99	128.78	139.47
South	48	123.84	124.72	126.77	139.9	140.33	147.13

Deflection Worksheet

11/9/2010 Cell 4 # of Passes 1 Wheel Path: South

Measurements

West ← ————— → East

		1	2	3	4	5	6
North	48	136.27	145.25	137.14	139.31	139.26	142.12
	42	142.87	152.88	138.62	138.82	141.98	147.22
	36	141.22	135.91	133.03	137	139.18	147.27
	30	120.84	136.79	143.97	138.68	138.67	143.24
	24	112.8	133.66	132.04	139.24	137.19	143.89
	22	116.78	129.75	144.11	134.28	139.32	140.08
	20	113.85	131.46	142.22	148.65	143.17	144.34
	18	110.46	121.45	142.42	141.09	143.29	146.96
	16	110.66	113.97	143.72	135.32	135.81	143.25
	14	111.8	121.41	149.49	140.87	138.37	142.81
	12	104.98	112.77	144.85	141.04	136.09	143.7
	10	105.02	113.19	149.49	145.69	138.21	150.21
	8	122.59	123.21	145.11	145.73	138.57	146.56
	6	113.63	121.08	147.54	145.29	142.9	150.13
	4	123.9	128.81	147.49	149.48	145.88	143.59
	2	116.71	126.73	149.07	148.45	146.43	147.56
CL	0	112.25	127.46	148.06	152.48	145.39	151.99
	2	108.99	121.63	149	148.13	144.88	148.08
	4	115.09	121.18	148.05	151.88	141.62	148.73
	6	106.45	120.77	148.8	151.81	143.25	152.7
	8	110.92	119.78	147.62	148.8	136.84	150.09
	10	104.96	114.72	146.97	153.57	135.82	150.3
	12	101.73	107.06	145.86	147.32	140.21	152.73
	14	102.05	105.72	138.92	148.82	142.57	135.13
	16	102.3	97.02	137.57	143.69	140.47	145.31
	18	100.66	101.63	139.7	150.7	133.11	139.51
	20	106.53	86.52	140.95	144.9	133.85	141.03
	22	100.44	97.19	131.38	148.32	138.61	145.61
	24	92.54	86.55	133.33	147.75	134.97	138.79
	30	94.96	97.05	134.88	149.32	130.51	135.03
	36	112.24	91.88	133.97	153.26	140.98	129.4
	42	117.16	122.27	130.11	145.61	134.47	144.8
South	48	119.63	133.7	124.57	139.92	135.84	144.38

Deflection Worksheet

11/10/2010 Cell 4 # of Passes 9 Wheel Path: South

Measurements

West ← ————— → East

		1	2	3	4	5	6
North	48	142.12	139.47	138.94	136.61	135.16	empty
	42	138.87	140.6	144.11	136.19	139.64	134.8
	36	130.59	133.13	137.06	135.45	137.04	145.33
	30	122.64	115.37	134.41	134.56	137.37	138.79
	24	109.39	110.36	144.05	132.31	131.95	138.52
	22	114.68	109.83	143.4	126.86	126.79	135.97
	20	107.83	108.08	136.75	133.85	129.22	135.06
	18	101.28	108.39	140.69	129.43	125.47	135.23
	16	102.1	110.51	141.9	131.08	125.47	137.33
	14	99.59	110.03	144.67	142.21	128.71	137.35
	12	108.02	105.43	147.14	148.11	132.5	141.69
	10	110.76	111.96	146.17	148.77	131.84	137.3
	8	152.8	138.25	148.88	167.69	136.01	143.3
	6	152.19	156.04	165.18	167.84	150.92	150.41
	4	154.5	160.92	162.66	163.42	161.26	157.03
	2	153.58	160.83	162.08	167.05	158.97	163.5
CL	0	154.96	153.93	166.24	166.29	158.61	162.83
	2	147.39	152.72	166.47	162.36	157.2	173.55
	4	146.95	148.91	161.83	170.99	154.98	171.17
	6	144.03	143.94	160.11	154.94	150.5	167.74
	8	141.48	136.37	159.61	143.16	145.22	161.9
	10	110.28	111.62	154.51	146.65	133.2	160.05
	12	103.85	97.11	140.34	150.58	129.34	142.52
	14	103.78	91.76	144.46	150.06	127.44	140.4
	16	95.73	84.28	143.79	141.85	121.37	134.03
	18	109.59	75.14	141.45	140.85	121.11	138.98
	20	100.32	72.37	133.49	134.57	118.94	134.34
	22	92.69	72.98	135.44	143.94	126.58	135.64
	24	88.56	87.27	135.41	142.87	120.56	133.9
	30	91.35	84.23	144.27	148.72	122.27	130.83
	36	90.56	93.55	141.38	150.88	128.12	138.78
	42	106.68	115.82	131.27	147.91	133.98	137.98
South	48	122.44	115.19	130.83	145	131.61	146.58

Deflection Worksheet

11/11/2010 Cell 4 # of Passes 97 Wheel Path: South

Measurements

	West			East			
	1	2	3	4	5	6	
North	48	135.64	not measured	137.62	138.78	141.85	139.23
	42	132.92		134.28	134.02	142.98	140.98
	36	115.35		139.85	132.79	135.97	137.82
	30	104.33		142.92	130.25	107.74	134.91
	24	68.56		121.71	120.11	72.43	113
	22	67.37		120.08	111.09	62.46	99.38
	20	69.55		116.77	118.93	59.31	89.7
	18	65.34		111.66	120.88	52.06	88.51
	16	77.24		110.42	117.04	55.79	80.05
	14	72.58		114.22	118.9	66.55	82.5
	12	88.21		115.05	150.12	73.63	84.47
	10	184.28		106.37	209.55	125.84	131.76
	8	228.6		186.45	209.55	198.3	202.87
	6	266.7		228.6	209.55	215.9	228.6
	4	266.7		228.6	209.55	215.9	241.3
	2	266.7		228.6	215.9	215.9	241.3
CL	0	260.35		228.6	215.9	215.9	241.3
	2	254		228.6	209.55	215.9	234.95
	4	254		222.25	209.55	215.9	234.95
	6	241.3		215.9	203.2	202.89	228.6
	8	203.33		215.9	182.62	172.71	203.67
	10	149.64		164.99	127.75	145.3	178.64
	12	135.94		114.81	124.86	66.01	136.26
	14	80.76		113.74	127.48	64.37	60.9
	16	45.75		116.07	124.42	78.14	67.46
	18	37.79		106.56	115.33	83.53	79.9
	20	33.61		107.27	129.08	86.05	94.44
	22	33.54		121.12	131.05	104.79	102
	24	36.22		108.26	127.58	106.54	130.74
	30	38.26		126.15	137.08	121.22	129.83
	36	43.91		150.61	157.16	127.14	133.56
	42	90.01		146.45	151.94	133.39	152.48
South	48	132.13		138.31	138.77	134.62	156.93

Deflection Worksheet

Cell 5 # of Passes 0 Wheel Path: North

Measurements

Date: 22nd October 2010

West ←  East

	1	2	3	4	5	6
48	131.15	128	127.43	126.62	129.65	132.25
42	127.64	128.57	123.45	122.71	128.95	127.89
36	131.22	126.54	121.77	121.66	122.88	128.41
30	127.99	126.37	122.36	119.11	121.32	128.37
24	128.36	127.68	119.72	114.16	124.24	123.28
22	122.26	129.62	123.06	117.37	124.15	122.85
20	131.71	130.42	120.23	122.7	121.93	129.44
18	134.24	128.83	120.2	113.74	127.24	122.69
16	124.95	129.55	123.78	113.06	118.51	121.74
14	130.98	127.34	116.66	115.64	118.57	127.28
12	127.98	132.84	120.07	115.85	119.18	122.95
10	128.94	132.54	121.22	110.08	123.64	129.61
8	129.36	128.48	114.98	113.03	123.06	120.64
6	135.18	127.39	115.54	111.56	123.08	120.36
4	129.49	127.5	114.1	108.59	122.42	121.46
2	126.97	128.09	117.73	112.61	119.04	118.39
0	121.4	124.72	117.3	106.13	120.65	116.95
2	126.46	126.21	117.93	110.95	122.59	117.85
4	126.18	124.26	110.87	110.76	114.65	120.73
6	121.07	127.67	111.75	111.5	116.22	119.95
8	126.94	132.03	114.83	110.67	117.55	116.09
10	127.01	127.26	117.05	110.77	118.2	117.28
12	125.91	130.43	112.62	110.63	112.10	114.43
14	126.28	120.39	118.81	108.18	114.83	113.39
16	127.46	120.41	109.54	108.01	115.69	118.42
18	128.12	126.61	116.95	112.03	115.68	118.7
20	124.54	123.18	116.52	110.73	115.67	117.08
22	129.14	125.37	113.33	110.73	114.41	113.01
24	121.4	122.36	121.73	108.01	116.87	117.18
30	130.2	122.71	115.94	121.73	112.81	113.74
36	130.2	127.41	111.74	109.42	112.23	124.75
42	119.09	129.34	111.06	122.56	109.25	115.33
48	116.16	124.73	114.64	121.73	110.28	110.63

North



CL



South

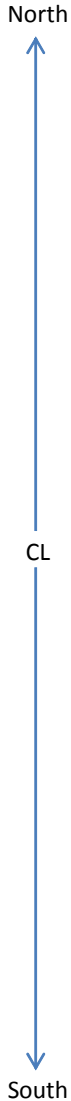
Deflection Worksheet							
10/25/2010	Cell	5	# of Passes	1	Wheel Path:	North	
Measurements							
West ← → East							
		1	2	3	4	5	6
North	48	132.07	130.14	130.62	127.51	128.19	130.21
	42	124.45	125.96	125.28	123.75	125.56	121.93
	36	124.87	125.45	123	119.66	121.19	125.29
	30	122.29	123.17	117.59	118.29	124.14	128.67
	24	124.29	133.8	118.8	120.15	125.74	122.7
	22	128.88	129.07	121.9	122.87	121.18	124.37
	20	126.41	129.14	125.45	116.3	118.02	120.93
	18	127.81	123.05	118.91	113.6	119.6	118.27
	16	122.68	128.28	124.37	116.13	121.98	116.89
	14	125.32	129.23	121.63	117.57	120.27	121.73
	12	136.05	129.7	114.78	116.94	123.27	117.4
	10	137.67	137.18	113.02	112.86	123.23	121.26
	8	136.19	136.1	114.96	112.15	118.45	121.21
	6	137.97	128.08	115.15	118.97	123.8	121.08
	4	132.01	136.68	119.26	115.52	117.19	132.51
	2	127.26	129.36	115.83	120.07	114.75	128.55
	0	131.88	125.25	114.44	109.87	116.29	126.18
CL	2	127.26	132.96	117.05	110.39	121.71	124.42
	4	128.78	124.6	121.98	115.33	119.25	117.04
	6	129.35	128.08	112.86	114.23	115.62	117.29
	8	137.2	134.98	122.43	106.73	114.26	121.18
	10	132.44	125.39	114.98	114.1	109.95	115.74
	12	133.51	127.48	113.59	116.14	113.08	111.39
	14	128.32	129.31	113.59	108.83	113.45	114.88
	16	126.52	126.08	107.49	107.24	108.37	113.29
	18	136.44	128.89	114.16	119.62	113.22	126.99
	20	130.37	124.12	107.26	114.36	113.5	125.92
	22	130.81	123.62	109.31	120.73	119	120.72
	24	121.27	128.53	123.16	114.39	109.5	117.96
	30	129.37	124.5	113.93	115.99	107.39	116
	36	124.03	123.91	120.42	111.42	117.08	112.98
	42	114.05	121.67	111.95	115.16	106.13	111.1
South	48	120.7	123.33	111.86	113.59	106.63	109.96

Deflection Worksheet

10/25/2010 Cell 5 # of Passes 10 Wheel Path: North

Measurements

	Measurements					
	West	1	2	3	4	5
48	128.93	131.29	129.43	127.21	137.55	128.62
42	129.72	127.79	121.11	124.33	129.97	121.6
36	123.5	130.65	125.53	121.71	128.35	131.93
30	126.71	123.12	123.13	118.82	123.91	126.44
24	132.03	128.57	116.64	113.6	121.09	130.85
22	121.9	133.17	119.8	118.71	120.22	131.29
20	121.78	132.56	120.78	115.31	119.88	116.74
18	124.62	132.18	115.53	114.56	126.67	115.98
16	124.11	130.35	123.2	114.26	117.14	123.54
14	124.47	129.09	124.57	122.83	119.13	123.99
12	135.12	132.3	112.1	116.75	116.8	122.11
10	134.8	133.16	117.05	110.67	114.94	123.86
8	123.32	127.33	112.33	107.55	124.23	114.02
6	133.58	135.77	123.58	129.21	125.56	131
4	136.23	135.09	122.84	114.95	125.34	129.15
2	130.91	127.85	127.15	118	131.09	134.04
0	136.84	128.56	131.54	118.37	129.1	129.99
2	135.64	136.78	128.6	125.09	130.74	130.57
4	134.82	128.36	120.33	123.46	129.3	121.32
6	133.07	134.93	122.49	115.03	120.22	121.77
8	132.18	139.2	118.53	113.09	119.19	123.92
10	132.93	130.26	104.25	111.03	112.43	112.63
12	127.41	130.24	104.87	108.6	109.15	114.97
14	121.24	124.38	113.64	113.98	111.51	111.76
16	137.39	119.65	108	121.25	109.77	116.55
18	127.97	125.87	111.71	120.5	123.88	127.09
20	121.77	122.32	115.55	106.47	118.23	118.79
22	120.17	122.5	120.58	110.62	121.45	117.14
24	125.5	121.49	118.61	113.11	119.42	116.81
30	121.78	130.88	114.51	115.18	116.09	121.64
36	134.76	129.68	113.29	113.2	118.5	121.91
42	121.61	125.28	115.59	108.17	106.93	120.15
48	118.78	126.41	117.4	108.06	113.08	114.13



Deflection Worksheet

10/25/2010 Cell 5 # of Passes 100 Wheel Path: North

Measurements

	Measurements					
	West	1	2	3	4	5
48	122.19	122.72	125.1	124.16	126.93	123.48
42	123.78	124.51	120.31	122.38	123.79	120.4
36	123.53	124.02	115.76	119.1	118.73	113.75
30	123.17	121.53	115.91	112.6	118.17	120.2
24	119.7	118.92	108.22	106.06	117.22	117.48
22	117.68	118.67	111.56	104.23	114.87	111.05
20	117	120.16	108.48	104.4	114.78	104.15
18	117.53	111.74	107.49	101.65	105.21	93.69
16	113.98	116.5	107.78	103.31	102.01	90.22
14	116.69	117.63	104.61	98.64	99.45	91.88
12	116.38	117.53	105.43	97	99.45	96.36
10	118.43	116.96	103.98	95.15	104.79	105.8
8	117.15	113.46	119.17	98.95	114.04	98.34
6	123.15	108.22	140.46	134.55	133.86	143.27
4	140.72	141.13	143.76	135.74	135.89	147.76
2	142.21	143.16	143.71	140.1	137.61	148.82
0	144	142.89	148.3	140.86	138.72	149.13
2	144.58	146.41	145.18	140.69	137.25	147.45
4	147.3	144.55	140.67	141.31	137.25	146.5
6	145.6	145.47	137.7	132.17	134.55	142.64
8	145.63	142.95	137.32	128.96	130.57	138.1
10	140.18	138.33	105.07	111.62	110.02	114.82
12	118.75	120.01	105.07	103.52	105.56	111.15
14	117.3	112.42	103.59	97.69	100.4	104.81
16	1909.15	113.82	102.13	97.38	109.19	103.23
18	120.34	109.95	107.27	95.76	106.44	104.78
20	112	111.42	105.28	100.68	107.08	107.44
22	111.86	109.77	114.24	100.34	110.62	107.35
24	113.92	112.96	107.79	103.93	109.67	112.96
30	116.27	112.84	111.88	105.82	108.01	109.81
36	114.64	117.93	110.11	106.44	104.88	109.06
42	113.15	117.86	109.77	112.31	105.61	110.14
48	114.77	117.29	109.59	105.6	105.14	111.91

North



CL



South

Deflection Worksheet

10/25/2010 Cell 5 # of Passes 290 Wheel Path: North

Measurements

	West						East
	1	2	3	4	5	6	
48	130.17	123.28	127.26	125.24	125.72	124.93	
42	128.27	125.29	124.72	122.22	125.41	119.48	
36	121.92	122.97	119.97	117.97	119.56	119.22	
30	119.84	118.76	116.29	110.94	118.19	118.54	
24	117.07	115.5	104.7	83.64	117.32	111.7	
22	113.02	113.29	94.23	85.81	104.09	89.9	
20	110.77	111.99	90.72	83.56	84.19	73.88	
18	107.74	102.64	88.32	75.09	68.74	43.84	
16	103.07	107.37	89.71	73.08	58.97	41.2	
14	103.77	105.94	89.76	73.3	63.35	43.08	
12	107.43	105.09	89.03	65.2	69.2	52.62	
10	112.84	103.28	92.01	70.68	68.02	112.23	
8	111.2	107.41	135.95	117.39	132.09	148.25	
6	127.91	108.11	160.55	154.14	157.44	181.81	
4	154.84	153.01	163.19	161.68	162.94	183.41	
2	156.39	156.47	168.97	162.61	157.33	184.39	
0	159.43	162.03	167.68	165.24	156.45	184.28	
2	159.99	162.91	164.44	158.86	156.27	184.23	
4	164	160.36	164.44	158.78	153.6	182.91	
6	162.42	161.03	158.73	155.95	146.86	184.49	
8	163.92	155.82	155.81	148.31	141.55	178.4	
10	153.43	151.32	113.01	116.51	106.38	125.49	
12	119.5	127.38	97.45	97.49	100.1	84.19	
14	105.59	113.74	95.98	89.92	97.53	66.99	
16	105.78	112.76	102.09	87.61	98.46	59.44	
18	113.82	112.63	97.73	83.39	96.48	68.8	
20	112.4	108.62	100.3	94.16	98.61	66.45	
22	109.24	106.37	105.18	88.2	99.77	72.6	
24	110.64	108.95	97.51	99.22	103.04	87.7	
30	114.46	113.4	109.19	107.78	109.4	108.65	
36	114.17	116.79	109.03	108.04	109.02	108.6	
42	114.13	117.08	105.57	107.63	106.02	110.28	
48	115.31	118.14	108.25	109.46	106.96	107.64	

North



CL



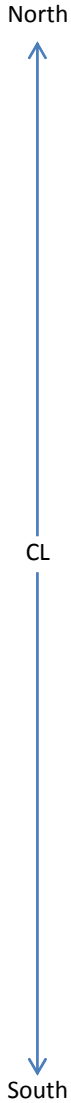
South

Deflection Worksheet

10/27/10 Cell 5 # of Passes 400 Wheel Path: North

Measurements

	Measurements					
	West	1	2	3	4	5
48	131.63	125.61	129.61	130.12	129.16	131.3
42	127.07	125.9	122.85	130.18	125.35	123.95
36	124.54	121.44	124.1	121.8	119.61	125.98
30	118.44	121.75	110.25	117.24	118	125.13
24	116.65	112.19	82.1	80.25	120.67	103.47
22	113.22	110.78	80.03	70.88	104.88	92.71
20	113.19	107.52	78.57	65.72	82.3	85.75
18	112.9	97.81	72.11	62.4	84.01	58.32
16	103.57	102.56	82.96	60.57	38.4	33.38
14	103.05	100.71	75.16	62.26	49.02	43.08
12	107.43	104.24	75.23	57.02	38.75	46.53
10	107.63	103.24	91.8	81.81	76.14	106.14
8	110.8	100.17	165.22	137.83	149.66	173.42
6	126.6	156.04	177.87	171.78	172.55	196.04
4	164.04	162.72	180.4	183.56	171.99	7.9 inches
2	162.69	184.74	181.4	182.41	175.13	8.1 inches
0	162.95	185.93	176.77	183.65	168.48	8.1 inches
2	167.55	167.85	179.34	182.41	170.31	8.1 inches
4	170.1	165.97	179.36	184.32	171.67	8.1 inches
6	170.04	185.47	176.56	178.16	169.99	8.1 inches
8	164.34	162.19	169.4	181.29	167.74	203.96
10	162.67	158.05	147.55	154.89	144.73	156.96
12	145.52	127.19	98.08	96.85	91.68	90.91
14	116.97	117.44	97.48	84.87	83.68	71.5
16	112.25	110.99	90.58	87.76	82.23	64.92
18	116.15	112.68	91.35	76.9	97.82	62.26
20	113.5	110.27	96.97	81.83	87.05	70.74
22	110.41	114.77	98.35	80.62	81.69	72.33
24	111.29	111.49	98.24	85.25	92.31	83.83
30	117.33	117.31	107.17	106.41	104.93	118.33
36	113.57	123.73	112.35	110.75	108.77	113.92
42	116.09	122.63	106.45	115.79	110.42	114.47
48	115.43	131.92	120.35	116.08	107.28	114.05



Deflection Worksheet

Cell 5 # of Passes 478 Wheel Path: North

Measurements

West ←  East

		1	2	3	4	5	6
North	48	129.71	126.3	128.98	125.91	126.45	133.98
	42	124.32	126.53	127.11	123.54	121.18	125.68
	36	121.6	129.96	123.96	117.8	123.39	125.91
	30	121.95	123.39	107.62	113.55	117.88	129.78
	24	114.05	113.06	48.46	67.61	111.35	125.97
	22	111.2	111.38	48.89	65.41	83.32	124.23
	20	108.86	107.91	72.69	49.31	69.63	59.98
	18	107.83	96.55	48.37	49.06	48.28	51.12
	16	98.75	104.71	48.88	45.7	46.9	33.81
	14	103.48	98.66	69.2	47.84	41.67	42.85
	12	98.37	101.56	75.12	56.35	43.17	44.18
	10	103.66	100.73	81.5	68.15	49.3	90.21
	8	107.37	98.94	146.11	119.4	134.66	143.68
	6	116.14	133.68	177.73	173.74	170.1	201.46
	4	157.22	166.33	182.95	186.34	178.58	8.5 in
	2	167.83	167.8	184.98	188.97	180.45	8.5 in
CL	0	167.44	168.56	184.37	191.95	182.65	8.5 in
	2	172.82	172.1	185.82	193.63	179.55	8.6 in
	4	170.12	178.45	184.55	191.81	184.77	8.6 in
	6	172.22	170.47	180.45	188.18	175.38	8.4 in
	8	167.29	170.31	177.92	186.47	176	8.6 in
	10	162.81	158.77	167.35	168.17	145.43	202.57
	12	149.17	123.54	121.05	99.62	81.51	131.86
	14	115.3	112.81	91.84	86.46	80.54	57.57
	16	112.56	110.93	86.56	70.43	77.85	51.12
	18	106.9	110.3	88.95	48.58	73.2	59.54
	20	108.19	112.57	90.47	74.57	70.18	58.75
	22	108.18	110.96	91.15	65.55	80.04	73.09
	24	113.83	111.75	89.62	49.53	90.02	97.56
	30	115.91	113.28	102.11	95.93	104.81	116.5
	36	116.76	117.23	117.34	112.6	107.27	110.99
	42	113.42	125.79	110.01	113.12	110.13	115.51
South	48	112.69	119.07	110.23	113.6	110.35	116.39

Deflection Worksheet

Cell 5 # of Passes 0 Wheel Path: 2

Measurements

	West					East	
	1	2	3	4	5	6	
48	133.93	129.59	135.16	128.81	131.96	135.92	
42	132.75	131.07	128.36	142.14	141.74	133.05	
36	128.21	133.8	132.45	139.04	138.25	125.91	
30	137.19	126.85	133.82	139.99	144.82	138.58	
24	130.42	127.06	134.99	142.03	145.08	140.83	
22	130.8	127.56	137.87	145.21	147.75	142.63	
20	124.67	131.34	132.42	146.41	142.85	145.43	
18	136.11	121.6	129.41	144.08	142.12	137.52	
16	133.11	124.74	135.59	144.23	142.15	143.36	
14	127.31	128.28	134.84	138.96	143.3	139.46	
12	126.66	128.29	132.3	138.31	142.45	142.29	
10	130.52	131.06	128.39	140.19	145.13	137.59	
8	129.24	127.44	128.8	144.46	145.88	140.08	
6	127.43	126.28	127.58	143.48	146.47	140.79	
4	125.14	122.73	129.25	143.5	146.55	142.32	
2	122.42	126.14	126.72	140.77	147.03	143.08	
0	122.37	126.97	126.22	143.34	147.11	138.59	
2	126.85	129.88	125.53	141.04	151.51	138.65	
4	123.52	124.22	126.6	141.95	149.1	141.68	
6	127.92	118.99	128.31	139.77	149.15	138.91	
8	136.66	127.77	125.01	141.85	148.3	145.27	
10	127.99	120.3	127.57	137.04	146.31	143.44	
12	133.49	126.27	129.02	140.87	146.78	140.18	
14	123.84	123.97	132.28	139.24	140.54	136.62	
16	125.2	124.01	131.19	137.13	143.44	135.84	
18	124.17	129.64	130.02	138.63	145.08	142.71	
20	120.93	124.74	126.38	138.37	141.98	140.67	
22	123.04	122.35	123.23	135.97	142.2	137.25	
24	126.23	125.24	124.8	135.89	141.23	135.53	
30	124.42	123.66	128.06	135.06	137.45	135.35	
36	122.89	127.45	128	133.15	137.74	135.87	
42	137.33	134.29	127.72	141.43	134.9	134.85	
48	132.33	143.13	128.69	143.06	132.42	128.34	

North



CL



South

Deflection Worksheet

10/28/2010 Cell 5 # of Passes 1 Wheel Path: South

Measurements

West ← ————— → East

	1	4	5	6		
48	135.8	132.48	124.16	137.5	130.12	135.91
42	125.38	131.51	132.94	128.3	133.13	132.46
36	127.04	131.04	135.59	127.05	133.14	132.53
30	119.55	126.57	133.96	132.52	142.23	135.24
24	127.91	125.42	128.56	132.21	142.24	140.65
22	128.42	125.1	134.51	144.72	140.47	142.96
20	120.39	134.57	131.41	133.17	139.8	142.89
18	126.59	120.18	128.96	140.07	139.96	142.87
16	124.53	127.01	130.56	133.82	141.16	142.86
14	128.73	125.29	134.48	128.63	137.77	132.77
12	123.46	138.45	133.7	132.87	144.01	136.22
10	123.48	128.41	133.32	130.09	139.95	142.27
8	122.3	130.23	132.7	135.12	138.88	136.1
6	127.32	131.37	126.85	138.72	142.22	138.61
4	122.58	131.44	129.13	135.3	142.9	138.45
2	123	123.65	131.17	132.25	144.04	137.68
0	125.69	123.2	129.6	130.68	146.88	149.8
2	125.04	124.37	129.18	134.09	150.35	144.94
4	121.72	126.53	133.53	133.03	151.37	138.7
6	122	129.24	130.6	133.02	150.46	139.09
8	116.4	133	129.93	130.11	146.14	139.35
10	120.2	120.47	124.89	127.57	148.84	141.97
12	128.48	121.8	125.06	131.19	147.35	139.94
14	127.97	120.64	127.03	130.25	140.08	139.77
16	123.35	116.94	125.24	127.57	149.84	133.3
18	120.6	129.82	124.64	125.41	137.23	143.85
20	120.36	126.33	128.85	118.55	142.85	136.66
22	120.39	131.35	114.59	133.56	142.9	137.13
24	123.29	132.48	122.96	123.26	140.48	134.54
30	122.63	122.93	137.82	124.8	143.41	130.94
36	126.05	126.32	129.65	122.35	136.72	129.3
42	129.05	132.78	132.46	128.31	140.97	138.81
48	129.77	126.6	123.37	124.44	141.11	124.02

North



CL



South

Deflection Worksheet

Cell 5 # of Passes 10 Wheel Path: South

Measurements

10/28/2010

West ←  East

		1	2	3	4	5	6
North	48	134.55	129.64	128.56	131.97	132.04	131.86
	42	135.16	125.92	126.53	127.73	138.42	131.71
	36	139.02	126.01	131.53	127.29	134.36	129.56
	30	131.32	129.36	131.22	134.82	139.68	135.52
	24	125.9	122.23	130.94	138.76	140.59	136.87
	22	120.6	127.13	130.21	137.29	141.49	134.45
	20	119.97	125.38	132.67	132.8	139.22	132.47
	18	119.87	127.01	128.5	136.22	137.38	135.82
	16	119.8	124.76	131.14	130.09	141.26	132.87
	14	123.4	134.43	128.57	127.35	136.21	133.57
	12	124.26	125.85	124.9	131.38	141.56	135.34
	10	119.26	128.82	128.5	130.72	141.28	134.84
	8	125.21	135.53	128.99	134.76	137.15	142.4
	6	134.28	131.01	137.46	141.3	150.1	145.51
	4	131.69	131.65	137.28	139.39	152.72	146.74
	2	133.41	138.19	140.37	141.42	151.54	152.66
CL	0	136.76	137.63	141.15	141.77	157.37	155.63
	2	134.31	139.14	134.15	141.73	157.71	150.09
	4	129.74	135.53	136.39	138.19	156.14	148.99
	6	124.11	134.44	130.65	138.85	153.33	148.84
	8	126.55	128.17	125.71	134.71	150.91	144.18
	10	122.5	129.93	122.95	129.19	140.83	140.46
	12	125.73	123.91	121.44	124.06	141.61	137.08
	14	122.43	127.31	119.72	127.64	143.59	133.83
	16	123.84	125.97	127	124.21	145.9	139.76
	18	123.37	117.46	124.11	123.34	143.38	134.46
	20	121.81	120.06	122.77	127.4	140.66	131.03
	22	118.57	128.52	125.71	125.88	139.69	135.13
	24	121.93	120.77	123	121.58	136.03	134.79
	30	116.84	124.53	127.63	128.61	133.66	132.51
	36	119.3	127.52	123.83	125.79	133.87	130.18
	42	125.97	129.53	129.54	127.42	134.29	131.27
South	48	134.05	124.28	134.05	130.83	132.67	131.72

Deflection Worksheet

10/29/2010 Cell 5 # of Passes 100 Wheel Path: South

Measurements

	West						East
	1	2	3	4	5	6	
48	131.3	136.71	138.97	136.35	134.3	129.22	
42	131.04	135.35	136.94	136.66	125.62	134.08	
36	128.32	132.24	129.76	127.21	134.76	134.86	
30	121.74	124.24	132.64	137.44	135.77	134.2	
24	124.41	125.5	136.81	134.44	114.09	111.03	
22	118.67	121.58	126.63	136.56	118.73	93.46	
20	117.53	131.66	131.21	130.94	103.45	85.62	
18	117.38	127.32	125.71	132.85	103.39	78.66	
16	118.06	127.15	126.5	129.76	97.33	71.84	
14	122.86	120.3	122.34	121.16	89.33	67.87	
12	117.16	125.55	121.58	128.1	90.61	64.24	
10	119.49	123.62	127.51	127.97	87.99	108.94	
8	128.19	142.95	143.79	137.2	146.05	182.64	
6	146.99	149.93	157.72	162.57	201.24	8 inches	
4	146.54	150.41	158.68	162.92	201.12	8 inches	
2	152.85	150.18	165.52	162.72	200.58	8 inches	
0	156.23	155.94	163.61	159.08	197.69	8 inches	
2	155.02	151.33	158.51	165.33	200.63	8 inches	
4	150.3	156.72	157.62	159.13	200.87	8 inches	
6	149.04	148.27	153.19	156.68	201.74	8 inches	
8	148.59	148.89	160.07	158.02	198.28	8 inches	
10	115.96	128.17	126.96	126.38	172.95	127.89	
12	126.37	117.98	119.6	122.09	100.7	69.61	
14	126.32	117.31	117.39	123.28	97.57	72.94	
16	124.56	121.48	122.26	117.56	91.82	80.61	
18	121.48	116.94	122.49	120.58	101.18	79.11	
20	127.09	122.19	120.89	123.34	95.87	100.11	
22	116.55	120.2	128.11	126.69	109.08	103.05	
24	120.15	119.88	127.27	125.26	119.26	118.9	
30	120.63	121.41	128.22	129.41	137.41	125.57	
36	117.57	123.37	122.79	121.96	130.58	134.06	
42	125.9	133.12	136.09	128.33	136.37	136.62	
48	126.23	123.93	142.38	131.06	137.76	131.71	

North



CL



South

Deflection Worksheet

10/29/2010 Cell 5 # of Passes 125 Wheel Path: South

	West				East	
	1	2	3	4	6	
48					134.23	125.19
42					134.57	125.8
36					134.23	125.73
30					127.4	130.14
24					117.63	94.32
22					106.62	90.4
20					97.95	75.84
18					92.26	70.64
16					83.44	62.31
14					81.68	59.5
12					84.36	57
10					163.64	126.17
8					8 (1/4) in	175.33
6					8 (3/8) in	8 (1/4) in
4					8 (3/8) in	8 (3/8) in
2					8 (1/2) in	8 (1/4) in
0					8 (1/2) in	8 in
2					8 (3/8) in	8 in
4					8 (3/8) in	8 (1/4) in
6					8 (3/8) in	8 (1/4) in
8					182.52	201.6
10					80.44	142.73
12					84.32	52.3
14					84.04	65.81
16					90.22	65.51
18					93.47	67.36
20					91.62	78.86
22					105.63	89.74
24					116.82	106.43
30					139.42	121.86
36					133.64	127.02
42					129.48	128.66
48					129.31	127.79

North



CL



South

Deflection Worksheet

10/29/2010 Cell 5 # of Passes 216 Wheel Path: South

Measurements

West ← → East

		1	2	3	4	5	6
North ↑ CL ↓ South	48	131.04	124.57	129.67	133.87		
	42	128.55	122.7	126.51	128.83		
	36	122.45	121.84	130.85	125		
	30	123.18	120.99	128.53	124.35		
	24	117.19	120.29	120.93	126.25		
	22	116.37	115.97	118.37	119.68		
	20	114.47	114.64	116.96	119.34		
	18	112.21	122.4	113.64	111.31		
	16	112.16	121.6	113.91	107.84		
	14	112.36	119.65	113.97	112.5		
	12	112.27	120.83	113.4	112.51		
	10	114.62	122.13	112.47	101.98		
	8	133.8	137.63	146.34	128.04		
	6	156.21	156.58	172.32	173.2		
	4	159.6	156.6	175.09	175.43		
	2	164.51	157.73	174.3	176.6		
	0	165.04	160.12	172.9	178.77		
	2	164.16	162.74	178.29	179.48		
	4	163.46	161.69	170.45	174.99		
	6	158.37	157.36	167.05	174.15		
	8	158.11	153.83	164.31	173.04		
	10	117.64	118.64	117.52	128.41		
	12	111.3	115.1	115.52	114.05		
	14	112.02	113.35	113.73	110.71		
	16	117.61	107.81	113.96	110		
	18	113.01	109.67	113.8	109.47		
	20	114.02	109.9	113.78	109.45		
	22	114.02	117.92	109.62	114.52		
	24	117.7	117.81	111.84	114.69		
	30	117.62	117.98	119.64	120.73		
	36	117.54	115.6	121.61	120.76		
	42	123.01	115.83	122.9	120.77		
	48	122.47	119.96	126.07	120.03		

Deflection Worksheet

Cell 6 # of Passes 0 Wheel Path: North

Measurements

West ← ————— → East

		1	2	3	4	5	6
North	48	124.33	130.41	139.03	120.68	125.36	121.07
	42	141.41	132.66	123.73	135.11	130.72	112.13
	36	130.34	125.75	134.25	122.61	129.01	111.39
	30	127.27	128	120.27	121.33	127.59	115.42
	24	130.93	124.61	129.5	121.62	130.42	117.58
	22	126.45	123.31	121.32	122.87	128	115.23
	20	126.18	123.37	121.29	124.84	127.5	115.53
	18	126.02	122.37	121.32	119.41	127.81	116.03
	16	131.62	128.38	123.88	123.94	130.22	116.85
	14	129.16	127.4	130.51	119.2	132.91	119.74
	12	127.68	129.85	123.42	115.82	131.34	120.18
	10	127.73	122.68	121.07	116.39	133.93	127.71
	8	127.2	123.97	122.21	115.05	131.99	131.68
	6	125.79	121.94	121.22	121.03	132.05	124.73
	4	125.96	122.03	125.34	120.87	137.36	132.42
	2	124.63	121.37	123.62	115.69	136.24	126.13
CL	0	126.95	125.91	124.37	120.32	141.04	128.45
	2	123.3	123.11	117.79	119.35	132.54	128.34
	4	121.75	121.33	120.38	115.34	136.63	129.86
	6	121.28	122.79	122.82	113.59	140.77	130.01
	8	121.92	122.79	126.9	112.87	132.69	129.3
	10	126.32	127.74	117.59	113.22	138.24	135.07
	12	128.5	121.79	120.93	112.37	141.42	129.59
	14	121.14	123.19	118.77	112.42	138.92	128.54
	16	120.04	119.56	118.67	111.44	126.95	132.76
	18	117.58	127.4	117.06	111.88	133.11	128.53
	20	120.66	120.89	122.6	112.14	137	130.05
	22	118.4	114.78	119.95	114.01	121.92	122.7
	24	120.92	125.95	117.72	111.35	136.02	117.26
	30	118.6	121.95	117.86	107.24	128.18	122.41
	36	109.87	122.81	115.42	106.55	119.19	110.29
	42	107.53	122.01	114.59	103.93	125.04	119.54
South	48	109.89	109.48	112.42	106.51	124.29	113.65

Deflection Worksheet

Cell 6 # of Passes 1 Wheel Path: North

Measurements

West ←  East

		1	2	3	4	5	6
North	48	127.98	129.67	125.73	125.41	128.06	124.19
	42	131.28	127.18	123.27	123.38	133.4	114.15
	36	133.61	124.74	122.46	126.54	131.04	111.8
	30	127.66	123.74	120.95	122.92	132.11	118.34
	24	131	121.46	122.11	119.61	132.32	115.21
	22	129.11	120.08	119.66	118.59	129.18	119.24
	20	126.49	125.2	119.19	122.5	133.85	118.54
	18	129.93	124.11	117.58	117.03	127.65	118.52
	16	132.91	122.15	118.49	120.82	137.16	120.54
	14	134.95	119.68	117.36	116.64	127.41	128.08
	12	129.08	128.81	123.04	120.39	130.49	122.28
	10	126.16	119.02	119.91	118.57	130.61	128.45
	8	129.94	127.04	126.23	117.33	131.36	125.18
	6	134.08	125.76	130.36	120.74	138.52	131.47
	4	132.13	123.07	124.34	120.26	136.68	136.52
	2	124.84	124.08	123.53	120.94	138.74	132.51
CL	0	135.05	128.21	127.17	114.69	139.32	132.03
	2	133.95	123.9	126.42	125.9	135.4	133.3
	4	131.34	125.99	122.55	118.43	136.98	130.65
	6	126.37	122.91	127.86	119.18	138.11	133.41
	8	132.91	121.51	118.54	116.81	132.39	129.74
	10	124.48	122.81	117.67	114.98	134.73	135.93
	12	123.04	119.44	116.09	111.68	134.31	137.95
	14	120.57	121.14	119.98	117.29	131.51	131.07
	16	117.04	115.92	118.8	113.61	139.83	138
	18	117.57	129.42	119.66	111.18	131.94	133.31
	20	117.6	127.14	115.62	116.14	135.9	125.66
	22	119.64	119.04	115.48	113.51	127.8	126.16
	24	128.74	128.95	116.68	109.9	124.22	113.15
	30	118.22	121.56	120.74	110.95	126.79	116.67
	36	118.78	122.47	114.63	108.87	115.35	110.85
	42	109.29	118.62	115.22	103.25	114.75	114.34
South	48	112.24	115.11	112.97	106.76	120.15	121.48

Deflection Worksheet

Cell 6 # of Passes 10 Wheel Path: North

Measurements

West ←  East

		1	2	3	4	5	6
North	48	131.94	127.24	123.31	125.89	126.84	122.54
	42	132.34	123.33	121.89	122.67	129.6	111.27
	36	128.74	122.51	123.92	120.65	130.62	110.12
	30	127.19	120.1	120.03	119.12	130.17	115.15
	24	128.2	120.7	121.16	118.56	133.36	112.43
	22	130.21	125.91	119.5	118.82	129.55	115.92
	20	129.3	117.68	117.9	125.62	132.74	115.65
	18	125.86	120.42	118.88	125.63	128.86	116.63
	16	129	124.25	118.66	119.84	141.75	118.12
	14	130.39	125.12	121.78	118.74	140.21	122.72
	12	129.95	128.72	120.84	120.81	137.81	126.07
	10	136.3	121.65	123.42	118.61	132.82	131.85
	8	136.13	129.18	134.84	131.73	141.9	129.79
	6	137.66	130.52	137.2	129.52	142.21	129.51
	4	137.85	135.06	138.31	132.03	146.03	133.21
	2	139.47	133.66	136.61	132.32	141.77	135.33
CL	0	141.74	133.75	137.96	126.86	142.08	135.68
	2	140.19	132.16	137.23	134.47	144.39	136.92
	4	136.88	135.4	136.75	127.75	141.44	136.23
	6	138.5	128.61	136.48	130.17	140.77	133.87
	8	125.31	123.06	125.21	122.32	133.46	136.18
	10	124.31	122.17	119.4	116.49	132.66	136.39
	12	120.51	120.27	118.99	113.28	130.25	129.56
	14	119.4	118.71	114.57	111.36	131.38	127.72
	16	122.72	109.91	115.7	111.2	137.38	130.72
	18	120.85	114.73	117.05	109.88	132.08	127.42
	20	119.18	114.37	117	111.53	131.21	129.22
	22	117.6	122.9	115.03	110.25	124.11	120.45
	24	118.28	127.07	116.62	107.82	123.21	116.32
	30	118.24	125.73	120.76	110.78	120.89	111.27
	36	106.79	120.46	120.28	106.13	119.36	112.34
	42	108.15	120.26	115.27	104.61	116.36	114.87
South	48	108.35	119.95	113.69	102.97	113.57	119.19

Deflection Worksheet								
Cell <u>6</u>		# of Passes <u>33</u>		Wheel Path: <u>N</u> Wheel out of stroke in the middle_				
Measurements								
		West ← → East						
		1	2	3	4	5	6	3.8 Worst Rutting
North	48	127.49	131.74	122.54	128.93	125.6	126.12	125.06
	42	135.82	123.37	118.92	127.13	129.34	115.48	124.75
	36	133.95	126.58	121.63	120.09	133.46	110.07	116.81
	30	124.81	119.87	118.62	112.21	130.37	114.59	119.92
	24	130.03	118.12	118.78	113.69	131.43	120.62	112.96
	22	130.56	121.1	121.01	109.59	131.15	118.46	110.49
	20	123.33	120.67	119.28	115.46	140.04	118.94	111.75
	18	125.82	121.35	115.89	108.78	129.19	119.96	121.51
	16	129.01	120.28	119.44	108.57	141.92	123.95	113.05
	14	129.72	120.2	120.79	112.72	145.99	122.4	114.43
	12	134.61	128.46	128.87	111.25	144.82	133.75	116.78
	10	147.46	131.46	134.26	119.38	144.91	137.33	181
	8	150.95	140.98	152.8	142.76	149.26	143.29	192.71
	6	151.96	145.76	157.09	165.71	151.91	139.28	194.2
	4	154.63	146.65	161.36	166.79	152.55	147.96	197.84
	2	152.12	148.48	161.96	169.74	147.68	150.93	197.16
CL	0	158.6	147.23	156.29	177.05	147.09	150.37	198.88
	2	153.15	147.37	157.95	175.14	152.47	148.93	197.76
	4	148.2	148.94	157.51	175.62	148.26	147.79	195.53
	6	145.83	141.86	149.76	174.43	144.39	141.99	195.25
	8	142.86	139.13	148.94	168.44	134.85	143.84	163.29
	10	130.14	120.41	120.14	144.88	130.67	142.26	144.93
	12	120.82	122.85	122.94	128.57	130	128.27	136.84
	14	118.3	117.85	117.49	118.75	141.96	133.1	133.81
	16	126.92	106.67	116.03	111.91	128.91	125.06	132.42
	18	123.55	123.17	116.97	110.22	136.45	132.51	129.81
	20	116.4	121.04	113.61	111.94	121.36	132.57	127.37
	22	117.56	123.46	115.62	113.38	129.31	125.25	124.74
	24	127.14	121.54	119.72	113.58	120.28	112.58	125.75
	30	117.38	119.18	116.97	108.79	130.01	124.71	125.62
	36	116.79	119.44	116.29	107.83	123.96	111.42	127.06
	42	108.84	123.33	118.38	107.93	126.17	122.59	118.5
South	48	114.15	124.93	117.03	103.28	115.87	121.27	127.56

Deflection Worksheet									
Cell _____		6		# of Passes _____		63		Wheel Path: _Wheel Stroke out of range after lowering machine_	
Measurements									
		West ← —————→ East							
		1	2	3	4	5	6	3.8	
North	48	131.94	128.96	120.17	122.26	129.89	122.11	122.09	
	42	126.97	119.98	119.06	116.58	131.74	109.83	115.16	
	36	130.63	117.05	116.92	98.79	132.58	108.79	99.97	
	30	122.77	111.91	114.91	90.99	135.09	116.72	86.73	
	24	119.78	112.43	112.62	82.7	136.59	110.93	88.91	
	22	122.7	113.92	114.65	84.86	132.26	116.14	83.05	
	20	122.57	112.87	113.87	82.7	133.21	113.2	85.17	
	18	127.5	110.76	113.33	79.42	130.6	122.34	83.23	
	16	124.76	111.29	120.77	83.01	135.78	126.9	84.04	
	14	129.03	117.43	123.24	86.27	142.39	128.34	83.88	
	12	122.07	118.84	125.06	93.96	135.81	131.47	85.4	
	10	143.98	143.21	151.22	203.01	142.59	131.76	228.6	
	8	158.65	164.98	171.17	250.83	154.42	143.89	254	
	6	160.46	168.68	174.9	250.83	154.52	150.33	254	
	4	163.22	172.84	175.25	250.83	160.59	151.23	254	
	2	167.01	175.2	182	250.83	156.02	153.11	254	
CL	0	176.2	174.18	184.52	250.83	159.19	156.62	254	
	2	161.04	166.78	180.99	250.83	157.57	153.78	254	
	4	160.91	164.71	179.86	250.83	152.44	148.65	254	
	6	156.85	160.51	175.8	250.83	150.81	148.15	241.3	
	8	147.27	139.22	150.12	203.63	141.95	135.68	228.6	
	10	135.52	122.94	125.28	113.65	139.3	138.15	127.99	
	12	134.43	118.6	119.7	116.54	131.23	134.56	120.56	
	14	124.09	118.9	120.91	116.77	131.23	125.6	115.6	
	16	124.1	110.87	115.96	103.92	130.72	129.76	115.3	
	18	116.35	113.3	119.2	107.17	128.92	128.07	116.71	
	20	124.55	119.21	119	98.62	124.01	130.48	114.75	
	22	117.9	117.83	112.73	100.22	118.52	123.05	113.09	
	24	117.62	116.91	115.24	101.89	121.48	115.09	119.33	
	30	114.04	116.02	119.36	100.17	129.17	111.33	116.77	
	36	119.99	116.73	116.41	106.82	116.98	117	119.19	
	42	107.92	117.84	114.75	107.87	118.44	118.91	117.85	
South	48	116.84	122.62	114.56	107.56	119.75	114.16	114.87	

Deflection Worksheet

Only Section 1 (Fairmount) and Section 3 (Lincoln) loaded from 63 passes to 100 passes.

Cell 6 # of Passes 100 Wheel Path: Manteno was stopped loading at 63 passes.

Measurements

	West ← ————— → East						
	1	2	3	4	5	6	
North	48	128.76	128.46	X	X	128.22	123.19
	42	134.07	118.82	X	X	128.37	110.15
	36	131.04	116.74	X	X	129.8	109.55
	30	121.5	105.64	X	X	129.17	112.18
	24	122.32	99.29	X	X	132.69	111.03
	22	120.08	101.15	X	X	132.37	112.52
	20	116.88	97.71	X	X	135.66	114.25
	18	116.77	98.72	X	X	129.91	115.64
	16	127.27	100.49	X	X	141.36	117.68
	14	123.1	116.9	X	X	135.04	122.35
	12	125.78	117.36	X	X	138.64	135.39
	10	141.74	172.49	X	X	143.8	137.55
	8	169.42	185.61	X	X	162.1	149.02
	6	177.03	198.15	X	X	161.9	156.22
	4	174.41	202.76	X	X	164.63	151.07
	2	174.3	201.14	X	X	169.34	163.4
CL	0	185.04	200.16	X	X	169.54	160.58
	2	173.36	200.12	X	X	168.15	155.76
	4	177.89	197.51	X	X	162.28	151.83
	6	170.87	193.21	X	X	156.5	158.8
	8	161.8	171.12	X	X	139.53	133.79
	10	130.55	120.1	X	X	137.3	128.18
	12	124.14	107.94	X	X	133.43	131.1
	14	121.57	105.86	X	X	134.95	125.99
	16	113.99	98.7	X	X	134.23	123.4
	18	119.18	109.93	X	X	127.75	121.4
	20	120.64	114.35	X	X	127.63	133.57
	22	111.94	121.71	X	X	120.5	115.89
	24	119.51	118.52	X	X	118.73	113.24
	30	113.71	122.22	X	X	118.88	107.69
	36	113.43	121.86	X	X	116.32	109.2
	42	107.82	119.69	X	X	117.24	113.84
South	48	111.42	127.23	X	X	118.85	117.14

Deflection Worksheet

Cell 6 # of Passes 159 Wheel Path: _____
 Measurements

	West ← Measurements → East						
	1	2	3	4	5	6	
North	48	130.83	116.5	X	X	X	X
	42	128.16	109.81	X	X	X	X
	36	122.03	95.81	X	X	X	X
	30	120.53	84.98	X	X	X	X
	24	115.07	72.42	X	X	X	X
	22	115.06	74.67	X	X	X	X
	20	109.43	77.66	X	X	X	X
	18	112.57	79.53	X	X	X	X
	16	115.73	81.04	X	X	X	X
	14	114.92	90.91	X	X	X	X
	12	124.23	107.24	X	X	X	X
	10	165.6	202.74	X	X	X	X
	8	182.05	9 in	X	X	X	X
	6	187.72	9.5 in	X	X	X	X
	4	188.52	9.5 in	X	X	X	X
	2	119.76	9.5 in	X	X	X	X
CL	0	205.33	9.25 in	X	X	X	X
	2	185.55	9.25 in	X	X	X	X
	4	190.88	9.25 in	X	X	X	X
	6	182.27	9 in	X	X	X	X
	8	182.4	204.16	X	X	X	X
	10	129.66	118.43	X	X	X	X
	12	130.63	97.27	X	X	X	X
	14	119.92	91.18	X	X	X	X
	16	116.49	85.03	X	X	X	X
	18	114.97	101.53	X	X	X	X
	20	119.25	100.06	X	X	X	X
	22	108.21	98.13	X	X	X	X
	24	123.69	109.06	X	X	X	X
	30	110.8	103.93	X	X	X	X
	36	115.29	120.3	X	X	X	X
	42	107.59	119.7	X	X	X	X
South	48	112.12	121.86	X	X	X	X

Deflection Worksheet

Cell 6 # of Passes 171 Wheel Path: N

Measurements

West ← → East

		1	2	3	4	5	6	5.5
North	48	X	X	X	X	126.32	130.45	126.24
	42	X	X	X	X	120.06	113.98	113.87
	36	X	X	X	X	114.23	113.28	101.69
	30	X	X	X	X	115.55	115.05	101.16
	24	X	X	X	X	119.91	110.6	100.46
	22	X	X	X	X	121.1	116.57	112.46
	20	X	X	X	X	127.93	119.27	97.71
	18	X	X	X	X	128.63	125.3	104.91
	16	X	X	X	X	137.27	115.53	102.58
	14	X	X	X	X	147.89	126.1	107.01
	12	X	X	X	X	162.71	135.1	100.05
	10	X	X	X	X	9 in	151.66	126.3
	8	X	X	X	X	10.25 in	163.31	147.28
	6	X	X	X	X	10.25 in	161.12	147.02
	4	X	X	X	X	10.25 in	162.55	157
	2	X	X	X	X	10.25 in	164.32	160.72
CL	0	X	X	X	X	10.25 in	164.24	154.98
	2	X	X	X	X	10 in	167.92	156.45
	4	X	X	X	X	10 in	160.04	147.99
	6	X	X	X	X	9.5 in	157.67	147.77
	8	X	X	X	X	8.5 in	143.35	141.65
	10	X	X	X	X	146.47	141.71	113.65
	12	X	X	X	X	143.3	136.26	109.52
	14	X	X	X	X	136.3	131.78	108.07
	16	X	X	X	X	135.98	123.95	105.55
	18	X	X	X	X	128.9	126.9	113.59
	20	X	X	X	X	122.63	127.45	103.48
	22	X	X	X	X	129.44	120.6	108.89
	24	X	X	X	X	116.38	116.99	110.25
	30	X	X	X	X	115.83	114.71	110.53
	36	X	X	X	X	124.06	108.57	100.04
	42	X	X	X	X	118.62	117.4	109.66
South	48	X	X	X	X	116.52	115.79	117.43

Deflection Worksheet

Cell 6 # of Passes: 223 (from 180 to 223 @ 4 mp) Wheel Path: N

Measurements

West ← ————— → East

		1	2	3	5.5	5	6
North	48	X	X	X	120.07	122.4	126.1
	42	X	X	X	109.03	115.02	112.4
	36	X	X	X	103.29	110.14	113.84
	30	X	X	X	97.37	106.72	115.04
	24	X	X	X	100.04	116.05	112.91
	22	X	X	X	92.88	117.63	118.61
	20	X	X	X	92.57	128.69	112.73
	18	X	X	X	90.52	124.88	124.46
	16	X	X	X	98.01	139.17	114.46
	14	X	X	X	95.31	145.14	125.78
	12	X	X	X	107.1	154.79	133.82
	10	X	X	X	145.29	9 (3/8) in	151.72
	8	X	X	X	160.34	10 in	165.32
	6	X	X	X	169.82	10.75 in	171.48
	4	X	X	X	176.43	10.75 in	171.93
	2	X	X	X	178.14	11 in	173.28
CL	0	X	X	X	180.19	11 in	181.23
	2	X	X	X	177.17	10.75 in	175.31
	4	X	X	X	179.05	10.5 in	172.8
	6	X	X	X	171.39	10 (3/8) in	166.95
	8	X	X	X	139.07	9 in	161.83
	10	X	X	X	101.34	144.75	132.69
	12	X	X	X	106.62	140.83	138.74
	14	X	X	X	101.61	129.18	126.38
	16	X	X	X	101.49	124.17	125.15
	18	X	X	X	102.61	126.56	132.82
	20	X	X	X	102.85	126.12	125.56
	22	X	X	X	101.52	126.48	123.54
	24	X	X	X	99.7	122.89	122.89
	30	X	X	X	105.94	112.48	116.31
	36	X	X	X	104.94	116.15	107.5
	42	X	X	X	107.66	123.28	111.82
South	48	X	X	X	113.15	131.81	120.49

Deflection Worksheet

Cell 6 # of Passes 0 Wheel Path: South
 Measurements

	West ← —————→ East					
	1	2	3	4	5	6
48	107.42	157.17	128.89	113.15	122.62	115.28
42	103.65	151.34	131.52	122.63	129.84	115.12
36	105.91	155.26	134.9	125.39	126.01	113.45
30	113.44	153.41	126.8	115.86	128.28	111.3
24	106.39	152.26	126.07	121.5	123.93	117.24
22	100.89	154.86	130.19	119.43	122.85	116.61
20	107.76	153.2	128.27	119.8	126.33	114.57
18	109.79	160.18	132.94	117.26	128.42	120.63
16	110.05	156.18	133.16	119.97	124.21	112.61
14	99.38	154.74	130.13	116.85	123.1	111.25
12	101.96	152.31	130.24	117.47	126.36	112.95
10	107.62	152.3	125.42	120.53	122.74	116.97
8	108.83	155.75	129.39	119.54	124.53	115.82
6	106.9	158.3	130.83	122.84	124.97	117.04
4	110.63	157.51	126.91	119.85	128.72	123.59
2	110.3	152.22	125.53	123.36	125.97	116.59
CL	109.76	155.03	131.87	120.91	126.43	120.5
2	112.54	158.96	128.2	125.82	127.89	119.82
4	111.54	154.63	128.25	123.55	127.71	120.78
6	115.07	150.94	137.16	122.33	131.92	123.04
8	106.24	150.38	131.33	119.92	132.66	120.01
10	106.25	147.66	125.83	128.19	132.62	121.92
12	107.48	146.84	124.47	121.84	139.33	122.71
14	106.92	144.82	124.35	123.44	136.4	127.95
16	107.65	148.33	121.35	118.04	135.6	128.24
18	108.83	147.98	119.95	118.14	137.44	129.42
20	111.77	143.54	128.19	120.93	137.01	129.45
22	105.93	140.23	126.99	117.58	132.35	127.3
24	106.23	145.89	123.69	117.1	134.3	124.64
30	107.57	139.45	128.9	117.31	123.88	123.3
36	115.9	140.7	123.43	117.64	131.81	135.69
42	114.12	136.81	134.99	121.34	130.05	130.66
48	114.44	140.29	131.32	127.08	130.32	133.69

Deflection Worksheet

Cell 6 # of Passes 1 Wheel Path: South

Measurements

Date: 18th October 2010

West ← ————— → East

		1	2	3	4	5	6
North	48	106.33	157.23	125.50	112.75	111.6	114.54
	42	109.61	154.99	130.67	117.00	119.34	113.13
	36	100.73	148.31	133.98	118.84	118.32	112.38
	30	100.99	154.28	126.98	121.90	113.04	112.57
	24	100.11	153.63	132.76	114.26	119.18	110.88
	22	100.92	155.48	123.67	116.25	123.69	115.93
	20	100.83	150.15	125.83	114.51	124.74	119.88
	18	102.93	155.22	122.84	119.15	125.11	113.4
	16	98.01	152.74	124.83	115.74	128.86	112.04
	14	99.79	150.98	122.41	115.84	126.35	115.95
	12	102.69	158.67	124.33	116.41	126.93	114.38
	10	106.74	155.30	126.00	117.31	125.15	116.54
	8	113.71	158.20	129.83	121.59	125.59	115.88
	6	114.85	159.62	135.20	118.94	125.86	117.42
	4	123.12	162.18	132.81	119.42	126.91	117.86
	2	117.03	162.72	130.21	121.54	129.25	124.33
CL	0	121.79	160.14	133.55	123.28	128.85	122.15
	2	116.49	163.68	130.57	121.23	128.97	122.55
	4	117.4	162.02	131.98	127.46	128.15	121.76
	6	119.77	154.26	128.38	123.24	131.07	121.67
	8	109.03	148.39	128.74	121.5	131.09	121.04
	10	108.45	153.65	124.47	121.03	134.69	124.32
	12	102.17	146.97	124.27	124.98	134.56	125.88
	14	108.91	149.67	122.58	119.1	136.64	130.62
	16	107.28	142.79	121.78	116.96	134.56	125.47
	18	114.92	141.7	121.45	119.9	135.74	123.24
	20	113.86	141.74	120.06	122.88	134.78	129.04
	22	110.23	144.34	119.34	120.47	133.17	122.03
	24	110.25	143.93	128.38	119.73	130.29	118.66
	30	108.53	138.34	132.25	118.25	127.33	122.44
	36	110.11	139.63	121.74	117.26	128.12	128.38
	42	114.97	132.82	123.25	116.34	128.66	128.59
South	48	115.79	134.72	132.16	130.21	129.01	130.63

Deflection Worksheet

Cell 6 # of Passes 10 Wheel Path: South

Measurements

Date: 18th October 2010

West ← ————— → East

	1	2	3	4	5	6
48	102.44	152.36	125.05	112.04	114.94	110.73
42	94.88	143.11	125.51	110.72	120.51	109.59
36	97.44	147.9	127.15	116.1	120.57	106.82
30	89.89	149.35	120.54	113.57	117.79	114.15
24	96.53	148.67	123.61	117.94	119.87	114.97
22	93.8	146.06	119.39	117.08	122.43	112.25
20	97.62	147.37	126.49	113.63	123.59	115.01
18	105.87	144.54	120.88	116.23	123.51	113.92
16	99.40	152.33	121.41	115.56	124.37	117.12
14	99.72	147.52	120.44	116.39	123.37	115.78
12	104.448	148.72	125.38	115.26	122.42	115.02
10	107.21	150.19	127.32	118.77	121.52	113.34
8	125.98	162.24	146.00	123.81	124.54	123.08
6	126.95	165.68	148.09	129.11	132.98	123.51
4	134.72	169.48	145.47	126.51	132.68	125.71
2	134.59	175.04	147.97	130.9	133.63	126.18
0	132.58	175.75	146.19	128.39	135.58	127.48
2	134.79	173.63	146.54	128.72	135.93	127.84
4	132.6	170.42	150.43	128.31	137.55	128.74
6	136.29	165.77	145.16	128.23	136.3	132.63
8	120	156.01	129.07	123.95	132.74	126.75
10	109.02	150.36	126.71	123.29	131.54	123.99
12	101.31	145.44	125.15	117.45	134.50	121.88
14	104.56	143.1	124.52	119.28	135.54	125.9
16	101.33	136.95	123.69	118.32	132.76	126.73
18	104.58	141.22	119.6	117.38	137.43	122.79
20	105.76	137.1	122.34	120.08	133.49	127.6
22	103.78	140.31	119.73	117.7	131.79	123.79
24	104.4	137.94	123.66	117.42	131.31	123.17
30	101.84	139.27	132.12	116.53	128.85	123.6
36	107.21	137.55	121.79	123.50	129.27	124.02
42	111.37	131.89	127.93	117.79	129.04	135.13
48	120.55	134.46	129.50	135.23	130.51	125.72

North



CL



South

Deflection Worksheet

Cell 6 # of Passes 33 Wheel Path: South

Measurements

Date: 18th October 2010

West ← ————— → East

		1	2	3	4	5	6
North	48	110.06	148.24	122.43	114.21	114.07	113.97
	42	109.08	135.54	125.26	117.71	117.69	110.1
	36	97.88	139.5	122.31	115.11	119.34	109.11
	30	93.87	142.23	114.99	121.91	119.88	111.56
	24	88.38	147.05	116.00	113.36	118.89	111.92
	22	94.37	137.19	113.17	115.91	123.13	111.37
	20	88.76	136.87	113.59	114.86	120.37	117.38
	18	97.31	144.9	115.29	116.71	120.18	114.56
	16	98.98	147.57	121.61	112.43	121.92	114.23
	14	99.19	140.53	118.28	113.97	125.82	116.19
	12	102.99	142.93	124.44	115.95	124.61	117.27
	10	110.09	152.98	131.28	120.17	121.42	114.23
	8	134.73	177.56	162.32	121.78	127.95	126
	6	143.05	180.3	167.08	135.43	137.63	133.95
	4	151.04	180.8	166.69	137.38	139.37	138.29
	2	151.4	186.6	167.47	135.36	143.44	134.92
CL	0	150.2	182.73	161.59	137.89	141.54	139.06
	2	151.34	183.32	163.08	137.52	144.12	141.21
	4	150.89	183.99	164.95	136.39	144.25	140.58
	6	149.21	179.95	162.31	134.7	138.96	140.67
	8	126.64	172.55	147.81	130.1	136.17	140.67
	10	113.53	142.16	127.98	123.23	134.17	131.81
	12	97.93	137.47	124.81	121.79	134.22	124.57
	14	99.85	132.85	118.38	117.29	133.38	126.83
	16	97.49	131.07	116.83	116.28	130.53	123.28
	18	104.79	129.8	114.61	116.76	133.04	126.67
	20	100.17	127.28	120.99	120.53	133.12	123.65
	22	97.98	128.67	113.45	120.47	129.21	118.88
	24	94.46	127	121.81	116.62	126.32	123.03
	30	102.35	130.52	129.04	115.25	131.2	120.21
	36	106.83	129.94	120.19	117.62	125.06	119.74
	42	107.48	131.85	124.95	115.08	130.82	129.97
South	48	121.82	132.04	133.59	128.14	130.04	127.78

Deflection Worksheet

Cell 6 # of Passes 63 Wheel Path: South

Measurements

Date: 18th October 2010

West ← → East

	1	2	3	4	5	6
48	103	136.64	126.07	112.81	115.26	116
42	92.33	135.51	118.72	113.17	115.65	109.71
36	92.22	140.98	130.45	116.73	121.55	109.65
30	86.47	136.92	107.43	113.47	114.97	112.42
24	86.48	132.72	110.41	115.18	116.89	111.79
22	86.75	131.6	105.26	116.65	120.97	112.26
20	87.79	133.07	114.01	115.98	121.63	116
18	89.15	129.01	108.51	117.2	118.55	116.31
16	89.03	131.64	118.62	117.83	119.04	117.92
14	91.45	134.51	109.21	112.57	121.38	113.04
12	92.55	133.52	120.83	117.13	117.42	115.14
10	119.31	150.06	174.29	120.22	123.71	116.14
8	149.9	195.45	185.52	129.75	130.21	130.37
6	156.09	191.72	185.87	140.65	144.15	144.51
4	158.76	195.52	188.39	143.86	147.01	142.09
2	160.93	196.21	189.58	145.29	148.66	146.54
0	159.34	195.11	189.94	144.73	149.98	144.15
2	160.24	195.32	189.69	147.54	148.2	149.97
4	159.98	192.97	189.81	145.29	146.91	143.25
6	157.65	193.47	189.73	140.51	144.28	148.48
8	128.34	160.14	148.27	134.78	147.21	141.45
10	92.3	136.57	120.96	122.83	130.35	121.34
12	88.86	126.18	120.07	119.11	132.88	123.05
14	91.44	124.54	117.14	120.32	132.75	121.68
16	91.16	119.44	117.25	115.31	131.2	121.33
18	92.01	118.02	107.56	119.03	132.95	122.67
20	98.54	125.62	117.26	120.3	130.01	127.46
22	90.08	124.49	116.1	115.74	127.67	120.57
24	93.99	127.55	124.28	114.42	126.9	119.66
30	97.31	132.15	125.34	115.92	123.89	118.86
36	103.11	128.37	121.4	115.93	124.39	126.44
42	106.57	130.42	132.99	126.42	127.43	129.04
48	111.62	141.19	133.50	133.58	129.91	131.06

North



CL



South



Deflection Worksheet

Cell 6 # of Passes 100 Wheel Path: South

Measurements

Date: 18th October 2010

West ←  East

		1	2	3	4	5	6
North  CL  South	48	102.93	147.38	122.11	112.9	111.18	107.84
	42	104.26	141.1	117.38	110.07	114.99	108.13
	36	97.63	133.81	108.02	114.66	115.04	107.32
	30	89.48	142.1	103.28	110.38	115.58	107.66
	24	89.42	133.82	96.49	108.46	116.57	106.77
	22	82.16	128.01	93.71	108.45	116.57	110.12
	20	93.23	127.22	93.21	107.95	116.56	114.94
	18	89.23	122.39	99.13	109.63	118.17	109.09
	16	82.25	125.92	97.64	109.6	118.11	109.73
	14	90.16	123.28	97.76	110.01	118.32	108.21
	12	92.47	121.78	110.67	112.56	118.52	109.84
	10	121.95	175.02	159.04	113.52	123.4	113.56
	8	158.84	199.69	200.58	147.38	133.13	118.09
	6	164.02	203.2	203.2	151.8	150.56	148.06
	4	164.78	206.375	203.2	153.34	155.06	149.76
	2	171.29	209.55	206.375	160.84	152.12	152.66
	0	172.16	209.55	203.2	156.84	151.21	150.17
	2	170.24	209.55	203.2	155.08	151.97	150.12
	4	168.57	209.55	203.97	153.33	148.49	150.66
	6	169.38	203.2	203.97	152.83	147	148.32
	8	145.26	188.23	172.5	143.01	145.44	148.09
	10	102.44	115.56	111.66	125.7	133.58	134.17
	12	87.1	115.55	108.88	117.42	130.88	123.6
	14	87.93	110.9	103.92	113.41	129.68	124.44
	16	92.43	108.06	102.16	113.59	126.71	121.75
	18	86.6	110.25	103.11	113.59	126.52	121.52
	20	85.48	111.51	104.56	113.77	125.23	119.84
	22	93.81	113.6	110.48	111.62	124.63	117.65
	24	88.29	119.13	107.88	112.14	123.43	117.48
	30	96.22	120.83	116.14	112.65	124.59	117.16
	36	96.12	131.19	113.5	113.71	124.66	114.62
	42	111.95	132.99	122.56	128.18	127.4	127.17
	48	121.09	134.96	132.89	128.16	127.3	126.01

Deflection Worksheet

Cell 6 # of Passes 159 Wheel Path: South

Measurements

Date: 18th October 2010

West ← ————— → East

	1	2	3	4	5	6
48	107.59	146.64	122.01	111.56	110.88	108.82
42	103.52	134.53	117.24	109.76	115.84	108.82
36	91.88	133.11	107.5	111.36	114.68	105.77
30	83.99	130.17	90.07	103.36	114.68	105.24
24	82.44	114.74	83.44	103.2	113.89	104.74
22	82.44	109.59	83.14	97.21	113.93	107.78
20	81.74	103.62	74.81	95.09	119.07	101.3
18	81.76	100.08	75.12	93.28	118.2	109.29
16	81.77	96.29	75.98	97.86	118.07	112.64
14	81.93	94.4	79.35	93.41	117.59	107.73
12	85.61	90.69	86.01	94.46	116.16	108.78
10	130.78	203.96	188.3	135.82	121.05	114.92
8	167.17	228.6	231.90	165.21	145.03	133.1
6	176.29	228.6	238.125	191.8	155.99	152.04
4	179.12	234.95	238.125	188.73	161.27	153.91
2	179.3	234.95	241.3	190.33	162.57	157.98
0	178.02	234.95	241.3	187.97	162.95	158.64
2	178.08	238.125	241.3	187.88	165.93	158.73
4	177.36	231.775	234.95	186.05	157.67	159.05
6	177.19	222.25	228.6	180.98	153.93	155.79
8	168.89	203.12	200.35	161.68	143.15	150.9
10	101.49	89.62	94.62	136.49	128.39	123.51
12	85.59	80.48	87.09	107.89	128.32	119.89
14	80.64	78.75	89.73	102.77	127.16	122.76
16	85.77	77.28	82.99	96.8	125.13	119.01
18	85.86	77.69	83.29	96.99	124.55	117.77
20	84.87	81.75	85.15	97.06	124.5	117.83
22	81.18	88.52	85.19	96.7	122.33	115.55
24	82.15	95.49	88.86	98.69	120.12	115.65
30	91.45	106.29	89.45	99.99	120.16	117
36	100.75	121.67	105.85	106.51	121.87	119.7
42	106.31	129.84	115.24	117.73	124.75	127.68
48	114.16	130.53	135.34	121.2	128.4	127.85

North



CL



South

Deflection Worksheet

Cell 6 # of Passes 171 Wheel Path: South

Measurements

Date: 18th October 2010

West ← ————— → East

	1	2	3	4	5	6
48					108.48	110.94
42					121.81	108.75
36					118.85	109.98
30					118.66	108.47
24					116.13	105.51
22					115.2	111.83
20					116.37	118.17
18					120.31	107.35
16					122.08	112.49
14					119.2	107.21
12					117.97	111.64
10					119.64	113.52
8					136.54	143.03
6					163.75	151
4					161.8	160.76
2					162.5	156.66
0					162.51	158.63
2					160.4	165.7
4					160.44	162.64
6					159.25	164.01
8					154.33	158.99
10					127.67	125.77
12					129.64	121.64
14					129.33	125.49
16					129.19	120.65
18					125.35	123.04
20					127.59	117.54
22					124.71	117.19
24					125.36	123.65
30					128.31	122.77
36					120.93	123.56
42					131.66	128.03
48					129.03	123.5

North



CL



South

Deflection Worksheet

Cell 6 # of Passes 223 Wheel Path: South

Measurements

Date: 18th October 2010

West ← —————→ East

		1	2	3	4	5	6
North	48					113.62	110.09
	42					116.76	102.51
	36					118.46	102.61
	30					126.21	107.85
	24					112.96	105.05
	22					112.99	107.17
	20					116.35	108.13
	18					120.43	110.68
	16					116.85	114.74
	14					115.89	107.34
	12					114.44	111.57
	10					114.1	112.28
	8					134.06	142.57
	6					166.19	159.18
	4					170.39	164.74
	2					167.66	163.15
CL	0					167.41	164.88
	2					165.65	163.37
	4					168.83	167.39
	6					161.01	169.59
	8					164.13	158.66
	10					119.72	144.8
	12					125.31	120.3
	14					124.32	125.52
	16					124.19	121.44
	18					120.93	121.7
	20					123.3	119.44
	22					119.22	119.51
	24					123.96	119.53
	30					118.38	115.24
	36					121.53	127.07
	42					130.2	129.45
South	48					132.17	124.13

Deflection Worksheet

Cell 6 # of Passes 400 Wheel Path: South

Measurements

Date: 18th October 2010

West ← —————→ East

	1	2	3	4	5	6
48					124.18	104.31
42					117.82	104.31
36					119.16	109.55
30					109.7	106.62
24					103.39	100.26
22					104.68	109.98
20					107.84	109.32
18					103.82	101.17
16					104.68	105.74
14					98.95	101.16
12					99.47	103.44
10					111.5	98.34
8					157.04	152.36
6					189.71	171.84
4					195.44	174.75
2					195.5	178.08
0					199.86	180.61
2					196.87	180.26
4					192.86	179.82
6					185.68	176.74
8					184.87	171.97
10					151.77	142.26
12					107.82	119.62
14					108.86	124.86
16					107.84	121.15
18					111.99	115.33
20					108.99	119.32
22					112.93	113.04
24					107.03	111.98
30					112.78	118.38
36					115.93	123.46
42					130.19	127.52
48					131.51	129.81

North



CL



South

